School of Civil and Mechanical Engineering
Department of Civil Engineering

Numerical and Experimental study of pounding damages in adjacent bridge structures subjected to spatially varying ground motion and its mitigation method

Bipin Shrestha

This thesis is presented for the Degree of
Doctor of Philosophy
of
Curtin University

April 2016

Declaration

To the best of my knowledge and belief this thesis contains no material previously published by any other person except where due acknowledgment has been made.

This thesis contains no material which has been accepted for the award of any other degree or diploma in any university.

Signature: …….

Date: ……...

ABSTRACT

Bridge infrastructure is an integral component of the transportation network and usually considered as a lifeline structure having significant economic, social and strategic value. As valuable lifeline structures, bridge structures are expected to remain functional to facilitate rescue and relief operation in the damaged area immediately after a strong earthquake. However, previous experiences have shown that keeping the bridges safe and operational after a strong earthquake is very challenging.

During previous major earthquakes, seismic pounding between adjacent bridge components was commonly observed due to the insufficient gap width provided at the expansion joints. In the majority of the cases pounding between the bridge components led to damages at the impacting location of the bridge girders and abutments. Damages to shear keys, bearing pads, and restrainers, resulting in the partial closure of the bridge were also observed. In extreme events, pounding led to the collapse of bridge deck due to the unseating resulting in the complete closure of the bridge for a lengthy period. It is worth noting that both pounding and unseating damages are the results of relative displacements between the adjacent bridge segments. Significant numbers of studies on pounding responses of adjacent bridge components subjected to seismic excitations have been conducted in the past. However, most of these studies have neglected spatial variation of ground motions between the supports of the bridges, which could significantly affect the relative displacement between the bridge segments. Moreover, large-scale shake table testing on the pounding response of the adjacent bridge segments subjected to spatially varying ground motion are inexistent.

Realising the above-mentioned facts an extensive investigation comprising of experimental and numerical studies is conducted to study the response of bridges subjected to non-uniform ground motions including pounding responses at expansion joints. A large-scale shake-table testing is carried out on representative bridge models to identify the response of the bridge segments to spatially varying ground motions. Numerical studies are then carried out to study the effectiveness of various devices, such as steel or shape memory alloy cable restrainers, rubber bumpers or a hybrid combination of both devices to mitigate pounding and unseating damages on bridge structures. Moreover, the significance of spatially varying ground motion and soil structure interaction on the response of bridges with unseating restrainers are explored. The application of low-cost, high energy dissipating rotational friction hinge devices to mitigate damages on base-isolated highway bridges under spatially varying ground motions are explored.

Another form of damage commonly observed during the strong earthquakes, leading to the complete closure of the bridges, is residual displacement of the bridge piers. Reinforced concrete bridge piers designed based on the modern codes to achieve high ductility, although capable of avoiding collapse, might suffer from large residual displacement leading to the demolition of the bridge after earthquake events. Using superelastic SMA reinforcement could provide the re-centring capacity to the bridge piers that could make it serviceable even after a strong earthquake. Parametric studies on the seismic performance of superelastic shape memory alloy reinforced bridge piers are carried out revealing the effects of various design and geometric parameters, such as number and geometry of piers and reinforcement ratio of the SMA reinforcement on its performance. Application of superelastic SMA reinforcement in the plastic hinge regions of the bridge piers significantly reduced the residual displacements, however, the maximum deformation piers were increased due to the relatively lower hysteretic energy dissipation and lower modulus of elasticity of SMA bars. The investigation is then carried out using a recently formulated probabilistic performance-based seismic assessment methodology that considers both the maximum and the residual deformation simultaneously. The benefits of using SMA reinforcement in the plastic hinge region of bridge piers are elicited, particularly for those constructed at moderate-high seismicity regions.

ACKNOWLEDGEMENT

The work presented in thesis could not have been materialized without the input from many individuals. It is very hard to fit the contribution of so many people on a single page.

Firstly, my heartfelt thank goes to Prof. Hong Hao, my supervisor for PhD study, for his continuous support, patience, guidance, and encouragement at difficult periods of this long journey. I would also like to acknowledge Dr. Kaiming Bi for his contribution as not only the co-authors but also as a friend and an advisor. I gratefully acknowledge the contributions of Mr. Chao Li, Prof. Hong-Nan Li, Mr. Nazman HJ Ibrahim, Mr. Li-Xiang He, Prof. Wei-Xin Ren as the co-authors of the paper that are an integral part of the thesis.

My sincere thanks also go to Dr. Andrew Whyte, head of the Department of Civil Engineering, Curtin University and Prof. Guowei Ma, graduate research coordinator, The University of Western Australia (UWA).

I would also like to thank my colleagues Kinzang Thinley, Francesco Hernandez and many other members of Prof. Hao's research group at The UWA and Curtin University. Thanks also go to the students of Prof. Wei-Xin Ren's research group, Central South University and Hefei University for their efforts during the experimental study.

I am indebted to the UWA for providing full scholarship for my PhD studies, which continued for nearly half of my PhD candidature. Thanks also goes to Curtin University for continuing the research scholarship for the remaining half of my PhD candidature. I am thankful to Australian Research Council for supporting this research through a Linkage Project (LP 110200906). Thank also goes to Central South University, Hunan, China for supporting me as a visiting student to conduct experiments in their Laboratory. I would also like to acknowledge Prof. Mehdi Saiidi, University of Nevado Reno for sharing experimental results.

It was a great privilege to have Mrs Sucy Leong, Mr Frankie Sia, and Ms Ying Hong Lin and Ms Cheryl Cheng as our administrative officers. I would also acknowledge IT support, both at the UWA and Curtin University, for their technical support during the study.

Last but not least, I give my sincere gratitude to my wife Charitra for her continuous support. I am indebted to my mother for her never ending love and encouragement, which were the driving force behind this work. Thanks are due to my friends and family, without their encouragement and support I could not have survived the lengthy ordeal of PhD study.

LIST OF PUBLISHED WORK AND WORK PREPARED FOR PUBLICAITONS

The list of published paper and work prepared for publications, with the full bibliographic citations in the order they appear in the thesis, are listed below.

Chapter 2

Shrestha, B., Hao, H., & Bi, K. (2016). Devices for protecting bridge superstructure from pounding and unseating damages: an overview. *Structure and Infrastructure Engineering*. (Published online)

Chapter 3

Shrestha, B., He, L.X., Hao, H., Bi, K., & Ren, W.X. (2016). Experimental and numerical analyses on pounding interaction between adjacent bridge frames subjected to spatially varying ground motions. (Under Review)

Chapter 4

Shrestha, B., Hao, H., & Bi, K. (2014). Effectiveness of using rubber bumper and restrainer on mitigating pounding and unseating damage of bridge structures subjected to spatially varying ground motions. *Engineering Structures*, 79, 195-210.

Chapter 5

Shrestha, B., Hao, H., & Bi, K. (2015). Seismic response analysis of multiple-frame bridges with unseating restrainers considering ground motions spatial variation and SSI. *Advances in Structural Engineering*, 18(6), 873-891.

Chapter 6

Shrestha, B., Hao, H., Ibrahim, N.H.J. & Bi, K. (2016). On the effectiveness of rotational friction hinge damper to control responses of multi-span simply supported bridge to non-uniform ground motions. *Advances in Structural Engineering*. (Published Online)

Chapter 7

Shrestha, B., & Hao, H. (2015). Parametric study of seismic performance of superelastic shape memory alloy-reinforced bridge piers. *Structure and Infrastructure Engineering*, 12(9), 1076-1089.

Chapter 8

Shrestha, B., Li, C., Hao, H., & Li, H.N. (2016). Performance–based seismic assessment of superelastic shape memory alloy reinforced bridge piers considering residual deformations. *Journal of Earthquake Engineering*. (In press)

LIST OF RELEVENT ADDITIONAL PUBLICAITONS

The list of additional publications relevant to the thesis, with the full bibliographic citations, are listed below.

1. Shrestha, B., Hao, H., & Bi, K. (2013). *Pounding and unseating damage mitigation on bridge structures subjected to spatially varying ground motions using restrainers and rubber bumpers*. Proceeding of Australian earthquake engineering society annual conference 2013, Hobart, Australia.

2. Shrestha, B., He, L.X., Bi, K., Hao, H., & Ren, W.X. (2014). *Experimental study of seismic pounding effects on bridge structures subjected to spatially varying ground motions.* Proceeding of Australian earthquake engineering society annual conference 2014, Lorne, Australia.

3. Shrestha, B., Ibrahim, N.H.J., Bi, K., & Hao, H., (2014). *Numerical Investigation on Rotational friction hinge damper based restrainers to mitigate relative displacement induced damages in simply-supported bridges*. Proceeding of Australian earthquake engineering society annual conference 2014, Lorne, Australia.

4. Shrestha, B., & Hao, H., (2014). *Comparison of performance of shape memory alloy reinforced bridge piers with conventional bridge piers using incremental dynamic analysis*. Proceedings of 23rd Australasian conference on the mechanics of structures and materials, Byron Bay, Australia.

5. Shrestha, B., Li, C., Hao, H., & Li, H.N. (2015). *Performance–based seismic assessment of shape memory alloy reinforced bridge piers considering combined peak and residual deformations.* 10th Pacific Conference on Earthquake Engineering, Sydney, Australia.

6. Shrestha, B., Hao, H., & Bi, K. (2015). *Effects of ground motion spatial variation and SSI on the response of multiple-frame bridges with unseating restrainers.* 10th Pacific Conference on Earthquake Engineering, Sydney, Australia.

STATEMENT OF CONTRIBUTION OF OTHERS

This research was initiated by Prof. Hong Hao, who defined the overall scope of the work, the possible methodologies and research approaches, secured the funds to support the work, and coordinated and liaised with the colleagues in China for carrying out the large-scale shake table experiment. The works presented in this thesis were primarily designed, experimentally and numerically evaluated, interpreted and written by the candidate and also the first author of the publications, Mr. Bipin Shrestha. Significant input to the works was also provided by co-authors. Contributions of the co-authors are described below.

Chapter 2

Prof. Hong Hao and Dr. Kaiming Bi thoroughly revised and edited draft manuscript prepared by the first author.

Chapter 3

The experiments were conceived by Prof. Hong Hao. The financial support to these experiments was provided by ARC Linkage project LP 110200906. The first author prepared the detailed design and plans for the experiment. Dr. Kaiming Bi was responsible for simulating the ground motion for the testing and other technical supports. The experimental model was prepared at Central South University, China under the supervision of Mr. Li-Xiang He. Prof. Wei-Xin Ren provided all the technical and logistic support at Central South University. The experiments were conducted by the first author and Mr. Li-Xiang He. The first authors conducted the numerical investigation to supplement the experimental results with technical support from other co-authors. Based on the experiment and the numerical results the first author prepared manuscript with an intellectual contribution from all other co-authors.

Chapter 4

The first author conducted the literature review and prepared the numerical model for the analyses. Dr Kaiming Bi provided the spatially varying ground motion required for the analyses. Prof. Hong Hao's role was pivotal to ascertain the objective of the study. The first author prepared manuscript based on the numerical results, which after detailed scrutiny from both the co-authors was submitted for publication.

Chapter 6

The first author conducted numerical simulation on the seismic response of multiple-frame bridges with restraining devices. Dr. Kaiming Bi provided spatially varying ground motion

input used in the analyses. Based on the numerical results the first author prepared the manuscript that was thoroughly revised by Prof. Hong Hao and Dr. Kaiming Bi.

Chapter 6

The first author conducted the literature review on the rotation friction damper and prepared the plan for the work. The numerical investigations and evaluation of the results were carried out by the first author and Mr. Nazman HJ Ibrahim. Dr. Kaiming Bi and Prof. Hong Hao provided significant input to initiate the work. Based on the numerical results the first author prepared the manuscript that was thoroughly revised by all co-authors.

Chapter 7

The first author conducted the literature review, prepared the work plan and conducted all the numerical simulations. Prof. Hong Hao's critical evaluation of the work helped to improve the quality of work. The latter was also responsible for the finalizing the manuscript prepared by the first author.

Chapter 8

The first authors conducted the literature review, prepared the work plan and conducted the numerical simulations. Mr Chao Li provided a significant support in preparation of fragility curves and evaluation of the results. Prof. Hong Hao was responsible for uninterrupted intellectual contribution from the inception of work. The latter along with Prof. Hong-Nan Li also contributed to finalize the manuscript prepared by the first author with help of Mr. Chao Li.

TABLE OF CONTENT

LIST OF FIGURES

LIST OF TABLES

CHAPTER 1
INTRODUCTION

1.1 Background

Seismic pounding between adjacent frames in multiple-frame bridges, between adjacent girders, and girder and abutment in multi-span bridges has been commonly observed in almost all previous major earthquakes. The pounding phenomenon observed is attributed to the out-of-phase vibration of the adjacent bridge structures, which results from different dynamic properties of adjacent bridge segments as well as from spatially varying ground motions. The consequences of pounding range from damages to the impacting surfaces at bridge joint, piers, abutments, shear keys, bearings and restrainers, and possible collapse of decks. For example, after the 1994 Northridge earthquake, significant pounding damage was observed at the expansion hinges and abutments of standing portions of the connectors at the Interstate 5 and State Road 14 interchange, which was located approximately 12 km north-east of the epicenter (Hall, 1995). Reconnaissance reports from the 1995 Hyogo-Ken Nanbu earthquake in Japan identified pounding as a major cause of fracture of bearing supports and a potential contributor to the collapse of several bridge decks (Comartin et al., 1995). The 1999 Chi-Chi earthquake in Taiwan revealed hammering at the expansion joints in some bridges which resulted in damage to shear keys, bearings and anchor bolts (Usarski et al., 2001). Damages to girder ends and bearings due to pounding of adjacent simply supported spans were reported after the 2001 Bhuj earthquake in Gujarat, India (Jain et al., 2002). Pounding usually results in minor to moderate damages to bridge structures, which often results in partial or complete closure of the bridge immediately after the earthquake. In the extreme events, pounding could also result in the collapse of bridge decks due to the unseating. As most bridges are lifeline structures, even partial closure of a bridge may lead to significant consequences, such as by increasing commuting period to the damaged area immediately after the earthquake for rescue and relief operation leading to losses of life, economy and disruption to social life.

For better performance of bridge structures, pounding phenomenon needs to be well understood and incorporated into the design of the bridge structures. However, owing to the complexity in predicting the pounding and modelling the pounding force, this phenomenon is generally neglected in the bridge design. Another significant factor that is not included in the regular design as well as in pounding related researches is the spatial variation of seismic ground motions. Spatially varying ground motions significantly contribute to the out-of-phase responses between adjacent segments of an elongated bridge. This phenomenon needs to be considered while evaluating responses of bridges resulting from pounding. Ground motion spatial variations between the two consecutive bridge supports mainly result from the wave

passage effect leading to the different arrival times of waves at various locations, coherency loss effect owing to seismic waves scattering in the heterogeneous medium of the ground and site amplification effect due to different local soil properties (Der Kiureghian, 1996). Owing to the difficulty in modelling the spatial variability of ground motions, only a few researches in the past have considered this phenomenon in analyzing the relative displacement responses of the adjacent bridge structures (Chouw & Hao, 2005, 2008; Chouw et al., 2006; Zanardo et al., 2002; Tecchio et al., 2012; Lou & Zervas, 2004).

Even though there have been numerous researches on pounding response between the adjacent structures most of them are conducted numerically or analytically. Experimental studies on bridge pounding are very rare. The lack of experiments is due to the complexity involved in these types of investigation as well as the cost involved. Previous investigations (Zhu et al. 2002; Guo et. al. 2009, 2012a, 2012b) performed the experimental investigation of the pounding responses and mitigation techniques. However, Due to equipment limitations, these studies considered only the uniform ground motion hence may not give a reliable representation of the actual pounding conditions. Recently, Li et al. (2012, 2015) investigated the pounding response of adjacent structures to spatially varying ground motion using three separated shake tables. Even though the latter considered the spatially varying ground motion, similitude law was not strictly enforced when constructing the models of small-scale (1:125). Therefore, although the testing results gave some indications of spatially varying motion effects on bridge structure responses, they could not necessarily represent the true response characteristics associated with pounding between the adjacent structures.

Although poundings have been observed in every major earthquake, current design codes do not provide sufficient guides to mitigate pounding damages. The most common pounding and unseating mitigation measure suggested by the code is to adjust the fundamental period of the adjacent bridge segments and provide sufficient seating length. Various bridge design codes such as Caltrans (2001), ASSHTO (1996) and Japanese code (2004) provide procedure to determine the required seating length and to estimate the restrainer strength and stiffness to prevent unseating. However, these procedure do not account for relative displacement produced by spatially varying ground motion.

This study focuses on investigating the complex pounding phenomenon between adjacent bridge structures by conducting large-scale shake table tests of the adjacent bridge segments subjected to spatially varying ground motion. The study also focuses on searching for promising mitigation measure to alleviate pounding induced damages using various devices (Cable Hinge Restrainer (CHR), rubber shock absorbing pad with CHR and using superelastic

shape memory alloy as restrainers). Both experimental tests and numerical simulations are carried out.

In addition to pounding, strong earthquakes in previous few decades, such as 1989 Loma Prieta earthquake, 1994 Northridge earthquake, 1995 Kobe earthquake and many more, have showed that Reinforced Concrete (RC) bridge piers with high ductility capacity, though capable of mitigating catastrophic collapse, could suffer from large residual displacement. As a result, significant research focuses have been provided since the last decade to improve the seismic performance of the bridge piers using advanced structural system with re-centering capacity. In this study, seismic performance of one of such advanced structural system that uses superelastic Shape Memory Alloy (SMA) as reinforcement in plastic hinge region of the bridge piers is studied. Firstly, parametric investigation on the effects of various design parameters on the seismic response of the SMA reinforced bridge piers are carried out. The study primarily focuses on its ability of recovering the residual displacement after the strong earthquakes. Finally, a recently formulated probabilistic performance-based seismic assessment framework (Uma et al., 2010) is applied to evaluate the performance of SMA reinforced bridge piers. Using the joined fragility curve, defined by the pair of maximum and residual deformation, the likelihood of seismic demand exceeding the predefined damage limits, expressed as a probability of exceedance of the corresponding damage state, at a chosen seismic excitation level is presented.

1.2 Research Objectives

The goal of this study is to determine the effects of spatially varying ground motion on the relative displacement induced damages of the adjacent bridge segments. In order to achieve the goal experimental tests and numerical analyses are conducted. Moreover, numerical investigations are carried out on SMA reinforced bridge piers to evaluate its seismic performance and its benefits over conventionally reinforced bridge piers. The specific objectives of this research are:

- To conduct large-scale experiments on adjacent bridge frames subjected to spatially varying ground motions with and without restraining devices using a shake table array system.
- To study the effectiveness of using rubber bumper and restrainers together to mitigate pounding and unseating damages on multiple-frame bridges subjected to spatially varying ground motions. Two types of restrainers, i.e. conventional steel cable restrainers and SMA restrainers, are analysed in combination with rubber bumpers.

- To study the adequacy of the current restrainer design methods on mitigating unseating damages of adjacent bridge structures subjected to spatially varying ground motions and soil structure interaction.
- To investigate the effectiveness of rotational friction hinge dampers to mitigate pounding and unseating damages on the isolated bridges.
- To conduct a parametrical investigation on the effect of various design parameters on the seismic response of SMA reinforced bridge piers.
- To assess the seismic performance of superelastic SMA reinforced bridge piers using probabilistic performance-based assessment methodology that considers both the maximum and the residual deformation simultaneously.

1.3 Research Outline

This dissertation is organized into nine chapters with the following contents:

Chapter 2 presents a review of the devices used to mitigate seismic pounding and unseating damages in the bridge structures. Various mitigation devices and methods prescribed by the codes and previous researchers are discussed.

Results from the experimental investigation carried out on large-scale bridge models subjected to spatially varying ground motions with and without restrainers are presented in Chapter 3.

Numerical investigations on the effectiveness of using rubber bumpers and restrainers to mitigate pounding and unseating damages on bridge structures subjected to spatially varying ground motions are reported in Chapter 4.

The limitation of the present design method of restrainers that considers only the relative displacement resulting from different dynamics characteristic of adjacent bridge segments and neglects the spatial variation of ground motion and soil structure interaction and its consequence on the seismic responses of the multiple-frame bridges is discussed in Chapter 5.

Chapter 6 presents a study on the application of friction hinge damper to control the response of base isolated simply-supported bridges including the pounding and unseating response.

Parametrical investigation on the influences of various design parameters on the seismic response of superelastic SMA reinforced bridge piers compared to that of the conventional bridge piers with steel reinforcement is presented in Chapter 7.

Chapter 8 presents a probabilistic performance-based seismic assessment of the superelastic SMA reinforced bridge piers considering both the maximum and the residual deformations as the performance criteria.

The conclusions of the current study and recommendations for the future research are presented in Chapter 9.

1.4 References

AASHTO. (1996). *Standard Specification for highway Bridges, 16th edition*. Washington, DC.

Caltrans. (2001). *Seismic Design Criteria*. Design manual-version 1.2, California Dept. of Transportation, Sacramento, California.

Chouw, N., & Hao, H. (2005). Study of SSI and non-uniform ground motion effect on pounding between bridge girders. *Soil Dynamics and Earthquake Engineering*, 25(7), 717-728.

Chouw, N., Hao, H., & Su, H. (2006). Multi-sided pounding response of bridge structures with non-linear bearings to spatially varying ground excitation, *Advanced Structural Engineering,* 9(1), 55-66.

Chouw, N., & Hao, H. (2008). Significance of SSI and nonuniform near-fault ground motions in bridge response I: Effect on response with conventional expansion joint. *Engineering Structures*, 30(1), 141-153.

Comartin, C.D., Greene, M., & Tubbesing, S.K. (Eds). (1995). The Hyogo-ken Nanbu earthquake Jan 17, 1995. EERI, *Preliminary reconnaissance Report EERI-95-04*, Oakland, CA.

Kiureghian, A. (1996). A coherency model for spatially varying ground motions. *Earthquake Engineering & Structural Dynamics*, 25(1), 99-111.

Japan Road Association. (2004). Specifications for highway bridges –Part V: Seismic design. 5th ed., Tokyo, Japan.

Guo, A., Li, Z., Li, H., & Ou, J. (2009). Experimental and analytical study on pounding reduction of base-isolated highway bridges using MR dampers. *Earthquake Engineering & Structural Dynamics*, *38*(11), 1307-1333.

Guo, A., Li, Z., & Li, H. (2011). Point-to-surface pounding of highway bridges with deck rotation subjected to bi-directional earthquake excitations. *Journal of Earthquake Engineering*, 15(2), 274-302.

Guo, A., Zhao, Q., & Li, H. (2012). Experimental study of a highway bridge with shape memory alloy restrainers focusing on the mitigation of unseating and pounding. *Earthquake Engineering and Engineering Vibration*, 11(2), 195-204.

Guo, A., Cui, L., & Li, H. (2012). Impact stiffness of the contact-element models for the pounding analysis of highway bridges: experimental evaluation. *Journal of Earthquake Engineering*, 16(8), 1132-1160.

Hall, F.J. (Eds). (1995). Northridge earthquake Jan. 17 1994, EERI-Preliminary reconnaissance Report EERI-94-01.Oakland, CA.

Jain, S.K. Lettis, W.R., Murty, C.V.R., & Barder, J.P. (2002). Bhuj, India, Earthquake of January 26, 2001 Reconnaissance Report, Publication No. 02-01, EERI, Oakland, CA.

Li, B., Bi, K., Chouw, N., Butterworth, J. W., & Hao, H. (2012). Experimental investigation of spatially varying effect of ground motions on bridge pounding. *Earthquake Engineering & Structural Dynamics*, 41(14), 1959-1976.

Li, B., & Chouw, N. (2014). Experimental investigation of inelastic bridge response under spatially varying excitations with pounding. *Engineering Structures*, 79, 106-116.

Lou, L., & Zerva, A. (2005). Effects of spatially variable ground motions on the seismic response of a skewed, multi-span, RC highway bridge. *Soil Dynamics and Earthquake Engineering*, 25(7), 729-740.

Tecchio, G., Grendene, M., Modena, C. (2012) Pounding effects in simply supported bridges accounting for spatially variability of ground motion: A case study. *Advances in civil engineering,* Ar. ID 267584.

Uma, S. R., Pampanin, S., & Christopoulos, C. (2010). Development of probabilistic framework for performance-based seismic assessment of structures considering residual deformations. *Journal of Earthquake Engineering*, 14(7), 1092-1111.

Uzarski, J., & Arnold, C. (2001). Chi-Chi, Taiwan Earthquake of September 21, 1999 Reconnaissance report, Publication No. 01-02, EERI, Oakland, CA.

Zanardo, G., Hao, H., & Modena, C. (2002). Seismic response of multi-span simply supported bridges to a spatially varying earthquake ground motion. *Earthquake engineering & structural dynamics*, 31(6), 1325-1345.

Zhu, P., Abe, M., & Fujino, Y. (2002). Modelling three-dimensional non-linear seismic performance of elevated bridges with emphasis on pounding of girders. *Earthquake engineering & structural dynamics*, 31(11), 1891-1913.

CHAPTER 2
DEVICES FOR PROTECTING BRIDGE SUPERSTRUCTURES FROM POUNDING AND UNSEATING DAMAGES: AN OVERVIEW

2.1 Abstract

Previous earthquakes have highlighted the seismic vulnerability of bridges due to excessive movements at expansion joints. This movement could lead to the catastrophic unseating failure if the provided seat width is inadequate. Moreover, seismic pounding is inevitable during a strong earthquake due to the limited gap size normally provided at the expansion joints. Various types of restrainers, dampers and other devices have been proposed to limit the joint movement or to accommodate the joint movement so that the damages caused by the excessive relative displacements could be mitigated. To select and design appropriate devices to mitigate the relative displacement induced damages to bridge structures during earthquake shaking, it is important that results from the previous studies are well understood. This paper presents an overview on the various pounding and unseating mitigation devices that have been proposed by various researchers. Based on an extensive review of up-to-date literatures, the merits and limitations of these devices are discussed.

2.2 Introduction

Bridges with multiple spans are often constructed with joints to accommodate temperature and time-dependent deformations. These joints act as physical cuts on the bridge superstructure. During the seismic events, poundings between the adjacent bridge components (deck to deck and/or deck to abutment) can occur when the relative closing displacement is larger than the expansion gap size. Pounding of adjacent bridge segments not only results in the localized damages around impacting locations but also could increase the relative opening movement between adjacent components of a bridge structure (Rungrasamme & Kawashima, 2001). On the other hand, unseating failure occurs when the relative opening displacement is larger than the provided seat width. The damages related to pounding and unseating have been observed in many recent major earthquakes, e.g. the 2011 Christchurch earthquake (Chouw & Hao, 2012), 2010 Chile earthquake (Kawashima et al., 2011), 2008 Wenchuan earthquake (Lin et al. 2008), 2006 Yogyakarta earthquake (Elnashai et al., 2006), 1999 Chi-Chi earthquake (EERI 1999), 1995 Kobe earthquake (Kawashima & Unjoh, 1996) and 1994 Northridge earthquake (Hall, 1994).

Retrofitting of bridges to mitigate the damages resulting from strong earthquakes has become a common measure in many seismic prone regions. Caltrans initiated retrofitting of its bridges

to prevent unseating failure after the devastating 1971 San Fernando earthquake in California. During this earthquake, many bridges with typical narrow seat width collapsed due to the excessive longitudinal movements at expansion joints and supports (Jennings, 1971). To prevent unseating of the bridge spans, the spans were tied together with restrainers, typically made of steel cables or steel rods, at their hinges after the earthquake. These traditional restrainers have many limitations, such as small elastic strain range, and limited ductility capacity. To address the limitation of these restrainers, significant numbers of researches were carried out in the following years. These researches led to the use of various types of new materials or the use of energy dissipating devices as the restrainers. These new restraining devices alleviated the limitation of the traditional restrainers to a certain extent. However, these new devices also have some limitations, such as high cost of material, less durability, sensitive to earthquake ground motion characteristics (velocity dependent behavior), and sensitive to ambient temperature, etc.

This paper presents an overview of the devices that are proposed/used to mitigate the pounding and unseating damages on highway bridges. Up-to-date information on experimental and numerical works and present-state-of-practice on the devices used to mitigate the pounding and unseating failure of bridge superstructures are included in the review. The merits and limitations of these devices for practical applications on bridge structures are discussed and commented. The paper focuses on the devices that are applied externally to the bridge superstructure. The structural element built-in along the bridge structures, such as concrete shear keys, retainer blocks are not included in this paper.

2.3 Restrainers

2.3.1 Steel Restrainer

Steel cable/bar restrainers are the least expensive and the most widely adopted retrofit strategy to prevent unseating failure of bridge decks. The 1971 San Fernando earthquake revealed the vulnerability of typical bridges of that period to the unseating failures at hinges (Jennings, 1971). After the event, steel cable restrainers were extensively used in the USA to mitigate the unseating failure on bridges with narrow seat length. Additionally, the restrainers were also used in new bridges with adequate seat length as a secondary back-up member to prevent unseating failure.

A typical restrainer connection layout used in typical Californian multiple-frame bridges are presented in Figure 2-1. The typical restrainer cables used in California are 19 mm diameter (area 143 mm^2) steel cables and 32 mm diameter (area 3217 mm^2) high strength rods. The steel cables are made of 6x19 strands, galvanized with a wire strand core and have a yield

strength of 174 kN corresponding to the yield stress of 1210 MPa. The high strength steel rods have the yield stress of 827 MPa and ultimate strength of 1034 MPa. The initial modulus of elasticity of the cables is 69 GPa, which is approximately 1/3 of that of steel rods. The commonly used cable restrainers are 6.1 m long that can stretch approximately 107 mm at elastic limit and 267 mm at failure. The restrainers are designed to remain within the elastic range utilizing only the restrainer's spring-like ability while seismic energy is dissipated by the plastic hinging of the columns (Bridge design Aids 2008). These criteria make cables more practical than bars as the cables have a longer elastic range and thus, shorter restrainers can be used. The restrainers are threaded through a 150 mm diameter hole drilled on the top part of the hinge. Bolster are provided on one side of the hinge to distribute the restrainer force into the superstructure. The restrainer units are bolted to metal plates on the other side of the hinge. During installation, a slack of few millimetres is provided depending on the ambient temperature. This allows for thermal expansion without putting restrainers into tension. For steel/concrete simply supported bridge girders resting on a pier cap, a variety of restrainer configuration could be adopted to prevent unseating. If the bridge piers are strong enough, the restrainers can be wrapped around the girder and bent cap, as shown in Figure 2-2 (b) to provide additional restraint to the superstructure. Attaching restrainers from girder to girder (Figure 2-2 (a)) is preferable when the additional force applied by the restrainers to the bent cap may potentially damage the piers. In general, girder to girder attachment is less desirable because the girders are not directly attached to the pier on which they are seated. During a strong earthquake, flexible column may experience large deflections which may lead to unseating if the girders are not attached to the piers directly.

Typical Japanese bridge constructions do not use the flexible cable restrainers as in the USA. Instead, falling prevention devices are used, which do not allow the relative displacement between spans. These include devices that connect a girder and substructures (Figure 2-3 (a)), devices that protrude into a girder from bridge substructure (Figure 2-3 (b)), and device to connect two girders (Figure 2-3 (c)).

As mentioned above, steel restrainers were applied on many bridge structures in US after the 1971 San Fernando earthquake. The following major earthquakes, such as the 1989 Loma Prieta, the 1994 Northridge earthquakes and the 1995 Kobe earthquake provided good opportunities to evaluate the performance of these steel restrainers. Steel cable restrainers were found to be effective to prevent the span collapse. However, failures of restrainers were also observed in a few cases (e.g. Gavin Canyon under crossing), which resulted in the unseating of bridge decks. As the restrainers are designed to perform elastically, this tends to attract

large forces during an extreme event resulting in either the breaking of the cable or punching of the diaphragm wall at ends of the restrainer (Selna et al., 1989).

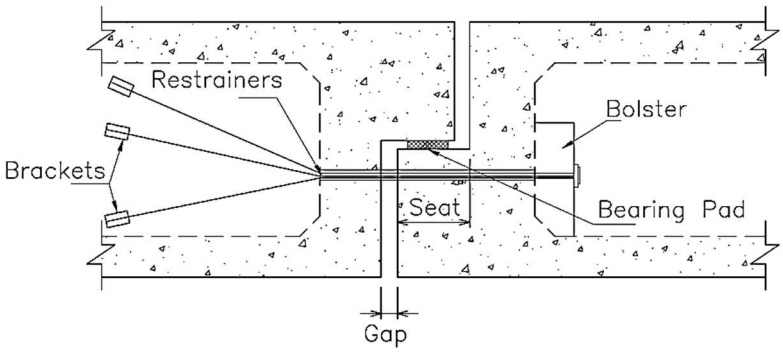

Figure 2-1 Hinge restrainer retrofit scheme.

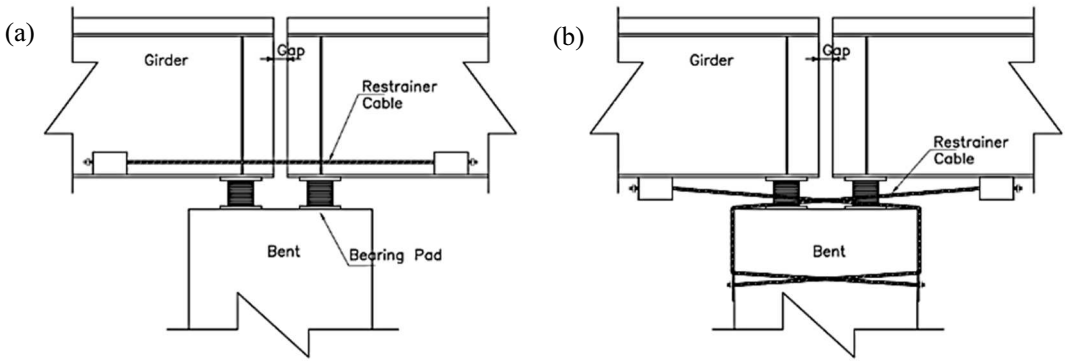

Figure 2-2 (a) Girder to girder and; (b) girder to column restrainer attachment for simply supported bridges.

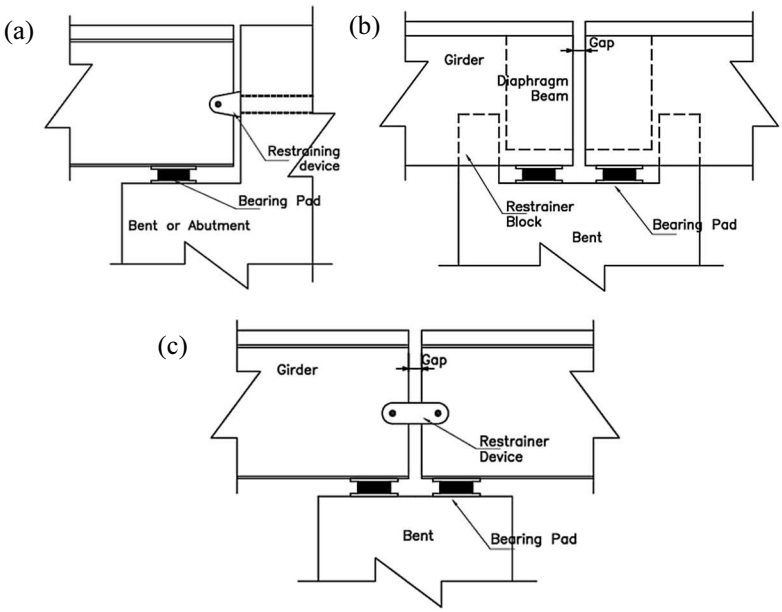

Figure 2-3 Japanese displacement restriction devices.

To improve the effectiveness of the steel restraining devices, significant studies have been conducted. Saiidi et al. (1993) investigated the seismic responses of bridge structures retrofitted with cable restrainer during the 1989 Loma Prieta earthquake. Their study concluded that restrainers are affected by many factors such as the amplitude and frequency contents of the ground motion, soil-structure interaction as well as the flexibility of substructure and nonlinear time history analysis is necessary for appropriate design. Abdel Ghaffar et al. (1997) studied the effects of the cable restrainers on the seismic response of the Aptos Creek Bridge during the 1989 Loma Prieta earthquake and found that restrainer had little impact on the overall structural response. However, restrainers were found effective to reduce the displacement at joints at higher acceleration. A parametric study on the cable restrainer effect on pounding response of multi-frame bridges was conducted by DesRoches and Muthukumar (2002) using SDoF model. It was revealed that the effectiveness of restrainers depend highly upon the period ratio of adjacent structures. The addition of restrainers increased the displacement of stiff frames. The effects of restrainers on the frame responses were mainly observed only for highly out-of-phase frames (i.e. frames with stiffness ratio which is significantly lower than unity) and was marginal for other stiffness ratios. Vlassis et al. (2004) conducted a large scale experiment to evaluate the efficacy of restrainers in reducing relative displacement across bridge hinge, and to examine the effects of restrainer stiffness and gap on the response of the hinge-restrainer system. It was found that restrainers were capable of inhibiting the relative hinge displacement and generally capable of reducing the intensity of impact between two adjacent decks. The restrainer force and ductility demand increase when restrainer gap is zero, which could happen at low ambient temperatures, resulting in extensive yielding of restrainer even under moderate earthquake excitations. It could result in high stress concentration at the location where the cables pass around the two 90° bends on the drum and could also result in failure of the restrainers.

Watanabe and Kawashima (2004) investigated on the effectiveness of cable restrainers to mitigate rotation of a skewed bridge during strong earthquake motions. Three configurations of cable restrainers were evaluated. In the first configuration restrainers were provided along the skewed longitudinal direction (x direction as shown in Figure 2-4), in the second configuration restrainers were provided along the Longitudinal direction (X direction) and in the final configuration restrainers were provided along the skewed transverse direction (y direction). Julian et al. (2007) evaluated the efficiency of using cable restrainers to mitigate unseating damage on isolated curved steel viaducts. The restrainers were generally found to be effective on minimizing the pounding forces at the expansion joint and on reducing the joint opening movements. It was revealed that due to the tendency of curved bridge rotating about the vertical axis irregular distribution of restrainer stresses were developed. Restrainers

located at the exterior girder of the curved bridges activated first and subjected to larger ductility demand.

Even though steel cable/bar restrainers had been used extensively in bridge retrofit, a satisfactory method for designing the restrainers was lacking. The old design codes (e.g. Caltrans 1990, AASHTO 1992 and Japanese bridge specifications) did not consider the relative displacement between the adjacent frames which is actually the reason behind the unseating of bridge spans. Researchers focused on this aspect and many design methods for seismic restrainers were proposed. Trochalakis et al. (1997) modified the equivalent static procedure for the design of the restrainers based on their numerical study. DesRoches and Fenves (2000) proposed a method to design the restrainer by predicting the expansion joints opening through modal analysis of the two adjacent bridge frames. This method had the advantage of considering the dynamic characteristics and the inelastic behavior of adjacent frames. The hinge displacements are estimated by combining the modal displacement using Complete Quadratic Combination (CQC). This method is adopted by the Caltrans to design the seismic restrainers in Californian bridges with multiple-frames (Bridge Design Aids 2008). Bridge Design Aids (BDA) also provides the guidelines for required properties of restrainer material. For simply supported bridges, BDA adopts the method proposed by Saiidi et al. (2001).

It is to be noted that out-of-phase vibrations between bridge segments are not only caused by different dynamic properties of adjacent structures, Spatially Varying Ground Motions (SVGM) along the different supports of bridge and Soil Structure Interaction (SSI) also results in the out-of-phase vibrations between the bridge segments. Relative displacements at hinges and the resulting pounding force and deformation of the restrainers are significantly affected by SVGM and SSI (Chouw & Hao, 2005, 2008; Li et al., 2012; Shrestha et al., 2015). However, most of the previous studies have neglected these sources of out-of-phase vibrations. The only study in the literature that proposes a restrainer design method considering spatial variation of ground motions is by Hudgings et al. (1997). However, due the complexity involved in calculating the relative displacement induced by the spatial variation of ground motion and SSI, the method have not found extensive applications.

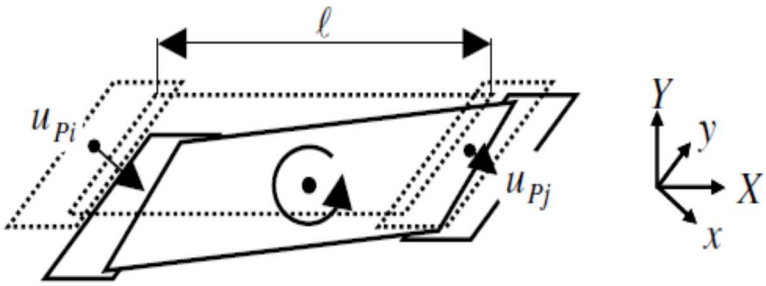

Figure 2-4 Skew bridge rotation due to incoherent response (Watanabe & Kawashima, 2004).

As mentioned above, steel restrainers do not have significant energy dissipation capacity, since they are designed to remain elastic. This results in a large number of restrainers required to limit the joint movement to an acceptable range, particularly for high seismic loads (DesRoches & Fenves, 2000). Restrainer systems with an excessive number of restrainers could induce large forces in other components of the bridge, such as bearings and columns. Additionally, the restrainer cables and bars have low yield strain of 1.75% and 0.2%, respectively. The limited elastic strain capacity results in a long length of restrainers to limit the joint movement at extreme earthquake scenarios to fulfil the requirement of elastic performance. These limitations of the steel restrainer have driven many investigations to find suitable alternatives to replace the steel restrainers.

2.3.2 Shape Memory Alloy Restrainer

Shape Memory Alloys (SMA) are a unique metallic alloy which can undergo large deformations while reverting back to their un-deformed shape through either the application of heat (shape memory effect) or the removal of the load (superelastic effect). These unique properties have led to the development of applications of SMAs in the biomedical field, aerospace field, and commercial industry. Recently, interests in the use of SMAs for seismic applications have also increased. The ability of SMAs to recover their shape is, in part, due to the ordered crystalline structure between the austenite and martensitic phases which allows the material to undergo a displacive martensitic phase transformation as a result of temperature change or applied stress (DesRoches et al., 2004). In the seismic application, the superelastic SMA has found a wide application due to its ability of recovering its shape without the application of heat (Shrestha & Hao, 2015).

Superelastic SMA displays a flag-shape hysteresis under cyclic axial loading, which can provide both re-centering and supplemental energy dissipation. Total recovery of axial deformation can be obtained for strains up to 6-8% with partial recovery being obtained for higher strain levels (DesRoches & Delemont, 2002). This large elastic strain along with the

hysteretic damping and strain hardening at large strains make SMA a suitable alternative material for the use as seismic restrainers (Andrawes & DesRoches, 2005).

Realizing the potential of SMA for application as a seismic restrainer, a significant number of researches have been carried out in the last few decades. DesRoches and Delemont (2002) conducted a series of cyclic test on a full-scale Nitinol (NiTi) SMA restrainer bar of length 280 mm and 25.4 mm diameter to investigate the mechanical properties of SMA restrainers. The study also investigated the effectiveness of the SMA restrainer bars in a multi-span simply supported bridge through nonlinear numerical analyses. The numerical results showed that SMA restrainers were extremely effective in limiting the response of bridge decks during strong ground motions. The strain hardening of SMA restrainers at strains beyond 6% increased the stiffness of the restrainers and provided additional restraint to limit the relative opening in the bridge.

Andrawes and DesRoches (2005) assessed the effectiveness of SMA restrainers on a typical Californian multiple-frame box girder bridge using numerical simulations. Superelastic NiTi restrainers were found significantly more effective than conventional steel restrainers to reduce the opening relative displacement. It was also found that the frame drifts were not significant different for two types of restrainers. Andrawes and DesRoches (2007a) conducted a comparative analysis of SMA tension only restrainer, and tension and compression restrainer with other bridge retrofit devices, such as steel cable restrainer, metallic dampers and viscoelastic dampers. The steel restrainer cables were found to be the least effective in limiting the joint displacement. The comparison between the SMA device and the metallic damper showed that superelastic behavior of the SMA is of more significance in limiting the joint opening compared to the higher damping of metallic dampers. Comparison with viscoelastic damper showed that the SMA devices have significantly lower forces while providing similar limits on joint opening. Johnson et al. (2008) conducted a large scale testing of NiTi SMA restrainers for retrofitting of the bridges. Padgett et al. (2010) used SMA restrainer to connect the deck-abutment interface of the bridge. The performance of the device for limiting the hinge opening was evaluated on a large scale four span concrete slab bridge. Guo et al. (2012) conducted an experimental study to investigate the performance of SMA restrainers to mitigate pounding and unseating on highway bridges. The experimental study was conducted for two connection schemes (deck to deck and pier to deck) with SMA restrainers.

One of the major drawbacks of SMA restrainers is their performance, which is dependent upon the ambient temperature. The superelasticity characteristics of SMA is exhibited only at the temperatures above the austenite finish temperature. In applications where the superelastic behavior is desired, the temperature of the SMA has to be kept above Austenite finishing

temperature, otherwise the SMA will experience residual deformations. Andrawes and DesRoches (2007b) evaluate the performance of SMA seismic restrainers under the effect of varying ambient temperature. The results indicated that the SMA restrainers are more effective in limiting the hinge opening at higher ambient temperature. At 20˚ F (-6.7˚ C) an average increase in the joint opening of approximately 41.5 % was observed for frames with moderate to high period ratio compared to that at 60˚ F (15.6˚ C). It is worth noting that one of the most used commercially nitinol SMA, NiTi45, have the lowest austenite finishing temperature of -10˚ C (Alam et al. 2008). According to ASTM 709 bridge steel specification (2005), the lowest temperature (AASHTO Zone 3) in bridge application is -51˚ C. Therefore, the use of NiTi SMA as a restrainer is limited by the cold temperatures.

To overcome the limitations of the NiTi SMA, investigators have proposed the CuAlBe alloys, which have the potential of providing both damping and re-centering properties. The most notable property of CuAlBe is its very wide operating temperature range from -80˚ C to 100˚ C. This property of CuAlBe alloys makes it a suitable restraining device for cold regions. Zhang et al. (2009) conducted the experiments of superelastic CuAlBe alloy bars at various temperatures (23, 0, -25 and -50˚ C) and developed a model to describe the stress-strain behavior under various temperature. The authors conducted a numerical simulation of isolated highway bridge with CuAlBe based SMA restrainers. It was found that the ambient temperature of -25˚ C have only minor effect on the control performance of the SMA device for the most cases.

Besides the dependence on ambient temperature, NiTi SMA restrainers also have other shortcomings, such as expensive cost and difficulty of machining. These shortcomings could be adequately addressed by using copper based SMA, which are relatively cheaper and easier to machine.

2.3.3 Fiber Reinforced Polymer Restrainer

The high tensile strength and versatility of Fiber-Reinforced Polymer (FRP) fabrics are the motivational properties that lead to the exploration of these materials as potential seismic restrainer (Saiidi et al., 2006; Johnson et al., 2005). FRP restrainers offer advantages over steel restrainer with respect to the ease of fabrication and installation. FRP connection to the superstructures is done by applying adhesives onto the bridge deck whereas installation of conventional restrainers is intrusive, requiring drilling of concrete. There are additional savings by elimination of the cost of connecting hardware (Saiidi et al., 2006). Usually, the conventional restrainers are hidden at the interior of the box girder, making them hard to inspect, whereas FRP restrainers are visible.

Saiidi et al. (2006) developed the FRP restrainers and tested a representative bridge hinge model with restrainer on a shake table. The developed FRP restrainers consisted of three segments: two end parts that were bonded to the superstructure surfaces, and the middle part that linked the two adjacent bridge frames as shown in Figure 2-5. The middle part of FRP restrainers needs to be flexible to allow the initial slack so the hinge opening due to the thermal movements could be accommodated and to deform out-of-plane without developing significant stresses during hinge closing. To allow this to happen, flexible silicon elastomer was used in the middle portion of the FRP restrainer. Three different types of restrainers, namely GFRP, CFRP and a hybrid restrainer made of glass and carbon fibers (CGFRP) were tested by the authors. During the testing, GFRP restrainer reached the maximum strain of 3.6%, 1.4% higher than the design strain. CFRP restrainer ruptured when it reached a strain of 1.7%, 0.5% higher than the specified design strain. CGFRP restrainer reached the maximum strain of 1.5%.

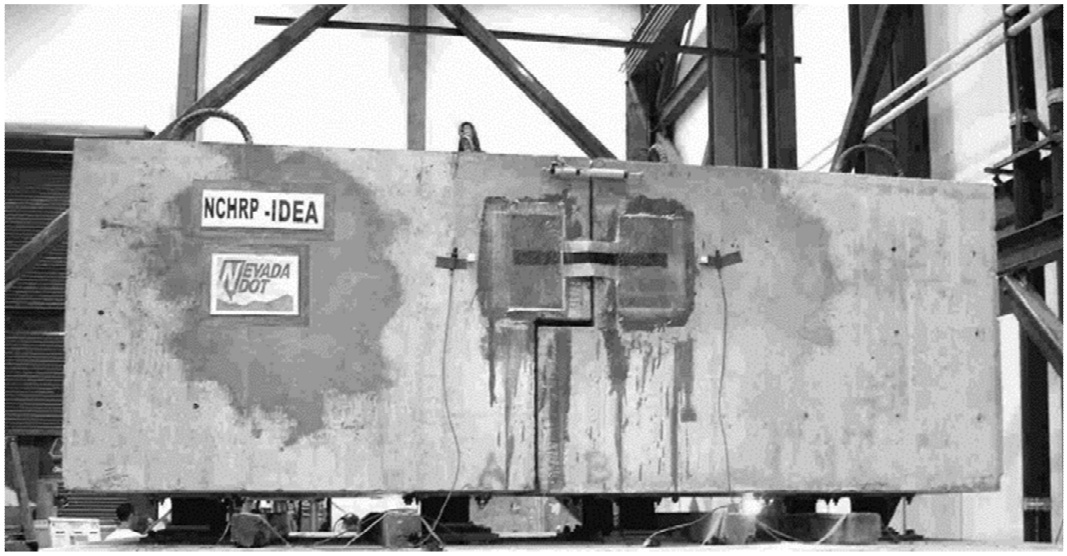

Figure 2-5 Test setup for FRP restrainer testing (Johnson et al. 2005).

A comparison of the relative hinge movement for GFRP, steel and SMA restrainers were made to evaluate the performances of these restrainers. Figure 2-6 (a) and (b) present the comparison of the relative hinge movement and superstructure acceleration with three types of restrainers. As presented in the figure, the maximum restrainer elongation (maximum hinge movement less the restrainer slack) for the SMA and FRP restrainers was 22.9 mm and 4.2 mm, respectively. The steel restrainer failed at $t \approx 14.7$ sec after it stretched by 105 mm. During the test run the peak superstructure acceleration was 4.97, 2.97, and 2.23 g for steel, SMA and GFRP restrainers, respectively.

The authors also developed a new design method for the FRP seismic restrainers. The basic assumption in the proposed method is that the FRP restrainers rigidly connect the two adjacent

segments of the bridge. The linkage of the two bridge frames reduces the two-degree-of-freedom system of the bridge frames to an SDoF system. The restrainers were assumed to link the two frames into an SDoF with a combined mass of $M = M1+M2$ and stiffness of $K = K1+K2$.

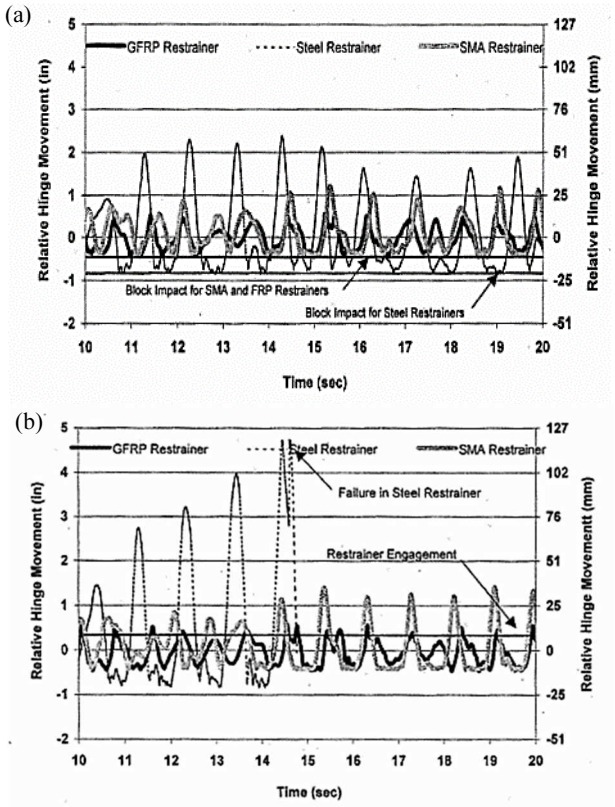

Figure 2-6 (a) Comparison of hinge movement; (b) superstructure acceleration for different restrainer types (Johnson et al., 2005).

It is to note that FRP restrainers suffer from similar deficiency as the steel restrainers since the performance of FRP are also governed by the linear response.

2.4 Damping Devices

2.4.1 Metallic Dampers

Metallic dampers are considered to be one of the most effective energy dissipating devices (Soong & Dargush, 1997). They are essentially displacement dependent energy dissipating devices which dissipate energy through the yielding of the metallic material. These devices typically exhibit hysteretic force-displacement behavior, which can be approximated as bilinear or trilinear curve. Metallic dampers could be used in the form of rectangular or circular tubes or bars. Alternatively, steel shear panels can also be used to function as a yielding damper. These devices tend to be inexpensive to produce, and their properties remain stable over the long periods. However, they often need replacement after a large seismic event. In

continuous bridge, they may be located either in one position to allow free movement of the bridge or distributed in several locations to allow thermal movements of the structure. Figure 2-7 shows typical metallic yielding dampers installed in Chilean highway bridges (Elnashai et al., 2010).

Chen et al. (2001) conducted extensive testing of metallic dampers on a 1:10 scale bridge model to reduce the dynamic response of the bridge structure. Their study focused on optimizing the metallic dampers for maximum energy dissipation and identifying the response of bridge model with dampers. Three full-scale dampers, two straight and one linearly tapered rods, were fabricated and tested under cyclic loading. It was found that at the same applied load the damper with tapered shape experienced large displacement thus more energy dissipation. Andrawes and DesRoches (2007) revealed that metallic dampers were capable of dissipating significantly more energy than other bridge retrofit devices. Vasseghi (2011) and Pan et al. (2014) proposed metallic yielding devices to improve the seismic performance and to prevent pounding between the superstructures and concrete shear keys under transverse seismic excitation. The energy dissipating shear keys transfer a fraction of the seismic load to the substructures and dissipate the seismic energy through inelastic deformations. Four full-scale specimens were tested under cyclic loading, good ductility and energy dissipation capacity of the device were observed. Furthermore, nonlinear time history response of a three span precast concrete girder bridge with proposed shear key indicated that seismic demands on the substructures were reduced when conventional concrete shear key were replaced by the proposed shear key. Deng et al. (2014) proposed a novel energy dissipation restrainer using steel shear panels to avoid bridge superstructure dislocation/unseating during a seismic event. Figure 2-8 shows the schematic application of such devices at bridge superstructure. To evaluate the performance of the steel shear panel devices and to identify its hysteretic behavior, five damper specimens were designed and tested to cyclic loading. The test result suggested that with proper design, the devices were capable of large deformation and energy dissipation. The authors used finite element model to supplement their experimental study. Based on the numerical results, a design procedure for the device was formulated along with a suggestion for the sizes of stiffener and flanges of the device for the stable performance.

A drawback of these kinds of devices is their dependence upon the hysteretic response of metal for the dissipation of seismic energy. Though, the dampers have good seismic energy dissipating capacity it also result in the residual deformation in the dampers. Thus, the devices may need to be replaced after a strong earthquake. Alternatively, this residual deformation could also result in the residual deformation in bridge superstructures that could influence the

traffic flow immediately after the earthquake. To resolve these problems, Choi et al. (2009) carried out investigations on the application of superelastic SMA bending bars. The superelastic SMA bending bars were upgraded version of SMA bar/cable restrainers that activate only in tension and do not resist compressive force. The authors analyzed the characteristic of the bending behavior of the SMA bar and investigated its effectiveness for the seismic application. The superelastic SMA under single and double bending was tested under a quasi-static loading. Figure 2-9 presents the test setup for the single bending test of SMA bars. The average damping ratio of the SMA bending bars were found to be just below 7%, which is slightly lower than that of metallic dampers that have damping ratio of around 10% (Chen et al. 2001). The bending behavior of the SMA bar was not affected by the loading rate, which is different from its behavior under tension. The SMA bars were assessed as seismic restrainer for a three-span simply-supported bridge. The bars reduced the joint openings and pounding forces at intermediate hinges and abutments. Choi et al. (2010) compared the seismic performances of bridge with SMA bending bar restrainers with the conventional steel restrainers and SMA bars in tension only. The fragility analysis revealed that SMA bars in bending were the most effective in improving the seismic resistance of the bridge. The other two restrainers increased the bridge fragility of the as-built bridge under slight and moderate damages and slightly reduced the seismic resistance for the extensive and complete damages. However, the SMA bars not only reduced the fragility under all performance levels but also significantly improved the performance for extensive and complete damages.

Figure 2-7 Metallic yielding dampers on Chilean bridges (Elnashai et al., 2010).

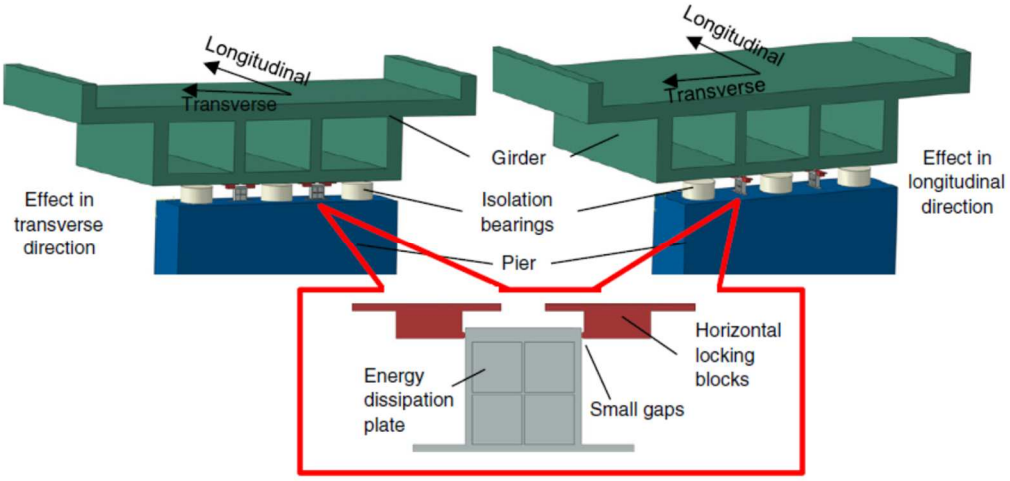

Figure 2-8 Installation of the device (Deng et al., 2014).

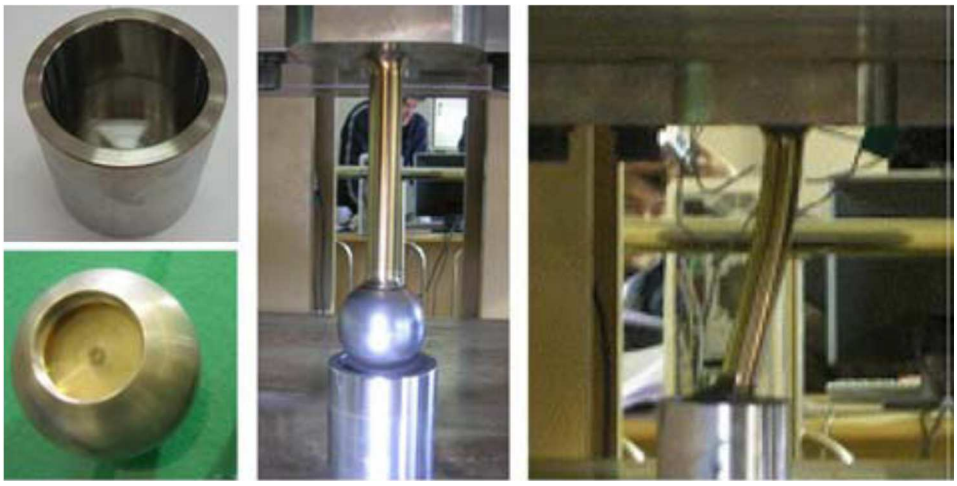

(a) (b) (c)

Figure 2-9 Test setup for SMA bar under single bending; (a) a ball and a cylinder; (b) a ball bolted to the SMA bar and the cylinder welded at the bottom; (c) bending shape of SMA bar under single bending (Choi et al., 2009).

2.4.2 Viscoelastic Dampers

Viscoelastic (VE) dampers belong to the family of the velocity dependent energy dissipating devices. The viscoelastic dampers, typically used for the structural applications, are made of copolymers or elastomeric substances, as presented in Figure 2-10. Energy is dissipated when they are subjected to shear deformation. Viscoelastic dampers consist of layers of the viscoelastic material sandwiched between steel layers. The mechanical behavior of the damper is frequency dependent. The stress-strain relationships of the VE dampers are characterized by an ellipse with a non-zero slope. The slope of the ellipse is controlled by the shear stiffness of the VE materials while the area of the ellipse is controlled by the shearing rate. The response can be regarded as the summation of a linear elastic component and a viscous (elliptical) component.

The elastic stiffness can be related with the viscous damping through the following equation

$$C_d = K_d \frac{\eta}{\omega} \tag{2.1}$$

where C_d is the damping coefficient, K_d is the elastic stiffness, and η is the loss factor. Many previous researches (e.g. Soong & Dargush, 1997) have found that η is almost constant at various frequency values.

Feng et al. (2000) and Kim et al. (2000) studied the effect of using viscoelastic dampers at the expansion joints of highway bridges to prevent the unseating of superstructures off their seats and pounding of decks during earthquakes. Finite element analyses were performed using Kelvin model (consists of an elastic spring and a viscous damper connected in parallel) and Maxwell model (consists of an elastic spring and a viscous damper connected in series) for the viscoelastic dampers. The research illustrated that using viscoelastic dampers reduces hinge openings without introducing a significant increase in the ductility demand in bridge piers. These investigations also revealed that viscous component of a viscoelastic damper were significantly more effective in reducing the relative displacement at the bridge expansion joints than the elastic spring component.

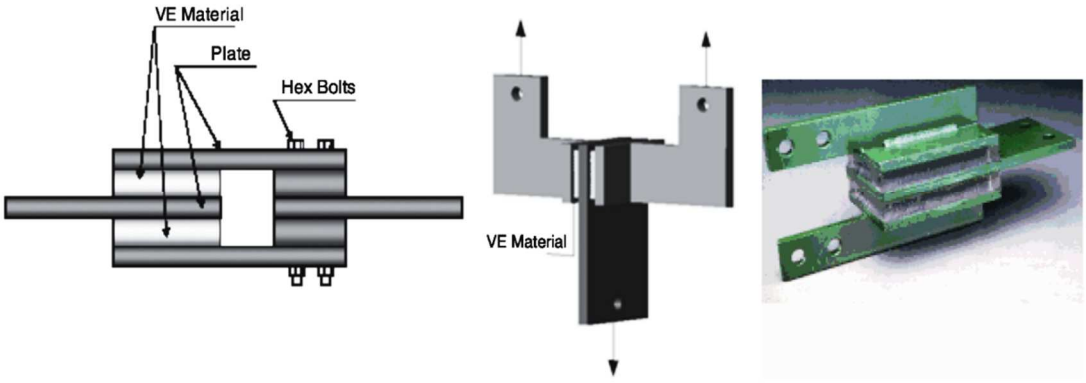

Figure 2-10 Typical viscoelastic dampers.

Andrawes and DesRoches (2007) compared the viscoelastic dampers with other bridge retrofit devices used to restrain the joint opening. It was found that the viscoelastic dampers are effective in reducing the joint opening and enhancing the re-centering capacity after the earthquake. However, force induced in the viscoelastic dampers are directly related to the frequency (relative velocity) of the joint opening rather than the joint opening displacement. Therefore, it may be very hard to control and design for specific force level.

It is worth mentioning that increase in temperature, due to cycling of the damper, can significantly reduce the storage and loss moduli, which in turn can result in the reduced

stiffness and energy dissipation capacity of the damper (Chang et al., 1993; Kanitkar et al., 2006). The viscoelastic dampers also have the disadvantages of limited deformation capacity and plausible deboning and tearing of viscoelastic material (Symans et al., 2008).

2.4.3 Fluid Viscous Dampers

Fluid viscous dampers are commonly used as passive energy dissipation devices for seismic protection of structures. Such dampers consist of a hollow cylinder filled with fluid. The fluid is typically silicone based. As the damper piston rod and piston head are stroked, fluid is forced to flow through orifices either around or through the piston head. The resulting differential pressure across the piston head can produce very large forces that resist the relative motion of the damper. The fluid flows at high velocities, resulting in the development of friction between fluid particles and the piston head. The friction forces give rise to energy dissipation in the form of heat. The associated temperature increase can be significant, particularly when the damper is subjected to long-duration or large-amplitude motions (Makris et al., 1998). The force generated by the device can be described as

$$P(t) = C\left|\dot{u}(t)\right|^{\alpha} \operatorname{sign}\left[\dot{u}(t)\right] \tag{2.2}$$

where P(t) is the force applied to the piston, $\dot{u}(t)$ is the piston velocity, C and α are constants depending on the fluid properties; α may range from 0.1 to 2, according to the type of valves. Force-displacement relations for devices with different values of α subjected to sinusoidal input are elliptical shaped. Force-velocity curves for different values of α are illustrated in Figure 2-11.

α with low values are preferred in the case where high energy dissipation per cycle is required. On the other hand, α with high value (for e.g. 2) is preferred when the difference of force at low and high velocities shall be maximized, in order to react stiffly as soon as the velocity increases, while allowing slow movements due to thermal variations, creep and shrinkage, and becoming rigid in case of dynamic actions (braking force and earthquake), or when energy dissipation is not essential. In this case they are normally named as Shock Transmission Units (STU). An example of an application of STU in bridges is presented in Figure 2-12.

Jankowski et al. (2000) conducted experimental and numerical investigations on the STU to mitigate pounding response of base-isolated bridge. The results of the experiment suggest that for the modelling purposes of STU under service loads caused by thermal, creep and shrinkage events, which result in slow movements, the Influence of the device can be neglected. On the other hand, the STU performed with high stiffness during earthquakes, which cause vibrations with a band of frequencies higher than 0.1 Hz. For the numerical investigation, the authors

modelled the STU using linear gap hook element. The STU acted as a link with very high stiffness during seismic events thus mitigating the pounding effects as well as limiting the moments on the piers.

Shinozuka et al. (2000) proposed retrofitting bridge structures using fluid viscous dampers in the form of dynamic restrainers. The authors evaluated the effectiveness of fluid viscous dampers with the damping exponent of 0.3 at the expansion joint of highway bridges. Through the extensive nonlinear analyses, it was found that the nonlinear dampers were very effective in limiting the relative opening displacements at expansion joints and pounding forces. The ductility demands in the substructures can also be suppressed by installing the viscous dampers at the expansion joints and both abutments. Strandgaard (2000) reported the first application of such dampers on a bridge structure with a length of 1270 foot (387 m) to absorb energy induced by earthquakes. The bridge was fitted with three fluid viscous dampers with capacity of 160 Kips (72.6 tonnes) and damping exponent of 0.4. It was found that with the application, it was able to reduce the seismic movement by approximately 45% and allow the use of smaller joint seal.

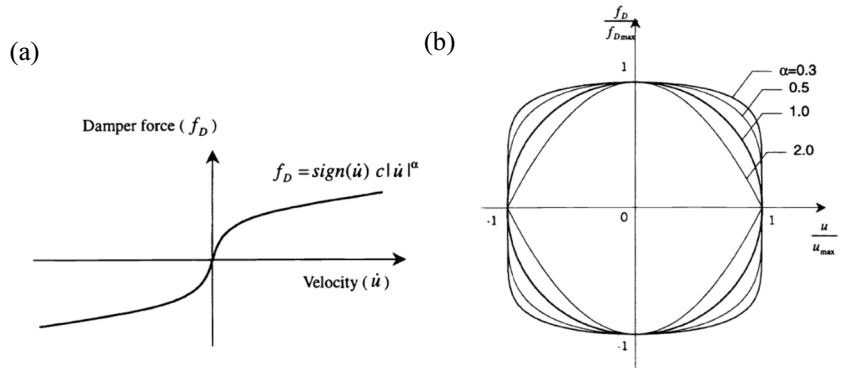

Figure 2-11 (a) Force-velocity relation for dampers with varying value of α, (b) hysteresis loop of a viscous damper for different value of α.

One of the noteworthy limitations of these devices is that it requires regular inspection of fluid seal that are liable to leakage (Symans et al., 2008). Usually the inspections are recommended to be carried out in an interval of few years.

Figure 2-12 Shock transmission unit installed in a bridge.

2.4.4 Magneto Rheological Dampers

The Magnetorheological (MR) dampers are a semi-active device containing MR fluid. MR fluid is composed of oil and varying percentages of iron particles that have been coated with an anti-coagulant material. When inactive, MR fluid behaves as ordinary oil but when exposed to a magnetic field, micron-size iron particles that are dispersed throughout the fluid align themselves along magnetic flux lines. Once this alignment is achieved, the iron particles resist being moved out of their respective flux lines and act as a barrier to fluid flow. Upon exposure to magnetic field, the MR fluid as a whole will appear to undergo a change in viscosity. The resistance caused by the iron particles on movement is what allows MR fluid to be applied in electrically controlled viscous dampers. A section view of a typical mono-tube MR damper is presented in Figure 2-13.

Recently many researchers have investigated the effectiveness of MR dampers to mitigate seismic induced poundings of bridge structures. Ruangrassamee and Kawashima (2003) studied the effectiveness of variable dampers in improving the structural seismic performance considering pounding effects of the highway bridges, in which the effectiveness of the friction-type damping force scheme and the two-step viscous damping force scheme were analyzed. The authors observed that the damping force in the two-step viscous damping force scheme was much smoother than that in the friction-type damping force scheme. The force of the friction-type damping scheme changes when the sign of velocity of the damper changes. The sudden changes of the damping force may cause shocks in the devices. Nonetheless, both the damping schemes were effective in reducing the seismic responses including the pounding forces and pulse-like acceleration responses in the bridge joint. The friction-type damping force scheme with total damping force of 32% of the deck weight was found to be most effective in reducing the deck displacement, flexural hysteretic curvature at the plastic hinge locations and acceleration pulses at joint.

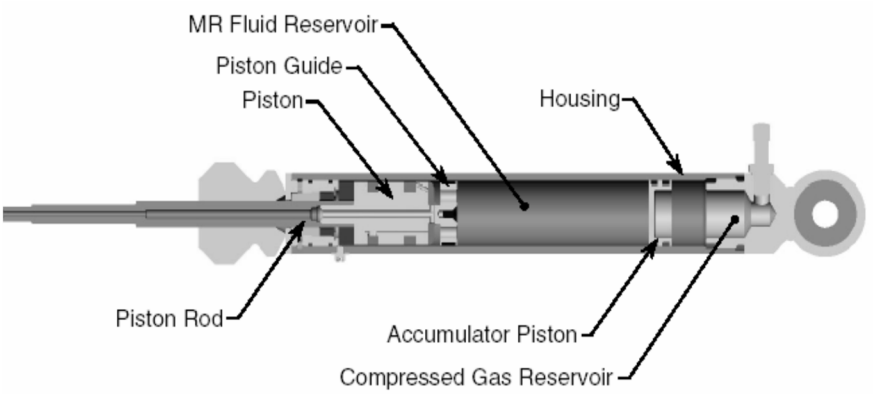

Figure 2-13 Mono-tube MR damper section view.

Guo and Li (2008) investigated the possibility of using MR dampers to reduce the pounding effect on adjacent segments of highway bridges in extreme earthquake events. MR dampers were designed to trace the instantaneous optimal control forces for manipulating the dampers. The damper control algorithm was then modified to incorporate the time-delay effect of the control system based on predictive control algorithm. Two types of installation scheme were analyzed by the authors, as presented in Figure 2-14. The first installation linked two adjacent superstructures and the second installation linked the superstructure with the substructure. The authors showed that semi-active control system can effectively reduce the structural acceleration response caused by pounding. Analyses also indicated that the time delay of the semi-active control system significantly deteriorates the performance of the control system. Li and Yue (2006) analyzed the effectiveness of using MR dampers to control pounding response in elevated bridge. It was found that installing MR dampers between deck and piers will have much better performance than installing it between adjacent decks, and the relative displacement and bearing deformation decreases remarkably by applying a semi-active control device.

Guo et al. (2009) carried out both analytical and experimental investigations on a 1:20 scaled base-isolated two-span simply supported bridge model. A series of shake table tests were performed to investigate the effects of pounding between adjacent superstructures. Furthermore, the experiments were carried out with MR dampers to identify the effectiveness of the dampers to mitigate bridge vibration. The bridge model with the MR dampers was experimentally compared for three control systems (passive-off, passive on and semi-active control). It was found that with the passive off MR dampers, the pounding of the bridge segments could be suppressed. However, pounding still occurred during an earthquake due to the low energy dissipation. In the case of passive-on damper, poundings between the bridge segments were effectively reduced but pounding still occurred. The semi-active control system was effective in reducing the bridge response and was able to eliminate pounding incidences. Sheikh et al. (2012) investigated the effectiveness of different control strategies (passive off,

passive-on and bang-bang control) of MR dampers to mitigate the pounding effect of base-isolated highway bridges. The authors conducted seismic response analysis of a three-segment bridge susceptible to pounding at the joints during an earthquake. It was revealed that all three control strategies are able to reduce the pounding responses.

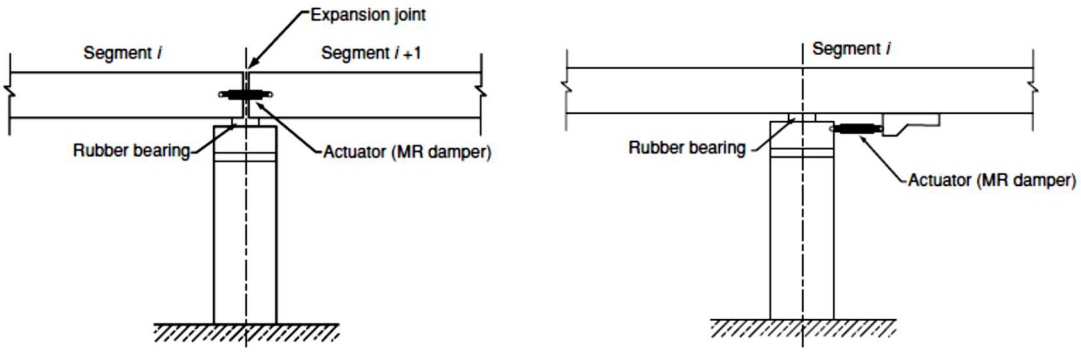

Figure 2-14 the installation schemes of the control devices (Guo et al., 2008).

The afore-mentioned researches have shown that semi-active control strategies of MR damper could be most effective in mitigating pounding and unseating damages. It is important to note that semi-active control requires external power source albeit small. Moreover, the performance of semi-active MR damper is also significantly depended upon the response delay time. The control algorithm is also rather complicated, which makes it difficult for general use in civil engineering applications.

2.5 Modular Expansion Joint

A Modular Expansion Joint (MEJ) system allows a large relative displacement between the bridge girders without compromising the bridge's serviceability and functionality. Using MEJs, it is possible to make the gap sufficiently large to cope with the largest expected closing girder movement, and consequently completely preclude pounding between adjacent girders and between girder and abutment. Originally, MEJ was developed to accommodate large thermal expansion and contraction of long bridges. Recently, investigators have focused on application of this device to mitigate relative displacement induced damages at bridge joints caused by seismic movement.

The cross section of the main components of an MEJ is presented in Figure 2-15. The bridge girders are joined by an edge beam at each girder end and by several centre beams. Seals cover the gaps between the beams and ensure the water tightness of the joint. The traffic load on the center beams is transmitted to the supporting bar via yokes. Sliding springs, bearings and yokes of the system ensure the beams move uniformly and enable the adjoined bridge girders to accommodate expected relative movements of the bridge. The MEJs are provided with a fuse box system, which permits the expansion joint to break out at one side of the connection

to the bridge girder. The fuse box prevents the expansion joints being damaged when unexpectedly large closing movement occurs and settle afterwards in a way to allow emergency vehicles to travel across the joint.

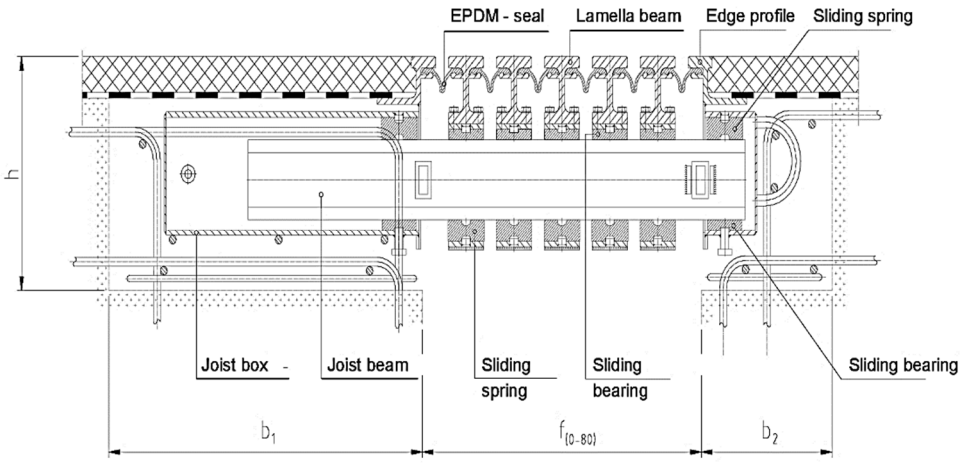

Figure 2-15 Section view of modular expansion joint.

Chouw and Hao (2008b) propose the use of MEJ to mitigate the pounding between the adjacent structures. The authors studied the minimum gap width that MEJs have to accommodate between two bridge frames to prevent pounding when subjected to SVGM and SSI. It was found that using MEJ with a large gap, pounding between the adjacent frames could be completely precluded, thus preventing any localized damage at bridge girder. However, a large girder movement results in a large bending moment in bridge pier, which compensates the advantages of using MEJ in bridges. Chouw and Hao (2009) further presented the minimum opening and closing movement required by MEJ to preclude the pounding. Bi et al. (2010, 2011) using stochastic method calculated the required separation distances between abutment and deck and between two decks to avoid pounding in a bridge structure subjected to SVGM and SSI.

McCarthy et al. (2014) developed an analytical model to represent a common MEJ including its critical component, such as friction element, equidistant devices, support bars and center beam and validated the model through full-scale experimental testing of the joint. To mitigate the damages to the MEJ due to the seismic events, Padgett and DesRoches (2013) developed a new shape memory alloy enhanced MEJ that can accommodate the heightened demands imposed during extreme events like earthquakes. The commonly used MEJ was enhanced by supplementing its equidistant system with SMA spring designed to supply additional displacement capacity during a seismic event while avoiding additional load transfer in the system that may damage other components. Yang and DesRoches (2015) developed a MEJ

with innovative buckling resistant SMA. The buckling resistant SMA can provide a much higher recentering strength than unconfined SMA, which significantly reduces the amount of SMA and thereby the cost of the smart MEJ system.

2.6 Shock Absorbing Device

Pounding of two adjacent bridge components (deck to deck or deck to abutment) results in an exchange of momentum and large acceleration pulses. It is also worthy to note that impact do not necessarily result in the contact between entire surfaces of contacting components. Due to the eccentric motions of bridge decks, it is observed that poundings more likely occur at the corners of the bridge decks. Large impact forces concentrated on the smaller area of the bridge deck and abutment could result in the localized damages such as crushing and spalling of concrete around impacting locations. Inserting a thin layer of a soft elastic material as shock absorbing devices between the impacting surfaces helps to alleviate the arbitrary eccentric contact (Leibovich et al. 2012). Shock absorbing devices such as natural rubbers, metallic honeycomb devices can be used as a layer of soft materials to mitigate large acceleration pulses and to limit the localized damage on the impact surface of the adjacent bridge components.

Kitahara et al. (2005) and Kajita et al. (2006) carried out a collision test between two steel solid bars in order to investigate the impact behavior of the natural rubber bumpers. The test setup is presented in Figure 2-16. Natural rubber bumpers with the hardness of 50 (JIS K 6301) was used for the experiment. The results revealed that the relationship between the collision velocity and the maximum deformation of the rubber bumpers can be approximated by using a linear curve. The relationship between the collision velocity and the maximum impact force, on the other hand, resembled a parabolic curve. The authors suggested that the maximum impact force depends strongly on the collision velocity and the thickness of the natural rubber. Therefore, the collision velocity could be used as a design variable for the rubber bumpers. The authors also conducted a numerical simulation of the impact behavior of rubber bumper using a general-purpose finite element code LS-DYNA, which specializes in dynamic structural crush analysis. The natural rubber bumper was discretized into a cube of 1 mm size using 8-node solid elements sandwich between the rigid plates. The constitutive law of the natural rubber bumper was modelled using the Ogden's Law as

$$W = \sum_{n=1}^{2} \frac{\mu_n}{\alpha_n} (\lambda_1^{\alpha_n} + \lambda_2^{\alpha_n} + \lambda_3^{\alpha_n} - 3) \tag{2.3}$$

where λ_i is the elongation ratio of i-direction, μ_n and α_n are material constants that are determined from the nominal stress-nominal strain curve of the natural rubber.

The numerical model was used to simulate the static and the dynamic behavior of the rubber bumper. However, the numerical analysis terminated when the compressive strain exceeds 0.6 due to tangling of finite elements. Collision simulation of rubber bumpers without the consideration of strain rate effect showed very poor match with the experimental results. Therefore, as presented in Figure 2-17, the strain rate effects have significant influence on the behavior of rubber bumpers.

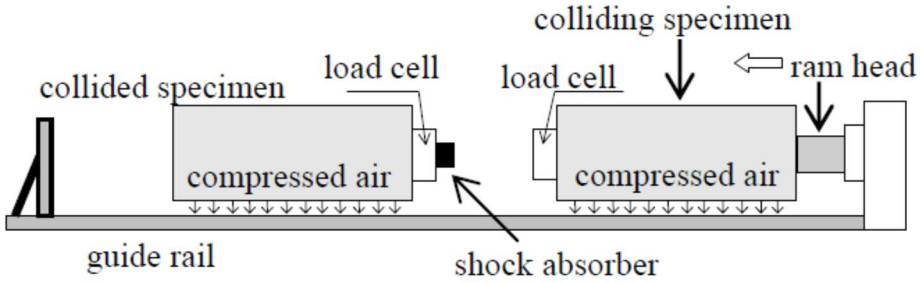

Figure 2-16 Test setup for the collision test of rubber bumper (Kajita et al., 2006).

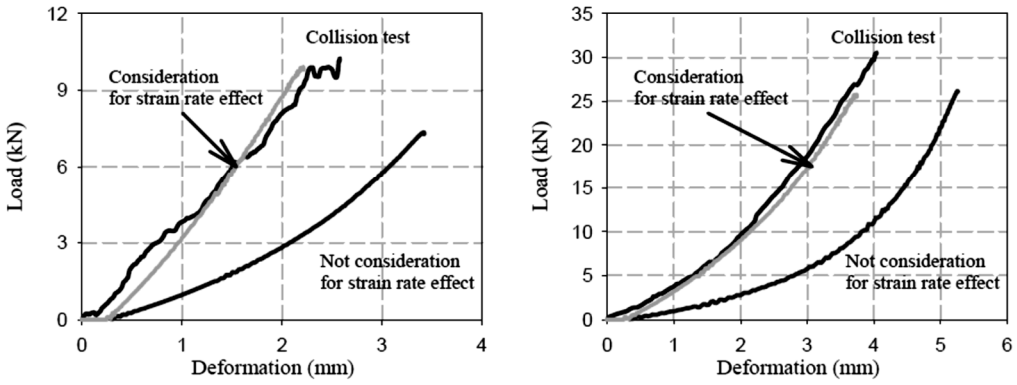

Figure 2-17 Load vs Deformation curve with and without consideration of strain rate effect at v=0.34 m/s (left); and v=0.68 m/s (right) (Kajita et al., 2006).

Leibovich et al. (2012) investigated the pounding response of concrete rods with and without softer filling materials at the joint between the impacting concrete surfaces. Concrete rods with diameter of 100 mm and length of 500 mm and 1000 mm were used in the test. The experimental setup is shown in Figure 2-18. Two guide rails were added on each side of the rods to limit the eccentric pounding between the rods. However, during the test it was found that the guide rails were not able to fully eliminate the eccentric poundings. A typical time history of the acceleration records during an impact is shown in Figure 2-19 (a). The acceleration signals due to the impact and its propagation along the length of the piles could be seen in the figure. It is evident in the figure that the main impact signal is followed by several lower magnitude high-frequency vibration waves that damped out within 3-4 cycles. These waves mentioned as noises by the authors, could in fact be the stress wave resulting from the axial compression of the material at the impacting surfaces. It could also be noted

that spike generated at target impacting face (sensor J) travelled to the middle of the rod (sensor F), which is approximately 500 mm from the impacting face. From the figure, the travel time of the spike from the impacting face to the target CM can be calculated approximately to be 0.2 msec. Upon dividing the distance by the travel time, the velocity of propagation of the compressive wave could be obtained as approximately 2500 m/s. For a straight, prismatic, free-ended rod with length L, the fundamental period of axial vibration, T is given by (Malhotra et al., 1995; Clough & Penzien, 1993)

$$T = \frac{2L}{c} \tag{4}$$

where L is the length of the concrete rod and c is the velocity of compressive wave. Substituting L = 1 m and c = 2500 m/s into the eqn. 4, T = 0.8 msec could be obtained which approximately matches the period of vibration waves following the main spike. Thus, the waves following the main impact spike are actually caused by the impact stress waves.

The acceleration pulse resulting from the impact of two solid surfaces could be eliminated by the introduction of soft materials between the surfaces. Leibovich et al. (2012) used white sponge that is characterized by a very low modulus of elasticity glued to target specimen impacting face to mitigate the contact pressure and acceleration due to the impact. The sponge also helps to overcome the surface irregularities that are responsible for partial contact and provide full contact between the piles on impact. Figure 2-19 (b) shows the peak acceleration at the target impacting face (J). As presented in the figure, a significant reduction the magnitude of the impact acceleration at the impacting face was observed. It could also be noted that the waves following the main impact during the impact test without any infill sponges were completely eliminated during the test with infill sponges. The result of the experiment prove that infill soft materials such as white sponge used in the test could not only reduce the large acceleration pulse but also completely eliminate the stress waves that are caused by the compression of the materials of the impacting elements. The softer infill material with low axial stiffness absorbs the high-frequency compressional waves, thus resulting in an elimination of high-frequency waves during an impact. However, as could be observed in Figure 2-19 (b), the duration of the impact is prolonged.

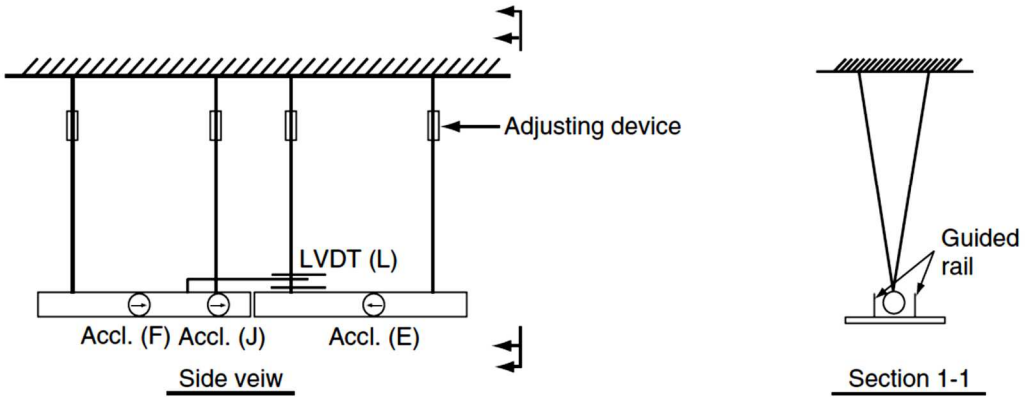

Figure 2-18 Experimental setup for impact test (Leibovich et al., 2012).

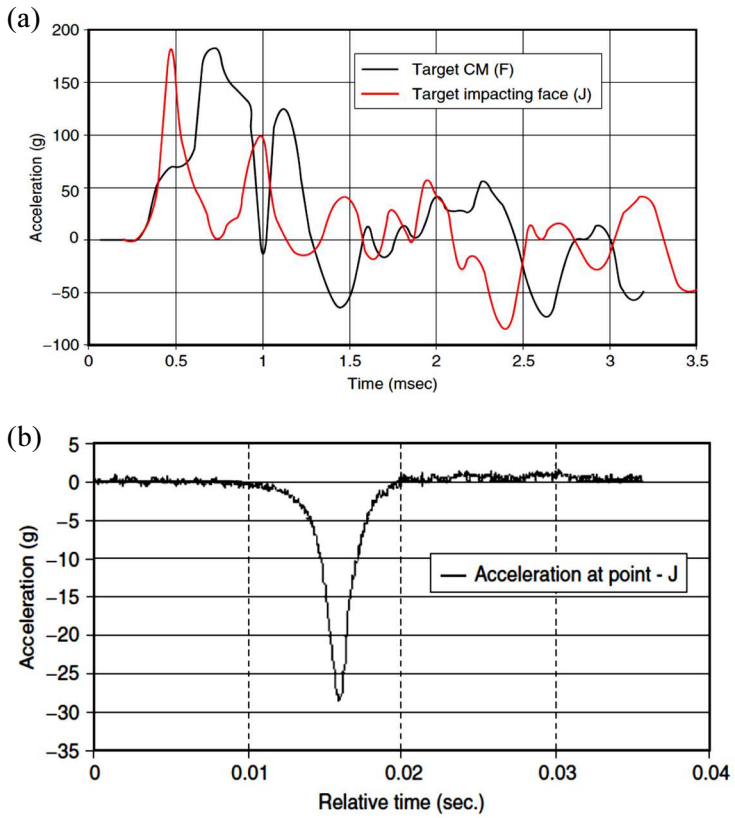

Figure 2-19 Acceleration record of concrete pile impact (a) without shock absorbing device; (b) with shock absorbing device (Leibovich et al., 2012).

Jankowski et al. (2000) investigated the effectiveness of rubber bumper and crushable devices to reduce the responses resulting from pounding of adjacent isolated bridge deck. The authors modelled the behavior of rubber bumper using linear spring-dashpot elements. The stiffness and damping of a rubber bumper were calculated as follows

$$k_p = \frac{E_r A_p}{t_p} \tag{2.5}$$

$$c_p = 2\xi\sqrt{k_p \frac{m_s}{2}} \tag{2.6}$$

where A_p is cross-sectional area of the rubber pad, t_p is its thickness and E_r is the Young modulus of rubber. ξ_r is damping ratio of the rubber and m_s is a mass of the superstructure segment. Two gap elements were modelled in series, the first to model the activation of rubber bumper when the gap between the bumper and bridge deck is closed. While the second gap element was placed with gap width equal to the separation between two bridge decks, to model the closing of the gap after full compression of rubber bumper. The authors also investigated the crushable devices that were designed to be crushed by compression, giving sufficient space for deck to move and absorb the energy at the same time. Under the normal conditions such devices allowed the transmission of vehicle over them. During the severe earthquakes the devices get destructed due to the crushing, allowing the superstructure segments to vibrate independently and the device could be replaced after an event. The authors concluded that using hard rubber bumper leads to reduction of reaction forces (bending moment) of piers and also could significantly reduce the pounding force. However, due to the earlier activation of bumpers contact period gets lengthened but maximum forces of collisions are reduced. Dissipation of energy due to the plastic deformation of crushable devices were not found to be of the great effectiveness, however, the benefits were derived from unrestrained vibration of superstructure segments after crushing of the devices.

Kawashima and Shoji (2000) numerically investigated the effectiveness of steel restrainers with rubber Shock Absorbing Devices (SAD) to mitigate pounding between adjacent bridge decks. Three types of rubber bumpers with strain-hardening, strain-softening and elastic type hysteretic behavior were investigated in the study. The study found that rubber SADs were effective in mitigating the impact forces as well as the acceleration impulse caused by pounding. The strain-softening devices were found to be more effective in reducing the impact indentation between the two decks with smaller compression force. Abdel Raheem (2009) investigated the effects of natural rubber pads on the isolated bridge structure. Rubber bumpers were modelled using exponential elastic impact element, without considering any impact damping. It was found that the rubber shock absorbers placed between the bridge segments significantly reduced the peak pounding force and the cable restrainers force was also reduced by rubber pad placed at the end of the restrainers. The author also suggested that rubber shock absorbing device with a half-gap slack size provides an economical and effective design that can reduce the impact force and acceleration response. Shrestha et al. (2014) evaluated the effectiveness of using rubber bumpers and restrainers to mitigate pounding and unseating damages on multiple-frame bridges subjected to SVGM. In this study, the rubber bumpers

were modelled by using the nonlinear strain hardening model proposed by Kawashima and Shoji (2000) without any damping.

Though the rubber bumper is effective to mitigate the pounding response, impact models capable of representing the behavior of rubber bumpers with sufficient accuracy are scarce. The researchers as mentioned above used the simplified model to represent the behavior of the rubber bumper. A linear model with viscoelastic damping or nonlinear spring with no energy dissipation was normally adopted. To overcome this limitation, a new nonlinear inelastic force-based impact model, able to appropriately describe the behavior of rubber under impact loading taking into account the limited thickness of the bumper was developed (Polycarpou et al. 2013a, Polycarpou and Komodromos 2013b). A simple and efficient nonlinear impact model with hysteretic damping for rubber bumpers was proposed and verified based on the experimental study by Kajita et al. (2006). As presented in Figure 20, the results obtained from the numerical analysis were very well correlated with the corresponding experimental data. The impact model was quite robust and it did not show instability problems at higher strains as those observed in LS-DYNA models by Kajita et al. (2006).

Though rubber bumpers are effective in reducing the pounding response of bridge structures, natural rubber is less durable to environmental loading. To overcome the durability problem Li et al. (2011) recently developed a novel shock absorber device-Shape Memory Alloy Pseudo Rubber (SMAPR). The energy dissipating and residual deformation self-recovery ability of the device was achieved by using the martensitic NiTi SMAPR. The mechanical properties, self-recovery ability of SMAPRs and recovery of SMAPRs on heating were investigated to identify its potential as shock absorbing device for impact applications. The mechanical properties of the SMAPR specimens under cyclic compression loading were experimentally investigated under a controlled temperature. Sinusoidal cyclic compression load was applied along the stamping and moulding directions of the specimens. It was observed that the tangent modulus of SMAPR increased dramatically when the strain was larger than 20%. The stress-strain curves were found to be independent of the loading frequencies as the elastic force of the micro-spring, and the internal Coulomb friction force were not affected by the loading rate. Figure 2-21 (a) shows the deformation of a specimen before and after compression to a strain of 45%. Figure 2-21 (b) shows the stress-strain curves of SMAPR specimens compressed to 30%, 40% and 48% strain amplitude. It was observed that no residual deformation was induced for 40% strain while 6% residual strain was found for the strain amplitude of 48%. Therefore, the fully restorable residual strain limit of SMAPR was somewhere between 40% and 48%.

Meng et al. (2011) conducted a shake table testing of high-pier bridge model to evaluate the efficacy of SMAPR to reduce seismic pounding in high-pier long-span bridges. Li et al. (2015) investigated the mitigation mechanism of SMAPR on a scaled model (1:30) of an isolated bridge with two deck segment. In the bridge models, R15α Acoustic Emission (AE) sensors were installed at the typical locations to capture the stress waves. The comparison of acceleration histories with and without the SMAPR shock absorbing devices showed that SMAPR not only significantly reduced the amplitude of impact but also eliminated the stress waves resulting from the impact.

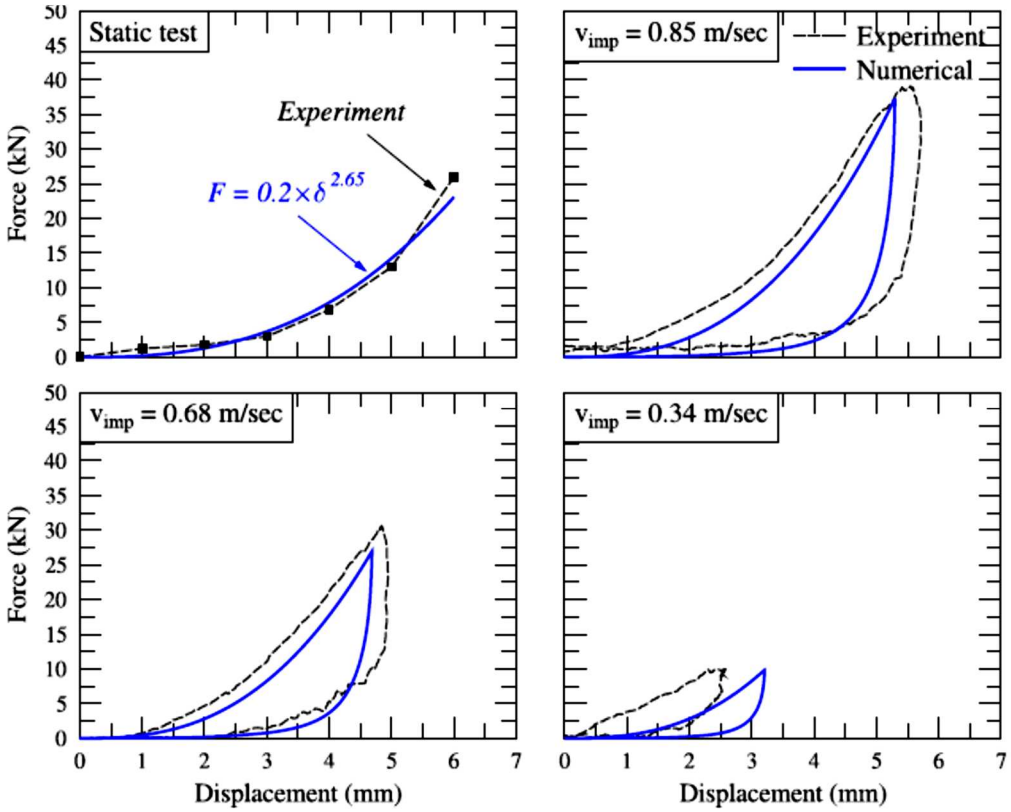

Figure 2-20 Comparison of experimental and numerical force-displacement diagram of a 10mm thick rubber shock absorber for static and dynamic tests (Polycarpou et al., 2013a).

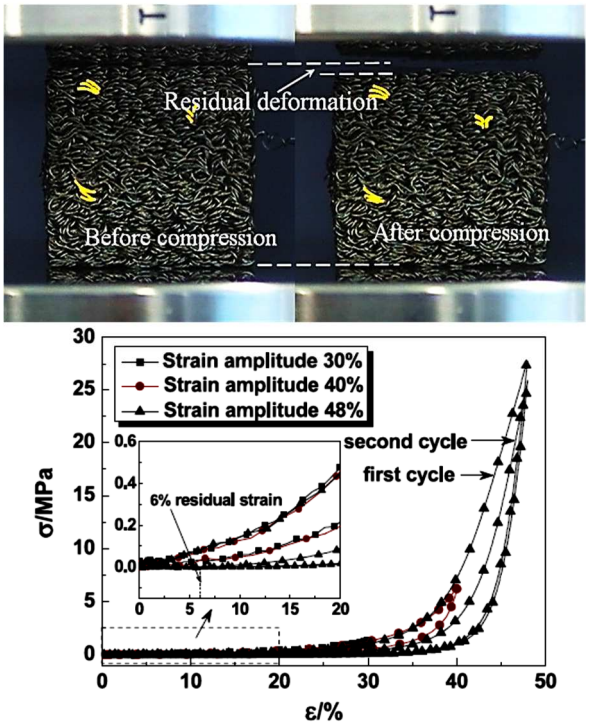

Figure 2-21 Self- restorable strain for SMAPR specimen (Li et al., 2011).

2.7 Hybrid Devices

In order to prevent unseating and pounding damages in the bridge structures, many researchers have investigated on the application of combination of devices to achieve the optimum protection. These devices complement each other to suppress the responses that may lead to the damage or failure of structures.

One of such hybrid device that has been widely used is the combination of rubber bumpers along with restrainers. The restrainers prevent the unseating failure but have limited effect on pounding impacts while rubber bumpers as presented earlier have superior performance in mitigating pounding impact and stress wave resulting from the pounding. Kawashima and Shoji (2000) revealed that the rubber bumper along with restrainers at the bridge joint were not only effective in reducing joint acceleration and relative joint displacements but also reduce the response of bridge piers to some extent. Zhu et al. (2004) proposed applying shock absorbing devices along with restrainers to counter pounding effects and to improve the serviceability of elevated bridges during a seismic event. Abdel Raheem (2009) investigated three different configurations of the hybrid device with rubber bumper and restrainers to prevent unseating and mitigate pounding effect at expansion joint of isolated multi-span bridges as shown in Figure 2-22. Recently, Shrestha et al. (2014) evaluate the effectiveness of using rubber bumper along with two types of restrainers (SMA and steel). The authors found that the effects of the rubber bumpers on the relative joint opening displacement were not always beneficial as rubber bumpers reduce the gap width, which in turn increased the number

of pounding incidences and prolonged the pounding duration although the amplitudes of pounding forces are reduced. As a consequence, the relative opening displacement at bridge joint may increase. Therefore, the authors suggested using rubber bumpers together with restrainers to mitigate the pounding damages whilst preventing deck unseating.

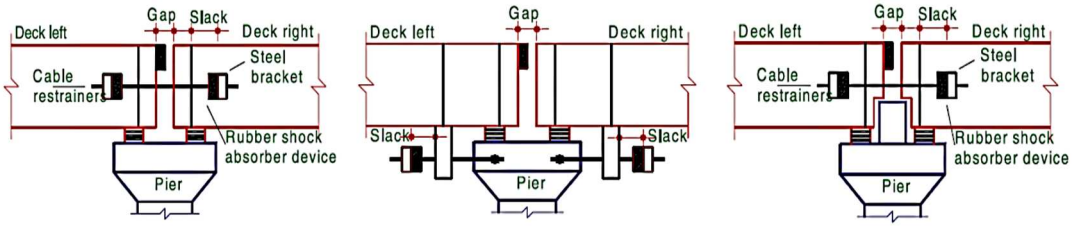

Figure 2-22 Schematic of various configuration of hybrid device at bridge expansion joint (Abdel Raheem, 2009).

Another form of hybrid devices that have been proposed to mitigate the damages induced by the relative displacement response of bridge structures is a combination of restrainers with dampers. Zhang, Hu and Zhu (2009) developed a restraining damping device to control the seismic response of a benchmark base-isolated bridge. The passive control hybrid device utilized stranded superelastic CuAlBe wires as restraining/self-centering component, which not only restrain the movement but also provide good re-centering capability through their unique hysteretic behavior at wide temperature range. As shown in Figure 2-23, the damper composed of two moving parts (denoted by block A and block B) that can slide past each other. When the dampers were subject to either tension or compression force, the CuAlBe SMA wires in one direction will be stretched. As the engagement of SMA wires would increase the stiffness of the isolated system and reduce the effectiveness of isolation, the SMA wires were designed to have a slack such that under the moderate earthquake the wires would not get engaged, and only the damping device would act. However, under larger earthquakes both the damper and SMA wires would engage to limit the movement of the bridge system.

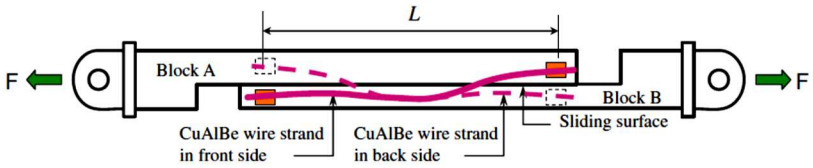

Figure 2-23 Schematic of passive control hybrid damping device (Zhang et al., 2009).

Berton et al. (2004) investigated the possibility of applying fluid viscous dampers along with modular expansion joints on a multi-span bridge to reduce the size of the modular expansion joint. The authors showed that for the studied case, the expansion joint size could be reduced up to the half of the size of the original design by using fluid viscous dampers. The study also showed that by using fluid viscous dampers, large girder movement could be restricted and

resulting bending moment on the bridge piers could also be reduced. The hybrid solution of combining MEJ with fluid viscous dampers to mitigate the damages due to the excessive movement of bridge superstructure has found significant application in long-span bridges. Application of such hybrid device not only mitigates the seismic induced damages but also prevents the premature failures of expansion joints of long span bridges in service conditions. Recently, Guo et al. (2014) reported a long-term displacement monitoring from three long span steel bridges in China, the Sutong Bridge, Runyan suspension Bridge and the Jiangyin Bridge, that used MEJ and fluid viscous dampers at the joints.

2.8 Conclusion

The paper presents an overview of the devices used to mitigate pounding and unseating damages on bridge structures. The interest within the structural engineering community in applying these devices in retrofit of existing structures and even in new structures is evident by the rapid growth of recent researches. Based on extensive review presented in the paper, the following general conclusions are drawn.

Steel cable hinge restrainers have been traditionally used in bridge retrofit because of its low cost. However, steel restrainers rely upon the elastic strength to reduce the joint opening between adjacent bridge girders, which could result in large forces within the restrainers and could in turn damage the restrainers or the connected structural members. Superelastic SMA has emerged as an alternative restraining device with energy dissipating and re-centering capacity. The temperature dependence of the NiTi SMA and its high cost compared to steel bar/cable as well as the difficulty of machining large diameter bars, however, have critically limited its application. Copper based SMAs, which are relatively cheaper, easier to machine and have a wide operating temperature, have attracted attention in the recent years. Alternatively, FRP restrainers could also be used, which are easy to install and inspect.

Using devices capable of dissipating the energy could provide protection against pounding and unseating failures. However, some of these devices have no re-centering ability and are frequency dependent, which make it difficult to be control the force during the design. Moreover, some of these devices could require regular inspection. Pounding of the bridge segments could be completely precluded by the application of MEJ. However, the larger girder movement has to be accommodated, which could result in a larger bending moment at bridge piers and thus compensate the benefits of MEJ. Rubber bumpers used as shock absorbing device are effective to mitigate large impact force resulting from the pounding of adjacent girders. SMAPRs that have similar behavior as natural rubber bumpers could be used as

alternative shock absorbing device to overcome the durability problem of natural rubber bumpers.

Recent researches have focused on the application of hybrid devices that combine the advantages of two or more materials or devices to mitigate pounding and unseating damages in bridge structure. Application of rubber bumpers with restrainers, combination of dampers with the restrainers and MEJ with damping devices have received considerable attention to reduce the damages as well as improve the serviceability of the bridge.

Although there have been significant researches on the design of restrainer devices, there are very limited works on designing the seismic restrainers considering spatially varying ground motion. As the spatial variation of earthquake ground motions are inevitable along the supports of extended structures such as long span bridges, more research focus should be provided into this. Additionally, there are limited studies on the effectiveness of these devices on the bridge with complex geometry (e.g. skewed and curved bridges).

2.9 References

AASHTO (1992). Standard Specification for Highway bridges. American Association of State Highway and Transportation Officials.

Abdel-Ghaffar, S. M., Maragakis, E., Saiidi, M. (1997) Effects of the hinge restrainers on the response of the Aptos Creek Bridge during the 1989 Loma Prieta Earthquake. Earthquake Spectra, 13(2):167-189.

Andrawes, B., & DesRoches, R. (2005). Unseating prevention for multiple frame bridges using superelastic devices. *Smart Materials and Structures*, *14*(3), S60.

Andrawes, B., & DesRoches, R. (2007a). Comparison between shape memory alloy seismic restrainers and other bridge retrofit devices. *Journal of Bridge Engineering, 12*(6), 700-709.

Andrawes, B., & DesRoches, R. (2007b). Effect of ambient temperature on the hinge opening in bridges with shape memory alloy seismic restrainers. *Engineering Structures*, *29*(9), 2294-2301.

ASTM. (2006). *Standard specification for structural steel for bridges, A 709/A 709M-05*. Vol. 01.04. ASTM International: West Conshohocken, PA: Annual Book of ASTM standards.

Berton, S., Strandgaard, H., & Bolander, J. E. (2004). *Effect of non-linear fluid viscous dampers on the size of expansion joints of multi-span prestressed concrete segmental box-girder bridges*. 13th World Conference on Earthquake Engineering. Canada: Vancouver, BC.

Bi, K., Hao, H., & Chouw, N. (2010). Required separation distance between decks and at abutments of a bridge crossing a canyon site to avoid seismic pounding. *Earthquake Engineering & Structural Dynamics*, *39*(3), 303-323.

Bi, K., Hao, H., & Chouw, N. (2011). Influence of ground motion spatial variation, site condition and SSI on the required separation distances of bridge structures to avoid seismic pounding. *Earthquake Engineering & Structural Dynamics, 40*(9), 1027-1043.

Bruneau, M., Wilson, J. C., & Tremblay, R. (1996). Performance of steel bridges during the 1995 Hyogo-ken Nanbu (Kobe Japan) earthquake. *Canadian journal of civil engineering,* 23(3), 678-713.

Caltrans, (1990) *Bridge Design Specification Manual*. Sacramento, CA: California Department of Transportation.

Caltrans (2008). *Caltrans Bridge Design Aids*, Sacramento, CA: California Department of Transportation. From http://www.dot.ca.gov/hq/esc/techpubs/manual/bridgemanuals/bridge-design-aids/bda.html

Chang, K. C., Soong, T. T., Lai, M. L., and Nielsen, E. J. (1993). *Development of a design procedure for structures with added viscoelastic dampers*. ATC-17–1 Seminar on Seismic Isolation, Passive Energy Dissipation and Active Control, Vol. 2, ATC, Redwood City, California.

Chen, G., Bothe, E., & Ger, J. (2001). Experimental characterization of metallic dampers for seismic retrofit of highway bridges. Transportation Research Record. *Journal of the Transportation Research Board*, (1770), 124-131.

Choi, E., Lee, D. H., & Choei, N. Y. (2009). Shape memory alloy bending bars as seismic restrainers for bridges in seismic areas. *International Journal of Steel Structures*, *9*(4), 261-273.

Choi, E., Park, J., Yoon, S. J., Choi, D. H., & Park, C. (2010). Comparison of seismic performance of three restrainers for multiple-span bridges using fragility analysis. *Nonlinear Dynamics*, *61*(1-2), 83-99.

Chouw, N., & Hao, H. (2005). Study of SSI and non-uniform ground motion effect on pounding between bridge girders. *Soil Dynamics and Earthquake Engineering*, *25*(7), 717-728.

Chouw, N., & Hao, H. (2008a). Significance of SSI and nonuniform near-fault ground motions in bridge response I: Effect on response with conventional expansion joint. *Engineering Structures, 30*(1), 141-153.

Chouw, N., & Hao, H. (2008b). Significance of SSI and non-uniform near-fault ground motions in bridge response II: Effect on response with modular expansion joint. *Engineering Structures*, *30*(1), 154-162.

Chouw, N., & Hao, H. (2009). Seismic design of bridge structures with allowance for large relative girder movements to avoid pounding. *Bulletin of the New Zealand Society for Earthquake Engineering, 42*(2), 75.

Chouw, N., & Hao, H. (2012). Pounding damage to buildings and bridges in the 22 February 2011 Christchurch earthquake. *International Journal of Protective Structures*, *3*(2), 123-140.

Clough, R. W., & Penzien, J. (1975). *Dynamics of structures.* Mc Graw-Hill.

Deng, K., Pan, P., Su, Y., Ran, T., & Xue, Y. (2014). Development of an energy dissipation restrainer for bridges using a steel shear panel. *Journal of Constructional Steel Research, 101,* 83-95.

DesRoches, R., & Fenves, G.L. (2000). Design of seismic cable hinge restrainers for bridges. *Journal Structural Engineering ASCE, 126*(4), 500-509.

DesRoches, R., & Delemont, M. (2002). Seismic retrofit of simply supported bridges using shape memory alloys. *Engineering Structures*, *24*(3), 325-332.

DesRoches, R., & Muthukumar, S. (2002). Effect of pounding and restrainers on seismic response of multiple-frame bridges. *Journal of Structural Engineering*, *128*(7), 860-869.

DesRoches, R., McCormick, J., & Delemont, M. (2004). Cyclic properties of superelastic shape memory alloy wires and bars. *Journal of Structural Engineering*, *130*(1), 38-46.

Earthquake Engineering Research Institute. (1999). Chi-Chi, Taiwan, Earthquake Reconnaissance Report. *Report No.01-02, EERI*, Oakland, California.

Elnashai, A. S., Kim, S. J., Yun, G. J., Sidarta, D. (2007). The Yogyakarta earthquake in May 27, 2006. Mid-America Earthquake Center, *Report No. 07-02*, Champaign, IL: The University of Illinois.

Elnashai, A. S., Gencturk, B., Kwon, O. S., Al-Qadi, I. L., Hashash, Y., Roesler, J. R., Kim, J.K., Jeong, S.H., Dukes, J. & Valdivia, A. (2010). *The Maule (Chile) earthquake of February 27, 2010: Consequence assessment and case studies*. MAE Center Report No. 10-04, Champaign, IL: The University of Illinois.

Feng, M. Q., Kim, J. M., Shinozuka, M., & Purasinghe, R. (2000). Viscoelastic dampers at expansion joints for seismic protection of bridges. *Journal of Bridge Engineering*, *5*(1), 67-74.

Guo, A., & Li, H. (2008). Pounding reduction of highway bridges with pounding effect by using magnetorheological dampers under earthquake excitations. *Advances in Structural Engineering, 11*(3), 305-322.

Guo, A., Li, Z., Li, H., & Ou, J. (2009). Experimental and analytical study on pounding reduction of base-isolated highway bridges using MR dampers. *Earthquake Engineering & Structural Dynamics, 38*(11), 1307-1333.

Guo, A., Zhao, Q., & Li, H. (2012). Experimental study of a highway bridge with shape memory alloy restrainers focusing on the mitigation of unseating and pounding. *Earthquake Engineering and Engineering Vibration*, *11*(2), 195-204.

Guo, T., Liu, J., Zhang, Y., & Pan, S. (2014). Displacement Monitoring and Analysis of Expansion Joints of Long-Span Steel Bridges with Viscous Dampers. *Journal of Bridge Engineering*, 04014099.

Hall, F. J. (Ed.). (1994). Northridge earthquake, January 17, 1994. Earthquake Engineering Research Institute, Preliminary reconnaissance report, *EERI-94-01*.

Hudgings, T., Eberhard, M.O., and Stanton, J.F. (1997) Design of Seismic bridge restrainers considering spatial variation of ground motions. Report WA-RD 387.2. Washington State Transportation Center, Seattle, WA.

Ishikawa, N., Nishimoto, Y., & Ukishima, T. (2006) Development of new bridge restrainer using laminated fiber reinforced rubber. In M. Pandey et al. (Eds.), *Solid mechanics and its applications. Advances in Engineering Structures, Mechanics & Construction*. 2006; 140:809–821.

Jankowski, R., Wilde, K., & Fujino, Y. (2000). Reduction of pounding effects in elevated bridges during earthquakes. *Earthquake engineering & structural dynamics*, *29*(2), 195-212.

Jennings, P. C. (1971). Engineering features of the San Fernando earthquake of February 9, 1971.Report EERL-71-02. Earthquake Engineering Research Laboratory, California Institute of Technology, Pasadena.

Johnson, R., Padgett, J. E., Maragakis, M. E., DesRoches, R., & Saiidi, M. S. (2008). Large scale testing of nitinol shape memory alloy devices for retrofitting of bridges. *Smart materials and structures*, *17*(3), 035018.

Johnson, R., Saiidi, M. S., & Maragakis, E. M. (2006). Fiber reinforced plastics for seismic bridge restrainers. CCEER 05-2, Dept. of Civil Engineering, Univ. of Nevada, Reno, Nevada.

Julian, F. D. R., Hayashikawa, T., & Obata, T. (2007). Seismic performance of isolated curved steel viaducts equipped with deck unseating prevention cable restrainers. *Journal of Constructional Steel Research, 63*(2), 237-253.

Kanitkar, R., Aiken, I., Nishimoto, K., and Kasai, K. (2006). *Viscoelastic dampers for the seismic retrofit of buildings: An overview of advancements in viscoelastic materials and analytical capabilities*. 8th U.S. National Conf. on Earthquake Engineering, EERI, Oakland, California.

Kajita, Y., Kitahara, T., Nishimoto, Y., & Otsuka, H. (2006, September). *Estimation of maximum impact force on natural rubber during collision of two steel bars.* First European Conference on Earthquake Engineering and Seismology, Geneva, Switzerland.

Kawashima, K., & Unjoh, S. (1996). Impact of Hanshin/Awaji earthquake on seismic design and seismic strengthening of highway bridges. *Structural Engineering/Earthquake Engineering JSCE* 1996; **13**(2):211–240.

Kawashima, K., & Shoji, G. (2000). *Effect of restrainers to mitigate pounding between adjacent decks subjected to a strong ground motion*. In Proceeding of the 12th World Conference on Earthquake Engineering, New Zealand.

Kawashima, K., Unjoh, S., Hoshikuma, J. I., & Kosa, K. (2011). Damage of bridges due to the 2010 Maule, Chile, Earthquake. *Journal of Earthquake Engineering*, *15*(7), 1036-1068.

Kim, J. M., Feng, M. Q., & Shinozuka, M. (2000). Energy dissipating restrainers for highway bridges. *Soil Dynamics and Earthquake Engineering*, *19*(1), 65-69.

Kitahara, T., Kajita, Y., Nishimoto, Y., & Katsuki, S. (2005). *Collision Test between Steel Bars with Shock Absorbing Rubber for Bridge Restrainer System using Frictionless Impact Testing Apparatus*. In Proceedings of the First International Conference on Advances in Experimental Structural Engineering (pp. 901-907).

Leibovich, E., Rutenberg, A., & Yankelevsky, D. (2012). Pounding Response of Adjacent Concrete Rods: An Experimental Study. *International Journal of Protective Structures*, *3*(3), 355-374.

Li, B., Bi, K., Chouw, N., Butterworth, J. W., & Hao, H. (2012). Experimental investigation of spatially varying effect of ground motions on bridge pounding. *Earthquake Engineering & Structural Dynamics*, *41*(14), 1959-1976.

Li, S., Mao, C., Li, H., & Zhao, Y. (2011). Mechanical properties and theoretical modeling of self-centering shape memory alloy pseudo-rubber. *Smart Materials and Structures*, *20*(11), 115008.

Li, S., Guo, A., Cui, L., Mao, C. & Li, H. (2015). *Pounding-induced stress wave analysis and mitigation of highway bridges under earthquakes*. In Proceedings of the 11th International conference in experimental structural engineering, University of Illinios, Urbana-Champaign.

Li, Z. X., & Yue, F. Q. (2006). *Analysis and control for seismic pounding response of urban elevated bridges*. 4th International conference of earthquake engineering. Taipei, Taiwan.

Lin, C. J., Hung, H., Liu, Y., & Chai, J. (2008). *Reconnaissance report of 0512 China Wenchuan earthquake on bridges*. 14th World Conference on Earthquake Engineering, China.

Makris, N., Roussos, Y., Whittaker, A. S., & Kelly, J. M. (1998). Viscous heating of fluid dampers. II: Large-amplitude motions. *Journal of engineering mechanics*, *124*(11), 1217-1223.

Malhotra, P. K., Huang, M. J., & Shakal, A. F. (1995). Seismic interaction at separation joints of an instrumented concrete bridge. *Earthquake Engineering & Structural Dynamics, 24*(8), 1055-1067.

McCarthy, E., Wright, T., Padgett, J. E., DesRoches, R., & Bradford, P. (2013). Development of an Experimentally Validated Analytical Model for Modular Bridge Expansion Joint Behaviour. *Journal of Bridge Engineering, 19*(2), 235-244.

Meng, Q. L., Zhang, M. Z., & Zhou, G. L. (2011). The study on SMA Pseudo-Rubber Metal damper's control efficiency on aseismic pounding in high-pier bridge in shaking table testing. *Advanced Materials Research, 163*, 4429-4441.

Padgett, J. E., DesRoches, R., & Ehlinger, R. (2010). Experimental response modification of a four-span bridge retrofit with shape memory alloys. *Structural Control and Health Monitoring*, *17*(6), 694-708.

Padgett, J. E., & DesRoches, R. (2013). *Shape memory alloy enhanced smart expansion joint.* Highway IDEA project 147, Transportation research board, The National Academies of Sciences, Engineering, and Medicine, Washington: DC.

Pan, P., Yan, H., Wang, T., Xu, P., & Xie, Q. (2014). Development of steel dampers for bridges to allow large displacement through a vertical free mechanism. *Earthquake Engineering and Engineering Vibration*, *13*(3), 375-388.

Polycarpou, P. C., Komodromos, P., & Polycarpou, A. C. (2013). A nonlinear impact model for simulating the use of rubber shock absorbers for mitigating the effects of structural pounding during earthquakes. *Earthquake Engineering & Structural Dynamics*, *42*(1), 81-100.

Polycarpou, P. C., & Komodromos, P. (2013). Numerical Investigation of the Effectiveness of Rubber Shock-Absorbers as a Mitigation Measure for Earthquake-Induced Structural Poundings. In *Computational Methods in Earthquake Engineering* (pp. 417-436). Springer Netherlands.

Raheem, S. E. A. (2009). Pounding mitigation and unseating prevention at expansion joints of isolated multi-span bridges. *Engineering Structures*, *31*(10), 2345-2356.

Ruangrassamee, A., & Kawashima, K. (2001). Relative displacement response spectra with pounding effect. *Earthquake engineering & structural dynamics*, 30(10), 1511-1538.

Ruangrassamee, A., & Kawashima, K. (2003). Control of nonlinear bridge response with pounding effect by variable dampers. *Engineering Structures, 25*(5), 593-606.

Saiidi, M., Maragakis, E., Abdel-Ghaffer, S., Feng, S., & O'Conner, D. (1993). Response of Bridge hinge resrainers during Earthquake- Field Performance, Analysis and Design. Report CCEER 93/06, Center for Civil Engineering and Earthquake Research, University of Nevada, Reno.

Saiidi, M., Randall, M., Maragakis, E., & Isakovic, T. (2001). Seismic restrainer design methods for simply supported bridges. *Journal of Bridge Engineering*, *6*(5), 307-315.

Saiidi, M. S., Johnson, R., & Maragakis, E. M. (2006). Development, shake table testing, and design of FRP seismic restrainers. *Journal of Bridge Engineering*, *11*(4), 499-506.

Selna, L.G., Malvar, L.J., & Zelinski, R.J. (1989). Bridge retrofit testing: hinge cable restrainer. *Journal of Structural Engineering, 155*(4), 920–934.

Sheikh, M. N., Xiong, J., & Li. W. H. (2012) Reduction of seismic pounding effects of base-isolated RC highway bridges using MR damper. *Structural Engineering and Mechanics 41*(6), 791-803.

Shinozuka, M., Feng, M. Q., Kim, J. M., Nagashima, F., & Kim, H. (2000, April). *Mitigation of seismic pounding effect on bridges using dynamic restrainers*. In SPIE's 7th Annual International Symposium on Smart Structures and Materials (pp. 377-387). International Society for Optics and Photonics.

Shrestha, B., Hao, H., & Bi, K. (2014). Effectiveness of using rubber bumper and restrainer on mitigating pounding and unseating damage of bridge structures subjected to spatially varying ground motions. *Engineering Structures*, *79*, 195-210.

Shrestha, B., Hao, H., & Bi, K. (2015). Seismic Response Analysis of Multiple-Frame Bridges with Unseating Restrainers Considering Ground Motion Spatial Variation and SSI. *Advances in Structural Engineering*, *18*(6), 873-892.

Shrestha, B., & Hao, H. (2015). Parametric study of seismic performance of superelastic shape memory alloy-reinforced bridge piers. *Structure and Infrastructure Engineering*, 1-14.

Soong, T. T., & Dargush, G.F. (1997) *Passive energy dissipation systems in structural engineering*. Wiley, London.

Strandgaard, H. (2000, April). *Design and application of energy-dissipating dampers on a new concrete bridge in California*. In SPIE's 7th Annual International Symposium on Smart Structures and Materials (pp. 400-411). International Society for Optics and Photonics.

Symans, M. D., Charney, F. A., Whittaker, A. S., Constantinou, M. C., Kircher, C. A., Johnson, M. W., & McNamara, R. J. (2008). Energy dissipation systems for seismic applications: current practice and recent developments. *Journal of Structural Engineering*, *134*(1), 3-21.

Trochalakis. P., Eberhard. M.O., & Stanton, J.F. (1997). Design of seismic restrainers for in-span hinges. *Journal of Structural Engineering ASCE, 123*(4), 469-478.

Vasseghi, A. (2011). Energy dissipating shear key for precast concrete girder bridges. *Scientia Iranica, 18*(3), 296-303.

Vlassis, A. G., Maragakis, E., & Saiidi, M. (2004). Experimental evaluation of longitudinal seismic performance of bridge restrainers at in-span hinges. *Journal of Testing and Evaluation, 32*(2), 96-105.

Watanabe, G., & Kawashima, K. (2004). *Effectiveness of cable-restrainer for mitigating rotation of a skewed bridge subjected to strong ground shaking*. 13th World Conference on Earthquake Engineering, New Zealand.

Yang, C. S. W., & DesRoches, R. (2015). Bridges with Innovative Buckling Restrained SMA Expansion Joints Having a High Symmetrical Tension/Compression Capacity. *Structures Congress 2015*, 452-461.

Zhang, Y., Hu, X., & Zhu, S. (2009). Seismic performance of benchmark base-isolated bridges with superelastic Cu-Al-Be restraining damping device. *Structural Control & Health Monitoring, 16*, 668-685.

Zhu, P., Abe, M., & Fujino, Y. (2004) Evaluation of pounding countermeasures and serviceability of elevated bridges during seismic excitation using 3D modelling. *Earthquake engineering & structural dynamics, 33*(5), 591-609.

CHAPTER 3
EXPERIMENTAL AND NUMERICAL ANALYSES ON POUNDING INTERACTION BETWEEN ADJACENT BRIDGE FRAMES SUBJECTED TO SPATIALLY VARYING GROUND MOTIONS

3.1 Abstract

Spatial variation of earthquake ground motions is inevitable at different supports of extended bridges structures. Relative displacements between bridge segments can be significantly amplified by the non-uniform ground motions, which in turn enhance the risk of pounding damages and unseating failures. This paper presents the results from large-scale shake table experiments, which were conducted at Central South University in China on two bridges models each with a total length of 16.67 m, to identify the effects of spatial variation of earthquake ground motion on the response of adjacent bridge segments. The emphasis is mainly put on pounding effect and relative displacement response. The experiments were also conducted to investigate the efficacy of superelastic Shape Memory Alloy (SMA) restrainers on mitigating relative displacement responses of the bridge models. The bridge models were subjected to stochastically simulated bi-directional spatially varying ground motions that are based on the Chinese code for the seismic design of Highway Bridges. Furthermore, numerical models based on the fiber section elements are developed and calibrated using the data from the testing. Parametrical investigations are performed on validated numerical models to study the effects of spatial variability of ground motions on the relative displacement responses of adjacent bridge segments.

3.2 Introduction

During major earthquakes adjacent segments of multiple-span bridges could suffer from damages resulting from out-of-phase vibrations of the bridge segments. The out-of-phase vibrations result in two major problems. Firstly, unseating failure of bridge span can occur if opening relative displacements between the bridge segments exceed the available seat widths. Many cases of the bridge collapse that occurred in recent earthquakes were attributed to this phenomenon (Kawashima et al., 2011; Comartin et al., 1995; Hall et al., 1996). Secondly, pounding of the adjacent segments occurs if the closing relative displacements exceed the limited expansion joint width usually provided in bridges. Poundings of the adjacent bridge segments have been observed in almost all major earthquakes, resulting in localized damages and crushing of concrete at the impacting location. Moreover, pounding between adjacent bridge segments results in the transfer of momentum that could lead to larger relative joint

opening displacement at expansion joints thus increasing the risk of unseating damage of bridge span (Ruangrasamme & Kawashima, 2001).

The out-of-phase vibration of extended bridge structures can result from the differences in the dynamic characteristics of adjacent bridge segments. Additionally, variations of earthquake ground motions along the length of the bridge can also lead to the out-of-phase vibrations. Spatially varying ground motions are inevitable along the support of extended bridges, which arise from the delayed arrival time of seismic waves as a result of finite wave speed, coherency losses due to reflection and refraction of seismic waves when they propagate through heterogeneous soil medium and site-response effect arising from different local soil sites at the bridge supports. Many previous investigations (e.g. Bi et al., 2011) have highlighted that the ground motion spatial variations have a significant effect on the seismic response, specifically on the relative displacement response of the bridge structures. However, when pounding of adjacent bridge structures is of concern, most of the previous studies focused on the influence of different dynamic characteristics of adjacent bridge segments, only very limited studies considered the spatial variation of the seismic ground motions (e.g. Shrestha et al., 2015; Bi & Hao, 2013; Bi et al., 2013, Bi & Hao, 2015; Chouw & Hao, 2005). It should be noted that it was demonstrated that spatially varying ground motions could lead to damaging seismic pounding between the adjacent bridge segments even when they have close fundamental periods (Chouw & Hao, 2008), indicating the recommended measure in many latest bridge codes (e.g. Caltrans, 2013) of adjusting the fundamental periods of adjacent bridge segments to mitigate the excessive relative displacement induced damages is inadequate. In other words, pounding cannot be completely precluded between adjacent bridge segments even with the same dynamic characteristics because of the inevitable spatial variation of earthquake ground motion.

Literature review reveals that studies on seismic pounding and unseating failure are not new (Hao et al., 2013), and several researches have been conducted in the past (Jankowski et al., 1998; DesRoches & Muthukumar, 2002; Muthukumar & DesRoches, 2005). However, most of the previous investigations used numerical or analytical methods to compute the pounding responses and experimental studies are rare. Experimental studies that consider the pounding of adjacent bridge segments resulting from inevitable spatial variation of ground motions are very limited due to the complexity as well as the cost involved and the special equipment required for this type of testing. To the best knowledge of the authors, only two previous investigations (Li et al., 2012; Li & Chouw, 2014) are found in the literature reporting the pounding response of adjacent bridge segments subjected to spatially varying input motions. However, due to the limitation of the available testing equipment, the experiments were

conducted on bridge models of very small scale (1/125). No experimental study of large-scale bridge model that considered pounding response of adjacent bridge frames to spatially varying ground motions has been reported yet in literature. Though the small-scale experimental studies shed some lights on the effects of spatially varying ground motion on the bridge pounding responses, they could not necessarily represent the localized damages, energy dissipation associated with pounding and inelastic responses of the bridge system due to the use of completely different materials than the prototype bridge in constructing the bridge model.

Restrainers are widely used in bridge retrofitting to prevent unseating of bridge span due to opening relative displacement exceeding the available bridge seat width. Conventionally steel restrainers were widely used to prevent unseating failures. However, its inefficiency was highlighted during the earthquakes in late 1980's and mid 1990's (Saiidi, 1993). The steel restrainers were found liable to yield during strong shakings, which greatly reduce the effectiveness of the restrainers in repeated cycles (Selna et al., 1989). Moreover, as steel restrainers are normally designed to remain elastic, it could also transfer large forces to adjacent bridge components. Recently, superelastic Shape Memory Alloy (SMA) restrainers, which can undergo large deformations without any significant permanent deformations owing to phase transformation, have received significant attention to mitigate unseating failure (Shrestha et al., 2016; Ozubulut et al., 2011). Various researches have been conducted numerically to investigate its effectiveness to avoid unseating failure on bridges subjected to uniform earthquake ground motions (DesRoches & Delemont, 2002; Andrawes & DesRoches, 2005; 2007) or non-uniform support motion (Shrestha et al., 2014). Some experimental studies were also conducted to identify the effectiveness of using superelastic SMA as bridge restrainers (Johnson et al., 2008; Padgett et al., 2010; Guo et al., 2012). However, it is to be noticed that previous experiments were either conducted on models of small-scale or did not consider full bridge system and spatial variability of the ground motions. All of these factors could have an influence on the response of the restrainers and the overall bridge system.

This paper presents results from experimental test recently carried out in Central South University, China, to identify the influence of spatially varying ground motions on the seismic response of a two-frame bridge, in which two large-scale models (scaled to 1/6). The length of the each frame comprising the two-frame bridge model was 8.33 m. The frames were separated by a gap in the middle of the bridge representing the expansion joint. A shake table array with two shake tables was used to excite the two adjacent bridges frames. Two sets of bridge models (i.e. in total four bridge frames with two frames in each bridge model) were

prepared to investigate bridge pounding responses and the effectiveness of superelastic SMA restrainer on mitigating pounding and unseating damages.

The main objective of this study is to carry out large-scale experiments to identify, i) the effects of spatially varying ground motions on the pounding response of the adjacent bridge segments, ii) the effectiveness of SMA restrainers to mitigate the relative displacement responses, and iii) to capture pounding induced localized damages to the bridge frames. A finite element software SeismoStruct is used to develop the numerical model, which are validated using the experimental data. Subsequently, parametric analyses are carried out numerically to supplement the findings from the experimental study. To the best knowledge of the authors, experiment of this nature and scale have not been performed previously. The pervious tests of large-scale bridge models either neglected the spatial variation of ground motions (Cruz Noguez & Saiidi, 2011; Weiser et al., 2014) or neglected the pounding effect (Saiidi et al., 2013; Johnson et al., 2008). Thus, the result provided herein could have a significant relevance to the design of the bridges that are susceptible to relative displacement induced damages such as pounding and unseating.

3.3 Experimental details

3.3.1 Bridge model

The test models for the experiment were scaled representations of a prototype two-frame bridge, scaled to 1/6 following the rules of similitude relations (Dove & Bennett, 1986) as presented in Table 3-1. The length of each pre-stressed box girder frame was 8.33 m, and the total length of the dual-frame bridge model was 16.67 m. The deck of the bridge model was 1.5 m wide, and the height varied from 0.4 m at bent cap to 0.2 m at the cantilever end of the deck. The bridge models were pre-stressed using two-15 mm diameter tendons on the both webs. The bent of the bridge frame contained two square piers of size 0.25 m x 0.25 m with 1.23% longitudinal reinforcement ratio. The integral layout of the test bridge is shown in Figure 3-1. Figure 3-2 presents schematic details of the test bridge.

The bridges models were tested for two conditions, i.e., without any mitigation device (referred as set 1 bridge model) and with superelastic SMA restraining devices (referred as set 2 bridge model). Due to the limitation of the testing facility (only two shake tables were available in the laboratory when the testing were carried out) abutments at the two ends of the bridge were not constructed. It should be noted that the presence of abutment can also influence the pounding responses (Li et al., 2013; Wieser, 2014), which cannot be considered in the present study. The tests were conducted progressively by gradually increasing the ground motion intensity until the safe operational capacity of the shake tables was reached.

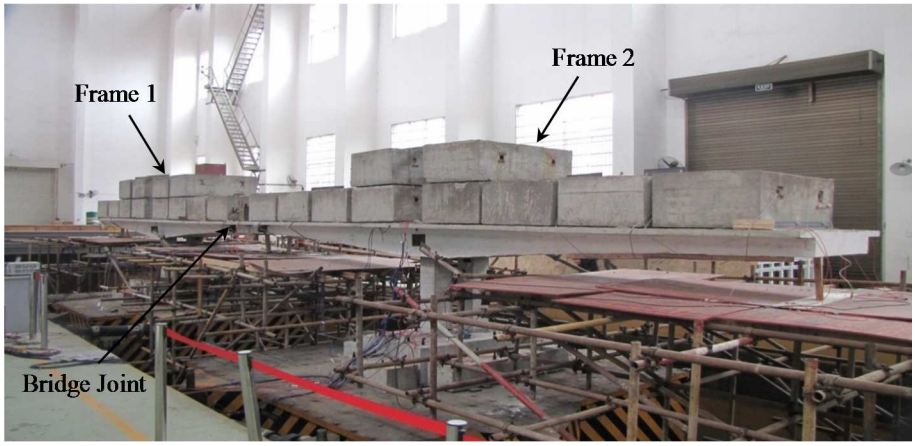

Figure 3-1 Experimental bridge model on shake table.

To realistically simulate the inelastic deformation of the structure, reinforced concrete of the same grade as the prototype bridge was used for the model. The specified concrete strength was 30 MPa and 40 MPa for the piers and the pre-stressed deck, respectively. The nominal yield strength of the reinforcement bars was 400 MPa. The self-weight of each bridge frame was 3.79 tons, and the weight of foundation was 1.95 tons. To simulate the seismic response of the prototype bridge frame, additional weights were added to the bridge frames using concrete blocks of 1.3 tons each. Twelve concrete blocks were placed on the first frame (frame 1) and ten concrete blocks were placed on the second frame (frame 2) to represent a bridge system having slightly different fundamental periods of two adjacent frames. The fundamental period of the frame 1 was 0.61 sec (t1), and that of frame 2 was 0.58 sec (t2). The fundamental periods of the frames were quite close (t2/t1 = 0.95) with each other following the requirement of the modern bridge codes (t2/t1 ≥ 0.70) (Caltrans, 2013). The total weight of the first bridge frame was 21.34 tons while the second frame was 2.6 tons lighter than the frame 1.

3.3.2 Shake-table array and Instrumentation

The experiments were conducted using a shake table array located at National Engineering Laboratory of High-Speed Railway Construction, Central South University, China. Two shake tables having size of 4 m x 4 m with a working frequency range of 0.1-50 Hz, and payload capacity of 30 tons were used for the testing.

The responses of the model bridges were recorded using an 80-channel data logger system. The channels were connected to accelerometers, strain gauges, LVDTs and load cells to measure the response of the bridge deck, piers and restrainers. Additionally, some data acquisition channels were used to record displacements and accelerations of the shake tables. Transverse and longitudinal displacements and accelerations of the bridge deck, relative displacement at the expansion joint, strains in the longitudinal and transverse reinforcement bars at critical sections of the piers and longitudinal bars in the bridge deck at expansion joint,

and curvatures at column plastic hinge zones were measured. As the primary objective of the experiment was to evaluate the pounding response and damages at expansion joint, a denser array of transducers was placed at the expansion joint of the bridge. Details of the instrumentation at the expansion joint are presented in Figure 3-3. Two accelerometers were placed at each corner of the bridge deck at the joint of both frames to record the longitudinal acceleration as well as the acceleration pulses generated during the impacts between the adjacent bridge decks. Additionally, accelerometers were placed in the same locations to record acceleration in the transverse direction. Two vertical accelerometers were used to measure the vertical vibration of the adjacent decks. Two LVDTs were placed at the corners of the deck to measure the relative displacement at the joint.

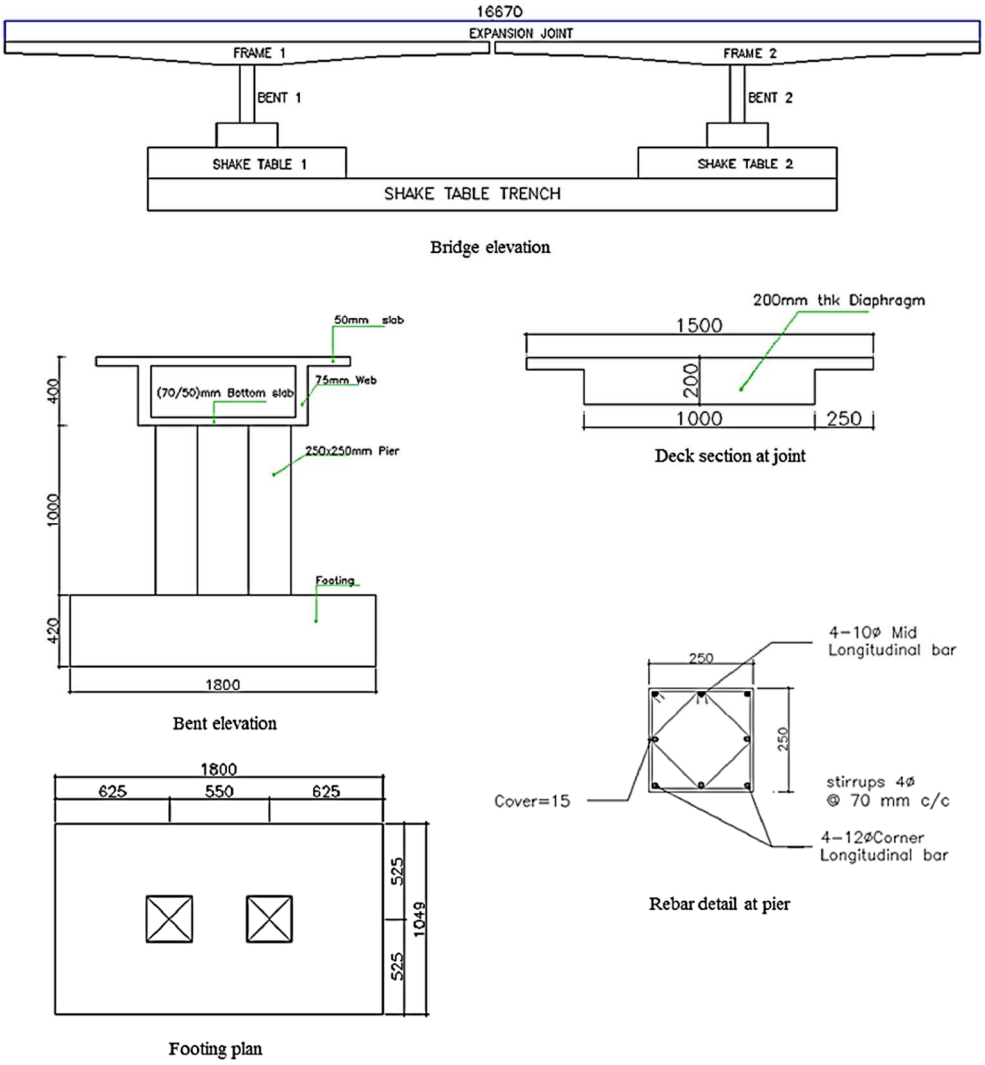

Figure 3-2 Details of the model bridge (dimension in mm).

Table 3-1 Similitude requirements of the bridge model

Type	Physical quantity	Similitude relation	Similitude parameter
Structural geometry	Length, L	N_L	1/6
	Displacement, δ	N_δ	1/6
Material properties	Elastic modulus, E	N_E	1
	Stress, σ	N_σ	1
	Strain, ε	N_ε	1
Dynamic Indicator	Mass, m	$N_m = N_E N_L^2 / N_a$	1/36
	Time, t	$Nt = \sqrt{(N_L / N_a)}$	1/2.45
Loads	Force, F	$N_F = N_m N_a$	1/36
	Moment, M	$N_M = N_F N_L$	1/216

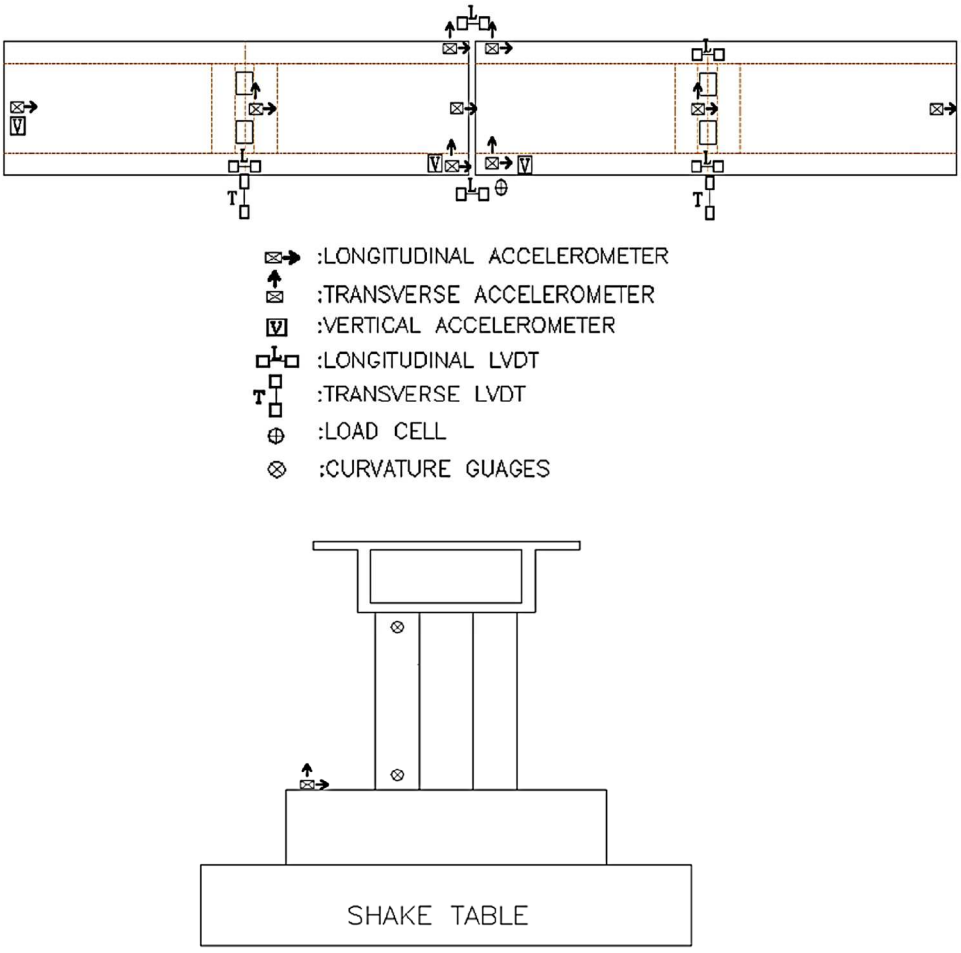

Figure 3-3 Arrangement of sensors on bridge model.

3.4 Loading Protocol

Spatially varying ground motions compatible with the design spectra of site class IV in the Chinese code for the Seismic design of Highway Bridge were stochastically simulated based on the method proposed by Bi and Hao (2012). These motions were used as inputs to the two shake tables.

The spatial variation properties between ground motions recorded at two locations *j* and *k* on the ground surface is modelled by an empirical coherency loss function (Sobcyzk, 1991).

$$\gamma_{jk}(i\omega) = \left|\gamma_{jk}(i\omega)\right| \exp(-i\omega d_{jk} \cos\alpha / v_{app}) = \exp(-\beta\omega d_{jk}^2 / v_{app}) \cdot \exp(-i\omega d_{jk} \cos\alpha / v_{app}) \quad (3.1)$$

where β is a constant reflecting the level of coherency loss, and β =0.0008, which represents an intermediate coherency loss between the two sites, was used in the present study. d_{jk} is the distance between the two locations in the wave propagation direction, f is the frequency in Hz, v_{app} is the apparent wave velocity, and α is the seismic wave incident angle. In the present study, v_{app} was assumed to be 500 m/s, and $\alpha = 60°$. In the simulations, the sampling and upper cut-off frequencies were set to be 100 and 25 Hz, respectively, and the duration of 20.47 sec was selected to have a convenient total number of points (2048) for a fast Fourier transform. Figure 3-4 (a) and (b) show the comparisons between simulated and model response spectra and coherency loss function. Figure 3-4 (c) shows the displacement time-histories at the two shake tables, where Site 1 and Site 2 represents the shake tables.

The simulated spatially varying ground motions were scaled from 0.25g to 0.90g and used for 8 test runs as shown in Table 3-2. For the uniform ground motion cases, ground motions simulated for site 1 (shake table 1) were also applied to site 2 (shake table 2). The time axis of the motions was compressed by 2.45 times to account for the scale of the model.

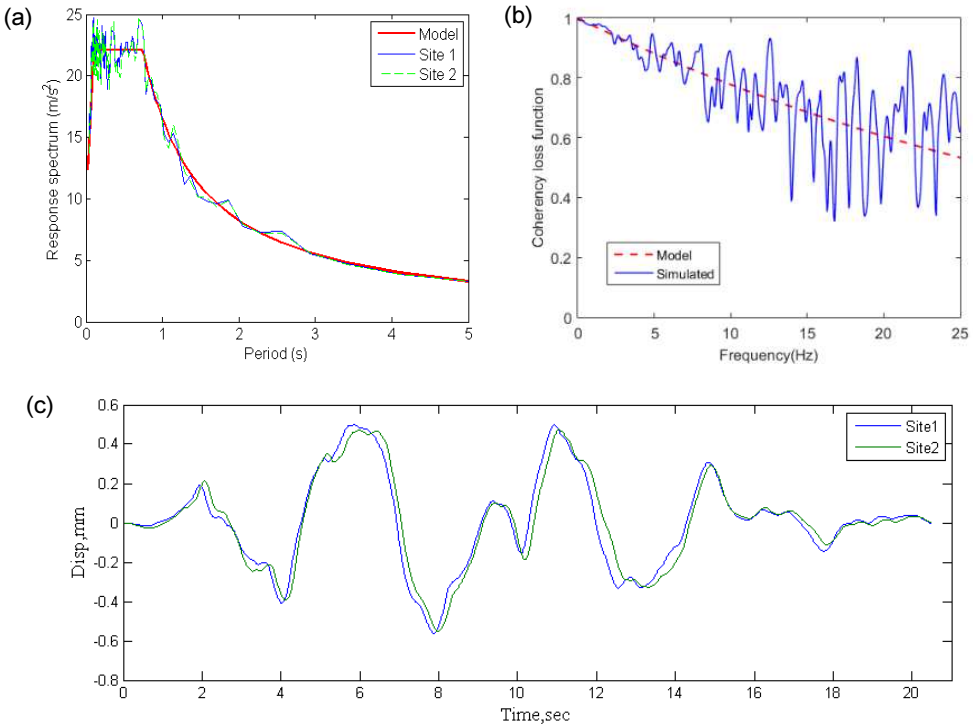

Figure 3-4. Comparisons between the simulated ground motions and corresponding models (a) response spectra; (b) coherency loss function; (c) displacement time history.

Table 3-2 Loading protocol for the testing

Test ID	PGA (g)	Motion type
Run1	0.25	Uniform
Run2	0.25	Spatially varying
Run3	0.40	Uniform
Run4	0.40	Spatially varying
Run5	0.50	Spatially varying
Run6	0.60	Spatially varying
Run7	0.75	Spatially varying
Run8	0.90	Spatially varying

3.5 Shape memory alloy restrainers

Nickel-Titanium (Nitinol) superelastic SMA wires of diameter 0.7 mm were used to form the restraining devices. Cyclic tensile loading tests were performed on the SMA wires at various frequencies. For the cyclic testing SMA wires were tested at a constant strain amplitude of 6%. In this study, the mechanical characteristics of the SMA wires observed at 2 Hz (two cycles of 6% strain per sec), as presented in Figure 3-5, is used to represent the stress-strain behavior of SMA restrainer under the seismic loading. The mechanical characteristics for the SMA wire at 2 Hz could be summarized as modulus of elasticity of 34000 MPa,

transformation stress of 340 MPa and equivalent damping ratio of 3.30%. The damping ratio was obtained based on the standard definition of the equivalent damping ratio as $\Delta W_D / (4\pi \Delta W_S)$, where ΔW_D is the dissipated energy and ΔW_S is the maximum elastic strain energy in a loading cycle.

The restrainers composed of bundled superelastic SMA wires were used to connect the two bridge frames. The length of the restraining cables was 200 mm and had the total cross-sectional area of 20.79 mm^2, i.e. 54 wires of 0.7 mm diameter. For the first four test runs a single restrainers were placed on each side of the bridge deck. For high-intensity testing runs (i.e. run 5 to run 8) two restrainers were placed on each side of the deck. The placement of the restrainers on the bridge deck can be seen in Figure 3-6 (b).

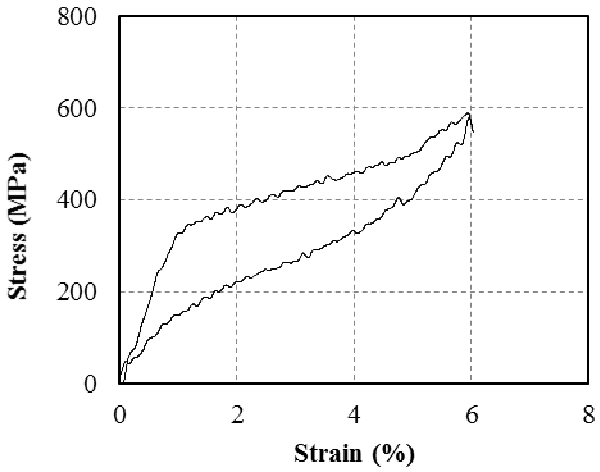

Figure 3-5 Stress-strain relationship of superelastic SMA at 2 Hz.

3.6 Experimental results

3.6.1 Seismic interaction at expansion joint

To investigate the pounding interaction at the expansion joint of the bridge, acceleration measurements from the sensors shown in Figure 3-3, as well as the observed damages are discussed in this section.

3.6.2 Observed Pounding damages

Pounding between adjacent bridge segments results in damages to the bridge superstructures, especially at impacting locations. Poundings between adjacent girders do not necessarily take place along the entire surface of the bridge deck. As shown in Figure 3-6 (a), poundings between the adjacent bridge segments were usually confined to the smaller region within the impacting surface. This concentration of impact in the smaller area resulted in high stresses in

the area, which in turn led to crushing and spalling of concrete. Poundings were also found to occur frequently at the edges of the bridge girder as shown in Figure 3-6 (b). These pounding behaviors could be attributed firstly to the imperfection during the construction of the bridge models, due to which the impacting surfaces were not exactly even. Secondly, the bridge responses in the longitudinal direction were coupled with that in the transverse direction due to the simultaneous action of spatially varying transverse ground motions. This coupling of motions in two lateral directions might have resulted in a slight torsional motion that led to the damages particularly at the edges of the deck as shown in Figure 3-6 (b). However, more noticeable pounding damages were found to be resulting from the longitudinal motion coupled with the large vertical vibration of the cantilevered bridge deck, as visible in Figure 3-6 (a), and further discussed in subsequent section.

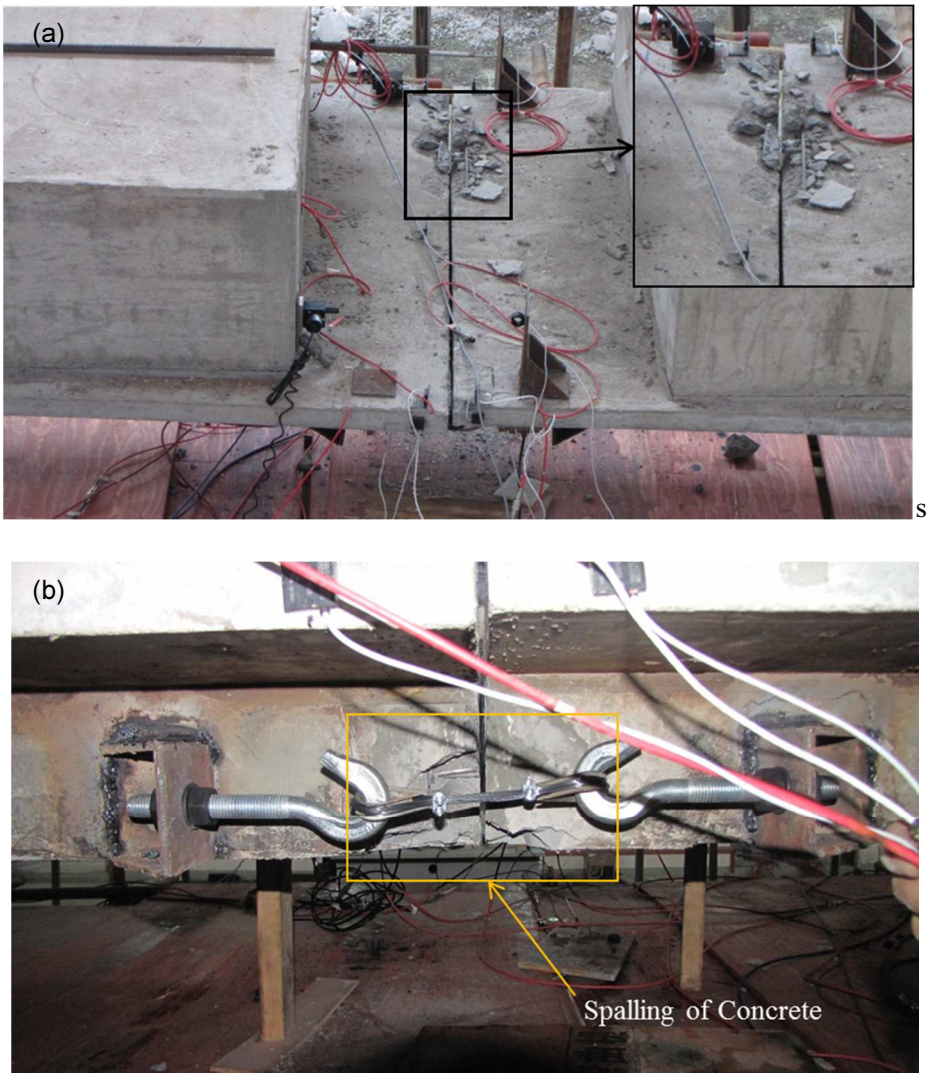

Figure 3-6 Pounding damages at the expansion joint.

3.6.2.1 Interaction mechanisms at expansion joint

Pounding between bridge segments created sharp spikes in the acceleration time histories resulting from short period forces generated during impacts between the adjacent segments and engagements of cable restrainers. Pounding interaction mechanisms could be classified into three different categories, namely, the frictional contact (Figure 3-7 (a) and (b)), oblique head-on contact (Figure 3-7 (c) and (d)) and cable engagement (Figure 3-7 (e)) (Malhotra et al., 1995). These three different mechanisms are discussed here.

3.6.2.1.1 Mechanism 1- frictional contact

In this contact mechanism, as illustrated in Figure 3-7 (a) and (b), only partial surface of the adjacent bridge segments contact each other owing to the vibration of bridge deck in transverse or vertical motion along with the longitudinal motion. Sliding between the surfaces in contact would occur once the frictional resistance between the two surfaces is overcome. The contact would result in a pair of equal and opposite friction force F_T, generated in the transverse direction or F_V, in the vertical direction. These forces result in equal and opposite acceleration spikes in the transverse or the vertical direction. These frictional forces are accompanied by axial compressive forces due to the compression of bridge decks while in contact, resulting in the acceleration spikes in the longitudinal direction.

3.6.2.1.2 Mechanism 2- head-on impact

Acceleration spikes are generated predominantly in the longitudinal direction resulting from head-on impacts between adjacent bridge segments undergoing mainly longitudinal motion. Though the response is predominantly in the longitudinal direction, some torsional and rocking responses in the transverse and vertical directions, as shown in Figure 3-7 (c) and (d), could occur simultaneously. Therefore, the acceleration spikes could also be presented in transverse and vertical directions in addition to the longitudinal direction. In this case, however, the forces developed in the transverse or vertical direction are in the same direction. Therefore, the resulting acceleration spikes will also have the same direction.

3.6.2.1.3 Mechanism 3- restrainer engagement

The two adjacent segments, undergoing longitudinal and transverse motions, can result in relative opening displacement between the adjacent segments and activate the restrainers. The forces generated in the restrainers would pull the two segments back. Cable forces in the longitudinal and transverse directions result in acceleration spikes in the respective directions. The longitudinal force, which is equal and opposite in magnitude in the axial direction of cable restrainers, results in the acceleration spikes in the longitudinal direction.

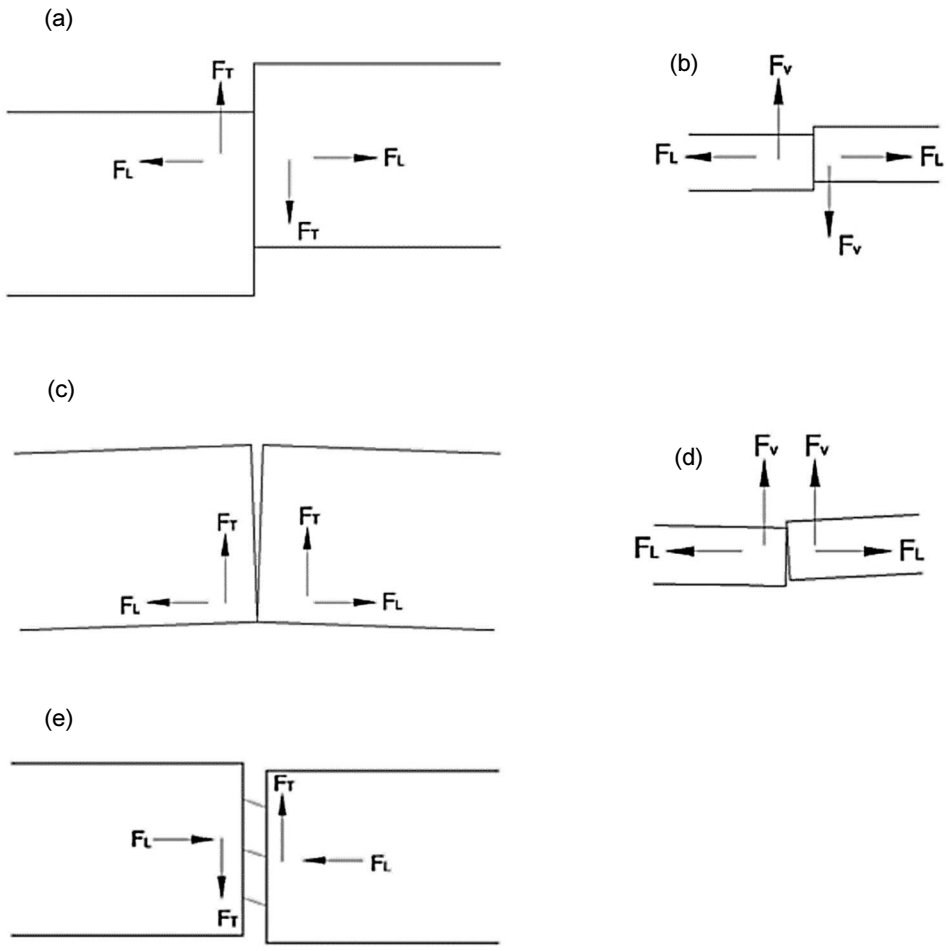

Figure 3-7 Interaction mechanisms at bridge expansion joint: (a) frictional contact between adjacent segments undergoing transverse motions, (b) elevation view of frictional contact between adjacent segments undergoing vertical motion, (c) Oblique head-on impact between adjacent segments undergoing predominantly longitudinal motion, (d) elevation view of oblique head-on impact with vertical movement combined with longitudinal motion, (e) cable engagement.

3.6.2.2 Observed interaction at expansion joint

Figure 3-8 presents the recorded acceleration time histories at the expansion joint of the model bridge set 1 during test run 4. Acceleration measurements in the longitudinal, transverse and vertical directions are presented in Figure 3-8 (a), (b) and (c), respectively. It is observed in Figure 3-8 (a) that nearly equal and opposite acceleration pulses were measured in the longitudinal direction of the two frames at three instances of around 1.75, 4.21 and 5.96 sec. However, only a single clear pulse around 5.96 sec is observable in the transverse direction as presented in Figure 3-8 (b). As shown in the zoom-in view (Figure 3-8 (d)), it is obvious that acceleration pulses at both the frames are in the same direction, implying that pounding forces are also in the same direction. Thus, these acceleration spikes are apparently the result of Mechanism 2, i.e. head-on impact with slight oblique angle. It is also noticeable that the third

longitudinal acceleration spike is accompanied by acceleration spike in the vertical direction, as shown in Figure 3-8 (c). This indicates the three-dimensional nature of the pounding because of the unrestrained movement of the cantilever deck ends in the vertical direction. Moreover, all three longitudinal acceleration spikes are accompanied by the vertical acceleration spikes, indicating a strong coupling between the vertical and the longitudinal motions. Zoom-in view of the second acceleration spike in the vertical direction is shown in Figure 3-8 (e). In this case, the acceleration spike measured at two frames showed opposite direction indicating Mechanism 1-frictional contact.

3.6.3 Effect of spatially varying ground motions

To evaluate the effect of spatially varying ground motions on the response of bridge system and pounding at expansion joint, the results from the first four runs of bridge models are analyzed. Figure 3-9 (a) shows the measured relative displacements at the expansion joint during run 1 and run 2 of set 1 model. Large relative opening and closing displacements are visible in the case of spatially varying ground motions (run 2) compared to the uniform ground motion (run 1). It is also observable that relative displacement is still substantial even when the uniform ground motion is considered. This observation could be attributed to the slightly different dynamic periods of the two adjacent bridge frames. It is also to be noted that relative displacement measurements at expansion joint were affected by the vertical vibrations of the cantilever bridge decks. As a result, the measured displacements could be slightly higher than the actual relative displacement in the longitudinal direction. As can be seen in Figure 3-9 (a), the measured closing relative displacement during run 2 is 8.57 mm at 4.74 sec, which exceeds the gap width of 8 mm. However, as shown in Figure 3-9 (b), acceleration spike resulting from poundings is not observable at this instant, suggesting that the actual closing relative displacements to be lower than the measured one. This is because the LVDTs placed at the bridge joint to measure horizontal relative displacements were influenced by vertical relative motion between the adjacent decks. Therefore, LVDT were measuring oblique separation distance between the two decks instead of the horizontal one when the bridge decks were not at same elevation. This phenomenon significantly influence the relative displacement measurement.

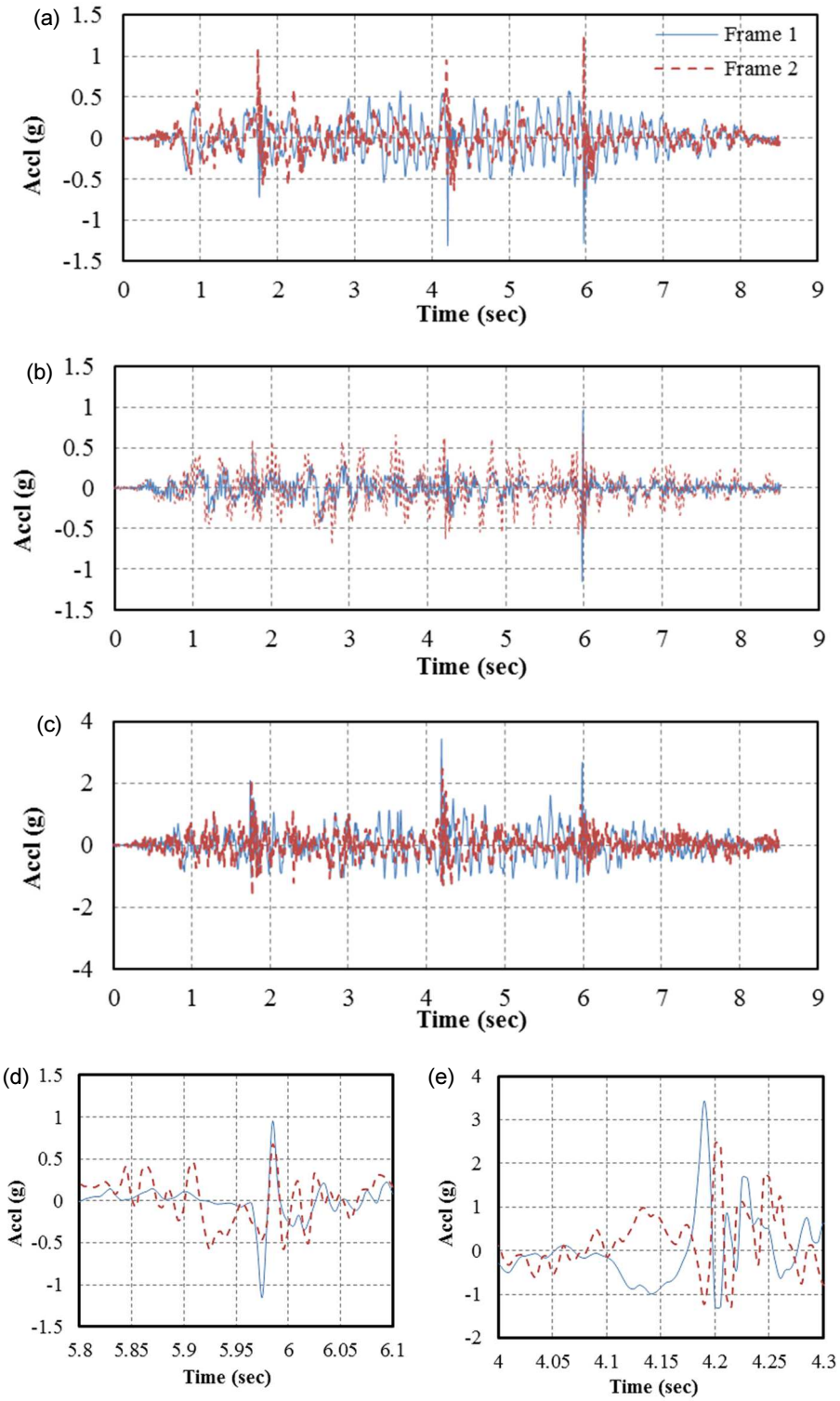

Figure 3-8 Measured acceleration time histories in the (a) longitudinal direction; (b) transverse direction; (c) vertical direction; (d) zoom-in view of acceleration in the transverse direction; (e) zoom-in view of acceleration in the vertical direction.

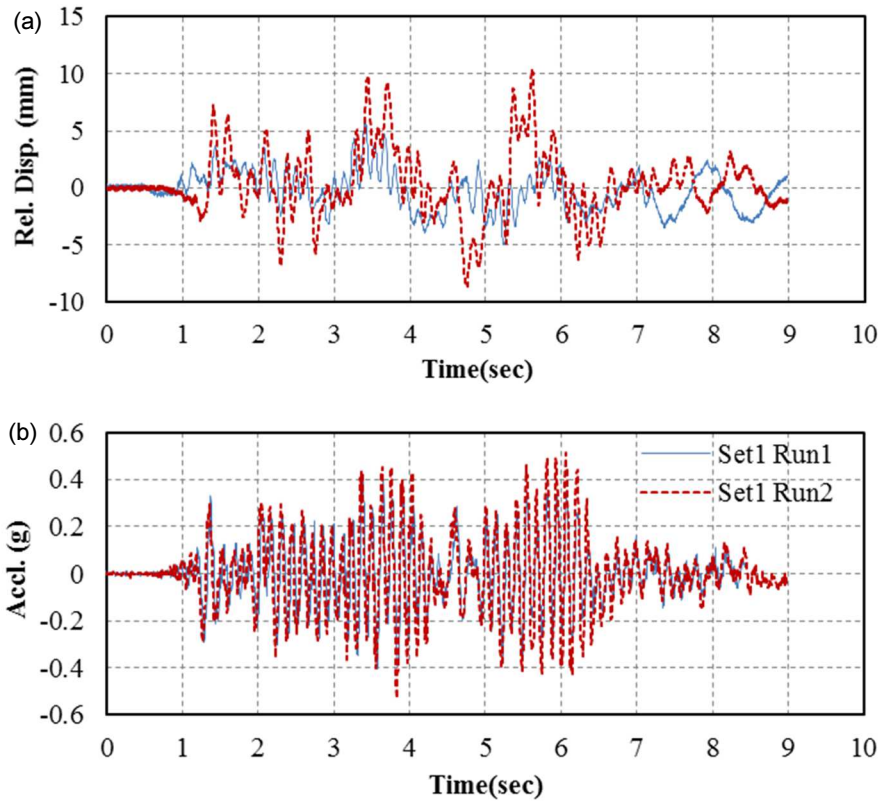

Figure 3-9 (a) Relative displacements; (b) acceleration time histories of set 1 bridge model during test run 1 and run 2

Figure 3-10 (a) shows relative displacements measured at expansion joints of set 1 bridge model during run 3 and run 4. Comparatively larger relative opening and closing displacements were observed when ground motions were spatially varying (set1 run 4). Figure 3-10 (b) shows the measured acceleration time histories at bridge expansion joint. Three acceleration spikes are clearly visible in run 4 due to strong poundings between the adjacent segments. However, as shown in Figure 3-10 (a) closing relative displacement exceed the gap width of 8 mm on more than these three occasions but no acceleration spikes are visible at these incidents. These phenomena again indicate towards to the inaccurate relative displacement measurement at bridge joints due to the influence of vertical vibrations of the cantilever decks as mentioned previously. Therefore, the relative displacements measured during the testing should be used with caution. In this study, numerical simulations calibrated against the other measurements (e.g. displacement measurement at middle of the frame and acceleration measurements) are thus used to identify the relative displacement at the bridge expansion joint and presented in the subsequent sections. Nonetheless, the experimental results clearly indicate that the relative displacement under spatially varying ground motions could be significantly larger than those under uniform ground motion. These large relative displacements could lead to pounding of adjacent bridge components under strong earthquakes even when the two adjacent structures with close fundamental periods.

Figure 3-11 (a) and (b) compare the measured longitudinal peak accelerations at the bridge joint corresponding to the uniform and spatially varying ground motion inputs at two intensities (0.25 g and 0.40 g). As presented in the figures, peak deck accelerations are quite similar for both cases (uniform and spatially varying ground motion) at the intensity of 0.25 g. However, a significant increase in peak deck accelerations is observed in the case of spatially varying ground motions at the intensity of 0.4 g, as pounding between the adjacent bridge segments occurred.

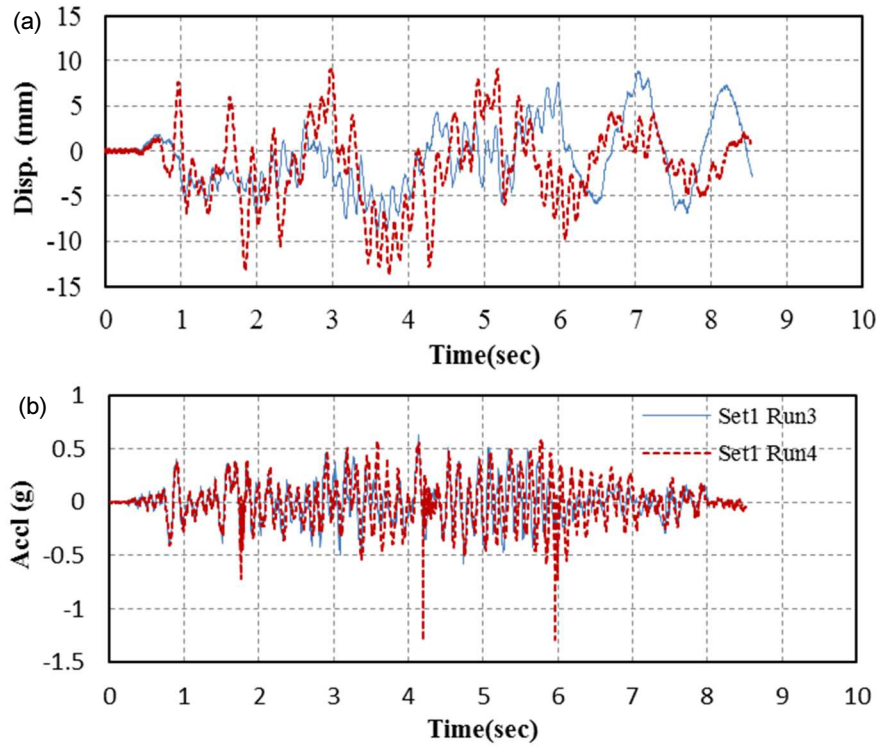

Figure 3-10 Relative displacements (a), and acceleration time histories (b) of set 1 bridge model during test run 3 and run 4.

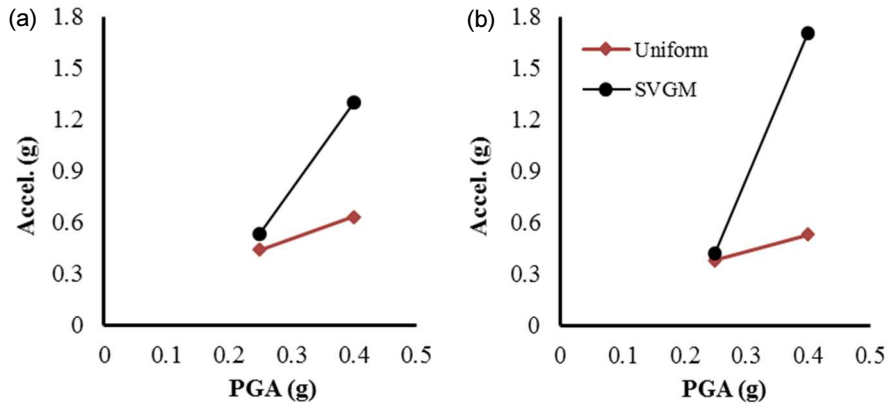

Figure 3-11 Measured longitudinal peak accelerations at decks of the model bridge at (a) frame 1, (b) frame 2.

Pounding between adjacent frames not only results in localized damages at the joint but also affects the response of the bridge system. The responses of the bridge piers could be altered due to pounding of adjacent bridge segments. This phenomenon is observed as pounding impedes the movement of bridge frames thus could result in lower drift of bridge piers. Alternatively, pounding of bridge segments could result in the transfer of momentum from a bridge segment to the other, leading to the larger deformation of stiffer bridge frame. Figure 3-12 shows the comparison of chord rotation at the pier base of frame 1 and frame 2 during run 3 and run 4. It is observed that uniform ground motion usually results in the larger rotation at pier base compared to the non-uniform ground motion. Careful observation of pier response at instance of poundings reveal slight reduction in the responses of the piers on both the frames. This is expected as the pounding impedes the movement of frames, which in turn reduced the responses of the bridge pier. The pounding between the adjacent decks occurred for a small fraction of a second therefore its effect on the response of bridge piers were slight. However, this observation may not be readily generalized, as previous investigations (Raungrasamee & Kawashima, 2001) have showed pounding might lead to adverse effects on pier responses particularly when adjacent segments have large differences in fundamental periods.

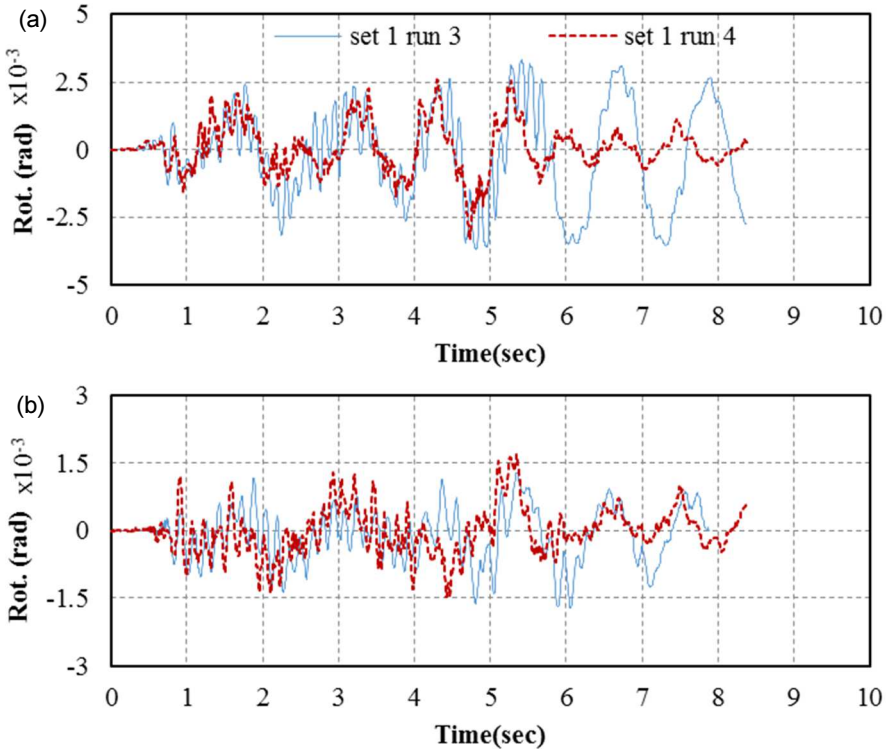

Figure 3-12 Rotations at the base of pier of (a) frame 1 and (b) frame 2 of set 1 bridge model.

3.6.4 Effect of restraining device

Restraining devices are provided to inhibit the relative opening movement at the bridge joint. Presence of the restrainers also affects the response of the bridge system. To investigate the effect of restraining device on the responses of the bridge subjected to spatially varying ground motions the results obtained from the both sets of bridge models are compared and discussed.

Figure 3-13 shows the comparison of longitudinal acceleration time histories at the joint measured at frame 1 for both sets of bridge models during test run 4. As shown, for bridge set 1, i.e. bridge model without the restraining devices, three acceleration spikes are visible at 1.75, 4.21 and 5.96 sec, respectively. It is also observed that the measured peak deck acceleration is 1.33 g. For Set 2 bridge model, four poundings occur at 1.67, 2.16, 4.66 and 5.61 sec and the peak acceleration is 0.89 g. The results suggest that due to the activation of the restrainer, acceleration responses of the bridge could be modified and the peak acceleration response could be reduced. However, the number of poundings between the adjacent bridge frames could increase.

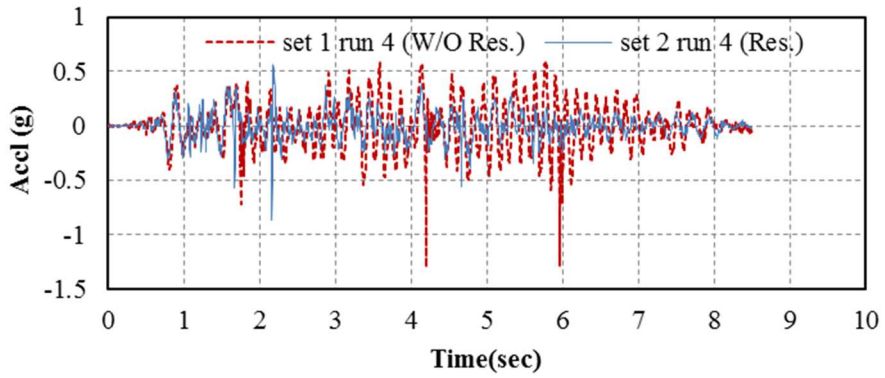

Figure 3-13 Longitudinal acceleration time histories measured at expansion joint of frame 1 of two models in test run 4.

Table 3-3 summarizes the testing results. The results from the set 1 bridge model are shown in normal fonts, and those from the set 2 bridge model are presented in bold italics fonts. Similar to the results observed in Figure 3-13, it is found that the restrainers, in general, result in lower peak deck acceleration but increases the number of impacts. This phenomenon could be attributed to the behavior of the restrainers that inhibit opening relative displacement, as a result of which the approaching velocity between the adjacent decks becomes lower. However, the restriction on the deck movement could increase the number of impacts between the adjacent frames. Significant difference in numbers of impact is observed for two sets of bridge models in run 8. During the test of set 1 bridge model the shake tables stopped at 6 seconds due to the excessive yawing movement of the tables, while the full run was completed for set 2 bridge model. This differences in run time between the two models caused the significant

difference in numbers of impact between these two cases. The restrainers also resulted in differences of the peak absolute displacements of the two bridge models. Due to the activation of the restrainers, responses of the bridge frames could either reduce or increase, however, in majority of cases slight increase is observed for frame 2 and vice versa for frame 1. A possible reason for this observation is described in subsequent paragraph. Unfortunately, due to the excessive movement and large acceleration impulse the LVDTs dislocated from their original positions during the final run. Therefore, the frame displacement during the last run (run 8) was not properly recorded and hence not presented in the table.

Table 3-3. Peak accelerations and displacements of bridge models.

Case ID	Motion type	Absolute Displacement		Peak Acceleration		Impact numbers
		frame 1 (mm)	frame 2 (mm)	frame 1 (g)	frame 2 (g)	
Set 1 run 1	Uniform	18.37	21.12	0.41	0.39	0
Set 2 run 1		***20.57***	***19.26***	***0.37***	***0.29***	***0***
Set 1 run 2	Spatially varying	26.33	27.56	0.54	0.43	0
Set 2 run 2		***27.19***	***26.38***	***0.38***	***0.30***	***0***
Set 1 run 3	Uniform	41.9	47.06	0.65	0.56	0
Set 2 run 3		***42.81***	***48.67***	***0.59***	***0.61***	***0***
Set 1 run 4	Spatially varying	43.46	44.07	1.33	1.18	3
Set 2 run 4		***38.06***	***43.68***	***0.89***	***1.40***	***4***
Set 1 run 5	Spatially varying	44.01	43.18	0.99	1.29	4
Set 2 run 5		***41.1***	***43.87***	***0.98***	***1.46***	***4***
Set 1 run 6	Spatially varying	57.31	66.44	1.94	3.37	5
Set 2 run 6		***51.49***	***72.84***	***1.16***	***1.47***	***10***
Set 1 run 7	Spatially varying	68.27	65.46	2.21	2.41	7
Set 2 run 7		***62.19***	***68.39***	***2.13***	***1.92***	***11***
Set 1 run 8*	Spatially varying	-	-	2.50	2.01	6
Set 2 run 8		-	-	***1.31***	***1.85***	***12***

* Test run terminated at 6 second.

Figure 3-14 (a) and (b) present the chord rotations at the base of the piers of frame 1 and frame 2 of the two bridge models. The responses of the bridge piers were also affected. As presented in the figure, piers of frame 1 of the bridge model with restrainers have lower response compared to the bridge model without restrainers. However, for the frame 2, the responses of the bridge model with restrainers were amplified. Therefore, piers of the frame 1 were beneficially influenced by restrainers while those of frame 2 were adversely affected. These

observations are consistent with the observation of absolute frame displacement discussed above and may have resulted due to the frame 1 pulling the slightly stiffer and lighter frame 2 resulting in the higher responses. These observation indicate that the connecting the adjacent frames with restrainers leads to larger responses of light and stiffer adjacent frames as the heavier adjacent frame pulls it.

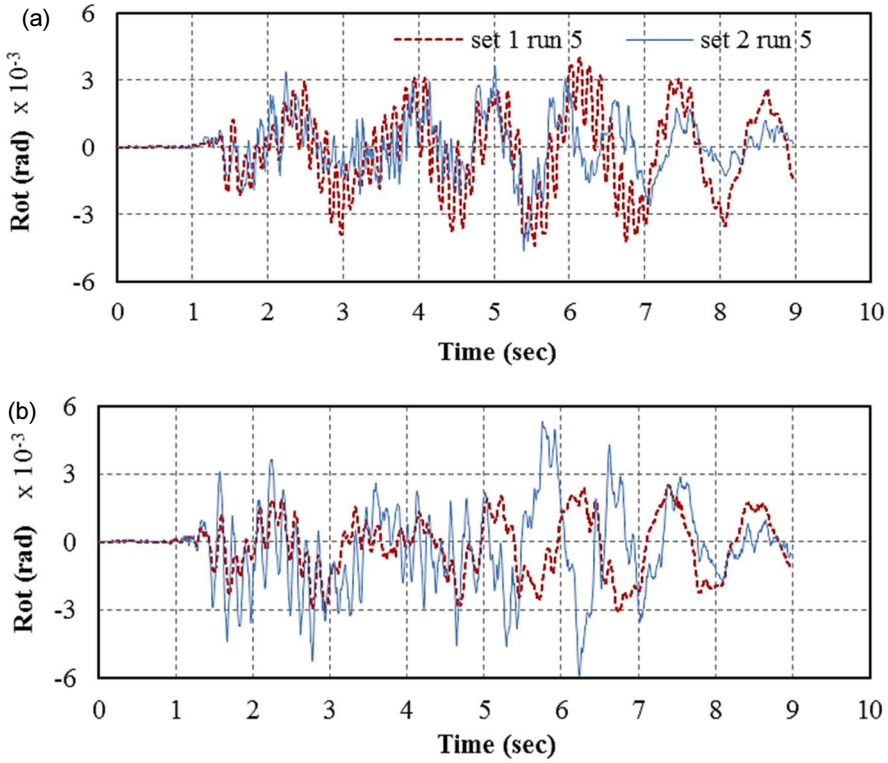

Figure 3-14 Chord rotations at base of the piers of (a) frame 1 and (b) frame 2.

3.7 Numerical Simulations

3.7.1 Numerical model

The numerical models of the test bridges are developed in a nonlinear software package Seismostruct (Seismosoft, 2006). Fiber section model capable of simulating the distribution of inelasticity along and across the reinforced concrete is used to model the inelastic response of the members. Force based inelastic frame elements are used to model piers of the bridge frames. The confined and unconfined concrete are modelled using the nonlinear constitutive relationships proposed by Mander et al. (1988). Steel reinforcements are modelled using Menegotto-Pinto steel model. The post-tensioned bridge decks are modelled using elastic elements.

Structural impacts are considered using the force-based method, where a contact spring together with a damper is used to simulate impact (Figure 3-15). This element is activated

when closing relative displacement exceeds the provided gap width. The interpenetration depth and the stiffness of the contact spring are used to estimate the contact forces that are applied to the structures according to the impact model. The damper is used to simulate the energy dissipation during the impact. In this study, modified linear viscoelastic impact model proposed by Komodromos et al. (2007) is used. This impact model has a distinct advantage over the conventionally used linear viscoelastic models of avoiding the tensile force arising at the end of the restitution period. The impact force can be calculated by:

$$F_{imp}(t+\Delta t) = k_{imp}.\delta(t) + c_{imp}.\dot{\delta}(t) \quad \text{when } F_{imp}(t) > 0 \tag{3.2}$$

$$F_{imp}(t+\Delta t) = 0 \quad \text{when } F_{imp}(t) \leq 0 \tag{3.3}$$

where k_{imp} is the stiffness of the linear impact spring, $\delta(t)$ is the interpenetration depth of the colliding bodies, c_{imp} is the impact damping coefficient, and $\dot{\delta}(t)$ is the relative velocity between the colliding structures. Anagnostopoulos (1988, 2004) has provided the following analytical expressions that associate the impact damping coefficient with the coefficient of restitution (e) and the masses m_1 and m_2 of the colliding bodies:

$$c_{imp} = 2\xi_{imp}\sqrt{k_{imp}\frac{m_1 \cdot m_2}{m_1 + m_2}} \tag{3.4}$$

$$\xi_{imp} = -\frac{\ln(e)}{\sqrt{\pi^2 + \ln(e)^2}} \tag{3.5}$$

where ξ_{imp} is the impact damping ratio. The coefficient of restitution, e, is defined as the ratio of the relative velocities between the colliding bodies after and before impact, which is assumed to be 0.65 in the present study (Anagnostopoulos, 1988; Jankowski, 2010).

The impact stiffness k_{imp} can normally be estimated as

$$k_{imp} = \gamma\frac{AE}{L} \tag{3.6}$$

where E, A, and L depends on the geometrical and material property of adjacent bridge girder and γ is the ratio of impact spring stiffness to the stiffness of the bridge superstructure. The impact stiffness of the springs is assigned 583500 kN/m in the present study, based on the preliminary analysis as this value led to the close match to the measured peak acceleration. This value represents γ of nearly 0.7. The numerical model of the bridge along with the contact

elements are presented in Figure 3-15. As shown in the figure, five distributed gap elements are used at the expansion joint to model impact concentration on the particular regions of the deck surface as shown in Figure 3-15.

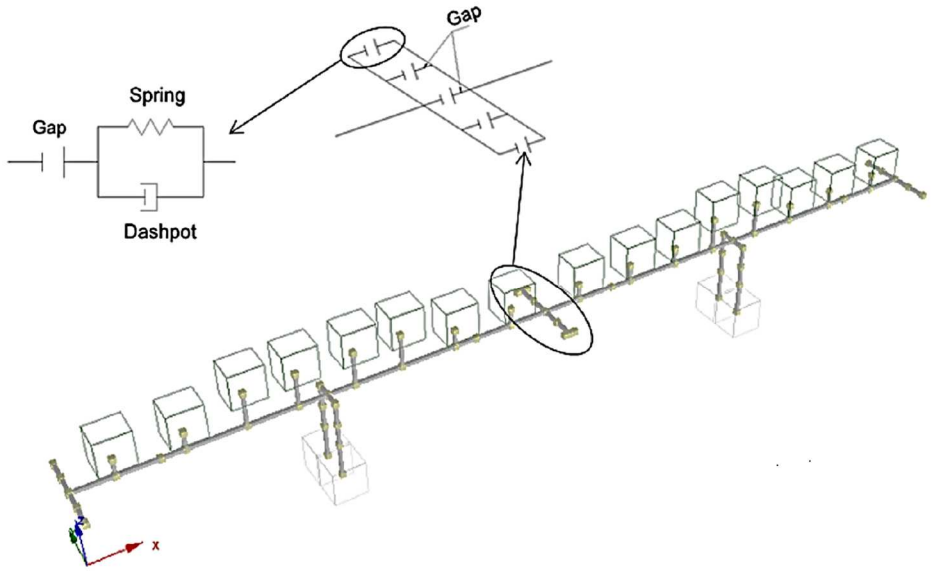

Figure 3-15. Finite element model of the bridge.

The SMA restrainers are modelled using the software inherent SMA model following the constitutive relationship proposed by Auricchio and Sacco (1997) and programmed by Fugazza (2003). This model is capable of describing the force-deformation relationship of superelastic SMA at constant temperature. The model is defined by six parameters, namely modulus of elasticity, austenite to martensite starting stress, austenite to martensite finishing stress, martensite to austenite starting stress, martensite to austenite finishing stress and superelastic plateau strain. The six parameters adopted in this study, based on the experimental results are presented in Table 3-4.

Table 3-4. Constitutive material properties of SMA restrainer.

Parameters		Value
Austenite to martensite starting stress	(MPa)	350
Austenite to martensite finishing stress	(MPa)	550
Martensite to austenite starting stress	(MPa)	420
Martensite to austenite finishing stress	(MPa)	210
Modulus of Elasticity	(MPa)	35000
Superelastic plateau strain		5%

Damping is specified through mass and stiffness proportional damping. The Rayleigh damping method is used to calculate the damping coefficients based on the estimated periods of first and second longitudinal modes of the frame 1, which are approximately 0.61 and 0.10 sec, respectively. In this study, the damping ratio of 5% and 7 % are assigned to the first two modes, respectively as the numerical results using this damping values provided the responses closer to the measured responses.

3.7.2 Comparisons with the experimental results

In order to evaluate the accuracy of the numerical model, numerical results are compared with the recorded experimental data. In the numerical simulations, the recorded displacement time histories measured at the two shake tables are taken as inputs. The acceleration and the displacement time histories are taken as primary responses to compare the numerical and experimental results.

Figure 3-16 compares displacement time histories of the two frames for set 1 bridge model in the longitudinal and transverse directions during run 4. As presented, the absolute frame displacements in the both directions are simulated accurately. Figure 3-17 (a) shows the acceleration time histories at expansion joint measured at frame 1 of the set 1 bridge model during run 4. Close-up views of the acceleration time histories during the impact are presented in Figure 3-17 (b), (c), and (d). The numerical model successfully predicts the number and occurrences of pounding with reasonable accuracy.

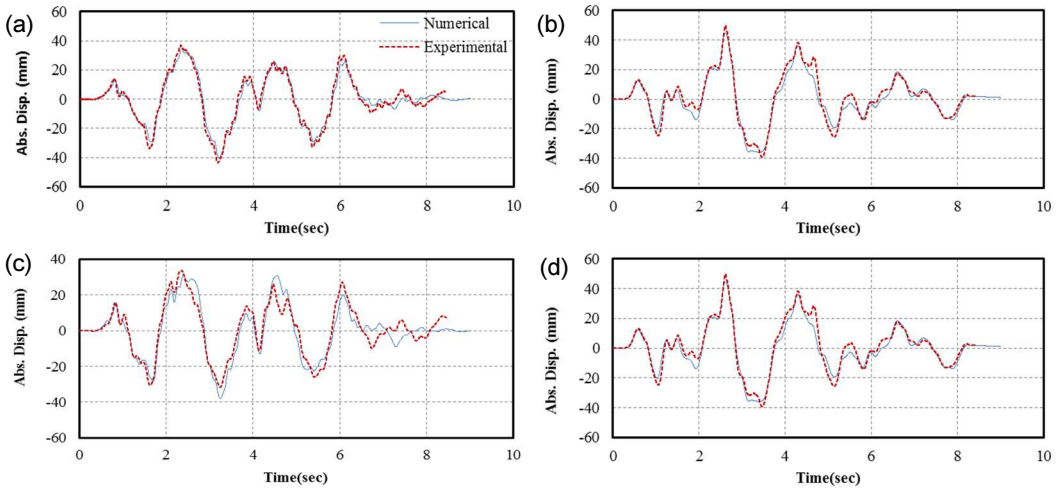

Figure 3-16 Absolute displacement time histories comparison between numerical result and testing data of set 1 model bridge during test run 4 (a) longitudinal displacement , (b) transverse displacement of frame 1, (c) longitudinal displacement, and (d) transverse displacement of frame 2.

Figure 3-18 shows the comparison of the measured and calculated peak deck accelerations at both bridge frames of bridge model set 1. As presented in the figure, a close match is observed

between the measured and calculated results. Figure 3-19 presents the peak accelerations at bridge frames of bridge model set 2. Here, the results of run 6 of bridge model set 2 could not be compared, as the shake table displacement record were lost. In overall, the results show that numerical models are reasonably accurate in predicting peak deck acceleration.

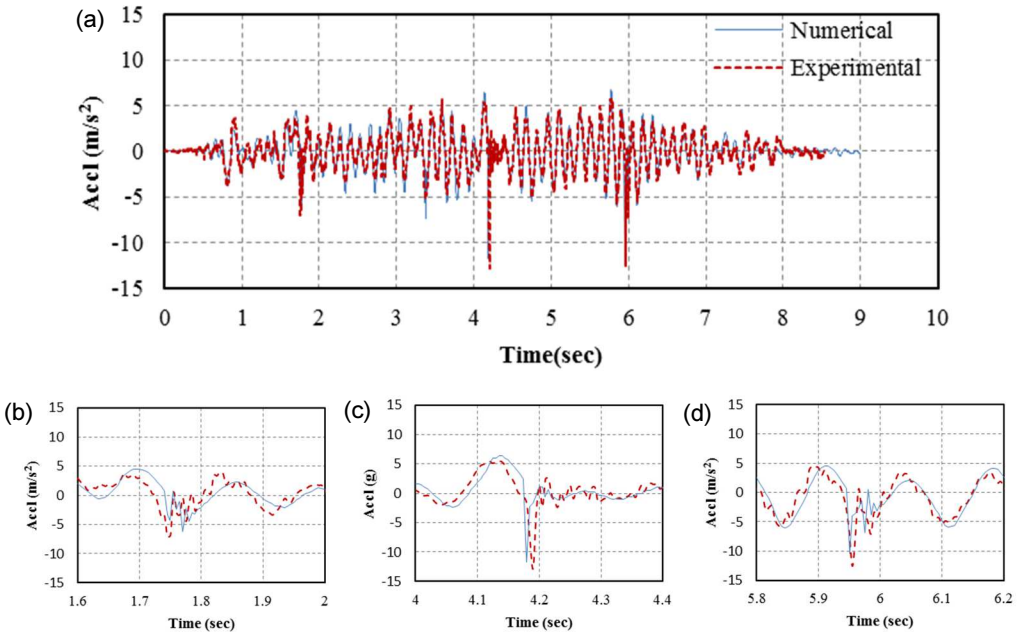

Figure 3-17 Acceleration time histories at expansion joint of bridge model set 1 during run 4.

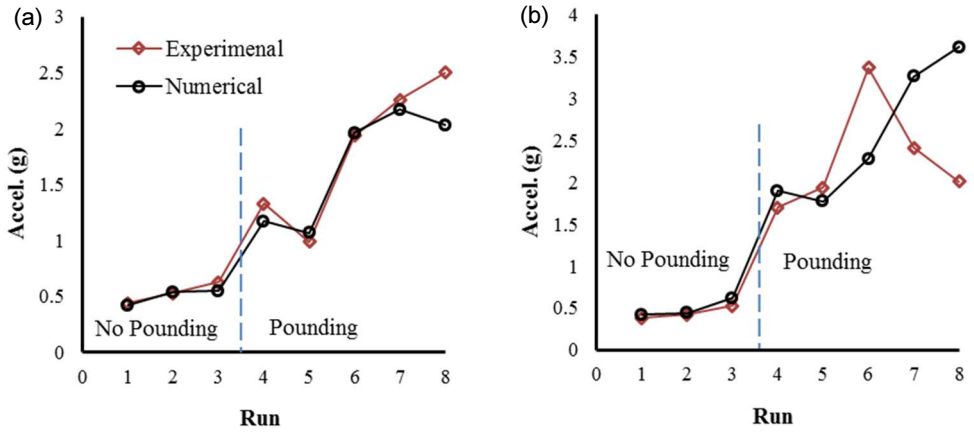

Figure 3-18 Comparison of peak measured and computed acceleration at (a) frame 1 and (b) frame 2 of bridge model set 1.

Figure 3-20 presents the comparison of the chord rotation at the base of the pier of frame 1 of set 1 bridge model during run 5. Figure 3-21 shows the comparison of the force in a SMA restrainer of set 2 bridge model during run 5. The results presented show that the numerical models are also capable to capture the response of the pier and the restrainers fairly accurately.

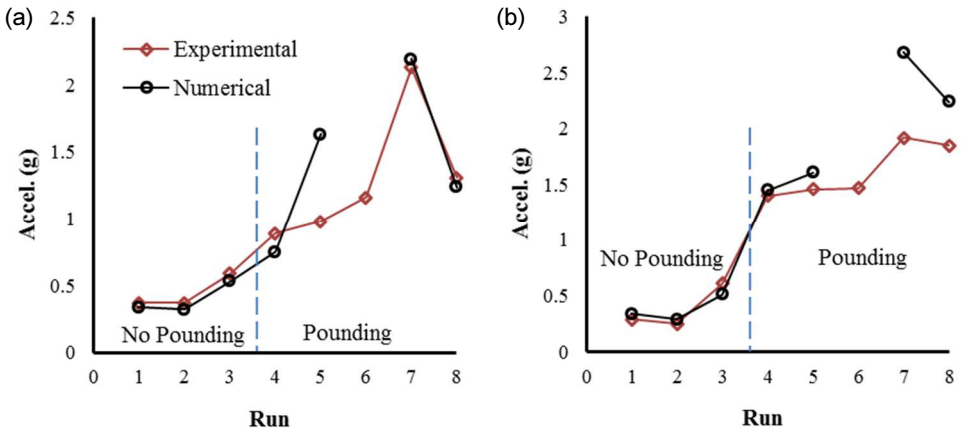

Figure 3-19 Comparison of peak measured and computed acceleration at (a) frame 1 and (b) frame 2 on the bridge model set 2.

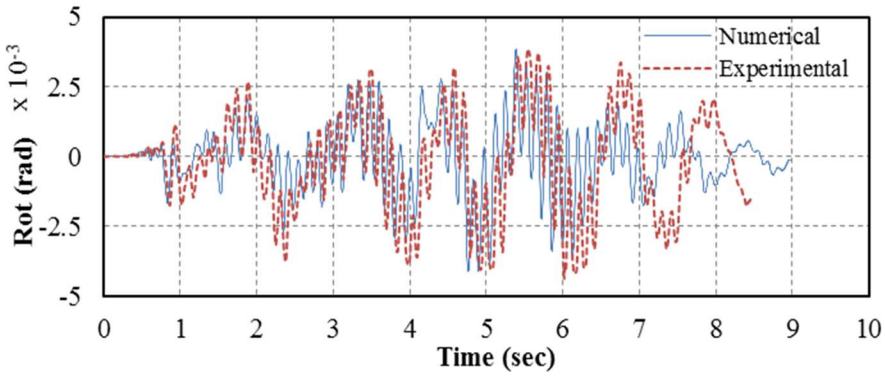

Figure 3-20 Comparison between the experimental and numerical results on the rotation time histories at the base of pier of frame 1 of bridge set 1 during run 5.

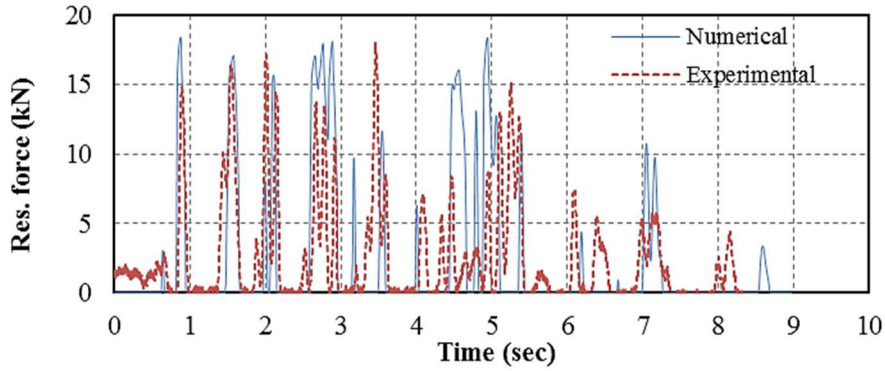

Figure 3-21 Restrainer force time history for model set 2 during run 5.

3.8 Parametric analysis

The calibrated numerical models are used to perform parametric studies on the response of adjacent bridge frames to spatially varying ground motions. Numerical investigation on bridge models subjected to spatially varying, ground motion considering wave passage effect only

and uniform ground motions are conducted. For the uniform ground motion, the displacement time history from shake table 1 is applied to the shake table 2. For the ground motion considering wave passage effect, the displacement time history from shake table 1 is applied to the shake table 2 again but with a time delay of 0.041 sec. In this study, only the runs with the spatially varying ground motions (i.e. runs 2, run 4 to run 8) are re-analyzed for the both sets of bridge models.

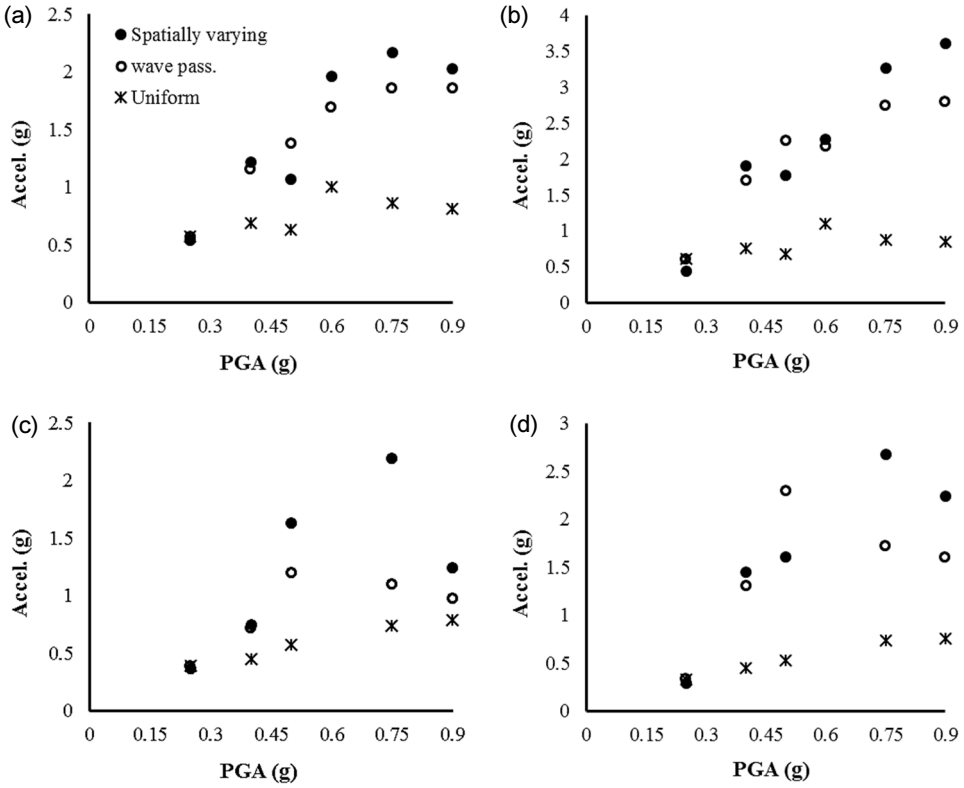

Figure 3-22 Peak deck accelerations at (a) frame 1 set 1; (b) frame 2 set 1; (c) frame 1 set 2; (d) frame 2 set 2 when subjected to different ground motions.

Figure 3-22 presents the comparisons of peak deck accelerations for the three ground motion assumptions. The peak deck accelerations for the three ground motion cases are similar at lower intensity (0.25g) as pounding between the adjacent frames are not observed at this intensity. However, as the intensity of the ground motion increases, the relative displacement between the adjacent structures also increases leading to pounding between adjacent frames subjected to spatially varying ground motions. Consequently, peak deck acceleration increases sharply. The comparison of the peak deck acceleration indicates spatially varying ground motion usually leads to stronger pounding. Peak deck accelerations are slightly smaller for the ground motion with wave passage effects. For uniform ground motion the peak deck accelerations are the smallest as the bridge frames move relatively in-phase and poundings do not occur. It is also observed that peak deck accelerations of the unrestrained model (set 1) are higher than those of the restrained bridge model (set 2). This phenomenon, as described earlier,

is because restrainers prevent large opening relative displacement and also helps to reduce the magnitude of pounding impact.

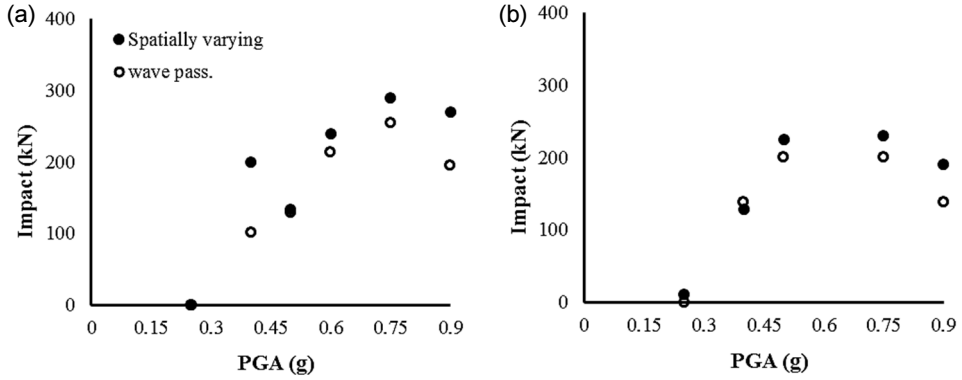

Figure 3-23 Peak impact force for (a) set 1; (b) set 2 bridge model when subjected to earthquake ground motions.

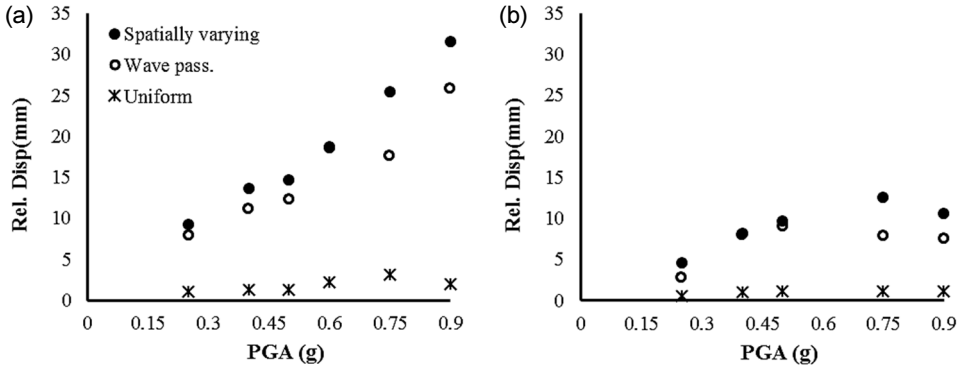

Figure 3-24 Peak relative displacement for (a) set 1; (b) set 2 bridge model subjected to earthquake ground motions.

Figure 3-23 shows comparisons of peak pounding forces for the bridge models, in which the results for the uniform case are not shown since no pounding occurs in this case. Similar to the peak deck acceleration, peak impact forces are also slightly higher for the bridge models subjected to spatially varying ground motions. The peak impact forces for set 1 bridge model is higher than that for restrained bridge model. Figure 3-24 shows the comparisons of peak opening relative displacements at the joint of both bridge models. As expected, when ground motion is uniform the relative displacement is the minimum. However, for the non-uniform cases, the relative opening displacement is significantly larger. Here again, the relative displacement for the cases with spatially varying ground motions are larger than those with wave passage effect only. The SMA restrainers are highly effective in reducing the relative opening displacement between the adjacent bridge frames. It is also observed that relative displacement obtained in the final run of restrained bridge model (set 2) is slightly smaller than that measured in run 7. This observation might have resulted from the period elongation

of bridge frames due to the cumulative damages from previous test runs, which in turn reduced the out-of-phase motions between the adjacent frames.

3.9 Conclusions

Seismic responses of large-scale bridge models with a pair of adjacent bridge frames having close fundamental periods, as recommended by the modern bridge codes, subjected to spatially varying earthquake ground motions were experimentally investigated in a shake table array system. The effects of superelastic SMA restrainers on the seismic response of bridge system was also experimentally evaluated. Numerical models were developed and validated using the experimental results. The validated numerical models were used for parametric analyses to comprehend the findings from the testing.

Pounding damages at the bridge joints, as observed during previous strong earthquakes, were successfully reproduced during the shake table tests. The mechanisms that might have resulted in pounding and consequential acceleration pulses are discussed. Based on the experimental and the numerical results following conclusions are drawn

The experiments revealed three-dimensional nature of pounding between the adjacent bridge frames resulting from motion of bridge deck in vertical and transverse directions along with longitudinal direction. Significant coupling between the motions mainly in vertical and longitudinal direction, leading to the frictional contact and head-on impact with an oblique angle, were observed. Spatial variation of ground motions significantly influenced the relative displacement between the adjacent bridge frames as a result of which poundings between the adjacent bridge frames with fundamental periods close to each other occurred leading to damages to bridge deck at the joint. Though poundings caused localized damages at the bridge joint, its effect on the response of bridge piers were rather beneficial as the chord rotation of both the piers were slightly reduced. Superelastic restrainers not only reduced the relative displacement but also were effective in reducing the magnitude of pounding impacts. However, the number of impacts increased with the application of restrainers. Moreover, restrainers also increased displacement response of the light and stiffer frame.

Numerical studies show that spatially varying ground motions results in the severer pounding and larger joint opening. It is also highlighted that considering only the wave passage effect of the spatially varying ground motion during the design is not sufficient as it will lead to the underestimation of the responses. Moreover, the effectiveness of superelastic restrainers in reducing the relative displacement induced damages is also demonstrated.

3.10 References

Anagnostopoulos, S. A. (1988). Pounding of buildings in series during earthquakes. *Earthquake engineering & structural dynamics*, *16*(3), 443-456.

Anagnostopoulos, S. A. (2004). Equivalent viscous damping for modeling inelastic impacts in earthquake pounding problems. *Earthquake Engineering & Structural Dynamics*, *33*(8), 897-902.

Andrawes, B., & DesRoches, R. (2005). Unseating prevention for multiple frame bridges using superelastic devices. *Smart Materials and Structures*, *14*(3), S60.

Andrawes, B., & DesRoches, R. (2007). Comparison between shape memory alloy seismic restrainers and other bridge retrofit devices. *Journal of Bridge Engineering*, *12*(6), 700-709.

Auricchio, F., & Sacco, E. (1997). A superelastic shape-memory-alloy beam model. *Journal of intelligent material systems and structures*, *8*(6), 489-501.

Bi, K., Hao, H., & Chouw, N. (2011). Influence of ground motion spatial variation, site condition and SSI on the required separation distances of bridge structures to avoid seismic pounding. *Earthquake Engineering & Structural Dynamics*, *40*(9), 1027-1043.

Bi, K., & Hao, H. (2012). Modelling and simulation of spatially varying earthquake ground motions at sites with varying conditions. *Probabilistic Engineering Mechanics*, *29*, 92-104.

Bi, K., & Hao, H. (2013). Numerical simulation of pounding damage to bridge structures under spatially varying ground motions. *Engineering Structures*, *46*, 62-76.

Bi, K., Hao, H., & Chouw, N. (2013). 3D FEM analysis of pounding response of bridge structures at a canyon site to spatially varying ground motions. *Advances in Structural Engineering*, *16*(4), 619-640.

Bi, K., & Hao, H. (2015). Modelling of shear keys in bridge structures under seismic loads. *Soil Dynamics and Earthquake Engineering*, *74*, 56-68.

Caltrans S.D.C. (2013) Caltrans seismic design criteria version 1.7. California Department of Transportation, Sacramento.

Chouw, N., & Hao, H. (2005). Study of SSI and non-uniform ground motion effect on pounding between bridge girders. *Soil Dynamics and Earthquake Engineering*, *25*(7), 717-728.

Chouw, N., & Hao, H. (2008). Significance of SSI and nonuniform near-fault ground motions in bridge response I: Effect on response with conventional expansion joint. *Engineering Structures*, *30*(1), 141-153.

Cruz Noguez, C. A., & Saiidi, M. S. (2011). Shake-table studies of a four-span bridge model with advanced materials. *Journal of Structural Engineering*, *138*(2), 183-192.

Cruz Noguez, C. A., & Saiidi, M. S. (2011). Shake-table studies of a four-span bridge model with advanced materials. *Journal of Structural Engineering*, *138*(2), 183-192.

DesRoches, R., & Muthukumar, S. (2002). Effect of pounding and restrainers on seismic response of multiple-frame bridges. *Journal of Structural Engineering*, *128*(7), 860-869.

DesRoches, R., & Delemont, M. (2002). Seismic retrofit of simply supported bridges using shape memory alloys. *Engineering Structures*, *24*(3), 325-332.

Dove R, Bennett J. (1986) Scale modeling of reinforced concrete category I structures subjected to seismic loading. Los Alamos National Lab., NM.

Fugazza D. (2003) Shape-memory alloy devices for earthquake engineering: mechanical properties, constitutive modeling and numerical simulations. Master's thesis. University of Pavia; Italy.

Guo, A., Zhao, Q., & Li, H. (2012). Experimental study of a highway bridge with shape memory alloy restrainers focusing on the mitigation of unseating and pounding. *Earthquake Engineering and Engineering Vibration*, *11*(2), 195-204.

Hall JF, Holmes WT, Somers P. (1996) Northridge earthquake of January 17, 1994: reconnaissance report: Earthquake Engineering Research Institute, Oakland, CA.

Hao, H., Bi, K., Chouw, N., & Ren, W. X. (2013). State-of-the-art review on seismic induced pounding response of bridge structures. *Journal of Earthquake and Tsunami*, *7*(03), 1350019.

Jankowski, R., Wilde, K., & Fujino, Y. (1998). Pounding of superstructure segments in isolated elevated bridge during earthquakes. *Earthquake engineering & structural dynamics*, *27*(5), 487-502.

Jankowski, R. (2010). Experimental study on earthquake-induced pounding between structural elements made of different building materials. *Earthquake Engineering & Structural Dynamics*, *39*(3), 343-354.

Johnson, N., Ranf, R. T., Saiidi, M. S., Sanders, D., & Eberhard, M. (2008). Seismic testing of a two-span reinforced concrete bridge. *Journal of Bridge Engineering*, *13*(2), 173-182.

Johnson, R., Padgett, J. E., Maragakis, M. E., DesRoches, R., & Saiidi, M. S. (2008). Large scale testing of nitinol shape memory alloy devices for retrofitting of bridges. *Smart materials and structures*, *17*(3), 035018.

Kawashima, K., Unjoh, S., Hoshikuma, J. I., & Kosa, K. (2011). Damage of bridges due to the 2010 Maule, Chile, Earthquake. *Journal of Earthquake Engineering*, *15*(7), 1036-1068.

Komodromos, P., Polycarpou, P. C., Papaloizou, L., & Phocas, M. C. (2007). Response of seismically isolated buildings considering poundings. *Earthquake Engineering & Structural Dynamics*, *36*(12), 1605-1622.

Li, B., Bi, K., Chouw, N., Butterworth, J. W., & Hao, H. (2012). Experimental investigation of spatially varying effect of ground motions on bridge pounding. *Earthquake Engineering & Structural Dynamics*, *41*(14), 1959-1976.

Li, B., Bi, K., Chouw, N., Butterworth, J. W., & Hao, H. (2013). Effect of abutment excitation on bridge pounding. *Engineering Structures*, *54*, 57-68.

Li, B., & Chouw, N. (2014). Experimental investigation of inelastic bridge response under spatially varying excitations with pounding. *Engineering Structures*, *79*, 106-116.

Malhotra, P. K., Huang, M. J., & Shakal, A. F. (1995). Seismic interaction at separation joints of an instrumented concrete bridge. *Earthquake engineering & structural dynamics*, *24*(8), 1055-1067.

Mander, J. B., Priestley, M. J., & Park, R. (1988). Theoretical stress-strain model for confined concrete. *Journal of structural engineering*, *114*(8), 1804-1826.

Muthukumar, S., & DesRoches, R. (2005). Effect of frame-restoring force characteristics on the pounding response of multiple-frame bridges. *Earthquake spectra*, *21*(4), 1113-1135.

Ozbulut, O. E., Hurlebaus, S., & DesRoches, R. (2011). Seismic response control using shape memory alloys: a review. *Journal of Intelligent Material Systems and Structures*, 1045389X11411220.

Padgett, J. E., DesRoches, R., & Ehlinger, R. (2010). Experimental response modification of a four-span bridge retrofit with shape memory alloys. *Structural Control and Health Monitoring*, *17*(6), 694-708.

Ruangrassamee, A., & Kawashima, K. (2001). Relative displacement response spectra with pounding effect. *Earthquake engineering & structural dynamics*, *30*(10), 1511-1538.

Saiidi, M. (1993). Response of bridge hinge restrainers during earthquakes: field performance, analysis, and design. Rep. no. CCEER93-6. *Center for Civil Engineering Earthquake Research, University of Nevada, Reno, Nev*.

Saiidi, M. S., Vosooghi, A., Choi, H., & Somerville, P. (2013). Shake Table Studies and Analysis of a Two-Span RC Bridge Model Subjected to a Fault Rupture. *Journal of Bridge Engineering*, *19*(8), A4014003.

SeismoSoft, S. (2010). A computer program for static and dynamic nonlinear analysis of framed structures. *Available from URL: www.seismosoft.com*.

Selna, L. G., Malvar, L. J., & Zelinski, R. J. (1989). Bridge retrofit testing: Hinge cable restrainers. *Journal of Structural Engineering*, *115*(4), 920-934.

Shrestha, B., Hao, H., & Bi, K. (2014). Effectiveness of using rubber bumper and restrainer on mitigating pounding and unseating damage of bridge structures subjected to spatially varying ground motions. *Engineering Structures*, *79*, 195-210.

Shrestha, B., Hao, H., & Bi, K. (2015). Seismic response analysis of multiple-frame bridges with unseating restrainers considering ground motion spatial variation and SSI. *Advances in Structural Engineering*, *18*(6), 873-891.

Shrestha B, Hao H, Bi K. (2016) Devices for protecting bridge superstructure from pounding and unseating damages: an overview. *Structure and Infrastructure Engineering*. (Accepted for publication).

Sobczyk K. *Stochastic wave propagation*. Netherlands: Kluwer Academic Publisher; 1991.

Wieser J. (2014) *Experimental and analytical investigation of seismic bridge-abutment interaction in a curved highway bridge*. Ph.D. Dissertation, University of Nevada, Reno; Nev.

Wieser, J. D., Maragakis, E. M., & Buckle, I. G. (2014, July). Experimental evaluation of seismic performance of seat-type abutments in a curved highway bridge. In *Proc. of the 10th National Conference in Earthquake Engineering*. Anchorage, Alaska: Earthquake Engineering Research Institute.

CHAPTER 4
EFFECTIVENESS OF USING RUBBER BUMPER AND RESTRAINER ON MITIGATING POUNDING AND UNSEATING DAMAGE OF BRIDGE STRUCTURES SUBJECTED TO SPATIALLY VARYING GROUND MOTIONS

4.1 Abstract

Pounding and unseating damages to bridge decks have been observed in almost all the previous major earthquakes. Recent studies have highlighted that adjusting the fundamental periods of adjacent structural elements close to each other, the only method suggested by the codes to mitigate pounding and unseating damage, is not sufficient to prevent such damages owing to the relative displacement induced by spatially varying ground motions. As pounding and unseating damage could lead to significant loss of economy and life owing to inability to quickly access the damaged area immediately after an earthquake, it is important to protect lifeline bridge structures. Past earthquakes have revealed that the commonly used steel cable restrainers have limited effectiveness. Additionally, only limited research has focused on mitigating pounding forces on the bridge joints that lead to localized damages and disruptions of the serviceability of the bridge after strong shakings. This study presents an extensive investigation on the effectiveness of combining rubber bumpers as a shock absorbing device along with Shape Memory Alloy (SMA) or steel cable restrainers to mitigate pounding and unseating damages on multiple-span bridges subjected to spatially varying ground motions. The responses of bridge structures with different restraining devices acting alone and in combination with rubber bumpers subjected spatially varying ground motions are compared and discussed. The result indicates that the SMA restrainers combined with rubber bumpers could lead to better performance in terms of reduction of joint opening and mitigation of large pounding forces.

4.2 Introduction

Seismic pounding between girders and/or between girder and abutment in multi-span bridges has been commonly observed in almost all major earthquakes. For example, during the 1994 Northridge earthquake, significant pounding damage was observed at the expansion hinges and abutments of standing portions of the connectors at the Interstate Freeway 5 and State road 14 interchange, which was located approximately 12 km north-east of the epicentre (Hall, 1994). Reconnaissance reports from the 1995 Hyogo-Ken Nanbu earthquake in Japan identified pounding as a major cause of fracture of bearing supports and potential contributor to the collapse of several bridge decks (Comartin et al., 1995). The 1999 Chi-Chi earthquake in Taiwan revealed hammering at the expansion joints in some bridges resulting in damages

to shear keys, bearings and anchor bolts (Uzarski & Jones, 2001). Failure of girder ends and bearing damage due to pounding of adjacent simply-supported spans were reported after the 2001 Bhuj earthquake in Gujarat, India (Jain et al., 2002). Pounding damages to adjacent bridge structures were also observed in the 2008 Wenchuan earthquake (Kawashima et al., 2009), 2010 Chile earthquake (Kawashima et al., 2011) and more recently in the 2011 Christchurch earthquake (Chouw & Hao, 2012). The multiple-frame and multiple-span simply supported bridges are most susceptible to pounding damages due to numerous independent components and lack of continuity in the structure. It has been observed that pounding impact could induce large acceleration spikes and contact forces on the component involved, resulting in local crushing and spalling of concrete and damages to shear keys, bearing pads and restrainers and possibly contributing to collapse of deck spans. However, there are contradicting views on how pounding affects the global bridges response and the response of the piers (Huo & Zhang, 2013). Some studies (Ruagrassamee & Kawashima, 2001) suggested pounding to be detrimental, while others (Kim & Shinozuka, 2003; Malhotra, 1998; Priestley, et al., 1996) concluded pounding has a less severe effect on the response of bridge piers depending the bridge model analyzed.

Restrainers have been in use since early 1970's as an effective device for preventing span collapse during an earthquake event (Andrawes & DesRoches, 2007). However, in large earthquakes such as the 1989 Loma Prieta, 1994 Northridge and 1995 Kobe earthquake, a number of cases of inefficiency of steel restrainers were observed, with serious damage or even collapse of a number of bridges retrofitted with restrainers (Saiidi et al., 1993). To improve the effectiveness of restrainers in bridge structure protection, many researchers have carried out research to provide appropriate design procedure for restrainers and to understand the influencing factors on the behavior of restrainers through parametric studies. Saiidi et al. (1996) have investigated four bridges retrofitted with cable restrainers during the 1989 Loma Prieta earthquake and concluded that restrainers are affected by many factors such as the amplitude and frequency of the ground motion, foundation flexibility as well as flexibility of the substructure and nonlinear time history analysis is necessary to design appropriate restrainers. Trochalakis et al. (1997) conducted 216 non-linear time history analyses for various frames, abutments, and restrainer properties and showed that the maximum relative displacement were sensitive to the stiffness of adjacent frames, the frame's effective periods, and the restrainer properties. DesRoches and Fenves (2000) suggested a new design procedure for steel restrainers and compared it with results of nonlinear time history analyses. DesRoches et al. (2003) carried out a series of full-scale tests of a simply-supported bridge to evaluate the force-displacement behavior of the cable restrainers. Based on these studies, it is concluded that the inadequate performance of restrainers during large earthquakes is a result of the fact

that the steel restrainers are designed to remain elastic; hence transfer large force to the bridge components (Selna et al., 1989). Additionally, when the ground shaking is strong enough to cause restrainer to yield, its effectiveness is greatly reduced for remainder of the ground motion due to the accumulation of plastic deformation. Recently, to overcome the limitation of steel cables and bars Shape Memory Alloys (SMA) with superelastic behavior have been widely investigated in analytical and experimental studies. In these studies (Andrawes & DesRoches, 2005,2007; DesRoches & Delemont, 2002; Padgett et al., 2010; Guo et al., 2012) SMA based restrainers have been proposed to avoid deck unseating owing to opening relative displacement, but the mitigation of pounding impact caused by closing relative displacement between adjacent decks were not considered in those studies.

It should be noted that the performance of restrainers depend on the relative displacement responses of adjacent bridge structures. Relative displacements between adjacent bridge structures are caused by out-of-phase vibrations owing to none identical vibration properties and inevitable ground motion spatial variations at the multiple bridge supports. However, in most of the previous studies uniform ground excitations along the bridge supports were assumed, which could significantly underestimate the responses (Chouw & Hao, 2008, 2009; Li et al., 2012).

Even though the destructive potential of structural pounding has been evident during almost all the previous major earthquakes, there is still not sufficient guideline provided by the seismic design codes to prevent the harmful effects of pounding. Most of the bridge design codes suggest adjusting fundamental periods of the adjacent structures close to each other as the only method to mitigate pounding damages in bridge structures. However, recent studies (Chouw & Hao, 2005, 2008, 2009; Li et al., 2012; Bi & Hao, 2013; Bi et al., 2013) showed that only adjusting the fundamental period of the adjacent structures is not sufficient to avoid pounding damages because of earthquake ground motion spatial variations. One of the mitigation measures for poundings of adjacent structures would be prevention of impact incidents by providing sufficient gaps. However, often the size of the expansion joints has to be limited for smooth traffic flow, making the adjacent structures susceptible to earthquake induced poundings. A method of mitigating pounding damages could be the incorporation of layers of soft material, such as rubber on the expansion joints to act as shock absorber. Previous studies (Kawashima & Shoji, 2000; Abdel Raheem, 2009; Polycarpou & Komodromos, 2011) assessed the effectiveness of this impact mitigation measure on the response of bridges and buildings.

During earthquake shaking, both pounding and unseating damages are possible because of the closing and opening relative displacement between adjacent bridge structures. To mitigate the

possible pounding and unseating damages, some codes (Japan Road Association, 2004) suggest using restrainers together with shock absorbing devices. Few researchers (Kawashima & Shoji, 2000; Abdel Raheem, 2009; Zhu et al., 2004) have investigated the effectiveness of using steel restrainers and rubber bumpers together to mitigate pounding and unseating damage between adjacent decks. The incorporation of rubber shock absorbers in the expansion joints was found to be effective to mitigate large pounding forces and acceleration pulses. Although ground motion spatial variation is inevitable owing to seismic wave propagation and non-uniform ground motion generates relative responses between adjacent structures, owing to the complexity in modelling such variations, all the above reviewed studies assumed uniform ground motion in the analysis. Moreover, no study that investigates the effectiveness of using SMA restrainers with rubber bumpers in mitigating pounding and unseating damage of bridge structures has been reported in the literature yet.

There is a clear consensus among the researchers that pounding results in localized damages at impact locations and could contribute towards unseating of the bridge spans. This paper investigates the effectiveness of combining rubber bumper with either SMA restrainers or steel restrainers on multiple-frame bridges with one or more intermediate gaps to mitigate these damages subjected to spatially varying ground motions. The study focuses on the bridge balanced frame geometry (Caltrans, 2010) which are emphasized by the prevailing codes as a method to mitigate relative displacement induced damages such as pounding and unseating. The study firstly compares the effectiveness of the steel and SMA restrainers to mitigate the large joint opening. Then, the effectiveness of rubber bumpers as a possible pounding mitigation device is investigated. Parametric studies are carried out to compare the effectiveness of the two types of restrainers along with rubber shock absorbing pads to mitigate pounding and unseating damage on bridges subjected to spatially varying ground motions corresponding to different site conditions. Based on the numerical results, conclusions on the effectiveness of using the rubber bumpers with restraining devices to mitigate pounding and unseating damage are drawn. This study sheds some light on the benefits and limitation of the aforementioned restraining devices and shock absorbers when acting alone or in combination. The results presented could assist bridge engineers on selecting the devices to effectively mitigate relative displacement induced damages on bridge structures.

4.3 Numerical Model

4.3.1 Bridge Model

Without loss of generality, two typical Californian Highway Bridges with five spans are selected for the analysis. The expansion joints are located nearly at the inflection points (i.e., 1/4 to 1/5 of span). The bridge deck consists of box-type girders with either reinforced or pre-

stressed concrete. The bridge details are described in Feng et al. (2000) and Kim et al. (2000). For readers' easy reference, the bridge parameters are also presented here in Table 4-1. Two 2-D nonlinear finite element models of the bridges shown in Figure 4-1 (a) and (b) are developed for the analysis, which represent

- Model 1: a five-span bridge with an expansion joint and equal column height of 19.83 m.

- Model 2: a five-span bridge with two expansion joint and equal column height of 19.83 m.

Table 4-1 Material and Cross-sectional Properties of Example Bridges

Structural component	Cross Sectional area [m^2]	Moment of Inertia [m^4]	Young's Modulus [MPa]
Girders	6.936	4.787	27790
Columns	4.670	1.735	27790

The bridge models are developed in the nonlinear software package Seismostruct (2012). Previous studies (Feng et al., 2000; Kim et al., 2000) used a bilinear hysteretic element at the plastic hinge location. In this study, a more rational fiber section model capable of simulating the distribution of inelasticity is adopted. The cross section is divided to multiple fiber elements, where each fiber is associated with a uni-axial stress-strain relationship. The sectional stress-strain state of beam-column elements is then obtained through the integration of the nonlinear uni-axial stress-strain response of the individual fibers in which the section has been subdivided. The analyses are conducted with a time step of $5x10^{-4}$ sec to adequately capture the peak pounding forces. The finite element model of the bridge is presented in Figure 4-1 (c). The sectional detail of the bridge is presented in Figure 4-1 (d).

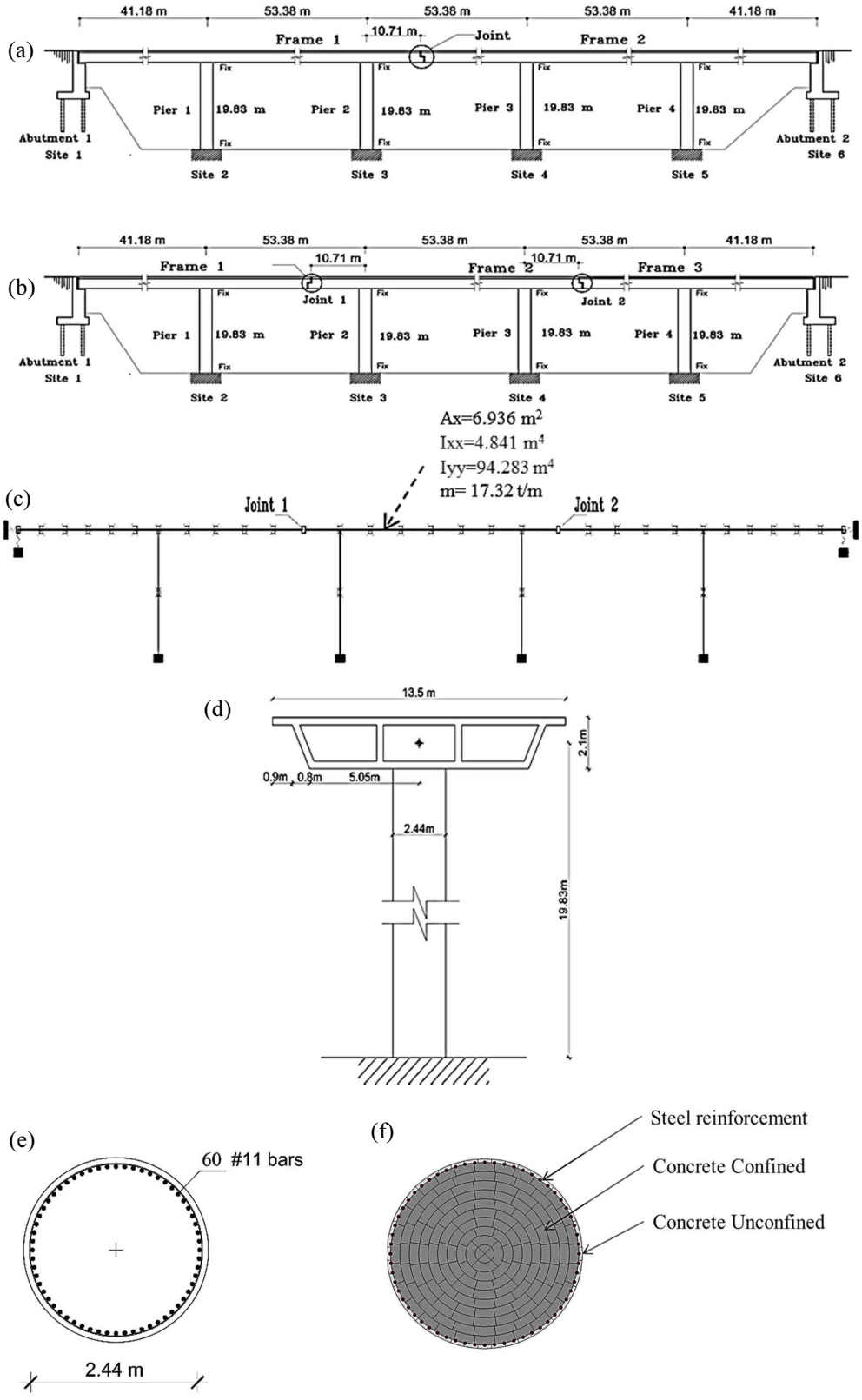

Figure 4-1 Bridge Models used for the study (a) model 1 with single intermediate hinge; (b) model 2 with two intermediate hinges; (c) finite element model of the bridge model 2; (d) section of the bridge; (e) pier cross section; (f) fiber discretization of the pier.

Concrete bents are modelled by force based reinforced concrete beam-column element. Pier reinforcement details and fiber element discretization are presented in Figure 4-1 (e) and (f), respectively. As shown reinforced concrete sections are constructed from three materials, namely unconfined concrete, confined concrete and reinforcing steel. The unconfined and confined concrete behaviors are modelled by using the nonlinear constitutive relationship proposed by Mander et al. (1988) and the cyclic rules proposed by Martinez-Rueda and Elnashai (1997), respectively. Confinement effects provided by the lateral transverse reinforcement are incorporated through the rules proposed by Mander et al. (1988), whereby constant confining pressure is assumed throughout the entire stress-strain range. To represent the behavior of the steel re-bars, Menegotto-Pinto steel model is used. The yield strength of the re-bars is 415 MPa, and the elastic modulus is assumed as *Es*= 200 GPa. The superstructure of the bridge is modelled using the elastic beam column elements. Elastomeric bearings consisting of an elastomeric rubber pad are modelled by the elastic perfectly plastic element to represent the frictional force developed at elastomeric pad. The initial stiffness, $k_{o,}$ of the bearing is given by (Choi, 2002).

$$k_o = \frac{GA}{hr} \tag{4.1}$$

where *A* is the area of the elastomeric bearing, *G* is the shear modulus of the elastomer and *hr* is the thickness of the elastomeric pad. In this study G= 1.38 MPa is assumed for the elastomers, the area and thickness of the bearings are assumed as 0.12 m^2 and 37.5 mm respectively, which gives an initial stiffness of k_o= 4.41 kN/mm. The frictional coefficient for concrete bridges takes into account the interface between the elastomeric rubber and the concrete surface. Some experimental tests have shown that the coefficient of friction for an elastomeric bearing is a function of the normal stress on the bearing, σ_m (MPa), and is given by (Scharge, 1981).

$$\mu = 0.05 + \frac{0.4}{\sigma_m} \tag{4.2}$$

In this study the coefficient of friction, μ, is taken as 0.36. 6 bearings are placed on each abutment and on each in-span expansion joint; the initial stiffness of the lumped bearing is thus 26.46 kN/mm. The yield force and yield displacement of the bearing are assumed to be 896.4 kN and 33.87 mm, respectively.

Abutments are modelled by two separate nonlinear springs representing the pile stiffness and passive soil stiffness at abutment. The nonlinear abutment behavior in this study reflects the design recommendation from Caltrans (1990, 2010). The Caltrans recommendation of

effective stiffness of 7 kN/mm/pile is used in this study with an ultimate strength of 119 kN/pile (Choi, 2002). The behavior of the pile, however, is not linear up to the ultimate strength. The initial stiffness degrades with soil surface yielding. Trilinear symmetrical models implemented by Choi (2002), which act in both active and passive loading of the abutments, are used to represent the pile stiffness. The piles become plastic at a deformation of 25.4 mm. It is also assumed that the first yielding occurs at 30% of the ultimate deformation. This corresponds to a yielding force equal to 70% of the ultimate force. 24 piles are placed in each abutment. Figure 4-2 (a) presents the load-deformation curve for abutment piles. Elastic plastic spring with initial stiffness, K_{ai}, of 28.7 kN/mm/m is used to represent passive soil behavior at abutment (Caltrans, 2010). Abutment stiffness can be calculated as (Caltrans, 2010):

$$K_{abut} = K_{ai} \times w \times \left\{ \frac{h}{1.7} \right\} \tag{4.3}$$

$$P_{bw} = A_e \times 239 \times \left\{ \frac{h}{1.7} \right\} \tag{4.4}$$

where K_{abut} is the stiffness of an abutment with initial embankment fill stiffness K_{ai}, effective width w, and height h. Based on an assumed elastic perfectly plastic force displacement relationship the passive pressure force P_{bw} can be calculated based on Eq. 4, where A_e is the effective area of the back wall, the height and width of the abutment back wall is h=2.25m and w=14.5m, respectively. Figure 4-2 (b) presents the load-deformation curve for soil embankment adopted in this study. The Pier foundation is assumed to be fixed. The foundation boundary condition is simplified so as to focus primarily on the response of structure with the restrainers and bumpers.

With the given properties of the two bridges, the natural periods of the bridge segments can be calculated based on Eigen value analysis. Natural periods of the target bridge segments and the ratio of their fundamental periods are presented in Figure 4-2. The ratios of fundamental natural periods of both the bridge models are above 0.7 (i.e. $T_i/T_j \geq 0.7$, where T_i is the natural period of stiffer frame and T_j is the natural period of flexible frame). Thus, both the considered bridge models meet the design guide of the balanced frame geometry, recommended by the code as a method to mitigate large pounding impact as well as unseating damage (Caltrans, 2010).

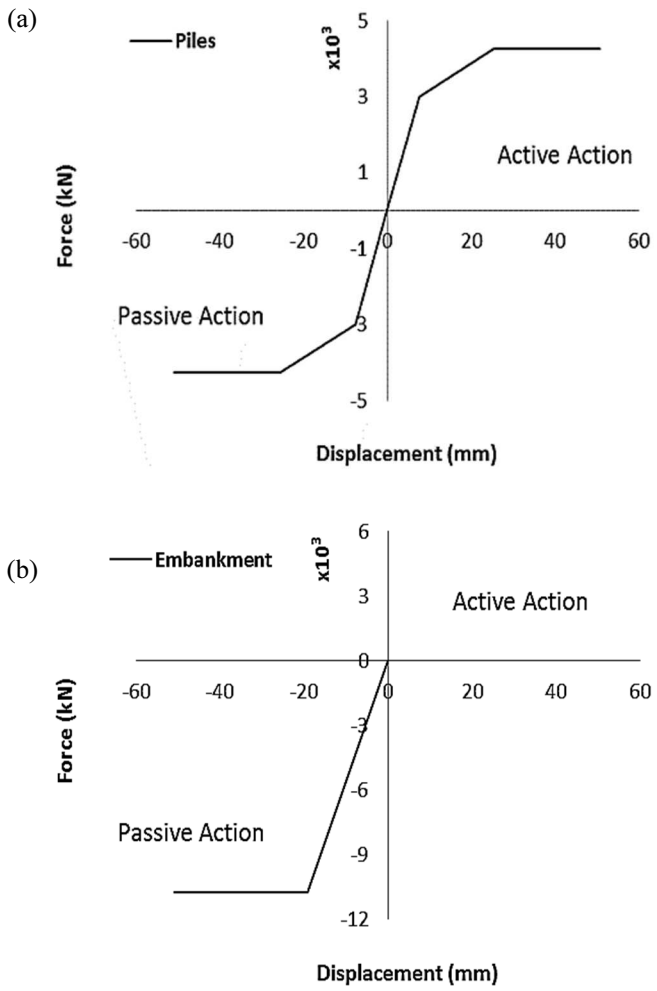

Figure 4-2 (a) Analytical modelling of Abutment piles; (b) Analytical model of soil embankment.

Table 4-2 Natural periods of model bridges

Bridge Model	Stiffer frame Fund. period [T_i, sec]	Flexible frame Fund. period [T_j, sec]	Period ratio [T_i/T_j]
Model 1 [Bridge 1H]	0.84 [Frame 1]	0.92[Frame 2]	0.91
Model 2 [Bridge 2H]	0.75 [Frame 2]	1.04 [Frame 1 & 3]	0.72

4.3.2 Expansion Joint and Impact Element

Expansion joints are provided to allow continuous traffic flow between adjacent bridge elements accommodating serviceability movements. During the large earthquake these joints are highly stressed as the gap provided between the segments are usually not sufficient to cope

with the movement. It is recognized that the pounding can affect the response of the bridge and hence must be considered in the seismic analysis. A common way of implementing this phenomenon is by using the contact element in the finite element model of the bridge. Essentially, the element monitors the gap between the adjacent sections of the bridge and is activated once the associated gap is closed. In this study a linear gap element with spring stiffness K_i, is used to model the impact between adjacent bridge structures. The impact stiffness, K_i, is proportional to the axial stiffness of the neighboring structural segment (Kawashima & Shoji, 2000; Abdel Raheem, 2009). The stiffness of the linear impact element, which activates after the gap closing, is given by:

$$K_i = \gamma \frac{AE}{L} \tag{4.5}$$

where E, A and L are the properties of the surrounding girders. In this study the stiffness of the gap element, K*i*= 3.6×10^7 kN/m is taken based upon the sensitivity analysis. To mitigate the large pounding forces rubber bumpers are proposed to be placed at the in-span hinges to act as shock absorbers as shown in Figure 4-3 (a). Figure 4-3 (a) also presents typical restrainer layout with anchoring details, details of the restrainer design is presented in following section. In this study the constitutive model of the strain hardening rubber bumpers as shown in Figure 4-3 (b), are adopted from Kawashima and Shoji (2000). The constitutive model is based on the uni-axial compressive load testing of the rubber bumpers. 10 rubber bumpers of 250mm x 150mm section and 50mm thick are used between the decks. The initial stiffness of the rubber bumper (Kb_1) is taken to be 12.5 KN/mm. A multi-linear strain hardening model is used in the study with second stiffness branch (Kb_2) of 12 times of the first stiffness branch and third stiffness branch (Kb_3) of 24 times of the first stiffness branch followed by a final spring with stiffness Ki, representing the impact stiffness after the full deformation of the bumpers. Similar modelling approach with multi-linear strain hardening model was used in some previous studies (Abdel Raheem, 2009; Abdel Raheem & Hayashikawa, 2012). The gap separating two frames and frame and abutments are taken as 100mm. Previous researches concluded that energy dissipation in the shock absorbing device have not significant effect on the response of structure (Kawashima & Shoji, 2000; Polycarpou & Komodromos, 2011). The energy dissipation of both the impact element and the rubber bumper is thus neglected in this study.

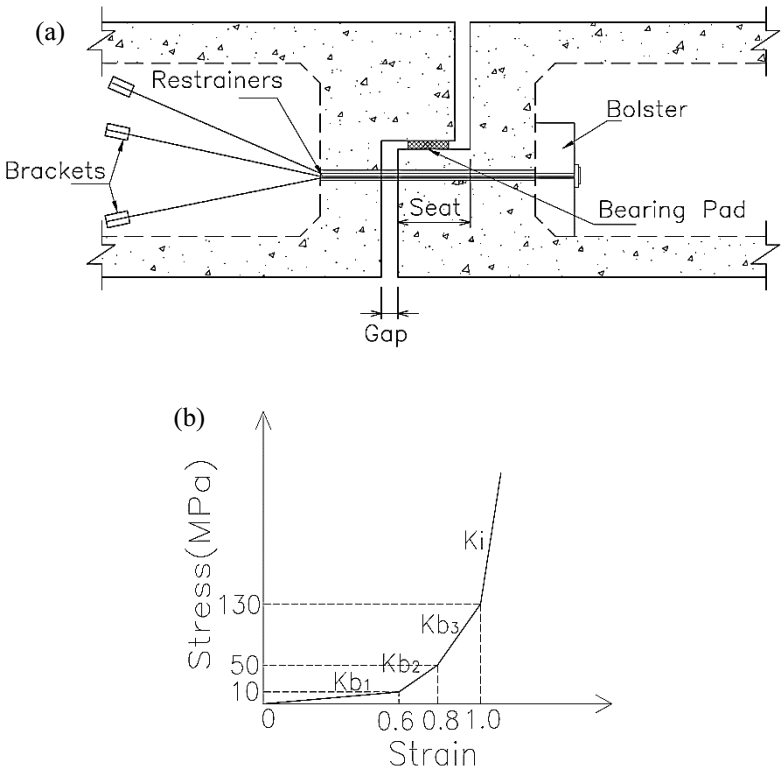

Figure 4-3 (a) Schematic illustration of expansion joint with bumper and restrainers; (b) Stress strain relationship of impact element including the rubber bumper.

4.4 Ground Motion Modelling

It is common in engineering practice to simulate spatially varying ground motions that are compatible with the specific design response spectra. Many stochastic ground motion simulation methods have been proposed by different researchers. For example, Hao et al. (1989) and Deodatis (1996) simulated the spatially varying ground motions in two steps, first the spatially varying ground motion time histories are generated using an arbitrary power spectral density function, and then adjusted through iterations to match the target response spectrum. Usually a few iterations are needed to achieve a reasonable good match. Recently, Bi and Hao (2012) further developed this method by simulating the spatially varying ground motions which are compatible with the ground motion power spectral densities that are related to the target design response spectra instead of arbitrary power spectral density functions. Compared with the methods suggested by Hao et al. (1989) and Deodatis (1996), less or even no iterations are needed in the latter approach (2012), the latter method is thus computationally more efficient. The method proposed by Bi and Hao (2012) is adopted in the present study to simulate the spatially varying ground motion time histories that are compatible with the design spectra specified in the New Zealand Earthquake Loading Code (2004).

The spatial variation properties between ground motions recorded at two locations j and k on ground surface is modeled by an empirical coherency loss function (Sobczky, 1991)

$$\gamma_{jk}(i\omega) = \left|\gamma_{jk}(i\omega)\right| \exp(-i\omega d_{jk} \cos\alpha / v_{app}) = \exp(-\beta\omega d_{jk}^2 / v_{app}) \cdot \exp(-i\omega d_{jk} \cos\alpha / v_{app}) \quad (4.6)$$

where β is a constant reflecting the level of coherency loss, and β = 0.0002 is used in the present study. d_{jk} is the distance between the two locations j and k in the wave propagation direction, f is the frequency in Hz, v_{app} is the apparent wave velocity, and α is the seismic wave incident angle. In the present study, v_{app} is assumed to be 400 m/s, and $\alpha = 60^{\circ}$.

To study the influence of different soil types, the spatially varying ground motions at strong rock site (Class A), shallow soil site (Class C) and soft soil site (Class D) are simulated. To obtain relatively unbiased structural response, 3 sets of ground motion time histories are simulated for each site condition. In the simulations, the sampling and upper cut-off frequencies are set to 100 and 25 Hz, respectively, and the duration of 20.47s is selected to have a convenient total number of points (2048) for a fast Fourier transform.

Figure 4-4 shows a set of simulated acceleration time histories based on the response spectra for shallow soil site condition specified in the New Zealand Earthquake Loading Standard normalized to 0.72g and 5% damping. Figure 4-5 compares the response spectra of the simulated ground motions and the target design spectra. It shows that the simulated ground motions match well with the target design spectra. Figure 4-6 shows the comparison of the empirical coherency loss function (Equation 6) between site 1 and the other sites and the corresponding values of the simulated motions. Good match can also be observed except for $|\gamma_{15}|$ and $|\gamma_{16}|$ in the high frequency range. This, however, is expected because as the distance increases, the cross correlation between the spatial motions or their coherency values decrease rapidly with the frequency. Previous studies (Hao et al., 1989) revealed that the coherency value of about 0.3-0.4 is the threshold of cross correlation between two time histories because numerical calculations of coherency function between any two white noise series result in a value of about 0.3-0.4. Therefore, the calculated coherency loss between two simulated time histories remains at about 0.4 even the model coherency function decreases below this threshold value.

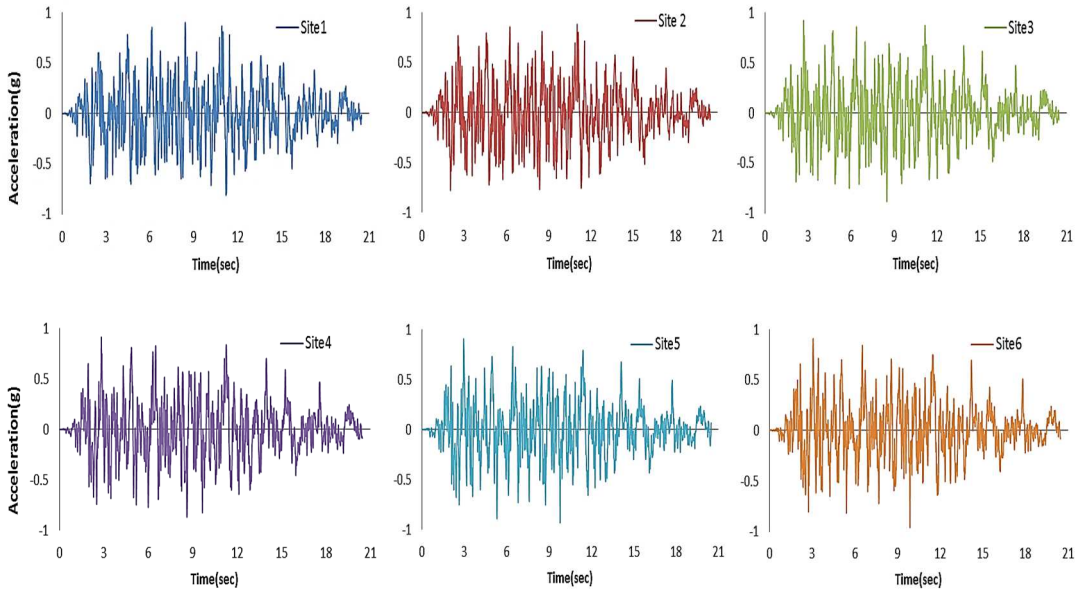

Figure 4-4 Simulated acceleration time histories.

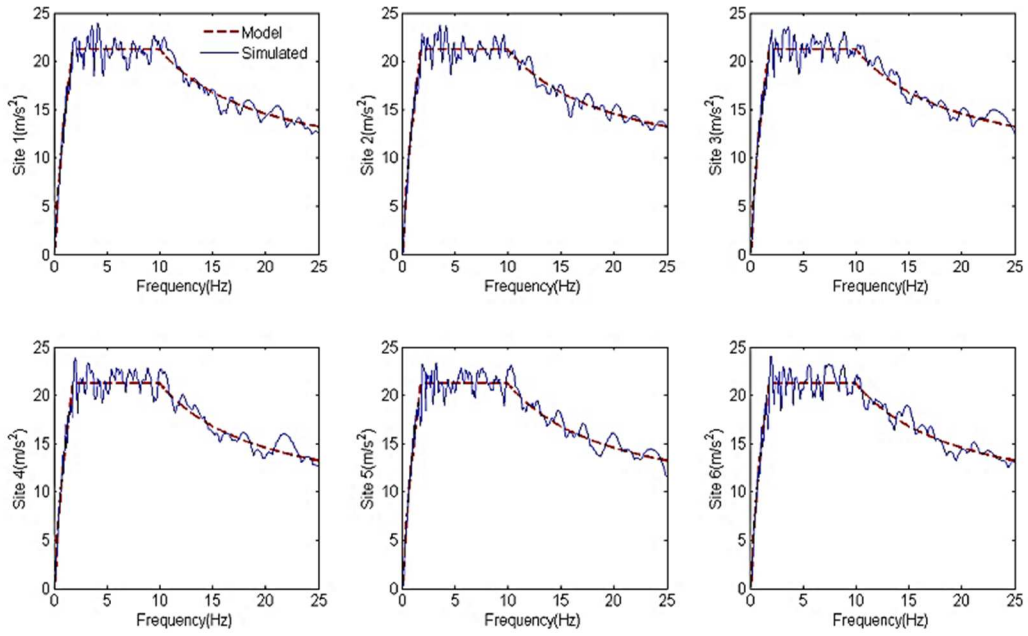

Figure 4-5 Comparison of the response spectra of the simulated ground motions and the target design spectra (shallow soil).

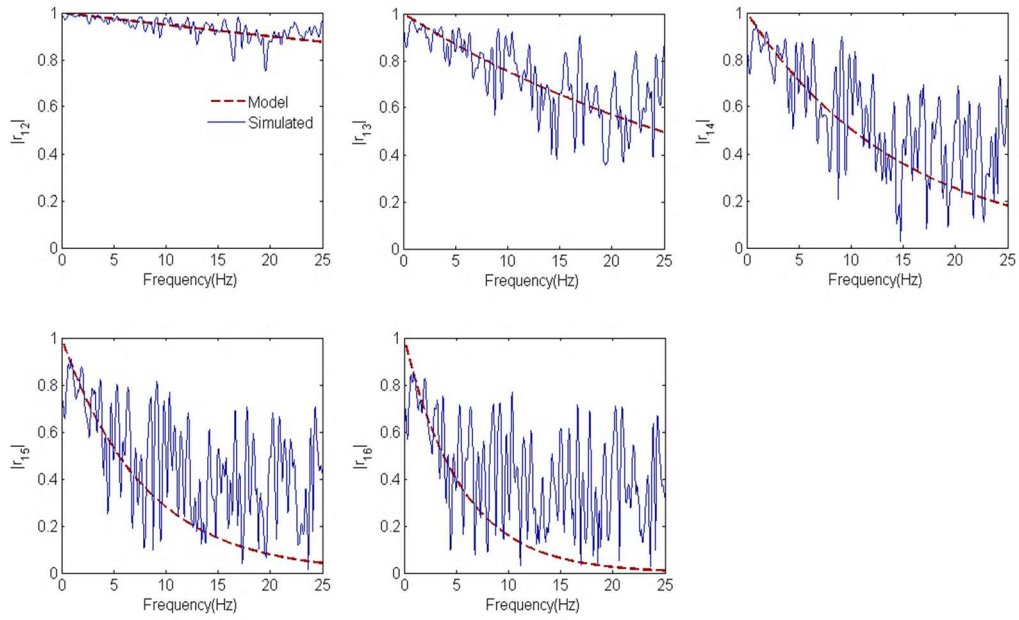

Figure 4-6 Comparison between coherency loss of simulated ground motions and model coherency loss function.

4.5 SMA and Steel restrainers modelling

Two different types of restrainers are investigated in this study, i.e., the steel cable restrainers and the SMA Cable restrainers. The steel cable restrainers are modelled by using the tension only bilinear elements. The length of the restrainers is fixed to 5.04m. The yield stress of the restrainers is 1210 MPa and initial modulus of elasticity is 69000 MPa, these values are the typical for the restrainers used by Caltrans. For the selection of the stiffness of the restrainers the design method suggested by DesRoches and Fenves (2000) is used in this study. The method has advantage of considering the out-of-phase vibration behavior of adjacent frames as well as the inelastic behavior. However, the design method does not consider the out-of-phase vibrations caused by spatially varying ground motion, but only those owing to different vibration characteristics of the adjacent spans. The restrainer's stiffness is calculated for the soft soil sites ground motions described in section 3. Table 4-3 presents the restrainer stiffness calculated for various ductility values, μ, for bridge 1 and 2 based on the analysis of two single degree of freedom systems. In this study, the initial stiffness of the restrainers of 30 kN/mm and strain hardening of 5% are assumed for both the bridges without losing the generality. This represents slight conservative value of stiffness of restrainers as during the strong earthquake high value of ductility could be achieved. However, this conservatism is justified considering the spatially varying ground motion used in this study. The initial slack of the cables is assumed to be 15 mm as specified in typical Caltrans bridges.

Table 4-3 Stiffness of designed restrainers for Bridge Model 1 and 2

	Restrainer Stiffness (kN/mm)		
Bridge Model	μ=1	μ=2	μ=4
Model 1	34.41	8.67	3.00
Model 2	58.08	25.97	13.32

Superelastic SMA has an ability to recover its original shape upon unloading. This property derives from the fact that SMA can transform from one phase to the other (austenite to martensite or vice versa) by applying or removing mechanical loading. The superelasticity phenomena provide SMAs with high re-centering capacity, which is demonstrated in Figure 4-7 (a) by the large elastic strain range (typically 6-8%). Additionally, hysteretic ductility of superelastic SMA limits the force transformed to the adjacent structure. Superelastic SMAs are also characterized by a sharp increase in stiffness once the elastic strain limit is exceeded. In this study, superelastic SMA restraining devices which are composed of the bundled or twisted SMA wires in the form of the cables are modelled using the uni-axial model for superelastic SMA programmed by Fugazza (2003) and that follows the constitutive relationship proposed by Auricchio and Sacco (1997). This model is capable of reproducing both super elasticity and damping properties of SMA. The parameters used to define the complete stress-strain relationship of SMA are listed in Table 4-4. The initial slack of the SMA cables are also assumed to be 15mm. To compare the effectiveness of the SMA cables with steel cable restrainers, it is necessary to ensure the effective stiffness added to the structures by each device is the same. In the case of the cable restrainers the yield strain is 1.75%. However, SMA devices are capable of reaching the elastic strain of approximately 7% with no residual strain. In this study, the effective stiffness of the SMA device at the elastic strain limit (7% strain) is assumed to be equal to the initial stiffness of the designed steel strain (1.75% strain) to ensure both the devices will experience the same force at their extreme elastic strain levels. This can be achieved by using a shorter SMA Cable of 1.26 m as compared to the 5.04 m long steel cable restrainer. Figure 4-7 (b) compares the force-displacement behavior of the superelastic SMA device with the steel restrainers.

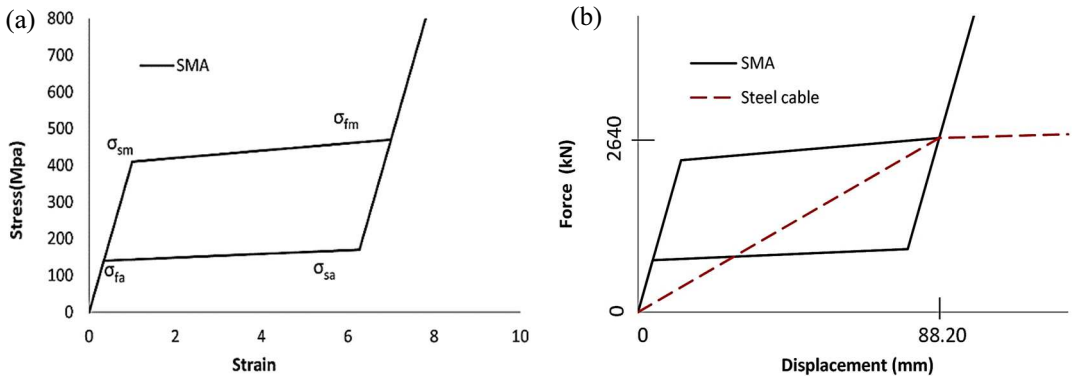

Figure 4-7 (a) Constitutive modelling of SMA based restrainers; (b) Force-displacement relationship of steel cable restrainers and SMA based restrainers.

Table 4-4 Constitutive material properties for NiTi based SMA

Parameters	Value
Austenite to martensite starting stress, σ_{sm} (MPa)	410
Austenite to martensite finishing stress, σ_{fm} (MPa)	470
Martensite to austenite starting stress, σ_{sa} (MPa)	170
Martensite to austenite finishing stress, σ_{fa} (MPa)	140
Yield strain limit,	1%
Recoverable pseudo elastic strain limit	7%

4.6 Effects of Restrainers

In order to evaluate the effectiveness of the steel cable and SMA restrainer, responses of two bridge models installed with the two types of restrainers are compared. Without losing generality, only the results corresponding to the soft soil site conditions are presented and discussed in detail. The responses of the two model bridges in terms of the joint opening, pier response, pounding force and restrainer's response are compared for three sets of simulated spatially varying ground motions.

Figure 4-8 presents the joint opening response at the in-span hinge of bridge model 1 to simulated 3 sets of spatially varying ground motions. The graph shows both the steel and SMA restrainer cables are effective in reducing the joint openings at the in-span hinge, however, the SMA restrainers are superior in terms of restricting hinge opening. Reductions of the peak joint opening with steel restrainers for the three ground motion cases are 34, 29 and 41%, respectively compared to the bridge model without restrainers. The corresponding reductions with the SMA restrainers are 66, 56 and 57% respectively. It is to be noted that the relative joint opening displacement for the bridge with relatively similar fundamental period is significantly large when restrainers are not considered. This clearly indicate that the present

code provision to balance the fundamental period of adjacent structure to mitigate unseating damage is not sufficient when spatial variability of ground motion is considered. Figure 4-9 presents the comparisons of the force-displacement relations of the steel restrainers and the SMA restrainers in bridge model 1 subjected to the three sets of simulated spatial ground motions. The reason for the lower joint opening with SMA restrainers could be clearly interpreted through the comparison of hysteretic curves. Due to the stiffening effect of the SMA after the achievement of martensite finishing stress joint opening is restricted at the cost of increased tensile forces. However, in the case of steel restrainers, after yielding the stiffness drops remarkably thus limiting the induced forces on the restrainers but increasing the joint opening rapidly. Also the SMA based restrainers are able to recover to its original length whereas the yielding of the steel cable restrainers always results in some residual displacement. The energy dissipating capacity along with the re-centering behavior of SMA makes it an ideal device to be used as restraining devices for the bridge structures.

The effects of the addition of the restrainers on the response of the bridge piers are presented in Figure 4-10 and Figure 4-11. Figure 4-10 presents the response of pier 1, which is located in stiffer frame shown in Figure 4-1. Figure 4-11 presents the response of pier 3 located in flexible frame. The results suggest that the inclusion of restrainers at mid span hinges results in a slight increment of responses in piers of the stiffer frame as suggested by the larger areas of hysteretic curves for frames with restrainers in Figure 4-10, and reduces the demand to some extent in the flexible frame piers as shown in Figure 4-11. This is expected because the stiffer frame restrains the response of the flexible one, while the flexible frame pulls the stiffer one to increase its response. It should be noted that the inclusion of the two types of restrainer results in slightly different pier hysteretic response, but it is very difficult to judge the performance of them in terms of the pier responses as on average both restrainers lead to nearly similar areas in hysteretic curves, suggesting approximately similar effects. Figure 4-12 presents the pounding force and joint acceleration of the intermediate hinge of bridge model 1. SMA restrainers result in lowest pounding force as well as the lowest joint acceleration among the three cases. Figure 4-13 presents the comparison of the joint opening for joints 1 and 2 of bridge model 2. The results presented are consistent with the observations made above for bridge model 1 that joint openings without the restrainers are larger than that with restrainers and SMA restrainers perform better in restricting the joint opening.

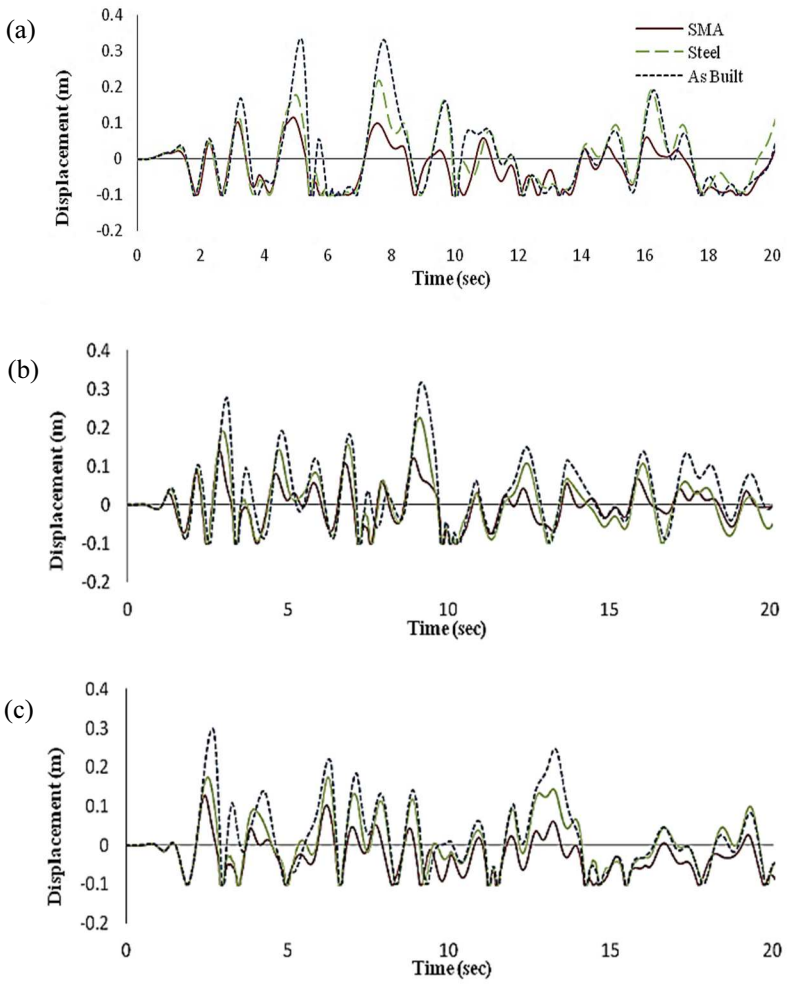

Figure 4-8 Joint opening at intermediate hinge of bridge model 1 without, with steel and SMA restrainers to three sets of simulated ground motions for Soft soil condition: (a) set 1, (b) set 2, (c) set 3.

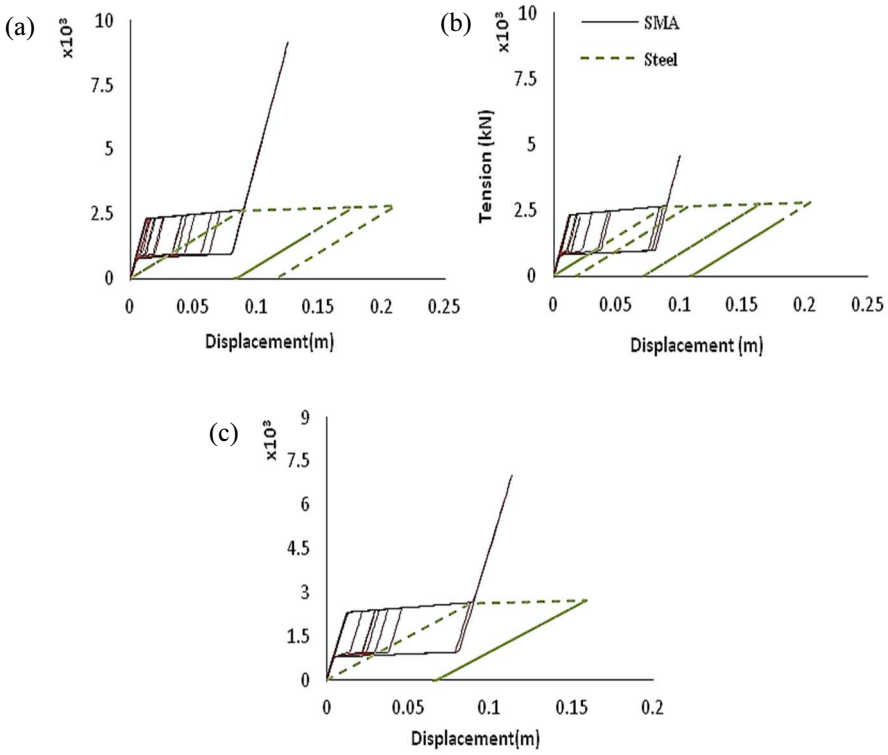

Figure 4-9 Comparison of the response of steel and SMA restrainers in bridge model 1 to three sets of spatial ground motions for soft soil condition: (a) set 1, (b) set 2, (c) set 3.

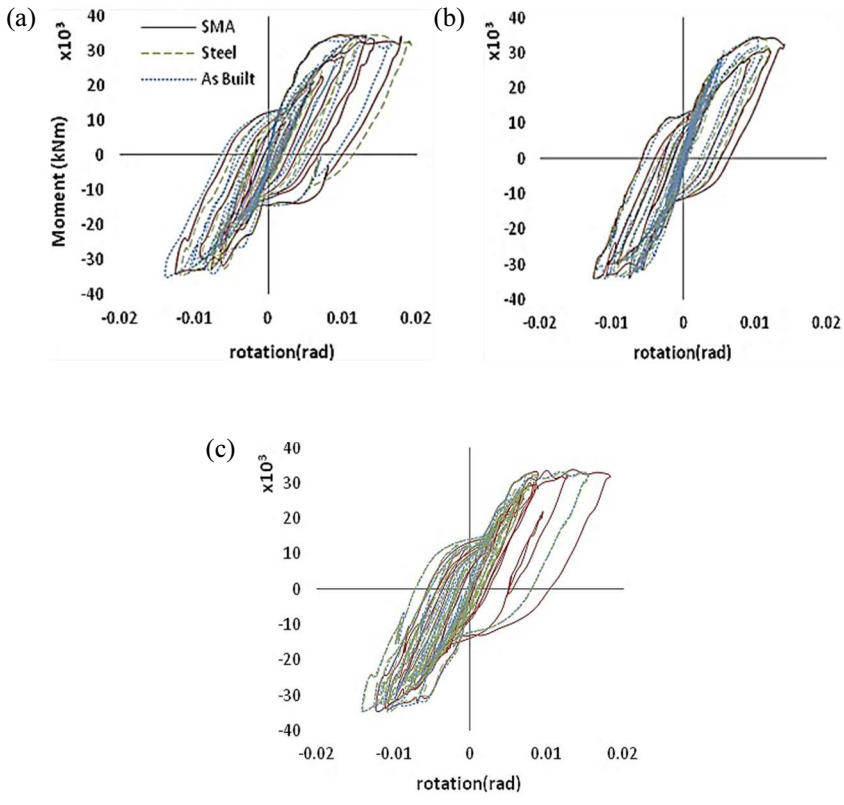

Figure 4-10 Response of pier 1 of bridge model 1 without and with restrainers to three sets of simulated spatially varying ground motions for soft soil: (a) set 1, (b) set 2, (c) set 3.

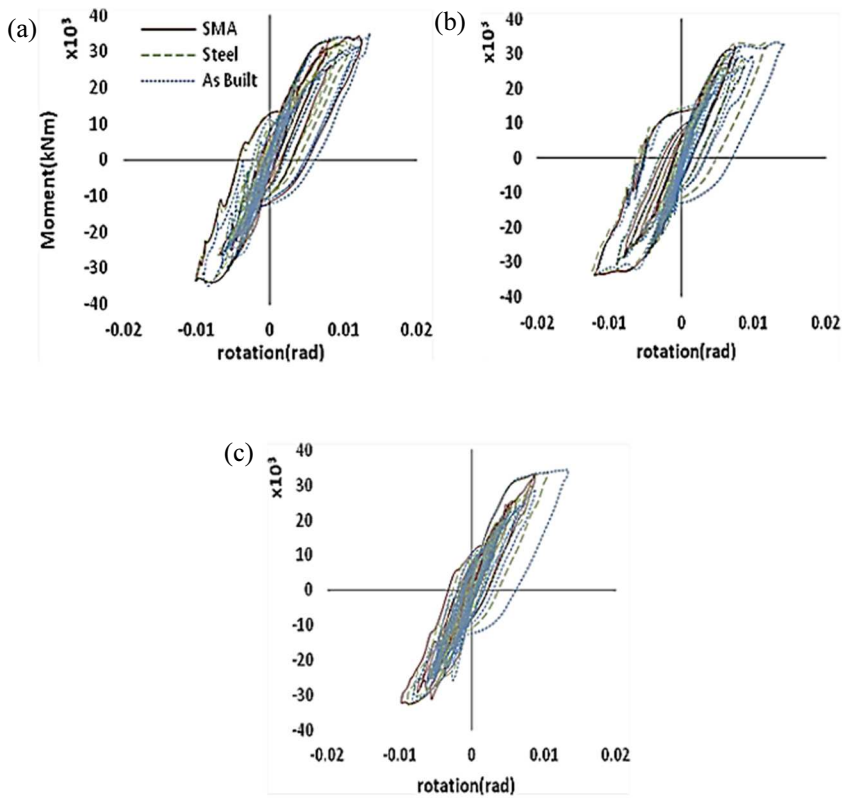

Figure 4-11 Response of Pier 3 of bridge model 1 without and with restrainers to three sets of simulated spatially varying ground motions for soft soil: (a) set 1, (b) set 2, (c) set 3.

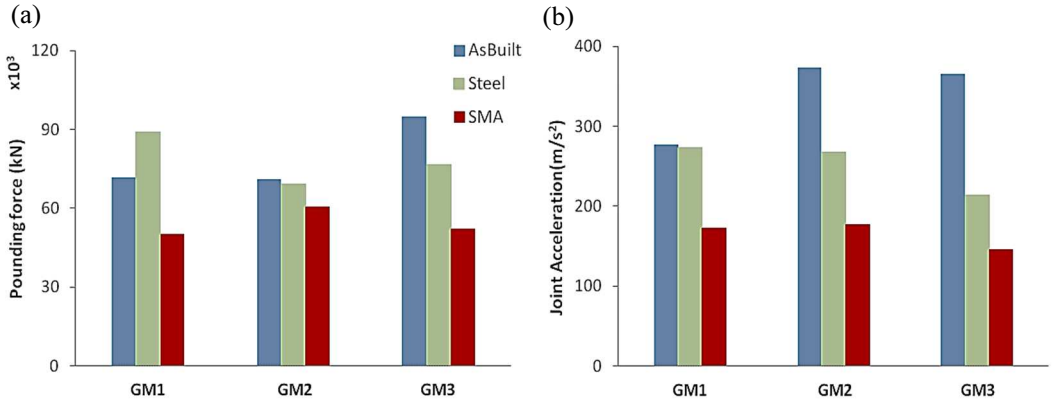

Figure 4-12 Comparison of (a) Pounding force and; (b) Joint acceleration of bridge model 1 for three sets of spatially varying ground motions.

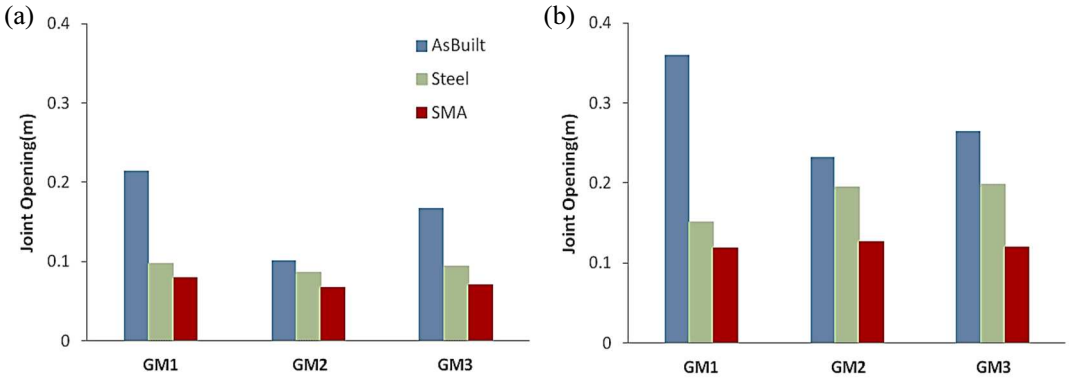

Figure 4-13 Comparison of relative joint opening displacement of bridge model 2 at: (a) Joint 1; (b) Joint 2 to spatial ground motion for soft soil condition.

4.7 Effects of Rubber Bumper

Poundings between adjacent bridge structures with limited gap sizes provided by conventional expansion joints are unavoidable. Pounding results in large impact forces and transfers large lateral force from one deck to another. The effect of such large impact forces and large lateral force transfer could result in localized damages in decks and abutments or even the collapse of the bridge structure. Using a layer of soft visco-elastic material as shock absorbing media between the decks of the bridge could mitigate such large impact force. A simple and inexpensive method of placing a rubber bumper between decks of the bridge could mitigate impact forces, and hence eliminate the large acceleration pulses caused due to the impacts.

In this study a series of analyses are conducted to investigate the effectiveness of natural rubber bumpers to mitigate large amplitude impacts. Without losing generality, again only the results corresponding to the soft soil site conditions are presented in detail. Six different models are investigated to examine the effect of addition of natural rubber bumpers on the responses of the bridge structures. Rubber bumpers are added to the expansion joints of the bridge models without restrainers and with steel cable or SMA restrainers. The rubber bumpers of thickness of 50mm are provided in the 100mm expansion joints of two bridge models. Figure 4-14 compares the pounding forces at mid-span hinges of the bridge model 1 with and without rubber bumpers. It is clear that inclusion of the rubber bumpers as a shock absorbing device results in a reduction of the pounding forces. Figure 4-15 compares the pounding forces at the hinge of the bridge model 1 with SMA restrainers only and SMA restrainers together with rubber bumpers from 4 to 10 seconds of the analysis subjected to set 3 of the spatially varying ground motions. As shown, the rubber bumpers reduce the pounding force but lead to more number of poundings due to reduction of the gap width. The rubber bumpers also elongate the pounding duration. Figure 4-16 shows the acceleration responses of the deck at impact location. As shown, incorporation of rubber bumpers eliminates

acceleration spikes. Figure 4-17 shows the peak impact force and opening relative displacement response of the bridge model 1 subjected to the three sets of ground motions for soft soil condition (GM1 to GM3), in which AB and RUB represent as built and with rubber bumpers, RES and RES+RUB represent the case of bridge model with steel restrainers and steel restrainers with rubber bumpers, respectively. SMA and SMA+RUB represent the case of bridge model with SMA restrainers alone and with rubber bumpers. As shown, inclusion of rubber bumpers not only affects the impact force, but also the relative opening displacement between the adjacent decks. This is because rubber bumper changes the impact force as well as reduces the separation gap between the adjacent decks, which may result in either an increase or decrease of the relative separation displacement.

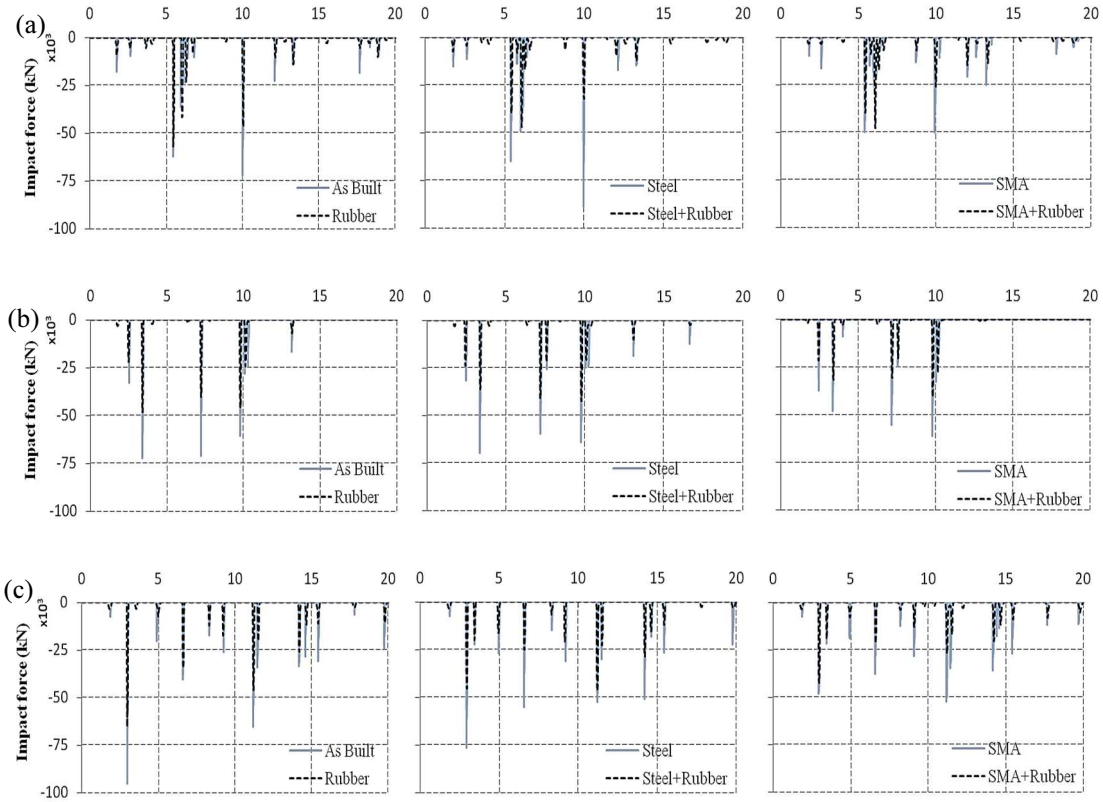

Figure 4-14 Pounding forces on bridge model 1 with and without rubber bumper for three sets of spatially varying simulated motions for soft soil site: (a) set 1, (b) set 2, (c) set 3.

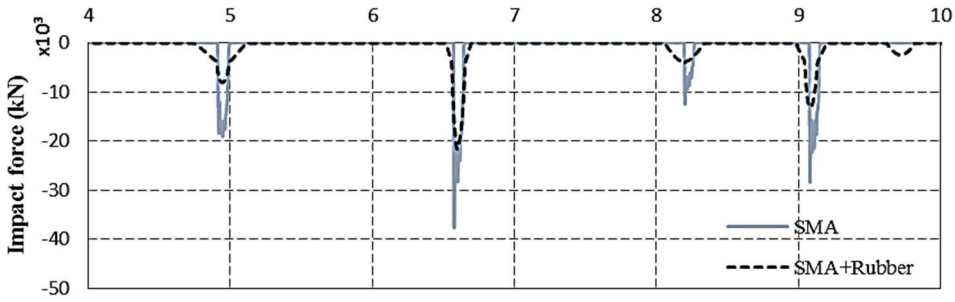

Figure 4-15 Pounding forces on bridge model 1 with SMA restrainer and SMA restrainer with rubber bumpers for set 3 ground motion between 4 to 10 second of analysis.

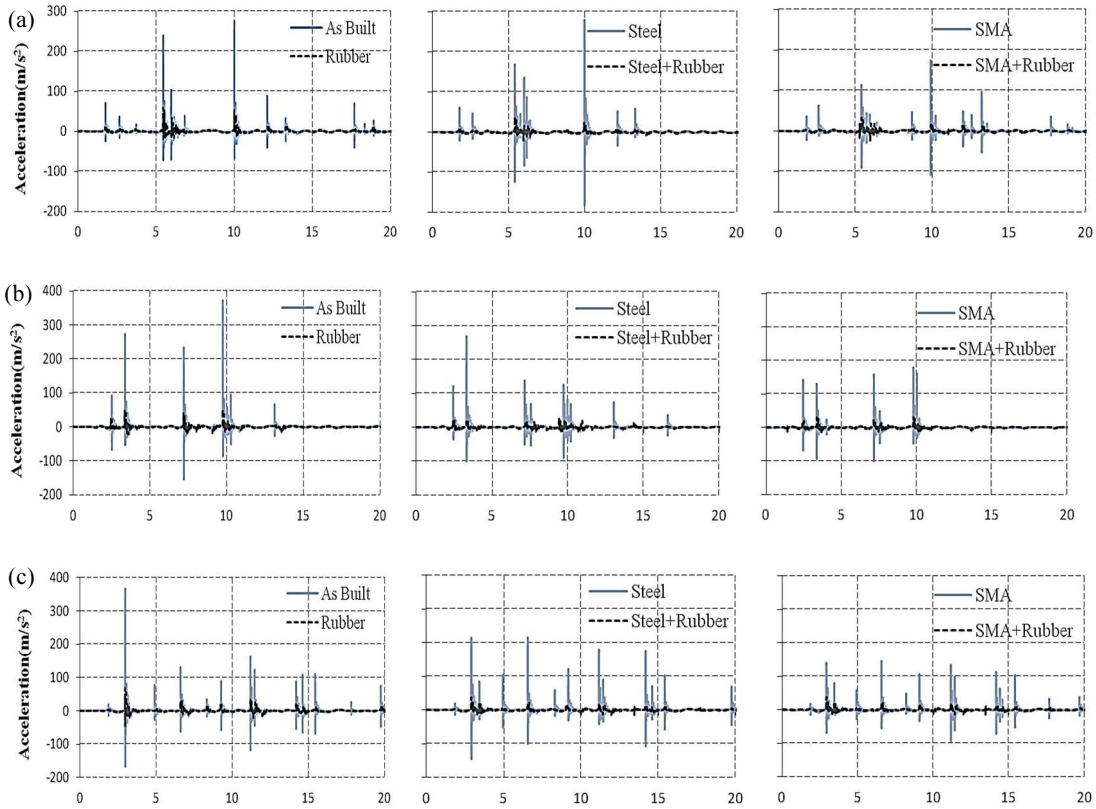

Figure 4-16 Pounding force with and without rubber bumpers for Model 1 subjected to the three sets of spatially varying motions: (a) set 1, (b) set 2, (c) set 3.

Figure 4-18 and Figure 4-19 depict the peak impact force and the maximum opening displacement of the joint 1 and joint 2 of the bridge model 2 corresponding to the different ground motions and mitigation measures. As shown, at the both joints it is clear that application of rubber bumpers alleviates the peak impact forces. However, the effects of the rubber bumpers on the relative separation response of the bridge joints are not always beneficial. Inclusion of rubber bumpers may result in a larger joint opening displacement because of the more number of impacts and prolonged impact duration, hence may lead to an increased unseating damage potential. Therefore, it is important to use rubber bumpers

together with restrainers to mitigate pounding damage while preventing deck unseating. Comparing the responses of bridge joints presented in Figure 4-17 to Figure 4-19, it can be summarized that SMA based restrainers combined with rubber bumpers could significantly improve the responses of bridge joints by not only reducing the relative joint opening but also the peak pounding forces.

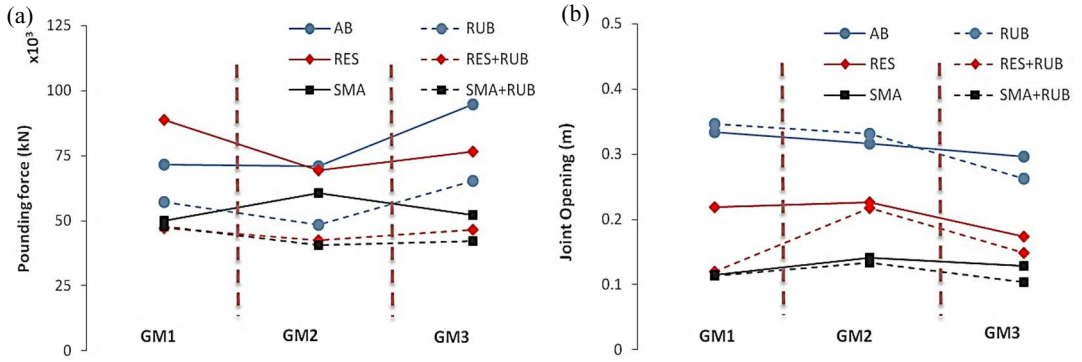

Figure 4-17 Comparison of the maximum pounding force with and without rubber bumpers; (b) Comparison of the maximum relative joint opening with and without rubber bumpers for Model 1.

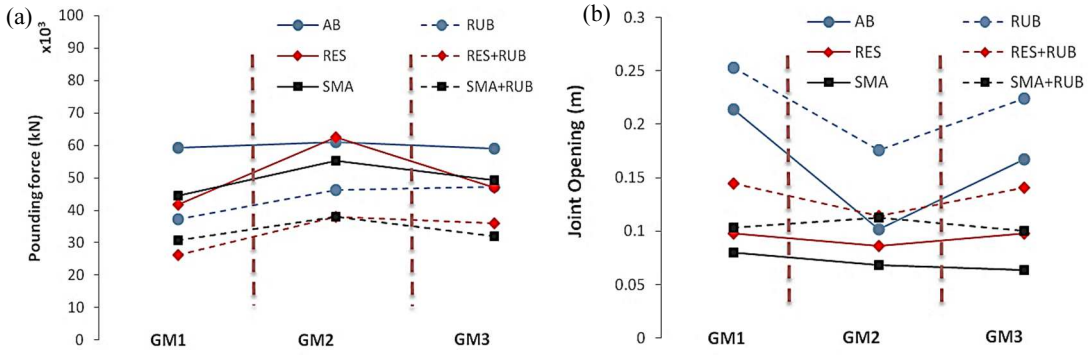

Figure 4-18 (a) Comparison of the maximum pounding force with and without rubber bumpers; (b) Comparison of the maximum joint opening with and without rubber bumpers for joint 1 of Model 2.

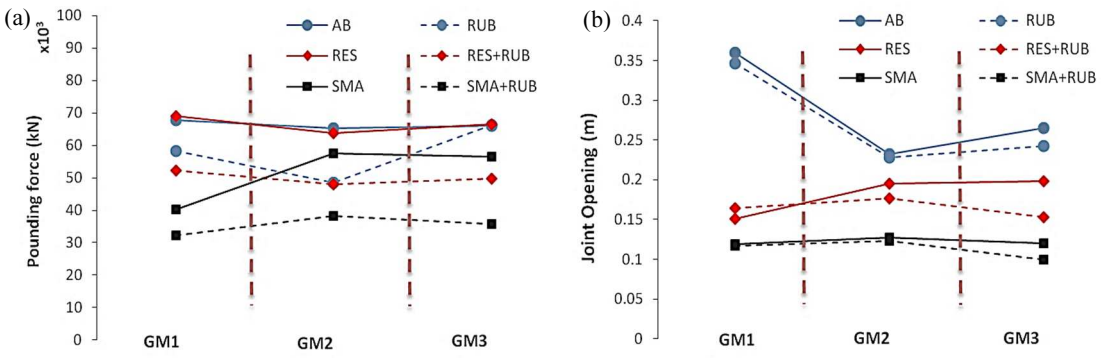

Figure 4-19 (a) Comparison of the maximum pounding force with and without rubber bumpers; (b) Comparison of the maximum joint opening with and without rubber bumpers for joint 2 of Model 2.

4.8 Effects of soil site conditions

A series of analyses are conducted to evaluate the performance of the considered pounding mitigation and unseating prevention devices when subjected to ground motions corresponding to different soil conditions. In this study three different site conditions namely; rock, shallow soil and soft soil are utilized to generate ground motions with different frequency contents. Figure 4-20 compares the mean maximum pounding forces and the mean maximum relative joint opening displacement for bridge model 1 corresponding to the different site conditions. The mean maximum pounding forces and the mean maximum relative displacement are the mean values of the maximum pounding force and relative joint opening displacement respectively from three ground motions simulated for each site condition. As shown the peak pounding forces obtained from the ground motion on shallow soil and rock site are smaller than those obtained from the ground motion on soft soil site owing to the relatively high frequency contents of ground motion. Because of the relatively small impact force generated from ground motion on shallow and rock site, the effectiveness of the rubber bumpers to mitigate pounding impacts are slightly reduced as compared to the soft soil condition. Nonetheless, the rubber bumpers are effective in reducing pounding forces on all the sites considered.

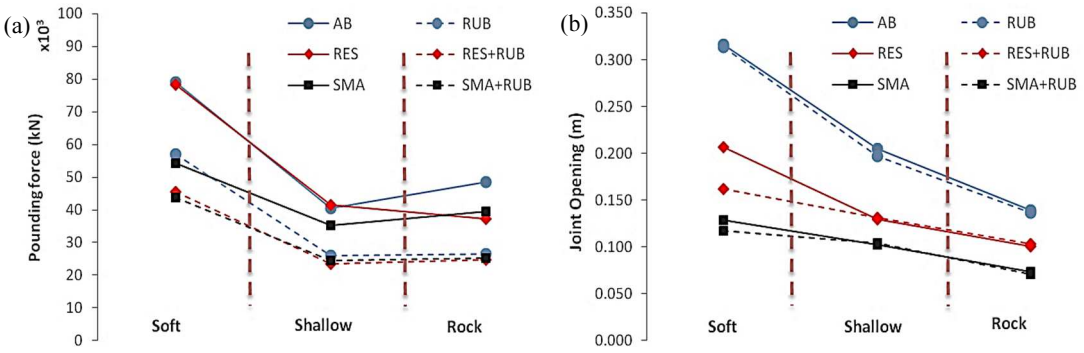

Figure 4-20 (a) Comparison of the mean maximum pounding force with and without rubber bumpers; (b) Comparison of the mean maximum joint opening with and without rubber bumpers for Model 1.

Figure 4-21 and Figure 4-22 show the mean maximum pounding force and the mean maximum relative joint separation displacements for the two joints of bridge model 2. The results presented in Figure 4-21 (b) and Figure 4-22 (b) suggest that inserting rubber bumpers in joints of as built bridge could induce larger joint separation particularly when the bridge locates on soft soil site. This is because the reduction of gap size in the joint due to the inclusion of bumpers increases the number of poundings which could influence pounding and the deck relative movement at another joint particularly when the pounding forces are large as in case of soft soil condition. Therefore there is not a definitive pattern on the rubber bumper influence on the relative joint opening responses on the bridges with multiple intermediate joints. The results presented in Figure 4-20 to Figure 4-22 indicate that the combination of SMA based restrainers with rubber bumper will lead to a superior performance in terms of pounding mitigation and reduction of relative joint opening for both bridge models in all types of site conditions considered in this study.

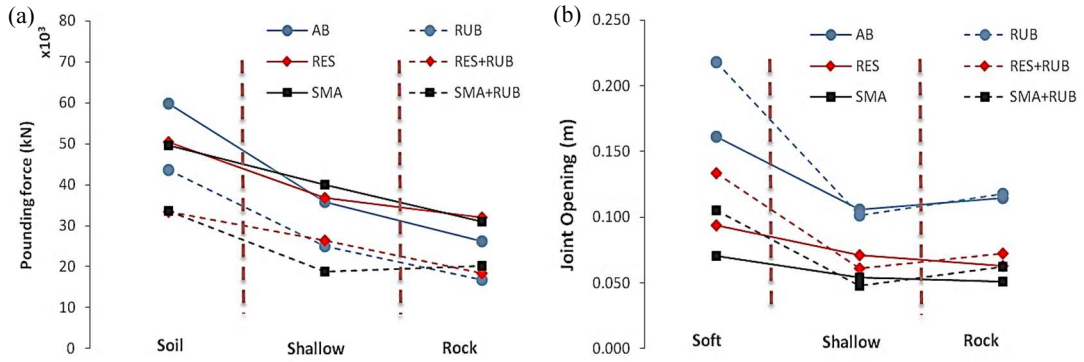

Figure 4-21 (a) Comparison of the mean maximum pounding force with and without rubber bumpers; (b) Comparison of the mean maximum joint opening with and without rubber bumpers for joint 1 in Model 2.

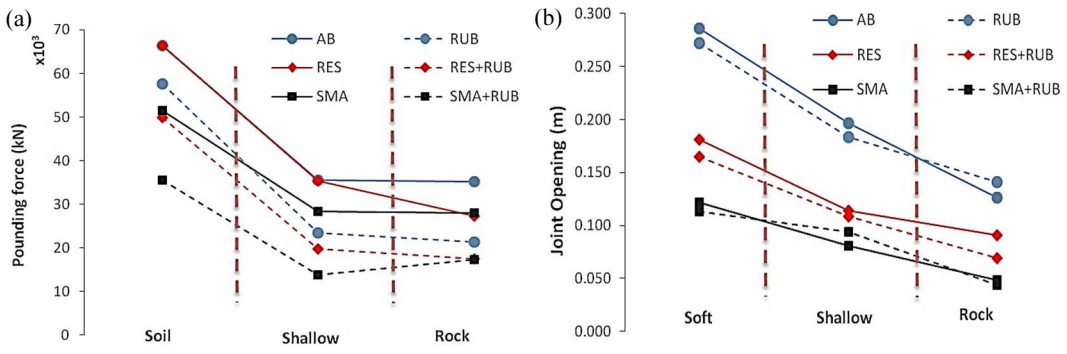

Figure 4-22 (a) Comparison of the mean maximum pounding force with and without rubber bumpers; (b) Comparison of the mean maximum joint opening with and without rubber bumpers for joint 2 in Model 2.

4.9 Parametric studies

A comprehensive parametric study is conducted to identify the various parameters affecting the performance of the rubber bumpers in mitigating pounding forces. This study focuses particularly on the rubber bumpers as the studies on the rubber bumpers are relatively rare. The parametric study is conducted on the bridge model 1 subjected to spatially varying ground motions simulated for soft soil conditions. The objective of this study is to find out the most influencing design factor that could affect the performance of the rubber bumpers.

4.9.1 Effects of the Gap Size

Pounding impacts between the adjacent frames are dependent upon the size of the gap provided. In this study the effects of gap sizes on the pounding of the bridge structures with the considered mitigation devices are conducted to evaluate the effectiveness of including rubber bumpers at the mid-span expansion joint of the bridge model with different gap sizes. In the numerical simulations, the expansion joint gap size is increased from 10 cm at an interval of 5cm to the width until the pounding is completely excluded. The rubber bumper with thickness of 50 mm is used in all the simulations.

Figure 4-23 (a) and Figure 4-23 (b) present the comparisons of the peak pounding forces and relative joint opening displacement with respect to different gap sizes. As shown, with the increase of the gap size between the adjacent decks the effectiveness of the rubber bumper in mitigating pounding forces reduces because the pounding force reduces with the gap size. However, the inclusion of rubber bumpers reduces the pounding forces at all gap sizes until pounding is completely precluded. It should be noted that inclusion of bumpers reduces the gap size, which may lead to occurrence of pounding events between adjacent structures when the gap size is large enough to preclude it if no rubber bumpers are used. However, the pounding force is relatively small since the gap width is relatively large in these cases. Similar

finding was also reported by Polycarpou and Komodromos (2011). This is a disadvantage of using bumpers in the expansion joint. Nonetheless the effectiveness of bumper in mitigating pounding forces is obvious when the expansion gap is not big enough to completely preclude pounding, which is the usual case in practice owing to the constraint for smooth traffic flow. Figure 4-23 (b) shows that the effects of the rubber bumpers on the relative joint openings are less eminent.

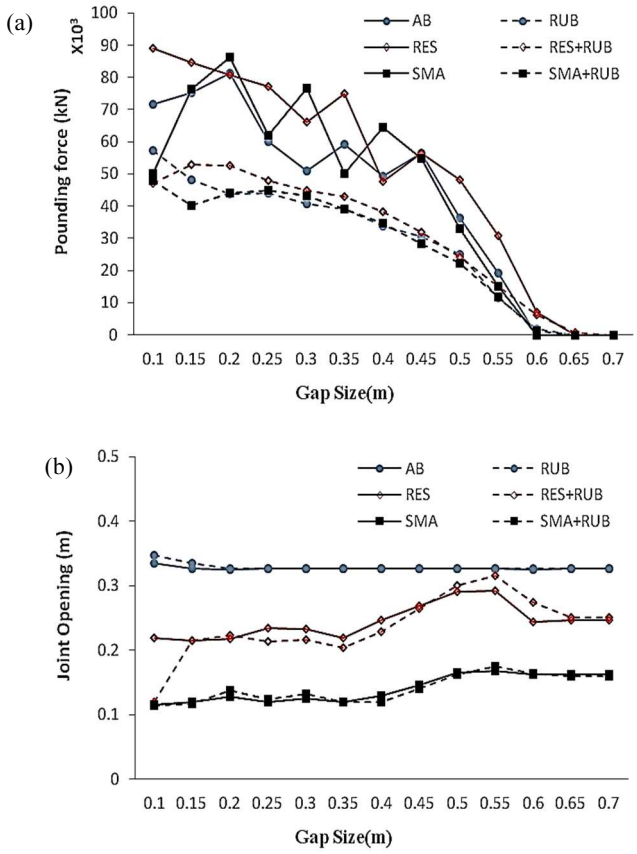

Figure 4-23 (a) Comparison of the maximum pounding force with and without rubber bumpers; (b) Comparison of the maximum joint opening displacement with and without rubber bumpers of Model 1 for various gap sizes from GM1 set of motion on soft soil site.

4.9.2 Effects of numbers of the Rubber Bumpers

The effects of the numbers of bumpers placed between the adjacent girders of the bridge structure are examined in this section. All previous studies were based on 10 bumpers placed in expansion joint. To find out the influence of the numbers of bumpers five different cases are considered including no bumper, 5, 10, 20 and 30 bumpers, respectively. The lumped stiffness of rubber bumpers is calculated by multiplying the stiffness of a bumper by the numbers of bumpers used. The pounding response and relative joint opening at mid-span hinge

of the bridge model 1 subjected to the three simulated ground motion for soft soils are calculated.

Figure 4-24 (a) and (b), respectively present the mean maximum pounding forces and the mean maximum relative joint opening displacement for the joint with varying numbers of rubber bumpers. As shown the rubber bumper for pounding reduction is highly effective when the number of bumpers is 10. When more than 10 bumpers are placed its effectiveness is slightly reduced. This is because increasing the number of bumpers increases the stiffness of the bumpers. The increase in stiffness of the bumper might lead to a slight increase in pounding force particularly for models with restraining devices. As can be noted, the number of bumpers or bumper stiffness has insignificant effects on joint opening responses.

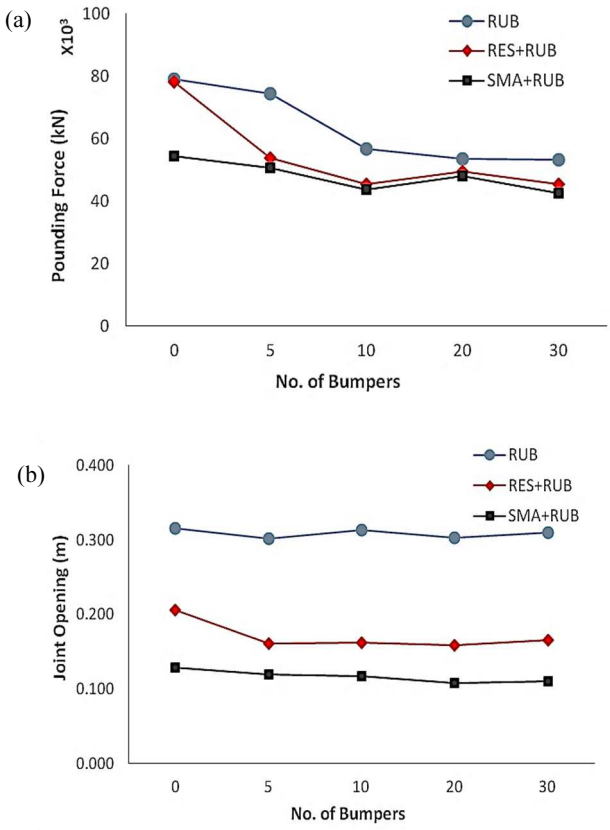

Figure 4-24 Comparison of the mean maximum pounding force; (b) Comparison of the mean maximum joint opening for varying number of rubber bumpers in bridge Model 1.

4.9.3 Effects of Rubber Bumper Thickness

It is expected that increasing the rubber bumper thickness might help to reduce the impact forces, but may result in more number of poundings and increase the pounding duration. In order to identify the effect of the thickness of the rubber bumpers on the current bridge system subjected to spatially varying ground motion, four cases of different bumper thicknesses are

considered. The parametric studies are conducted for bridge model 1with a gap of 100 mm and 10 rubber bumpers placed in the expansion joint subjected to three sets of spatially varying ground motions for soft soil site. Stress-strain model of rubber bumper defined in Figure 4-3 (b) is used to derive the force-displacement relations of bumpers with different thicknesses.

Figure 4-25 (a) and (b) present the mean maximum pounding forces and the relative joint opening displacement at mid-span joint. The results indicate that increase in the bumper thickness beyond 50% of the gap width would slightly decrease the peak pounding forces. The relative joint opening displacement is also slightly reduced by increasing the thickness of bumpers beyond 50% of gap size for the restrained bridge.

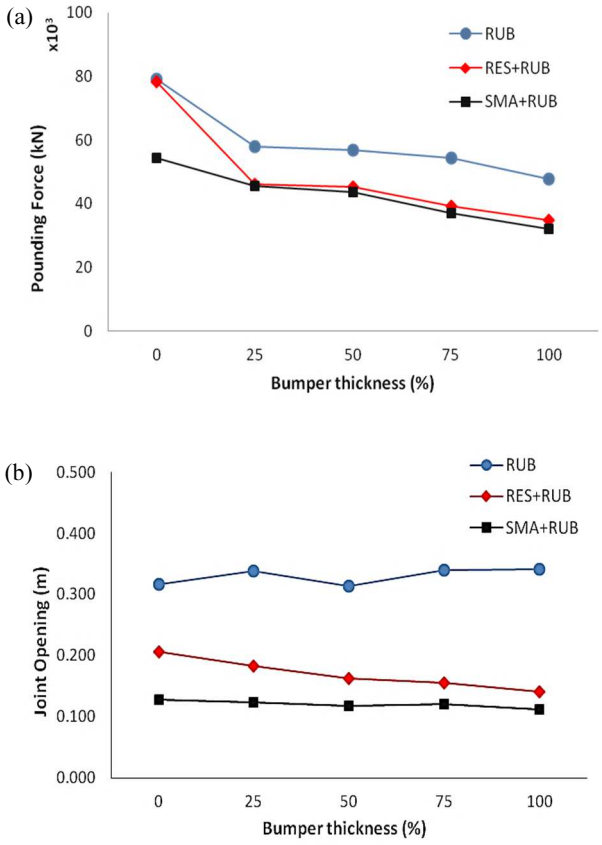

Figure 4-25 (a) Comparison of the mean maximum pounding force; (b) Comparison of the mean maximum joint opening for varying thickness of rubber bumper for Model 1.

4.10 Conclusions

The paper presents numerical studies on relative displacement responses of adjacent bridge structures with close fundamental periods to spatially varying ground motions. The study focuses on the comparison of the effectiveness of using two types of restrainers combined with the rubber bumpers on mitigating pounding and unseating damages of the adjacent bridge structures. Based on the results the following conclusions could be made:

SMA restrainers perform better than steel cable restrainers in terms of restricting the hinge opening. Unlike the steel cable restrainers, for which the effectiveness is lost after yielding, SMA restrainers showed stiffening effect which prevents large joint opening displacement. The SMA restrainers showed re-centering behavior, whereas the steel cable restrainers always resulted in residual displacement once the strain exceeded the yield strain limit. Additionally, energy dissipating behavior shown by the SMA restrainers with super elastic behavior makes it ideal for the application in bridge structures. The application of SMA restrainers did not further increase the demand on the adjacent frames compared to the steel restrainers. However, it did help to reduce the pounding impact and joint accelerations.

The results show that only adjusting the fundamental periods of the adjacent bridge frames close to each other as suggested in the current bridge design codes is not sufficient to mitigate large pounding forces and relative joint opening displacement when subjected to spatially varying ground motions. The rubber bumpers could be an effective method of reducing the large pounding forces. It also showed high effectiveness in eliminating the large acceleration spikes but resulted in more numbers of poundings due to the reduction of the gap width and increased the duration of the impact. The results suggest that use of SMA restrainers and the rubber bumper together at the joints could be the most effective in mitigating the damaging impact as well as the large separation between the adjacent structures.

The effectiveness of the rubber bumper depends upon the provided gap width and the amplitudes of impact forces. Using rubber bumpers is the most effective when the expansion joint gap is narrow and the induced pounding force is large. The results also demonstrated that the thickness and the numbers of rubber bumpers need to be effectively designed as providing thicker and more bumpers leads to only slight benefits in terms of mitigations of pounding damage between adjacent bridge structures.

4.11 References

Abdel Raheem, S. E. (2009). Pounding mitigation and unseating prevention at expansion joints of isolated multi-span bridges. *Engineering Structures*,*31*(10), 2345-2356.

Abdel Raheem, S. E., & Hayashikawa, T. (2012) *Effect of Expansion Joint Modelling on the Seismic Response of Bridges*. 15th World conference on Earthquake Engineering, Paper no. 3232, Portugal.

Andrawes, B., & DesRoches, R. (2005). Unseating prevention for multiple frame bridges using superelastic devices. *Smart Materials and Structures*, *14*(3), 60-67.

Andrawes, B., & DesRoches, R. (2007). Comparison between shape memory alloy seismic restrainers and other bridge retrofit devices. Journal of Bridge Engineering, 12(6), 700-709.
Auricchio, F., & Sacco, E. (1997). A superelastic shape-memory-alloy beam model. Journal of intelligent material systems and structures, 8(6), 489-501.

Bi, K., & Hao, H. (2012). Modelling and simulation of spatially varying earthquake ground motions at sites with varying conditions. *Probabilistic Engineering Mechanics*, *29*, 92-104.

Bi, K., & Hao, H. (2013). Numerical simulation of pounding damage to bridge structures under spatially varying ground motions. *Engineering Structures*, *46*, 62-76.

Bi, K., Hao, H., & Chouw, N. (2013). 3D FEM analysis of pounding response of bridge structures at a canyon site to spatially varying ground motions. *Advances in Structural Engineering*, *16*(4), 619-640.

Caltrans. (1990). Seismic Design Criteria. Design manual-first edition, California Dept. of Transportation, Sacramento, California.

Caltrans. (2010). Seismic Design Criteria. Design manual-version 1.6, California Dept. of Transportation, Sacramento, California.

Choi E. *Seismic analysis and retrofit of mid-America bridges*. PhD thesis, Georgia Institute of Technology, USA, 2002.

Chouw, N., & Hao, H. (2005). Study of SSI and non-uniform ground motion effect on pounding between bridge girders. *Soil Dynamics and Earthquake Engineering*, *25*(7), 717-728.

Chouw, N., & Hao, H. (2008). Significance of SSI and nonuniform near-fault ground motions in bridge response I: Effect on response with conventional expansion joint. *Engineering Structures*, *30*(1), 141-153.

Chouw, N., & Hao, H. (2009). Seismic design of bridge structures with allowance for large relative girder movements to avoid pounding. *Bulletin of the New Zealand Society for Earthquake Engineering*, *42*(2), 75.

Chouw, N., & Hao, H. (2012). Pounding damage to buildings and bridges in the 22 February 2011 Christchurch earthquake. *International Journal of Protective Structures*, *3*(2), 123-140.

Comartin, C.D., Greene, M., & Tubbesing, S.K. (Eds). (1995). The Hyogo-ken Nanbu earthquake Jan 17, 1995, EERI, Preliminary reconnaissance Report EERI-95-04, Oakland, CA.

Deodatis, G. (1996). Non-stationary stochastic vector processes: seismic ground motion applications. *Probabilistic Engineering Mechanics*, *11*(3), 149-167.

DesRoches, R., & Fenves, G. L. (2000). Design of seismic cable hinge restrainers for bridges. *Journal of Structural Engineering*, *126*(4), 500-509.

DesRoches, R., Pfeifer, T., Leon, R. T., & Lam, T. (2003). Full-scale tests of seismic cable restrainer retrofits for simply supported bridges. *Journal of Bridge Engineering*, *8*(4), 191-198.

DesRoches, R., & Delemont, M. (2002). Seismic retrofit of simply supported bridges using shape memory alloys. *Engineering Structures*,*24*(3), 325-332.

Feng, M. Q., Kim, J. M., Shinozuka, M., & Purasinghe, R. (2000). Viscoelastic dampers at expansion joints for seismic protection of bridges.*Journal of Bridge Engineering*, *5*(1), 67-74.

Fugazza, D. (2003). *Shape-memory alloy devices in earthquake engineering: mechanical properties, constitutive modelling and numerical simulations* (Doctoral dissertation, Istituto Universitario di Studi Superiori di Pavia).

Guo, A., Zhao, Q., & Li, H. (2012). Experimental study of a highway bridge with shape memory alloy restrainers focusing on the mitigation of unseating and pounding. *Earthquake Engineering and Engineering Vibration*, *11*(2), 195-204.

Hall, F.J. (Eds). (1994). Northridge earthquake Jan. 17 1994, EERI-Preliminary reconnaissance Report EERI-94-01.Oakland, CA.

Hao, H., Oliveira, C. S., & Penzien, J. (1989). Multiple-station ground motion processing and simulation based on SMART-1 array data. *Nuclear Engineering and Design*, *111*(3), 293-310.

Huo, Y., & Zhang, J. (2012). Effects of pounding and skewness on seismic responses of typical multispan highway bridges using the fragility function method. *Journal of Bridge Engineering*, *18*(6), 499-515.

Japanese Road Association. (1996). Specifications for highway bridges, part V, seismic design. *Tokyo, Japan*.

Jain, S. K., Lettis, W. R., Murty, C. V. R., & Bardet, J. P. (2002). Bhuj, India Earthquake of January 26, 2001 Reconnaissance Report, Publ. No 02-01.*Earthquake Engineering Research Institute (EERI), Oakland, CA*.

Kawashima, K., & Shoji, G. (2000, January). Effect of restrainers to mitigate pounding between adjacent decks subjected to a strong ground motion. In *Proceeding of the 12th World Conference on Earthquake Engineering*.

Kawashima, K., Takahashi, Y., Ge, H., Wu, Z., & Zhang, J. (2009). Reconnaissance report on damage of bridges in 2008 Wenchuan, China, earthquake. *Journal of Earthquake Engineering*, *13*(7), 965-996.

Kawashima, K., Unjoh, S., Hoshikuma, J. I., & Kosa, K. (2011). Damage of bridges due to the 2010 Maule, Chile, Earthquake. *Journal of Earthquake Engineering*, *15*(7), 1036-1068.

Kim, J. M., Feng, M. Q., & Shinozuka, M. (2000). Energy dissipating restrainers for highway bridges. *Soil Dynamics and Earthquake Engineering*, *19*(1), 65-69.

Kim, S. H., & Shinozuka, M. (2003). Effects of seismically induced pounding at expansion joints of concrete bridges. *Journal of engineering mechanics*, *129*(11), 1225-1234.

Li, B., Bi, K., Chouw, N., Butterworth, J. W., & Hao, H. (2012). Experimental investigation of spatially varying effect of ground motions on bridge pounding. *Earthquake Engineering & Structural Dynamics*, *41*(14), 1959-1976.

Malhotra, P. K. (1998). Dynamics of seismic pounding at expansion joints of concrete bridges. *Journal of Engineering Mechanics*, *124*(7), 794-802.

Mander, J. B., Priestley, M. J., & Park, R. (1988). Theoretical stress-strain model for confined concrete. *Journal of structural engineering*, *114*(8), 1804-1826.

Martínez-Rueda, J. E., & Elnashai, A. S. (1997). Confined concrete model under cyclic load. *Materials and Structures*, *30*(3), 139-147.

Padgett, J. E., DesRoches, R., & Ehlinger, R. (2010). Experimental response modification of a four-span bridge retrofit with shape memory alloys. *Structural Control and Health Monitoring*, *17*(6), 694-708.

Polycarpou, P. C., & Komodromos, P. (2011). Numerical investigation of potential mitigation measures for poundings of seismically isolated buildings. *Earthquake and Structures*, *2*(1), 1-24.

Priestley, M. N., Seible, F., & Calvi, G. M. (1996). *Seismic design and retrofit of bridges*. John Wiley & Sons.

Ruangrassamee, A., & Kawashima, K. (2001). Relative displacement response spectra with pounding effect. *Earthquake engineering & structural dynamics*, *30*(10), 1511-1538.

Saiidi, M. (1993). Response of bridge hinge restrainers during earthquakes: field performance, analysis, and design. Rep. no. CCEER93-6. *Center for Civil Engineering Earthquake Research, University of Nevada, Reno, Nev*.

Saiidi, M., Maragakis, E., & Feng, S. (1996). Parameters in bridge restrainer design for seismic retrofit. *Journal of Structural Engineering*, *122*(1), 61-68.

Schrage, I. (1981). Anchoring of bearings by friction. In *Joint Sealing and Bearing Systems for Concrete Structures, World Congress on Joints and Bearings* (Vol. 1), Niagara Falls, NY.

Seismosoft Inc. (2010). Seismo-struct user Manual for version 6, Pavia, Italy.

Selna, L. G., Malvar, L. J., & Zelinski, R. J. (1989). Bridge retrofit testing: Hinge cable restrainers. *Journal of Structural Engineering*, *115*(4), 920-934.

Sobczky, K. (1991) Stochastic Wave Propagation. Kluwer Academic Publishers, Netherlands.

NZS 1170.5. (2004). Structural Design Actions, Part 5: Earthquake actions–New Zealand.

Trochalakis, P., Eberhard, M. O., & Stanton, J. F. (1997). Design of seismic restrainers for in-span hinges. *Journal of Structural Engineering*, *123*(4), 469-478.

Uzarski, J., Arnold, C. (2001). *Chi-Chi, Taiwan Earthquake of September 21, 1999 Reconnaissance report*, Publication No. 01-02, EERI, Oakland, CA.

Zhu, P., Abe, M., & Fujino, Y. (2004). Evaluation of pounding countermeasures and serviceability of elevated bridges during seismic excitation using 3D modelling. *Earthquake engineering & structural dynamics*, *33*(5), 591-609.

CHAPTER 5
SEISMIC RESPONSE ANALYSIS OF MULTIPLE-FRAME BRIDGES WITH UNSEATING RESTRAINERS CONSIDERING GROUND MOTION SPATIAL VARIATION AND SSI

5.1 Abstract

Unseating damages of bridge decks have been observed in many previous major earthquakes due to large relative displacement exceeding the available seat length. Steel cable restrainers are often used to limit such relative displacements. Present restrainer design methods are based on the relative displacements caused by the different dynamic characteristics of adjacent bridge structure. However, the relative displacements in bridge structures are not only caused by different dynamic characteristics of adjacent bridge segments. Recent studies indicated that differential ground motions at supports of bridge piers and Soil Structure Interaction (SSI) could have a significant influence on the relative displacement of adjacent bridge components. Thus the present design methods could significantly underestimate the relative displacement responses of the adjacent bridge components and the stiffness of the restrainers required to limit these displacements. None of the previous investigations considered the effects of spatially varying ground motions in evaluating the adequacy of the restrainers design methods. Moreover, the code recommendation of adjusting the fundamental frequencies of adjacent bridge structures close to each other to mitigate relative displacement induced damages is developed based on the uniform ground motion assumption. Investigations on its effectiveness to mitigate the relative displacement induced damages on the bridge structures under the influence of spatially varying ground motion and SSI are made. This paper discusses the effects of spatially varying ground motions and SSI on the responses of the multiple-frame bridges with unseating restrainers through inelastic bridge response analysis.

5.2 Introduction

During an earthquake, adjacent bridge segments can vibrate out-of-phase because of their different dynamic characteristics and variations in the ground motion inputs at multiple bridge supports. The out-of-phase motion results in two main problems. Firstly, when the relative displacement between the bridge segments exceeds the available seat width, unseating of the bridge span occurs. Many cases of bridge collapse that occurred in recent earthquakes were attributed to this phenomenon (Saiidi et al. 1993, Moehle 1995, Comartin et al., 1995, Kawashima et al. 2011). On the other hand, when the bridge spans vibrate towards each other pounding might occur if the relative displacement is larger than the expansion gap size. Pounding could cause significant impact forces that can result in local damages and crushing of concrete. Additionally, large impact forces can increase opening at hinges between simply

supported spans or at in-span hinges, which in turn could increase the possibility of unseating of the bridge spans.

Unseating of bridge decks during the 1971 San Fernando earthquake in the USA was a major reason behind the collapse of several bridges. This earthquake triggered the development of seismic restrainers to prevent the excessive relative movement of girders at superstructure hinges and at girder supports. Seismic restrainers since then have been installed as a retrofit measure in bridges with narrow supports to restrict the movement. It has also been used in new bridges with wide supports as a backup system. Steel cables and high strength steel rods attached to steel connections are the most widely used restrainer types. During the earthquakes such as the 1989 Loma Prieta, 1994 Northridge and 1995 Kobe earthquake restrainers were found effective in protecting the bridges against the unseating failures. However, a few bridges that had been retrofitted with cable restrainers still collapsed due to the unseating at hinges (Moehle 1995), indicating better understanding the performances of restrainers during strong shaking and improvement in the design are needed. Many researchers have since carried out researches to understand the influencing factors on the behavior of restrainers, its influence on the overall performance of the bridge structures and to provide appropriate design procedure for restrainers. Saiidi et al. (1996) investigated four bridges retrofitted with cable restrainers during the 1989 Loma Prieta earthquake and concluded that the performances of restrainers were affected by many factors such as the amplitude and frequency contents of the ground motion, foundation flexibility as well as flexibility of the substructure and recommended that nonlinear time history analysis is necessary to design appropriate restrainers. Trochalakis et al. (1997) conducted 216 non-linear time history analyses for various frames, abutments, and restrainer properties and showed that the maximum relative displacement was sensitive to the stiffness of adjacent frames, the frames' effective periods, and the restrainer properties. DesRoches and Fenves (2000, 2001) suggested a new design procedure for steel restrainers and compared it with the results from nonlinear time history analyses. DesRoches and Muthukumar (2002) carried out a comprehensive study on the effects of pounding and restrainers on seismic response of multiple-frame bridges. It should be noted that all these studies neglected the effects of ground motion spatial variations, which, as will be demonstrated later in this paper, might be the detrimental factor that generates relative displacement between bridge spans.

As mentioned, most of the previous studies neglected the relative displacement arising from the non-uniform ground motions thus could underestimate the relative response of adjacent structures. For example, the design method of the restrainers developed by DesRoches and Fenves (2000) takes into account only the out-of-phase vibration caused by different

fundamental vibration frequencies of adjacent bridge components. As a result, it could underestimate the required stiffness and strength of the restrainers when subjected to spatially varying motion. This is realized by the current Caltrans code (Caltrans 2010), which states that "a satisfactory method for designing the size and number of restrainers required at expansion joints is not currently available". Researches on the response of bridge structure with cable restrainers to spatially varying ground motion including the SSI effect are inexistent. Though Won et al. (2008) investigated the effects of restrainers and pounding on the bridge responses subjected to non-uniform ground motion, due to the complexity of modelling coherency losses the study considered only the wave passage effect of spatial ground motion variations. Shrestha et al. (2014) presented the comparison of the response of different restrainers to spatially varying ground motions, in which ground motion spatial variation was modelled in detail. However, the study did not consider the SSI effects, which was demonstrated significantly influencing the relative responses between adjacent bridge structures (Chouw & Hao, 2008). The latter study demonstrated the importance of considering ground motion spatial variations in calculating the relative displacement. As spatial variability of the ground motions at multiple supports of bridge structures are inevitable due to the wave propagation and different soil conditions along the length of the bridge, the existing restrainers design method must be evaluated considering the additional relative motion caused by spatially varying ground motions and SSI to effectively prevent catastrophic unseating failures.

The only method presently suggested by bridge design codes to mitigate pounding and unseating damage of bridge girders is to adjust the fundamental frequencies of the adjacent structures as close as possible (Caltrans, 2010). It is recommended for all new constructions to adjust the ratio of fundamental period of the adjacent frames to at least 0.7. This provision of the code is proven to mitigate the pounding effects by reducing out-of-phase vibration of the adjacent bridge structures resulting from the different natural frequencies (DesRoches & Muthukumar, 2002). However, the out-of-phase vibration is not only caused by the different natural frequencies of the adjacent bridge components, spatial variations of the ground motions and the characteristics of soil-structure systems also significantly affect the relative displacement response of the adjacent structures (Chouw & Hao,2005, 2008; Sextos et al., 2003; Bi et al., 2011; Li et al., 2012). However, study that has considered spatially varying ground motions and SSI on the response of the adjacent structures with restraining devices are not yet reported in literature. In this paper a numerical investigation is carried out to examine the adequacy of the codes provision of adjusting the fundamental periods of the adjacent bridge components with unseating restrainers considering uniform and non-uniform ground motions and SSI effects.

This paper extends the previous study by the authors by performing extensive parametric calculations to investigate the influences of the ground motion spatial variations and SSI on the response of bridge structures with cable restrainers. The effects of SSI on the responses of bridges are considered using the frequency independent soil springs and dashpots. To realistically represent the response of the structure, fiber section model capable of considering the spread of inelasticity throughout the entire section is adopted. Parametric analyses are conducted to investigate the effects of spatially varying ground motions, SSI on the response of bridge as well as unseating restrainers at the bridge hinges.

5.3 Model Description

In this study four five-span bridge models are used for the analysis representing two bridge geometries. The expansion joints in the bridge are located nearly at inflection points (i.e., 1/4 to 1/5 of span). The bridge deck consists of box-type girders with pre-stressed concrete. The bridges are adopted from Feng et al. (2000), Kim et al. (2003) and are representative of typical Californian bridges. 2-D nonlinear finite element models are used for the analysis, representing a wide variation in ratio of fundamental periods of adjacent structures. Following lists the four bridge models considered in the study:

- Model Bridge 1(a): a five-span bridge with single intermediate expansion joint and equal column height of 19.83 m and diameter of 2.44m.
- Model Bridge 1(b): a five-span bridge with single intermediate expansion joint and equal column height of 19.83 m and the stiffer frame column diameter 3.66m and the flexible frame column diameter 2.44m.
- Model Bridge 2(a): a five-span bridge with two intermediate expansion joints and equal column height of 19.83 m and diameter of 2.44m.
- Model Bridge 2(b): a five-span bridge with two intermediate expansion joint and equal column height of 19.83 m and the stiffer central frame column diameter 3.66m and the flexible frame column diameter 2.44m.

The geometry, boundary conditions and finite element model of these bridges are shown in Figure 5-1. The bridge structures are modelled using the nonlinear software package Seismostruct (Seismosoft 2012). Concrete bents are modelled using force based reinforced concrete beam column elements. Reinforced concrete sections are constructed from three materials namely unconfined concrete, confined concrete and reinforcing steel. The unconfined and confined concrete behavior is modelled using the nonlinear concrete model that follows the constitutive relationship proposed by Mander et al. (1988) and the cyclic rules proposed by Martinez-Rueda and Elnashai (1997). The confinement effects provided by the

lateral transverse reinforcement are incorporated through the rules proposed by Mander et al. (1988), whereby constant confining pressure is assumed throughout the entire stress-strain range. To represent the behavior of the steel re-bars, Menegotto-Pinto steel model (Menegotto and Pinto 1973) is used. The yield strength of the rebars is 415 MPa, and an elastic modulus, E_s is 200GPa. The superstructure of the bridge is modelled using elastic beam column elements. As shown in Figure 5-1 (c) each deck element is discretized into six elements and each pier element, which is modelled using force based beam column element, is subdivided into two elements. Elastomeric bearings at the bridge abutments and bridge joints are modelled using the elastic-plastic element. The bridges consist of 6 elastomeric bearing of 0.4 m by 0.3 m area each. The initial stiffness of the elastomeric bearing, *Ko*, is given by Eq. (1).

$$K_o = \frac{GA}{h_r} \tag{5.1}$$

where A is the area of the elastomeric bearing, G is the shear modulus of the elastomers and h_r is the thickness of the elastomeric bearing pads. The initial stiffness of each bearing is calculated to be 4.41 kN/mm. The initial stiffness of a bearing is 26.46 kN/mm and coefficient of friction, μ, at the interface of concrete surface and elastomeric bearing is taken as 0.20. The yield force of the bearing is thus calculated to be 498 kN.

5.3.1 Soil-Structure Interaction (SSI)

SSI at pier base is incorporated using the frequency-independent lumped spring-dashpot systems. The bridge piers analyzed rest on the spread footings with size of 7 m x 7 m. In this study dynamic soil stiffness (springs and dashpot) of the foundation are calculated based on the study of Mylonakis et al. (2006) using graph and tables for different modes of vibration based on assumption of surface foundation on homogeneous half space. To be compatible with the time-domain nonlinear inelastic analysis framework of the computational platform frequency-independent values are assigned to the foundation impedances corresponding to a frequency of 1.11 Hz (T = 0.9 sec), according to the common assumption of calculating the dynamic impedance matrix based on the predominant frequency range of the input motion. The selected frequency for calculating the foundation impedance is close to the fundamental period of the bridge segments thus would lead to higher responses. Two linear translational and one rotational springs and dashpots are used to represent the stiffness and damping introduced due to SSI. All coefficients of springs and dashpots for sway, vertical and rocking degrees of freedom used to define the soil-foundation model are summarized as follows:

$$K_z = k_z\left(\frac{4.54GB}{1-\nu}\right), \qquad C_z = (\rho V_{La} A_b)\hat{c}_z \tag{5.2}$$

$$K_x = k_x\left(\frac{9GB}{2-\nu}\right), \qquad C_x = (\rho V_s A_b)\hat{c}_x \tag{5.3}$$

$$K_{ry} = k_{ry}\left(\frac{0.45GB^3}{1-\nu}\right), \qquad C_{ry} = (\rho V_{La} I_{by})\hat{c}_{ry} \tag{5.4}$$

where K_z, C_z, K_x, C_x, K_{ry}, C_{ry} are the vertical stiffness, vertical viscous damping, sway stiffness, sway viscous damping, rocking stiffness and rocking viscous damping, respectively. k_z, k_x, k_{ry} are vertical, sway and rocking dynamic stiffness coefficients. $\hat{c}_z$, $\hat{c}_x$, $\hat{c}_{ry}$ are vertical, sway and rocking dynamic dashpot coefficients. B, A_b, I_{by} are the length, area and moment of inertia about the y-axis of the square foundation as shown in Figure 5-1. G, ρ, v, V_s and V_{La} are the shear modulus, soil density, Poisson's ratio, shear wave velocity and Lysmer's analog wave velocity, respectively. In this study without losing generality only the local soil site classes presented in Table 5-1 are considered based on Caltrans (2010) and FEMA 356 (2000). In this study soil with shear wave velocity of 400 m/s, Poisson's ratio of 0.4 and soil density of 1.9 tons/m^3, respectively is adopted for soil site class C. For soil site class D, the shear wave velocity of 220m/s, Poisson's ratio of 0.4 and soil density of 1.8 tons/m^3, respectively is adopted. The elastic shear modulus, G_o, is calculated by following equation (Richart and Whitman 1967).

$$G_o = \rho (V_s)^2 \tag{5.5}$$

Under seismic shaking the soil behavior is strongly nonlinear. In this study to approximately include the soil nonlinearity, the reduced shear modulus, G, equal to 67% of the G_o based upon FEMA 356(2000) is used. To investigate the effects of SSI the response of bridge on two soil site classes are compared against fixed base cases.

Table 5-1 Local soil site classes

Site Class	Shear wave Velocity, Vs (m/s)	Selected value of Vs (m/s)
C. Very dense soil	360-760	400
D. Stiff soil	180-360	220

The abutments of the bridges on the raised embankments are supported on the pile foundation. The bridge abutments are modelled using two separate nonlinear springs to model the pile stiffness and passive soil stiffness at abutment. The nonlinear abutment behavior in this study reflects the design recommendation from Caltrans (Caltrans 2010). The Caltrans recommendation of effective stiffness of 7kN/mm/pile is used in this study with an ultimate

strength of 119kN/pile. Tri-linear symmetrical models implemented by Choi (2002), which act in both active and passive loading of the abutments, are used to represent the pile stiffness at abutments. 24 piles are present in each abutment. It is assumed that the piles become plastic at a deformation of 25.4 mm, and first yield occurs at 30% of the ultimate deformation. This corresponds to a yielding force of 70% of ultimate force. Elastic plastic spring with initial stiffness of 28.7 kN/mm/m is used to represent the passive soil stiffness at abutment back-wall (Caltrans 2010). Abutment stiffness and yield capacity can be calculated in SI units as (Caltrans 2010):

$$K_{abut} = \left(\frac{K_{ai} w h}{1.7} \right) \tag{5.6}$$

$$P_{bw=} \left(\frac{239 A_e h}{1.7} \right) \tag{5.7}$$

where K_{abut} is the stiffness of an abutment with initial embankment fill stiffness of K_{ai}, effective abutment width of w, and height h. The yield strength of the abutment back wall, P_{bw} can be calculated based on (5.7). A_e is the effective area of the back wall, the height and the width of the back wall is 2.25 m and 14.5 m, respectively.

Fundamental period of the bridge segments and the ratio of their fundamental periods are presented in Table 5-2 Fundamental periods of model bridges. The ratios of fundamental natural periods of the fixed bridge models 1(a) and 2(a) are above 0.7 (i.e. Ti/Tj≥0.7, where T_i and T_j are the natural period of the stiffer and flexible frames, respectively). To investigate response of the bridge segments with distant fundamental frequencies, the diameters of piers of the stiffer frame of the both bridge models are increased by 1.5 times to that of the original model, i.e., stiffness is increased to change its vibration frequency. This resulted in the two new bridge models with the ratio of the natural frequencies lower than 0.7. However, the inclusion of soil spring affects the natural frequencies of the bridge structures. Due to the flexibility introduced by the soil springs the natural period of the bridge structures increases and the ratio of the periods of the adjacent frames with soil springs shifts closer to unity.

5.3.2 Impact Element

It is recognized that pounding between adjacent bridge decks during strong earthquake shaking can affect the bridge response. Pounding resulting from the out-of-phase motion of the adjacent bridge structures could result in damages at the joints and may even result in the unseating of the adjacent spans. Hence it is essential to include the effects of pounding in the numerical model. This can be done in finite element model by using a gap element to monitor

the relative displacement between the adjacent sections of the bridge. Once the closing relative displacement is larger or equal to the associated gap pounding occurs. The concept of the gap element is hence quite simple. However, actual modelling of pounding behavior can be quite cumbersome. Linear impact model which has been widely adopted to model the pounding between the adjacent structures has a limitation of not allowing energy dissipation and thus may overestimate the system response due to the impact. The impact model such as Kelvin, Hertz damp model etc., which considers the energy dissipation during the pounding, is difficult to implement in nonlinear software packages. Muthukumar (2003) recommended a simplified bilinear spring model to capture the effects of impact including the energy dissipation. The impact model is an approximate representation of the Hertz damp model (Muthukumar & DesRoches, 2006). In this study the impact model proposed by Muthukumar (2003) is used to represent the contact and pounding during the seismic event. Figure 5-1(d) shows the typical representation of the bilinear spring model used to model pounding. In this study the maximum deformation or penetration δ_m is assumed to be 25.4 mm and δ_y is assumed to be 0.10(δ_m). The coefficient of restitution, e is assumed to be 0.8. The K_{t1} and K_{t2} are calculated to be 10.68 GN/m and 3.68 GN/m respectively. More details on determination of these pounding parameters can be found in Muthukumar (2003). In this study, without losing generality the gap length of the internal expansion joints is assumed to be 25 mm and that between abutment and deck is assumed to be 50 mm.

Table 5-2 Fundamental periods of model bridges

Bridge Model	Stiff frame period (T_i, sec)	Flexible frame period (T_j, sec)	Period ratio (T_i/T_j)
Model 1a(Fixed base)	0.84 (Frame 1)	0.92(Frame 2)	0.91
Model 1b (Fixed base)	0.55(Frame 1)	0.92 (Frame 2)	0.60
Model 2a(Fixed base)	1.00 (Frame 2)	1.25 (Frame 1&3)	0.72
Model 2b(Fixed base)	0.88 (Frame 2)	1.25 (Frame 1&3)	0.50

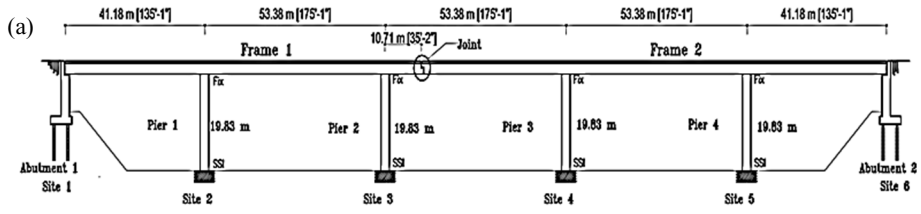
(a)
41.18 m [135'-1"]
53.38 m [175'-1"]
53.38 m [175'-1"]
53.38 m [175'-1"]
41.18 m [135'-1"]
10.71 m [35'-2"]
Joint
Frame 1
Frame 2
Fix
Pier 1
19.83 m
Pier 2
19.83 m
Pier 3
19.83 m
Pier 4
19.83 m
SSI
Abutment 1
Site 1
Site 2
Site 3
Site 4
Site 5
Abutment 2
Site 6

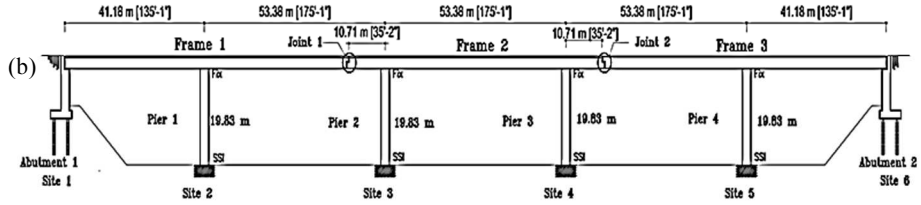
(b)
41.18 m [135'-1"]
53.38 m [175'-1"]
53.38 m [175'-1"]
53.38 m [175'-1"]
41.18 m [135'-1"]
Frame 1
Joint 1
10.71 m [35'-2"]
Frame 2
10.71 m [35'-2"]
Joint 2
Frame 3
Fix
Pier 1
19.83 m
Pier 2
19.83 m
Pier 3
19.83 m
Pier 4
19.83 m
SSI
Abutment 1
Site 1
Site 2
Site 3
Site 4
Site 5
Abutment 2
Site 6

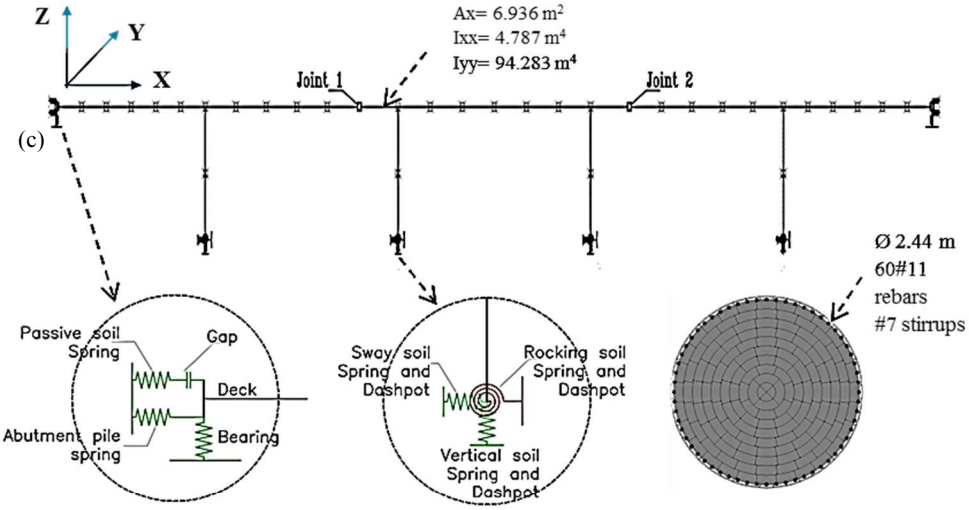
(c)
Z
Y
X
Ax= 6.936 m²
Ixx= 4.787 m⁴
Iyy= 94.283 m⁴
Joint 1
Joint 2
Ø 2.44 m
60#11
rebars
#7 stirrups
Passive soil
Spring
Gap
Deck
Abutment pile
spring
Bearing
Sway soil
Spring and
Dashpot
Rocking soil
Spring and
Dashpot
Vertical soil
Spring and
Dashpot

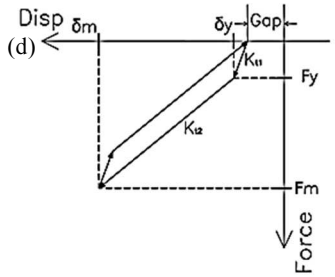
(d)
Disp
δm
δy
Gap
Ku1
Fy
Ku2
Fm
Force

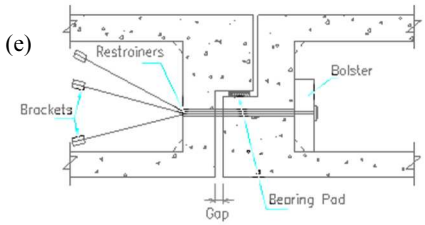
(e)
Restroiners
Bolster
Brackets
Bearing Pad
Gap

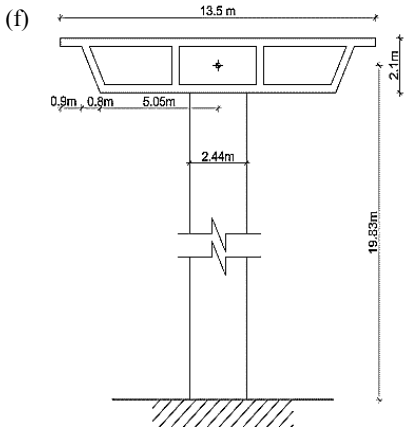
(f)
13.5 m
2.1m
0.9m
0.8m
5.05m
2.44m
19.83m

Figure 5-1 Bridge Models used for the study (a) Bridge 1(with single expansion joint); (b) Bridge 2 (with two expansion joint); (c) Finite element model of Bridge 2; (d) Analytical model of impact element; (e) Typical joint detail; (f) Bridge pier details.

5.4 Ground Motion Modelling

It is common in engineering practice to simulate spatially varying ground motions that are compatible with the specific design response spectra. Many stochastic ground motion simulation methods have been proposed by different researchers. For example, Hao et al. (1989) and Deodatis (1996) simulated the spatially varying ground motions in two steps: first the spatially varying ground motion time histories are generated using an arbitrary power spectral density function, and then adjusted through iterations to match the target response spectrum. Usually a few iterations are needed to achieve a reasonably good match. More recently, Bi and Hao (2012) further developed this method by simulating the spatially varying ground motions which are compatible with the ground motion power spectral densities that are related to the target design response spectra instead of arbitrary power spectral density functions. The method proposed by Bi and Hao (2012) is adopted in the present study to simulate the spatially varying ground motion time histories that are compatible with the design spectra specified in the Japanese Highway Code (2004). The acceleration response spectrum of a Type II ground motions, which represent the ground motion generated by inland earthquake at short distance (Near-fault), developed by smoothing the response spectra that are computed from the ground motion records obtained in the 1995 Kobe earthquake is used in this study. The spatially varying ground motions for group 2 sites, i.e., the medium soil site conditions, are simulated. In the simulations, the sampling and upper cut-off frequencies were set to 100 and 25 Hz, respectively, and the duration of 40.95s is selected to have a convenient total number of points (4096) for a fast Fourier transform.

The spatial variation properties between ground motions recorded at two locations j and k on ground surface is modelled by a theoretical coherency loss function (Sobczky 1991)

$$\gamma_{jk}(i\omega) = \left|\gamma_{jk}(i\omega)\right| \exp(-i\omega d_{jk}\cos\alpha / v_{app}) = \exp(-\beta\omega d_{jk}^2 / v_{app}) \times \exp(-i\omega d_{jk}\cos\alpha / v_{app}) \tag{5.8}$$

where β is a constant reflecting the level of coherency loss. In order to gain the wider perspective on the response variation due to the non-uniform ground motions, simulation of the ground motions is carried out for three levels of coherency losses, i.e., β = 0.0005, 0.0010 and 0.0015 to represent highly, intermediately and weakly correlated ground motions respectively. To obtain relatively unbiased structural responses, 3 sets of ground motion time histories are simulated for each coherency loss levels. d_{jk} is the distance between the two locations j and k in the wave propagation direction, f is the frequency in Hz, v_{app} is the apparent

wave velocity, and α is the seismic wave incident angle. In the present study, v_{app} is assumed to be 400 m/s, and $\alpha = 60^{\circ}$. The values of v_{app} selected is realistic for typical highway bridge sites in California in consideration of the measured shear wave velocities, such as the Painter Street Bridge and Meloland Road Overcrossing (Zhang and Markis, 2002a, b). The same value of v_{app} has been adopted in previous studies for Californian bridges (Huo and Zhang, 2013). It is to be noted that bridge model used in the analysis are 2D models and the spatially varying ground motions are only applied along the longitudinal direction (X-axis) of the bridge (Figure 5-1 (c)).

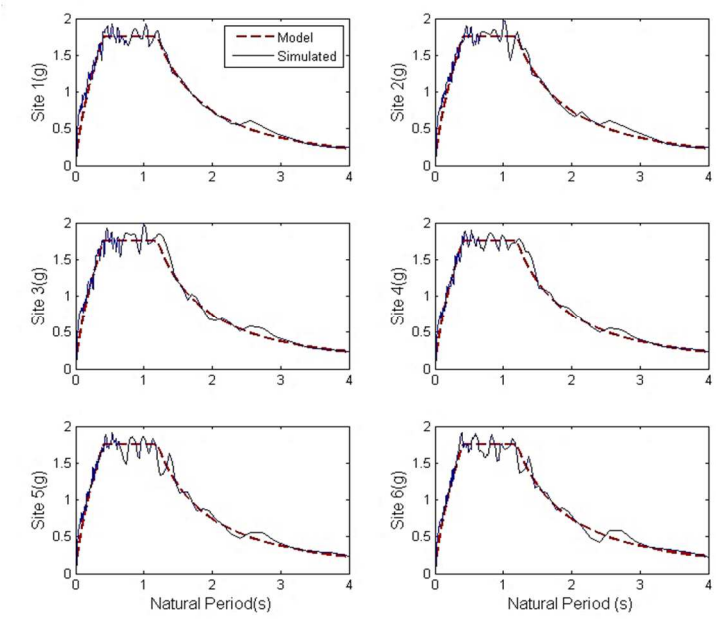

Figure 5-2 Comparison of the response spectra of simulated ground motions with the target spectrum.

Figure 5-2 compares the response spectra of the simulated ground motions and the target design spectra at the 6 sites shown in Figure 5-1. It shows that the response spectrum of the simulated ground motions match well with the target design spectrum for the respective site. Figure 5-3 shows the comparison of the empirical coherency loss function (Equation 8) between site 1 and other sites and the corresponding values of the simulated motions. Good match can also be observed except for $|\gamma_{15}|$ and $|\gamma_{16}|$ in the high frequency range. This, however, is expected because as the distance increases, the cross correlation between the spatial motions or their coherency values decrease rapidly with the frequency. Previous studies (Hao et al. 1989) revealed that the coherency value of about 0.3-0.4 is the threshold of cross correlation between two time histories because numerical calculations of coherency function between any two white noise series result in a value of about 0.3-0.4. Therefore, the calculated

coherency loss between two simulated time histories remains at about 0.4 even the model coherency function decreases below this threshold value.

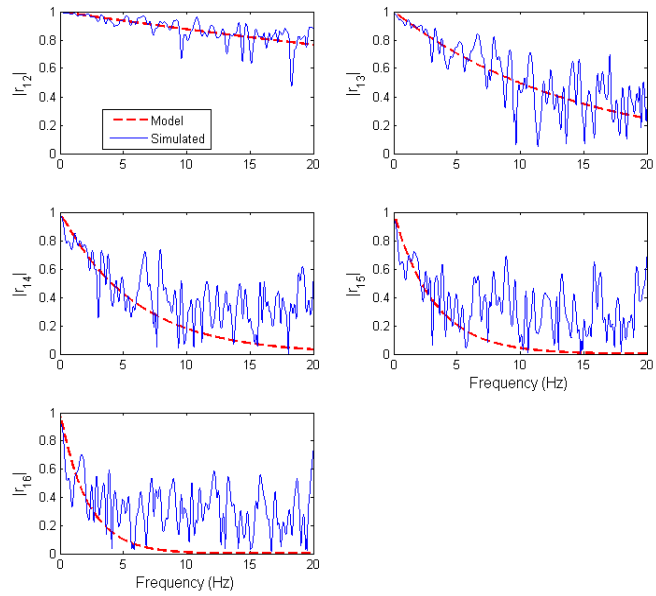

Figure 5-3 Coherency losses of simulated ground motions.

5.5 Restrainer Design and Modelling

In this paper a widely used restrainer design method proposed by DesRoches and Fenves (2000) is evaluated to identify its adequacy to prevent unseating damage of bridge decks subjected to spatially varying ground motions. The method, developed to predict the restrainer stiffness required to limit the hinge movement to a certain acceptable limit subjected to uniform ground motion, is briefly discussed here. The method is based on the analysis of a two-degree-of-freedom system as shown in Figure 5-4 (a), representing the fundamental vibration mode of adjacent bridge frames. The relative hinge displacement, D_{eq}, is estimated by combining the modal response using the complete quadratic combination (CQC) rule (Der Kiureghain 1980):

$$D_{eq} = \sqrt{D_1^2 + D_2^2 - 2\rho_{12} D_1 D_2} \tag{5.9}$$

where D_1 and D_2 are modal displacements and ρ_{12} is the correlation coefficient between the response of the two single-degree-of-freedom system defined as:

$$\rho_{12} = \frac{8\sqrt{\xi_1 \xi_2}\left(\xi_1 + \beta \xi_2\right)\beta^{3/2}}{\left(1-\beta^2\right)^2 + 4\xi_1\xi_2\beta\left(1+\beta^2\right) + 4\left(\xi_1^2 + \xi_2^2\right)\beta^2} \tag{5.10}$$

where β is the ratio of the frame fundamental periods, T_2/T_1, and ξ_1 and ξ_2 are the corresponding modal damping ratios. The main design parameters are the frame stiffness, masses, ductility demand and allowable hinge displacement. The schematic view of relative displacement at the bridge expansion joint during an earthquake event is shown in Figure 5-4 (b), where D_{eq} represents the Maximum Relative Hinge Displacement (MRHD) that could be expected during the seismic event and D_{hinge} is the available hinge seat width. The allowable hinge displacement, D_r, is calculated by subtracting the minimum required bearing length, D_b which is required for spans to remain seated without losing the functionality of the bridge, from the available seat width, D_{hinge}. The target yield displacement of the restrainers, D_y, is the difference between the allowable hinge displacement, D_r and the restrainer slack, D_s. Using *Deq*, the restrainer stiffness, *Kr*, needed to limit the hinge displacement to D_r is determined from the sensitivity of the hinge displacement to the restrainer stiffness:

$$\frac{\delta Deq}{\delta Kr} = -\frac{1}{Km + Kr} Deq \tag{5.11}$$

where 1/Km=1/K1+1/K2 is the sum of the flexibilities of the two frames. Performing a Taylor series expansion about the current estimate of the hinge displacement, Deq_j, and solving for an improved estimate of the restrainer stiffness at the next step, Kr_{j+1}, gives

$$Kr_{j+1} = Kr_j + (Km + Kr_j)\frac{(Deq_j - Dr)}{Deq_j} \tag{5.12}$$

Each iteration of the procedure consists of a 2-DOF modal analysis for *Deq*, followed by the use of the updated estimate of restrainer stiffness. The yielding behavior of ductile frames is accounted for in the restrainer design procedure by determining an equivalent stiffness and damping ratio based on the maximum displacement of the frames (Gulkan & Sozen, 1974). A typical case requires three to five iterations to converge. Parametric studies and case studies showed that the procedure limits the relative hinge displacement to a specified value for a wide range of bridges subjected to uniform ground motions (DesRoches & Fenves, 2000).

In this study available hinge seat width, D_{hinge}, is taken to as 200 mm, which represents narrow seated bridges of pre-San Fernando earthquake. The restrainer slack, Ds, is assumed to be 25mm. Minimum required bearing length, $D_{b,}$ is assumed 87 mm. The target yield displacement, D_y, of the restrainer is thus calculated to be 88 mm. Letting, D_y be the same as the yield displacement of restrainers at 1.75% strain, the restrainer length is calculated to be 5.04m. The stiffness of the restrainers required to restrict the hinge movement to the prescribed value, i.e., D_r =113 mm in this study, is determined using the modal analysis with multiple trials.

Typical 19 mm diameter high-strength cable used in Caltrans bridges with area of 143 mm^2 and the yield strength of 1210 MPa are used in this study. The numbers of restrainers required to limit the hinge opening subjected to design earthquake motion calculated for bridge model 1(a) and model 2(a) are 2 and 8, respectively. In this study, without losing generality a practical number of 10 restrainers are provided for each bridge model at each joint, implying slight over-design of the required cable restrainers. It is assumed that the connection between the deck and the restrainers are strong so that all the deformation will concentrate on the restrainers.

The drawback of the above design method is that it only considers the relative displacement induced due to the different fundamental periods of the adjacent structures. Due to this reason only 2 restrainers are calculated when the adjacent bridge frames have close vibration frequencies. Influences of spatial variation of ground motion, which results in further out-of-phase vibration, are not considered thus could underestimate the relative displacements between the adjacent segments. This underestimation of the relative displacement could significantly affect the required stiffness and strength of the restrainers. As spatial variation of the ground motions are unavoidable and the failure of the restrainers could lead to the unseating of the bridge spans, it is essential to evaluate the effectiveness of the method by including the effects of ground motion spatial variations.

In numerical simulations the restrainers are modelled using a truss elements with tension only behavior. The slack of 25mm is provided to accommodate the thermal movement of the deck. Bilinear steel model is used to model the constitutive behavior of the restrainers. As the restrainers are designed considering only the uniform ground motions, which might significantly underestimate the relative joint displacements, it is likely that restrainers will be significantly stressed and may even get fractured. Therefore, the failure of the restrainers is taken into account and the ultimate strain of the restrainers is taken as 4.50%. Once the ultimate strain capacity is reached the adjacent span can vibrate freely without any restriction provided by the restrainers. The hysteretic behavior of the restrainer is presented in Figure 5-5.

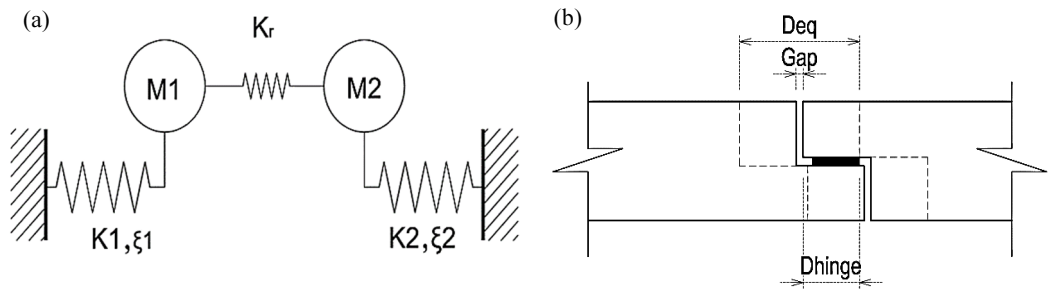

Figure 5-4 (a) Linearized analytical model of the hinge; (b) Bridge intermediate hinge.

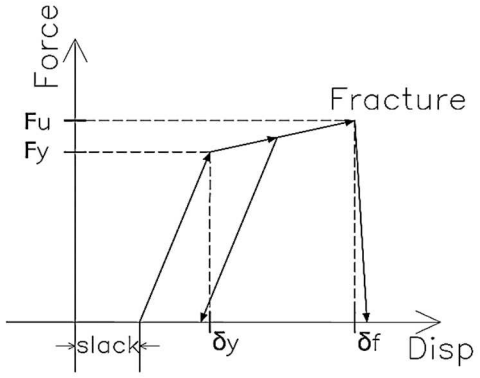

Figure 5-5 Hysteretic behaviour of steel restrainers.

5.6 Effects of Spatial Variation of Ground Motion

5.6.1 Wave Passage Effect

One of the sources for the variation of the ground motion at different bridge supports is the travelling seismic wave. Wave passage effect is primarily described by the apparent wave passage velocity, v_{app}, which depends on incident angle of seismic waves into the site and the site condition. A study of the recorded time histories revealed that the apparent wave velocity is frequency dependent and quite irregular in nature (Hao et al., 1989). To consider the randomness of the apparent wave velocity three different values (i.e. 400, 800, 1600 m/s) of wave velocity is considered in this study. Ground motion simulated for site 1 is used in the analysis with appropriate time delays to represent the wave passage effect. Without losing the generality, only the responses of the bridges on soil site C (Vs = 400 m/s) is presented. Bridge structure responses to the three independent sets of spatially varying ground motions are analyzed, and the average responses are calculated and discussed. In order to quantify the effects of spatially varying ground motions normalized values of response are used. The normalized value is defined as below

$$Normalized\ value = \frac{Average\ \ response\ \ to\ \ spatially\ \ varying\ \ ground\ \ motion}{Average\ \ response\ \ to\ \ uniform\ \ ground\ \ motion} \tag{5.13}$$

Figure 5-6 (a) and (b) present comparison of the normalized average drift subjected to the three sets of simulated ground motions for Pier 2 and Pier 3 of bridge model 1(a), respectively. In the figure, WP(1600), WP(800) and WP(400) represents the non-uniform ground motions with apparent wave passage velocity as presented in parenthesis. As shown, ground motions considering wave passage effects result in reductions in the seismic demand for piers of both stiff and flexible frames. This is because, as shown in Figure 5-7, spatially varying ground motions result in more frequent and severe pounding between the adjacent girders and between the girder and abutments. This impedes displacements of bridge frames because pounding restrain movements of adjacent structures. However, differential support motions adversely influence the relative displacement responses. Normalized Maximum Relative Hinge Displacement (MRHD) and normalized Restrainer Deformation (RD) at intermediate hinges, as presented in Figure 5-8 (a) and (b), are significantly increased due to the non-uniform ground motion caused by wave passage effect. Generally speaking, smaller apparent wave velocity results in larger MRHD and RD. For comparison, the deformations when the restrainer yield and fracture are also presented in the figure. As shown, when the apparent wave velocity is 400m/s, the restrainer might be fractured and cannot restrain the bridge opening displacement anymore. It should be noted the allowable hinge displacement, D_{hinge}, plotted in Figure 5-8 (a) is only for the indicative purpose and the unseating of the bridges is not explicitly modelled.

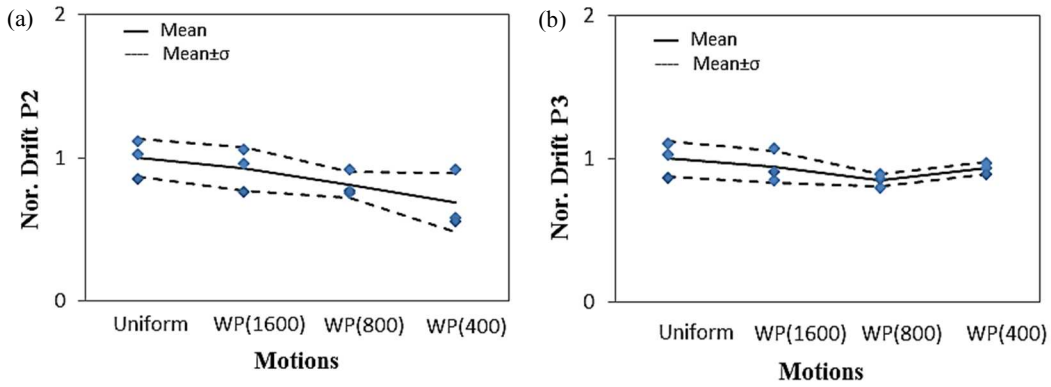

Figure 5-6 Normalized drift of (a) Pier; (b) Pier 3 of bridge 1(a).

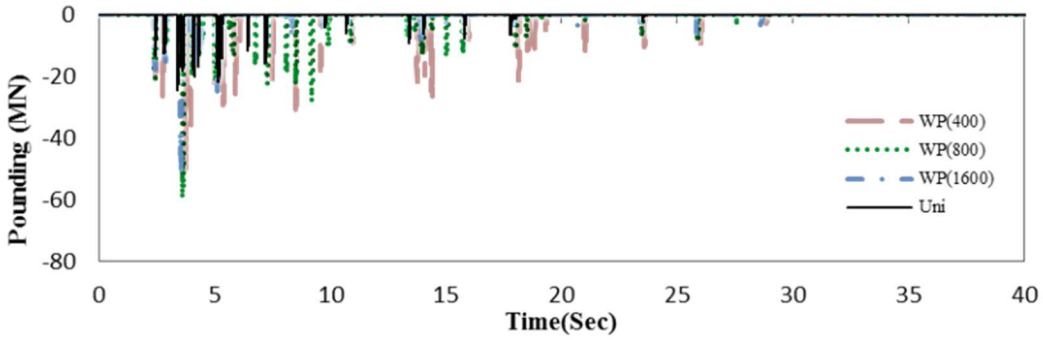

Figure 5-7 Pounding forces at intermediate hinge of bridge 1(a).

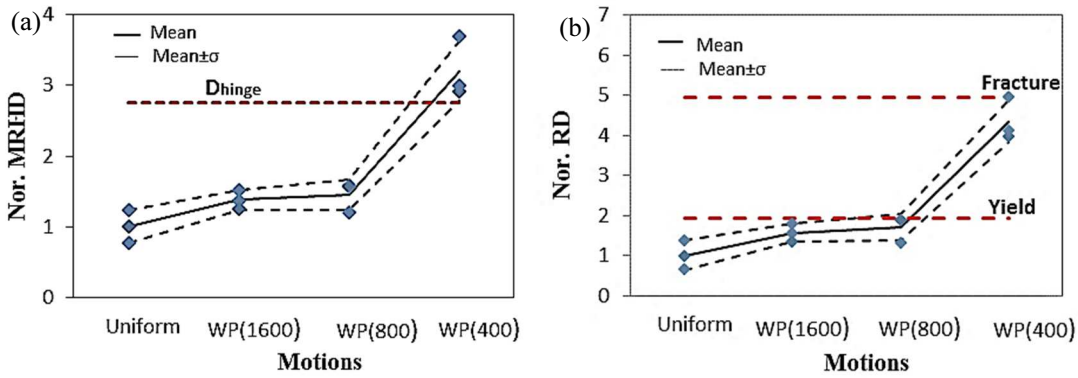

Figure 5-8 (a) Normalized MRHD; (b) normalized RD for bridge 1(a).

5.6.2 Coherency Loss

Effects of the coherency losses between the ground motions at different bridge supports on the response of bridge structures are parametrically evaluated for three different coherency loss levels as discussed previously. Figure 5-9 (a) presents the comparison of MRHD and Figure 5-9 (b) presents the normalized RD for spatial ground motions with different levels of coherency losses with uniform ground motion. In the figure, WP (400) represents the ground motions considering the wave passage effect only. CH (Hig), CH (Int) and CH (Wea) represent the cases with highly coherent, intermediately coherent and weakly coherent motions, respectively. As shown, the largest relative displacement response at the intermediate hinge corresponds to the case considering only the wave passage effect, the coherency losses of spatially varying ground motion, in fact, have beneficial effects on relative responses between the adjacent bridge components. However, the normalized MRHD for all the cases of spatially varying ground motions are significantly higher than that from the uniform ground motions. It can also be noticed that the restrainers yielded for all the cases of the ground motions with exception of the uniform ground motions, as presented in Figure 5-9 (b), indicating the restrainers designs are inadequate to resist spatially varying ground motions. A set of ground motion considering only the wave passage effects resulted in the relative displacement large

enough to fracture the restrainers resulting in unrestrained movement of the adjacent spans. Figure 5-10 (a) and (b) present the normalized MRHD and RD for joint 2 of bridge model 2(a). In this case, however, the spatially varying motions considering coherency losses resulted in higher relative displacement. These results indicate that the effects of the coherency losses on the response of the bridge structures are not only dependent upon the ground motions, but also on the bridge geometry and its vibration frequency. Considering only the wave passage effects of the ground motion spatial variations may lead to inaccurate predictions of bridge structural responses. Uniform excitation assumption significantly underestimates both the MRHD and the RD. The restrainers designed for uniform ground motion assumption may lose its functionality due to yielding or may even get fractured due to the large relative displacements caused by ground motion spatial variations.

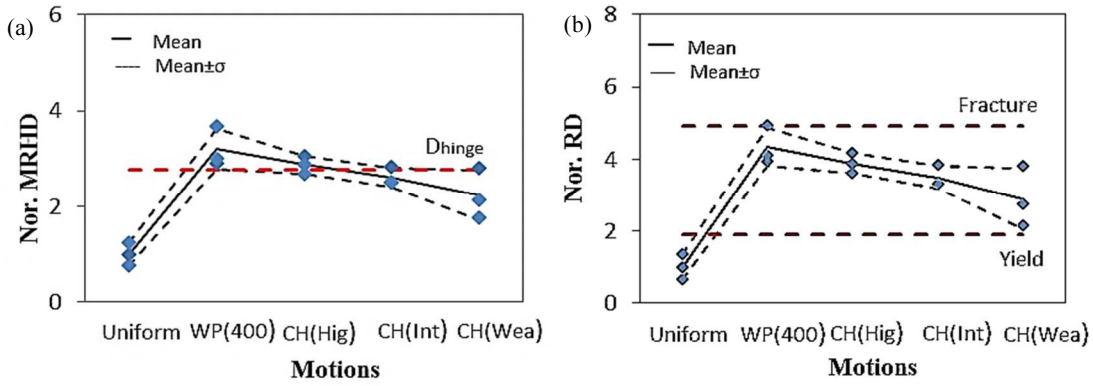

Figure 5-9 (a) Normalized MRHD; (b) normalized restrainers deformation of bridge 1(a).

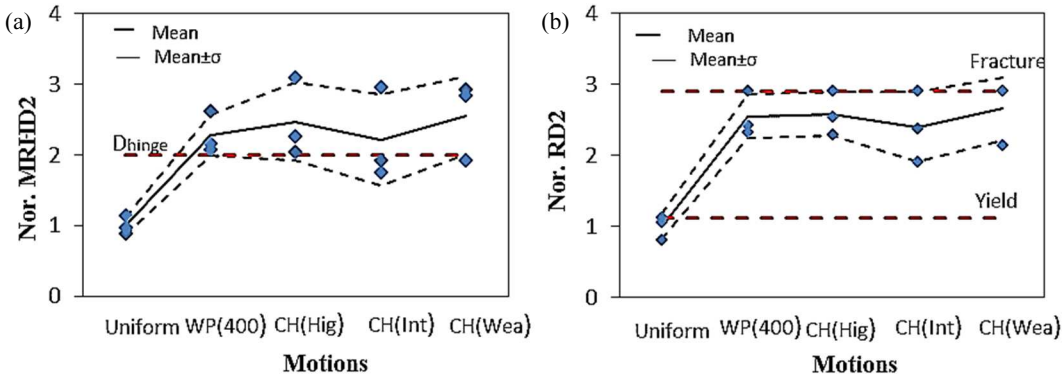

Figure 5-10 (a) Normalized MRHD; (b) normalized RD at joint 2 of bridge 2(a).

Figure 5-11 (a) and (b) show response of Pier 2 and Pier 3 of the bridge model 1(a) subjected to uniform and spatially varying ground motions. The results again show that pier drift are reduced due to spatially varying ground motion compared to uniform ground motions.

Figure 5-12 (a) and (b) present the normalized peak pounding forces for the bridge model 2(a) at joint 1 and joint 2, respectively. As shown, the spatial variation of the ground motions results in out-of-phase motion of adjacent bridge components. This leads to amplification of peak pounding forces.

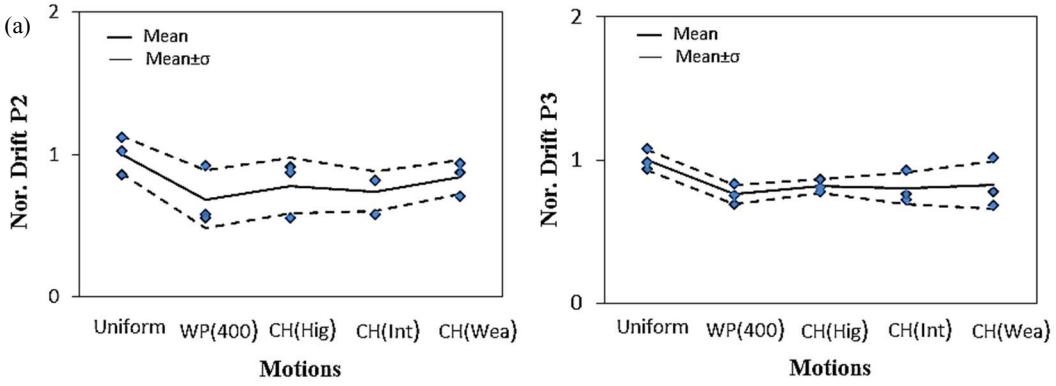

Figure 5-11 (a) Normalized peak Drift of Pier 2; (b) Pier 3 of bridge 1(a).

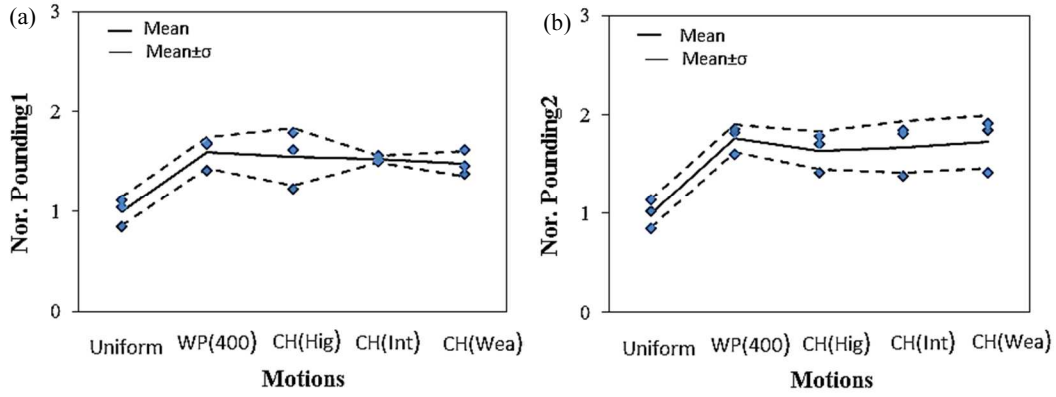

Figure 5-12 Normalized pounding force at (a) joint 1; (b) at joint 2 of bridge 2(a).

5.7 Effects of Frame Period Ratio

To investigate the influence of the spatially varying motions on the relative response of the adjacent bridge frames with close and different fundamental frequencies, a parametric study is conducted on four bridge models. Bridge codes such as Caltrans (2010) recommend constructing the adjacent structures with close fundamental periods. However, there still lacks investigations on its effectiveness on the bridges subjected to spatially varying ground motions including the SSI effect. In this study the two bridge model 1(a) and 2(a) with close fundamental periods are compared against bridge models 1(b) and 2(b) with relatively distant fundamental periods. In this case also the bridge model including the SSI for soil class C is discussed, without losing the generality. The response of the structures to uniform motion,

ground motion considering wave passage effects only and spatially varying motion considering intermediate coherency losses are investigated.

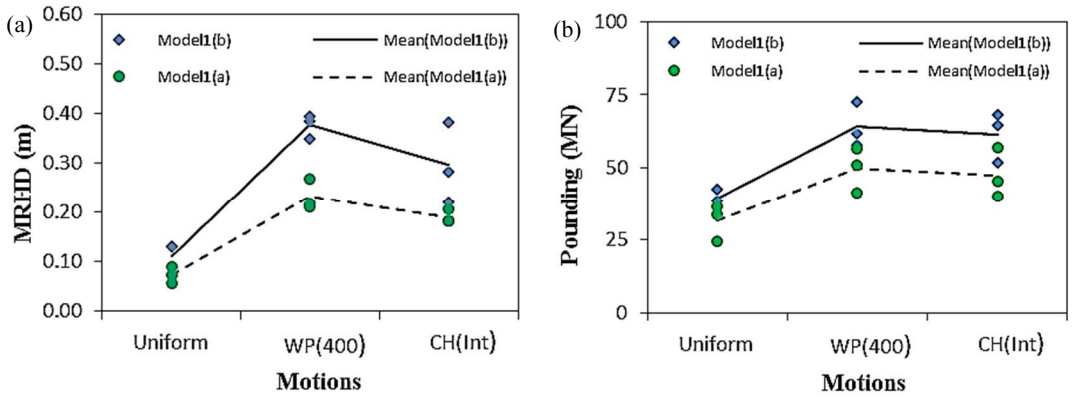

Figure 5-13 Comparison of (a) MRHD; (b) Peak pounding force bridge models 1(a) and 1(b).

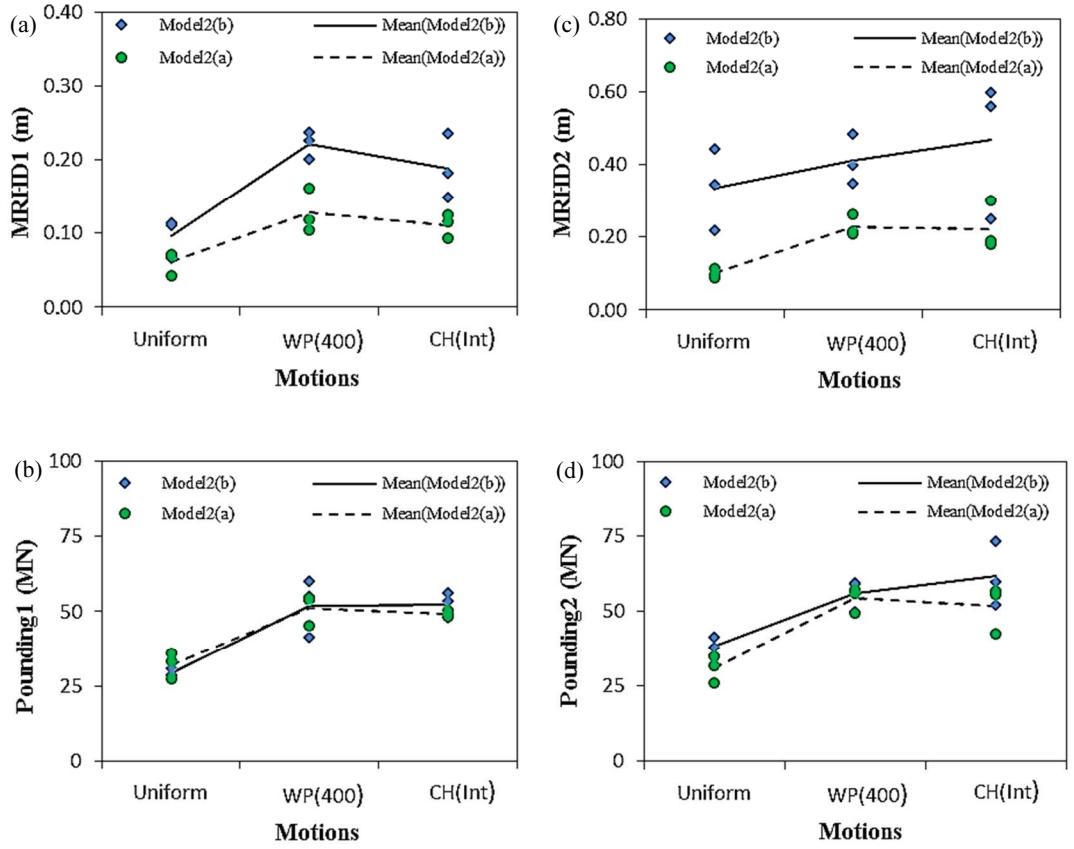

Figure 5-14 Comparison of (a) MRHD; (b) Peak pounding forces at Joint 1; (c) MRHD; (d) Peak pounding forces at joint 2 of bridge models 2(a) and 2(b).

Figure 5-13 (a) and (b) present the comparison of MRHD and peak pounding forces for bridge model 1(a) and 1(b). Figure 5-14 (a) to (d) compare the pounding forces and relative opening displacement at the two joints of the bridge model 2(a) and 2(b). The results show that code provision of adjusting the natural frequencies of the adjacent structures close to each other is

an effective method to mitigate pounding forces and relative displacement on bridges under influence of spatially varying ground motions as well. Pounding forces and relative joint opening for bridges with close fundamental periods are significantly lower compared to the bridge with distant fundamental periods. Hence, the code provision of adjusting the fundamental periods of adjacent structures close to each other is justifiable regardless of ground motion input. However, as shown in Figure 5-13 and Figure 5-14, only this might not be sufficient to prevent the bridge structures from relative displacement induced damages caused by spatially varying motions. Though the relative displacement and pounding forces are reduced, spatially varying ground motions still results in relative displacements large enough to induce some damages at bridge joints even for the bridges with relatively close fundamental periods.

5.8 Effects of SSI

The interaction of the foundation with the surrounding soil and the structures could lead to a very complex and case dependent dynamic response. In this study to identify the influence of SSI on the seismic responses of the bridge a comparative study of the bridges with fixed base and with SSI (for two different soil site conditions) subjected to uniform and spatially varying ground motions are carried out. Figure 5-15 (a) and (b) present the MRHD and the RD at intermediate hinge of bridge model 1(a). As presented, inclusion of SSI reduces the relative displacement response of the adjacent bridge structures. This is because, as presented in Figure 5-16, vibration period of the structures increases when SSI is considered. Due to this shift in the fundamental vibration period, the ratio of the periods of the adjacent structures shifts closer to the unity. Hence, the adjacent frames tend to vibrate more in-phase, which in turn decreases the relative displacement between the frames compared to the fixed foundation cases. Similar results were also observed by the previous authors (Chouw & Hao, 2003). The SSI, however, has detrimental effect on the relative displacement at abutment joints as shown in

Figure 5-17 (a). The period elongation of the adjacent frames due to the SSI results in an increase in out-of-phase motions with stiffer abutments. This causes an increase in relative displacement at both abutments joints.

Figure 5-17 (b) presents the peak pounding responses at intermediate joint of the bridge. As shown the pounding response of the adjacent bridge structure is dependent upon the soil site type considered. Pounding forces on the bridge joints with SSI considering soil site class C are always higher compared to the fixed base condition. However, the pounding force for the bridge in softer soil (site class D, Vs= 220 m/s) is lower compared to the fixed base condition, except for the uniform ground motions. The results presented highlight that the effects of SSI

on the pounding response of adjacent bridge structure is case dependent and it is difficult to generalize the results based on the limited cases considered in the present study. However, the results demonstrate the importance of considering the SSI effects in bridge response calculations.

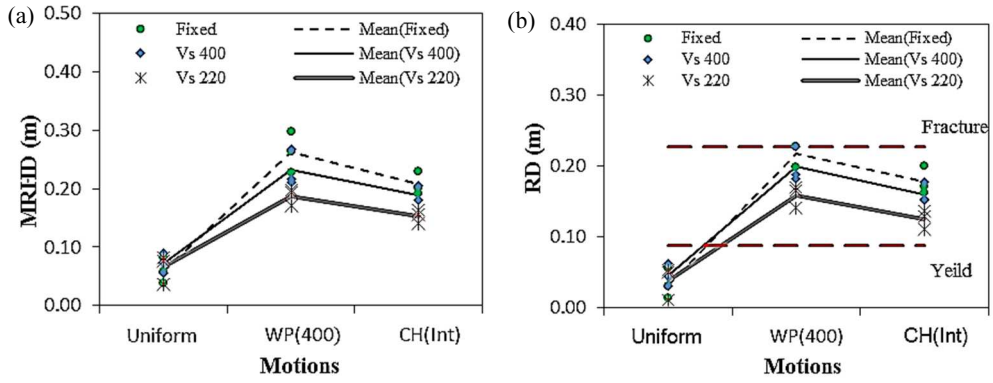

Figure 5-15 Influence of SSI on (a) MRHD; (b) RD at in-span hinge of bridge model 1(a).

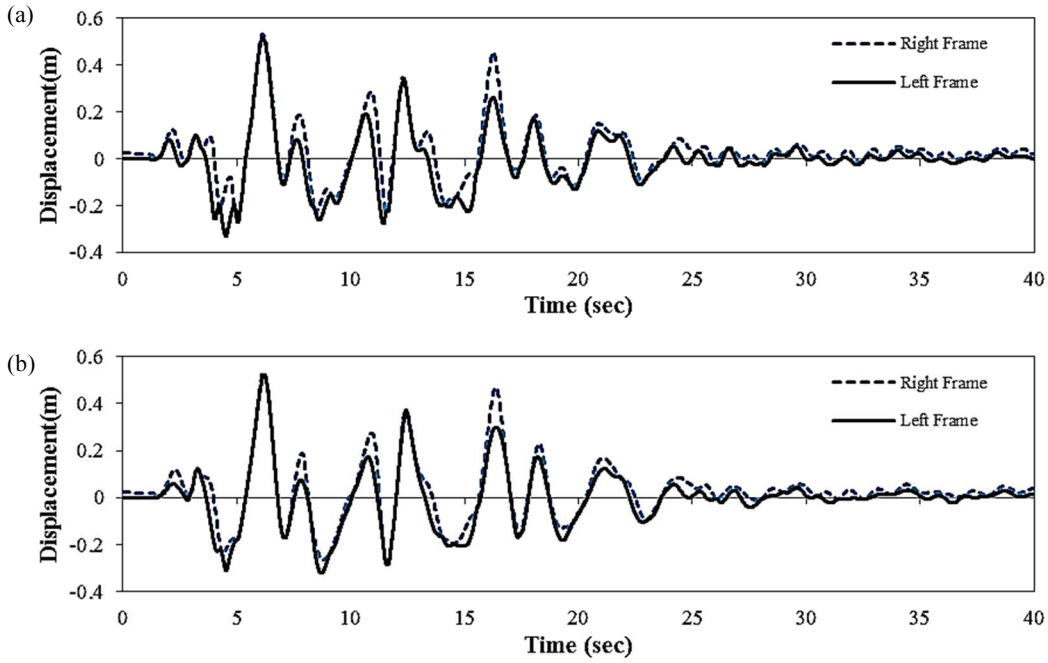

Figure 5-16 Displacement time-history of bridges girders for (a) Fixed foundation; (b) With SSI (Vs 220) subjected to spatially varying ground motion.

Figure 5-18 (a) and (b) compare the drift of pier 2 and pier 3 of bridge model 1(a). As shown, inclusion of SSI increases the overall displacements of both frames. It is interesting to note that considering SSI reduces the relative displacement (as shown in Figure 5-15) but increases the drift of both the frames. The softer the soil, the more will be the drift of the frames. However, the relative displacements at intermediate joints are reduced. In order to find out the

effects of SSI on the response of the bridge piers, section curvature demand at the top and the base of the bridge piers are compared.

Figure 5-19 (a) and (b) present the section curvatures of the base of pier 2 and pier 3 of bridge model 1 (a), respectively. The results show that the inclusion of SSI reduces the curvature demand at the base of the pier. However, as presented in

Figure 5-20 (a) and (b), larger displacements caused by the SSI could result in an increase of curvature demands at the top of the piers. The above observations demonstrate that the flexibility and additional damping introduced in the system by inclusion of soil spring benefits the response of piers by reducing the curvature demand at the base. On contrast, larger displacement demands resulting from SSI could result in an increase of curvature demand at the top of the bridge piers. Hence, in multiple-frame bridges SSI could induce more damages at the top of the piers compared to the fixed base condition.

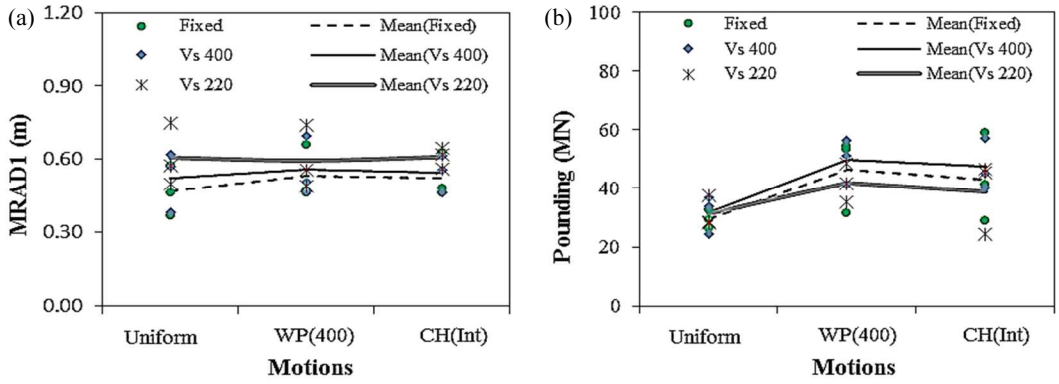

Figure 5-17 Influence of SSI on (a) MRAD 1; (b) Peak pounding force at the internal joint.

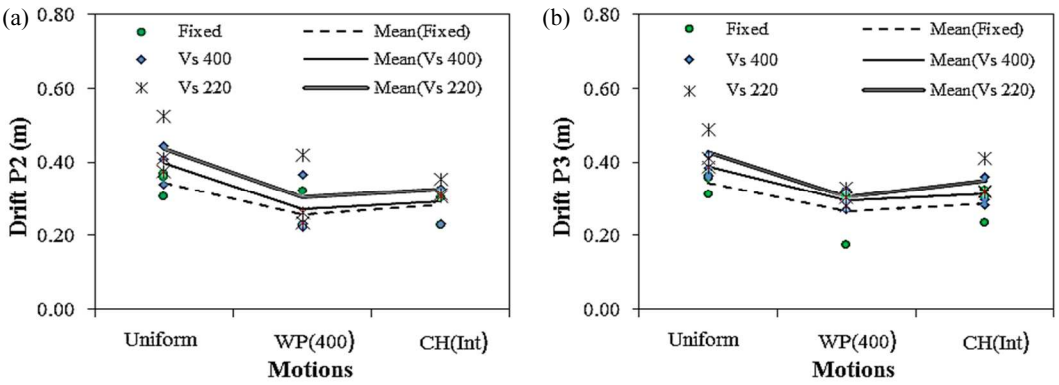

Figure 5-18 Influence of SSI on the drift of (a) Pier 2; (b) Pier 3.

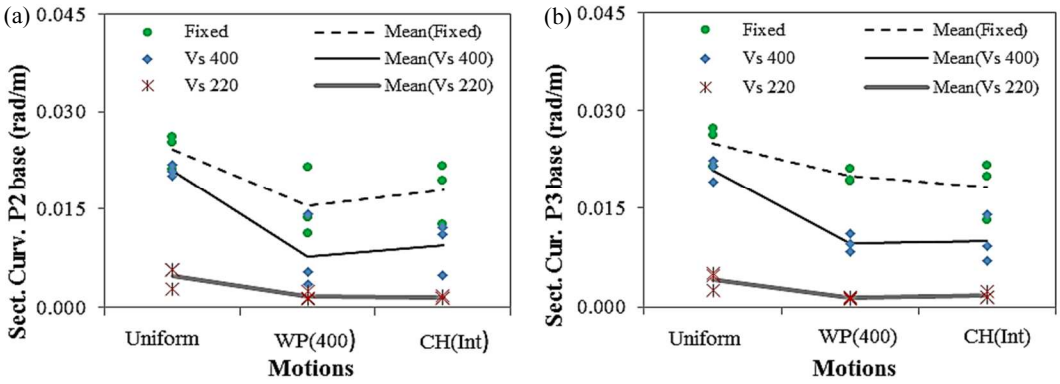

Figure 5-19 Comparison of section curvatures at base of (a) Pier 2; (b) Pier 3 of bridge model 1(a).

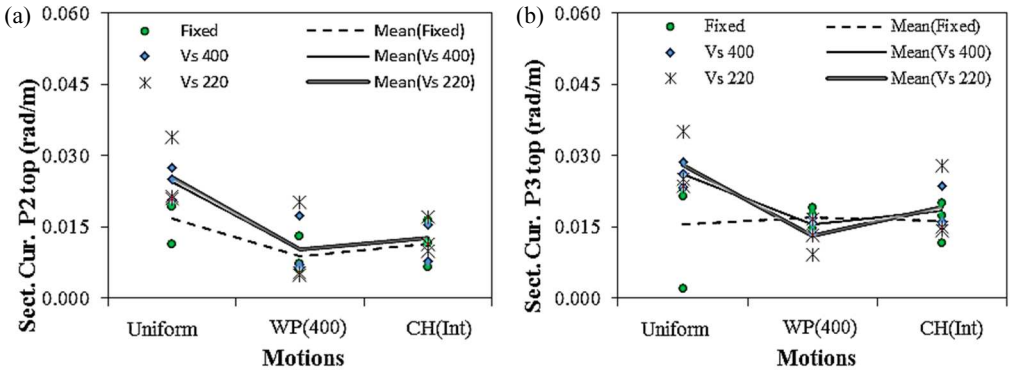

Figure 5-20 Comparison of section curvatures at top of (a) Pier 2; (b) Pier 3 of bridge model 1(a).

5.9 Conclusion

This paper presents parametric studies on the response of multiple-frame bridges with unseating restrainers to spatially varying ground motions and SSI. The nonlinear finite element model of multiple-frame bridges includes pounding and energy dissipation during pounding, foundation flexibility and damping, frictions at supports, superstructure-abutment soil interaction and non-uniform ground motions to represent realistic bridge response. Based on the parametric studies conducted the following conclusions can be drawn

Spatially varying ground motion resulted in the reduction of the seismic demands on the piers of both stiff and flexible frames in the longitudinal direction. However, its effect on the relative displacement responses such as relative hinge displacement, pounding forces and restrainer deformation are always detrimental. The present design method of the restrainers based on the uniform ground motion assumption could significantly underestimate the required stiffness and strength of the restrainers to limit the joint opening movement. The numerical results

indicate that the restrainers designed for uniform ground motion could suffer yielding or even fracturing under the influence of spatially varying ground motions.

Adjusting the fundamental periods of the adjacent bridge components close to each other, as suggested by various codes, is indispensable to mitigate the relative displacement induced damages. However, this might not be sufficient to prevent the damages on bridge structures because of the relative displacements caused by inevitable ground motion spatial variations.

Though SSI results in an increase in drift of the bridge frames, the relative displacement between the bridge frames at intermediate joints are reduced. This could be attributed to reduction of relative phasing of motion caused by the increase in flexibility of the frames due to the introduction of SSI. The SSI also benefits the response of bridge piers by reducing the curvature demands at the base of the piers. However, the larger displacement induced due to the SSI results in an increase in curvature demand at the top of the bridge piers.

It should be noted that present study investigates the seismic responses of multiple-frame bridges subjected to longitudinal spatially varying ground motions only. The influences of multi-dimensional seismic excitations are not considered. Future studies are needed to consider the influence of all three components of ground motions on bridge response analysis.

5.10 References

Bi, K., & Hao, H. (2012). Modelling and simulation of spatially varying earthquake ground motions at sites with varying conditions. *Probabilistic Engineering Mechanics*, *29*, 92-104.

Bi, K., Hao, H., & Chouw, N. (2011). Influence of ground motion spatial variation, site condition and SSI on the required separation distances of bridge structures to avoid seismic pounding. *Earthquake Engineering & Structural Dynamics*, *40*(9), 1027-1043.

CALTRANS (2010). *Seismic Design Criteria: Design manual-version 1.6*, California Dept. of Transportation, Sacramento, CA.

Choi, E. (2002). *Seismic analysis and retrofit of mid-America bridges*, PhD thesis, Georgia Institute of Technology, GA.

Chouw, N. & Hao, H. (2003). Effect of simultaneous spatial near-source ground excitation and soil on the pounding response of bridge girders. *Journal of Applied Mechanics*, 6, 779-788.

Chouw, N., & Hao, H. (2005). Study of SSI and non-uniform ground motion effect on pounding between bridge girders. *Soil Dynamics and Earthquake Engineering*, *25*(7), 717-728.

Chouw, N., & Hao, H. (2008). Significance of SSI and non-uniform near-fault ground motions in bridge response II: Effect on response with modular expansion joint. *Engineering Structures*, *30*(1), 154-162.

Comartin, C.D., Greene, M., & Tubbesing, S.K. (Eds.) (1995) *The Hyogo-ken Nanbu earthquake Jan 17, 1995*, EERI, Preliminary reconnaissance Report, EERI-95-04, Oakland, CA.

Deodatis, G. (1996). Non-stationary stochastic vector processes: seismic ground motion applications. *Probabilistic Engineering Mechanics*, *11*(3), 149-167.

Der Kiureghian, A. (1980). *A response spectrum method for random vibrations. Rep. No*. UCB/EERC-80-/15, Earth. Eng. Research Center, Univ. of California, Berkeley.

DesRoches, R., & Fenves, G. L. (2000). Design of seismic cable hinge restrainers for bridges. *Journal of Structural Engineering*, *126*(4), 500-509.

DesRoches, R., & Fenves, G. L. (2001). Simplified restrainer design procedure for multiple-frame bridges. *Earthquake Spectra*, *17*(4), 551-567.

DesRoches, R., & Muthukumar, S. (2002). Effect of pounding and restrainers on seismic response of multiple-frame bridges. *Journal of Structural Engineering*, *128*(7), 860-869.

FEMA 356 (2000) *Pre-standard and commentary for the seismic rehabilitation*, American Society of Engineers, Virginia.

Feng, M. Q., Kim, J. M., Shinozuka, M., & Purasinghe, R. (2000). Viscoelastic dampers at expansion joints for seismic protection of bridges. *Journal of Bridge Engineering*, *5*(1), 67-74.

Gulkan, J., & Sozen, M. (1974). Inelastic response of reinforced concrete structures to earthquake motion. *ACI Structural Journal*, 71(2), 604–610.

Hao, H., Oliveira, C. S., & Penzien, J. (1989). Multiple-station ground motion processing and simulation based on SMART-1 array data. *Nuclear Engineering and Design*, *111*(3), 293-310.

Huo, Y., & Zhang, J. (2012). Effects of pounding and skewness on seismic responses of typical multispan highway bridges using the fragility function method. *Journal of Bridge Engineering*, *18*(6), 499-515.

Japanese Road Association. (1996). Specifications for highway bridges, part V, seismic design. *Tokyo, Japan*.

Kawashima, K., Unjoh, S., Hoshikuma, J. I., & Kosa, K. (2011). Damage of bridges due to the 2010 Maule, Chile, Earthquake. *Journal of Earthquake Engineering*, *15*(7), 1036-1068.

Kawashima, K., Unjoh, S., Hoshikuma, J. I., & Kosa, K. (2011). Damage of bridges due to the 2010 Maule, Chile, Earthquake. *Journal of Earthquake Engineering*, *15*(7), 1036-1068.

Li, B., Bi, K., Chouw, N., Butterworth, J. W., & Hao, H. (2012). Experimental investigation of spatially varying effect of ground motions on bridge pounding. *Earthquake Engineering & Structural Dynamics*, *41*(14), 1959-1976.

Mander, J. B., Priestley, M. J., & Park, R. (1988). Theoretical stress-strain model for confined concrete. *Journal of structural engineering*, *114*(8), 1804-1826.

Martínez-Rueda, J. E., & Elnashai, A. S. (1997). Confined concrete model under cyclic load. *Materials and Structures*, *30*(3), 139-147.

Menegotto, M., & Pinto, P.E. (1973). Method of analysis for cyclically loaded RC plane frames including changes in geometry and non-elastic behavior of elements under combined normal force and bending. In *Proc. of IABSE symposium on resistance and ultimate deformability of structures acted on by well-defined repeated loads*, Zurich, Switzerland.

Moehle, J. P. (ed.) (1995) *Northridge Earthquake of January 17, 1994: Reconnaissance Report, Volume 1*—Highway Bridges and Traffic Management. Earthquake Spectra 11 (4):287–372.

Muthukumar, S. (2003) *A contact element approach with hysteresis damping for the analysis and design of pounding in Bridges.* PhD thesis, Georgia Institute of Technology, GA.

Muthukumar, S., & DesRoches, R. (2006). A Hertz contact model with non-linear damping for pounding simulation. *Earthquake engineering & structural dynamics*, *35*(7), 811-828.

Mylonakis, G., Nikolaou, S., & Gazetas, G. (2006). Footings under seismic loading: Analysis and design issues with emphasis on bridge foundations. *Soil Dynamics and Earthquake Engineering*, *26*(9), 824-853.

Saiidi, M. (1993). Response of bridge hinge restrainers during earthquakes: field performance, analysis, and design. Rep. no. CCEER93-6. *Center for Civil Engineering Earthquake Research, University of Nevada, Reno, Nev*.

Saiidi, M., Maragakis, E., & Feng, S. (1996). Parameters in bridge restrainer design for seismic retrofit. *Journal of Structural Engineering*, *122*(1), 61-68.

Seismosoft Inc. (2010). Seismo-struct user Manual for version 6, Pavia, Italy.

Sextos, A. G., Kappos, A. J., & Pitilakis, K. D. (2003). Inelastic dynamic analysis of RC bridges accounting for spatial variability of ground motion, site effects and soil–structure interaction phenomena. Part 2: Parametric study. *Earthquake Engineering & Structural Dynamics*, *32*(4), 629-652.

Shrestha, B., Hao, H., & Bi, K. (2014). Effectiveness of using rubber bumper and restrainer on mitigating pounding and unseating damage of bridge structures subjected to spatially varying ground motions. *Engineering Structures*, *79*, 195-210.

Sobczky, K. (1991) *Stochastic Wave Propagation*. Kluwer Academic Publishers, Netherlands.

Trochalakis, P., Eberhard, M. O., & Stanton, J. F. (1997). Design of seismic restrainers for in-span hinges. *Journal of Structural Engineering*, *123*(4), 469-478.

Won, J. H., Mha, H. S., Cho, K. I., & Kim, S. H. (2008). Effects of the restrainer upon bridge motions under seismic excitations. *Engineering Structures*, *30*(12), 3532-3544.

Zhang, J., & Makris, N. (2002a). Kinematic response functions and dynamic stiffnesses of bridge embankments. *Earthquake engineering & structural dynamics*, *31*(11), 1933-1966.

Zhang, J., & Makris, N. (2002b). Seismic response analysis of highway overcrossings including soil–structure interaction. *Earthquake engineering & structural dynamics*, *31*(11), 1967-1991.

Notations

MRHD	Maximum relative hinge displacement
RD	Restrainer deformation
MRAD	Maximum relative abutment displacement
γ_{jk}	Coherency loss function between the ground motions at points j and k
d_{jk}	projected distance between points j and k in the wave propagation direction
α	incident angle of incoming wave to the soil site
β	coefficient depending on the level of coherency loss
vapp	apparent wave velocity on the base rock
K_z	vertical stiffness of foundation
K_x	sway stiffness of foundation
K_{ry}	rocking stiffness of foundation

C_z	vertical viscous damping of foundation
C_x	sway viscous damping of foundation
C_{ry}	rocking viscous damping of foundation
G	shear modulus of soil
ρ	soil density
v	Poisson's ratio
V_s	shear wave velocity
V_{La}	Lysmer's analog wave velocity
G_o	elastic shear modulus of soil
D_{eq}	relative hinge displacement
D_1	modal displacement of system 1
D_2	modal displacement of system 2
ρ_{12}	correlation coefficient between system 1and system 2
β	ratio of the fundamental periods of two systems
ξ	modal damping of system

CHAPTER 6
ON THE EFFECTIVENESS OF ROTATIONAL FRICTION HINGE DAMPER TO CONTROL RESPONSES OF MULTI-SPAN SIMPLY SUPPORTED BRIDGE TO NON-UNIFORM GROUND MOTIONS

6.1 Abstract

Base isolation techniques have been extensively used to improve the seismic performance of bridge structures. The decoupling of the bridge decks from piers and abutments using rubber isolator could result in significant reduction of seismic forces transmitted to bridge substructures. However, the isolation devices could also increase the deck displacement thus enhance the possibility of pounding and unseating damage of bridge decks. Moreover, previous investigations have shown pounding and unseating damages on isolated bridges exacerbate due to the spatial variation of earthquake ground motions. Recent earthquakes revealed that isolation bearing could also be damaged due to the excessive movements of decks during large earthquake events. This study proposes the use of Rotational Friction Hinge Dampers (RFHD) to mitigate the damages that could be induced by large displacement of bridge decks, particularly focusing upon pounding and unseating damages and bearing damages. The device is capable of providing large hysteretic damping and the cost of installing the devices is relatively economical. This paper presents numerical investigations on the effectiveness of these devices on a typical Nepalese simply supported bridge subjected to spatially varying ground motions. The results indicate that RFHDs are very effective in mitigating relative displacement and pounding force, as well as controlling the bearing deformation and pier drift. It is also revealed that the effectiveness of the device is not significantly affected by small changes in the slip forces, thus small variations of the optimum slip forces during the lifetime of the bridge do not warrant any adjustment or replacement of the device.

6.2 Introduction

Highway bridges are one of the key components of a transportation network and they carry significant importance in providing emergency services after an earthquake. Past and recent earthquakes, such as 1971 San Fernando earthquake, 1994 Northridge earthquake, 1995 great Hanshin earthquake, 2010 Chile earthquake and many more revealed that bridges are vulnerable to large ground shakings. In order to improve the seismic performance of both new and existing bridges, seismic isolation devices have been widely used since last few decades. Seismic isolation is an innovative seismic resistant design approach that decouples the bridge superstructure from the substructures, reducing the transmitted forces to the piers and

abutments. The incorporation of the seismic isolator introduces flexibility at isolation level. As a result, the displacements of bridge decks increase. Since adjacent bridge decks/abutments might have different vibration frequencies, and ground motion input at different bridge supports are not exactly the same owing to seismic wave propagation, the adjacent bridge decks and abutments usually do not vibrate exactly in phase. This out-of-phase vibration results in relative displacement responses between bridge decks and between a deck and an abutment that leads to two main problems. Firstly, poundings between adjacent decks or between a deck and an abutment occur if the closing relative displacement exceeds the provided gap size at bridge expansion joints. Pounding of adjacent bridge structures could cause damages at expansion joints and could damage adjoining bearings and piers. It can also amplify relative displacements and contribute towards unseating of bridge spans (Otsuka et al., 1996). The bridge design codes, such as the Japanese Road Association (2004) specify that the gap size between bridge segments should be large enough to avoid poundings. However, the sizes of the expansion joints have to be limited to allow the traffic to flow smoothly. Therefore, it is often impossible to avoid pounding between adjacent bridge components with conventional expansion joints during large earthquake ground excitations. On the other hand, unseating of the bridge spans occur if the opening relative displacement is larger than the provided seat length. Unseating of a bridge span can lead to complete closure of the bridge. As bridges are key components in transportation networks and essential for providing emergency rescue and relief operation after a major earthquake, it is desirable for bridges to not only avoid collapse but also remain functional immediately after an earthquake. Therefore it is necessary to mitigate unseating and pounding damages of bridges induced by large relative displacement between adjacent bridge components.

In addition to pounding and unseating damages large relative displacement during an earthquake could also damage isolation bearings. For example, during the Tohoku earthquake, Japan in 2011, bearing rupture was observed in multiple bridges, such as the Tobu viaduct where the rupture was caused possibly due to the interaction of adjacent bridge components (Takahashi, 2011). The failure of the bearing could result in large residual vertical gaps between the girders (Zhu et al., 2004). According to the design specification of highway bridges in Japan (JRA, 2004), the shear strain in the isolation bearing shall be within 250%. Though several researches have been done in the past on preventing unseating damages in bridges, only limited researches have focused on the damages to the bearing during seismic events. Zhu et al. (2004) using a 3D model evaluated the serviceability of highway bridge with pounding countermeasures. The authors concluded that bearings to be the weakest link in the bridge and are likely to fail during strong earthquake resulting in permanent vertical gaps that could impede the traffic flow. Bi and Hao (2013) used a detailed 3D model of an isolated

bridge and reported that bridge girder could dislocate from the bearing and the dislocated girder could pound against rubber bearing leading to further damages. Only limited studies have focused on the bearing protection devices (Ghosh et al., 2011; Wilde et al., 2000; Choi et al., 2005; Ozubulut & Hurlebaus, 2011). It should be noted that these studies did not consider pounding between adjacent bridge components that could amplify/reduce the bridge displacement. The performance of bearings during earthquake excitations, especially when pounding between adjacent bridge decks occurs, is not well studied yet.

In order to mitigate the adverse effect of relative displacement in bridges different devices have been used. Among them, cable restrainers are the most widely used retrofitting method. However, cable restrainers are only effective to mitigate unseating damages caused by opening relative displacement but could not directly mitigate pounding impacts caused by closing relative displacement. Moreover, the commonly used cable restrainers relies primarily upon their stiffness to limit the opening relative displacement, which can induce a large tensile force which could result in either failure of restrainers or connecting element. The large tensile forces transferred to adjoining frame/deck/abutment may also alter the seismic responses of the bridge. To overcome the limitation of cable restrainers Feng et al. (2000) and Kim et al. (2000) investigated the use of energy dissipating restrainers to mitigate the damages at expansion joint. These studies reported that energy dissipating devices could be a practical solution to the seismic problem arising on bridges with expansion joints. Additionally, it was found that the supplemental damping could be significantly more effective than the stiffness on reducing the relative displacement at bridge expansion joints. Other researcher such as (Rungrassamee & Kawashima, 2003; Guo et al., 2009) investigated the active and semi-active devices such as Magneto-Rheological (MR) dampers to improve the seismic responses of bridges.

One of the important factors affecting the relative displacement responses between adjacent bridge components that have been commonly neglected is the spatial variation of seismic ground motions. Spatial variation of the ground motions along the length of an extended bridge is inevitable due to the different arrival times of seismic waves at the supports of bridge and loss of coherency due to scattering of seismic waves and different soil conditions. Some previous studies, e.g., (Bi & Hao, 2013; Zanardo et al., 2002; Chouw & Hao, 2008; Li et al., 2012) have demonstrated that structural response of bridges subjected to spatially varying ground motions can be drastically different from that under the usually adopted uniform ground motions. Despite the presented facts, most of the previous studies have either neglected the spatial variability of ground motions by assuming uniform ground motion or only partially considered it by including the wave passage effects (Jankowski et al., 2000) when studying

the effectiveness of retrofit devices to mitigate relative displacement induced damages. To the best knowledge of authors, none of the previous studies, apart from the study of Shrestha et al. (2014, 2015) have modelled the ground motions spatial variability in detail in evaluating the effectiveness of pounding and unseating mitigation devices. Since ground motion spatial variation is inevitable, and it causes significantly different responses between adjacent bridge components, the study on the retrofit devices to mitigate the relative displacement induced damages without considering the spatial ground motion variations along the length of bridge may provide unrealistic results.

In this study, Rotational Friction Hinge Dampers (RFHD) devices are proposed to mitigate damages in bridge structures subjected to spatially varying ground motions. These devices have large hysteretic energy dissipation capability at a reasonable cost and are easy to install and maintain. The behavior of the device are nearly unaffected by amplitude, frequency or the number of the applied loading cycles (Mualla & Belev, 2002). Recently, several friction devices have been tested experimentally and some of these have been implemented in buildings around the world (Mualla & Belev, 2002; Nielsen et al., 2004). However, its efficacy in mitigating the relative displacement induced damages in bridge structures has not been explored yet. This study focuses on evaluating the effectiveness of the RFHD on mitigating relative displacement induced damages in simply supported bridges caused by spatially varying earthquake ground motions. This study does not focus on comparison of responses of isolated simply supported bridges to spatially varying ground motions with those subjected to uniform ground motion, which could be found elsewhere (Zanardo et al., 2002). It focuses on mitigating the adverse responses of isolated multi-span simply supported bridges subjected to spatially varying ground motions, particularly pounding and unseating damages as highlighted by (Zanardo et al., 2002). The analysis is conducted on a typical Nepalese simply supported bridge with four spans of 25 meters each. Extensive numerical analysis is conducted to identify the effectiveness of RFHD on mitigating the damages in bridge structures. Parametric analyses have been conducted to ascertain the optimum slip force of the RFHD. The investigation also compares the bridge structural responses with two configurations of RFHD.

6.3 Rotational Friction Hinge Damper

In recent years, friction dampers have found several applications in both steel and concrete buildings for seismic rehabilitations and up-gradation of the existing structures as well as applications in newly constructed structures (Mualla & Belev, 2002). A key point in the use of the friction dampers in seismic protection of structures is that their response is not affected by frequency and duration of ground motions. However, their mechanical behavior is likely

to induce residual displacement that may require some recovering operations after the earthquake event.

In this study, a type of friction damper, Rotational Friction Hinge Damper (RHFD), is used to mitigate the damages arising in bridge structures due to relative displacements of adjacent bridge components. RFHD consists of rigid steel plates connected in rotational hinge, and the plates are separated by several shims of friction pads as seen in Figure 6-1 (a). The moment-rotation behavior in the hinge is elastic-frictional. The hinge connection is meant to increase the amount of relative rotation between the rigid plates, which in turn enhances the energy dissipation in the system. During the seismic events the distance between connection points and the angle between the damper plates in the hinge changes due to the induced seismic motion. Upon reaching the frictional resistance of the device in torsion, slip and relative rotation between the damper plates take place, thus dissipating a portion of the kinetic energy of the structure. The sticking and sliding modes of the RFHDs succeed each other until the end of motion (Nielsen et al., 2004).

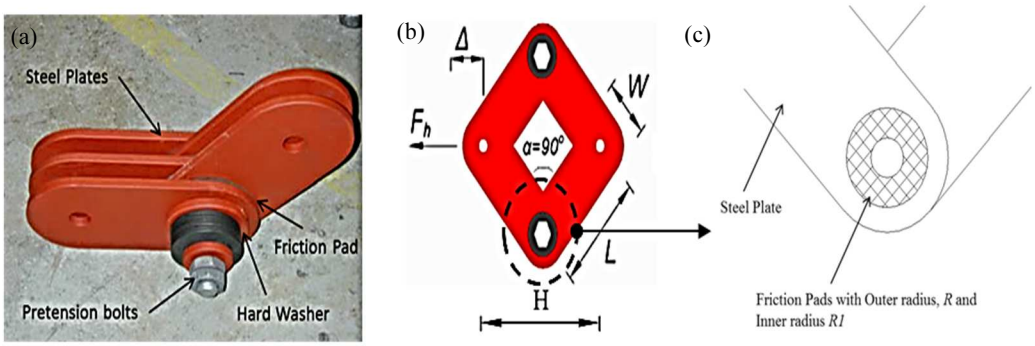

Figure 6-1 (a) Damper details; (b) Details of Rhombus shape damper with double hinges and (c) Sectional detail of hinge including friction pads.

In order to investigate the effects of different configurations of dampers on the bridge responses two damper configurations as shown in Figure 6-1 (a) and (b) are studied. The damper configurations are referred as V-type and R-type, respectively. The geometrical features of the friction dampers are provided in Figure 6-1 (b). Figure 6-1 (c) shows details of friction pads at rotational hinge. The friction plate has length L, width W and thickness t. The angle between the two adjacent plates is α. The slip force of the friction damper is calculated using the relations given by Chen and Hao (2013).

$$F_h = \frac{nM}{\sqrt{L^2 - (H/2)^2}} = \frac{nM}{L\cos(\alpha/2)} \tag{6.1}$$

where M is the rotational friction resistant moment at each hinge, n is the number of hinges in a device, L is the effective length of plate. The included angle is given by α, and the height of the device is H.

The value of rotational friction resistant moment, *M*, depends on the friction coefficient, the preload and the frictional area. The friction force is given by

$$dF = \mu dN = \mu pds = \mu p \times 2\pi r dr \tag{6.2}$$

The resistant moment is given by

$$dM = rdF = 2\pi r^2 \mu p dr \tag{6.3}$$

$$M = \int_{R_1}^{R} dM = \int_{R_1}^{R} 2\pi r^2 \mu p dr = \frac{2}{3}\pi\mu p (R^3 - R_1^3) \tag{6.4}$$

where F is the rotational friction force at each joint; μ is the friction coefficient; p is the preloading provided by the bolts; R1 is the inner radius of friction pad ; R is the outer radius of friction pad as shown in Figure 6-1(c).

The two ends of a V-type damper can be connected to pier and deck of the bridge, respectively, as shown in Figure 6-2 to mitigate relative displacement response. The connection detail of the R-type damper is presented in Figure 6-3. As shown, for an R-type damper the connection is between deck to deck at intermediate joints. In the figures only the connection scheme to control the longitudinal bridge motion are presented as this study considers only the longitudinal bridge responses that are responsible for pounding and unseating. The connection scheme could be easily extended to control both the longitudinal and the transverse bridge responses.

As presented, the damper has a very simple mechanism that makes it easy to be assembled and installed. The simplicity allows for installing devices with multiple units in order to meet the required frictional resistance. While applying, the dampers should be placed parallel to the longitudinal axis of the bridge to mitigate relative displacement responses in the longitudinal direction. In addition, a hydraulic lock-up device to allow slow movements such as thermal expansion but transmit the shocks from high frequency movement such as earthquake could be placed along with the device.

Previous investigation had showed that the behavior of friction damper is essentially bilinear (Mualla & Belev, 2002; Mualla, 2000). Due to this behavior it is quite common to represent a friction damper using rigid plastic link (Mualla & Belev, 2002; Vafai et al., 2001) or elastic

perfectly-plastic link in numerical modelling. Bhaskararao and Jangid (2006) studied the response of MDOF structures connected using friction dampers modelled using fictitious springs. The fictitious spring was assumed to having large stiffness during the non-slip mode and zero stiffness during the slip mode. The same concept is utilized here to model the RFHD with a high initial stiffness (k_d) during non-slip mode as shown in Figure 6-4. The slip takes place whenever the force in the dampers exceeds the slip force F_h, which is the limiting force in that friction damper.

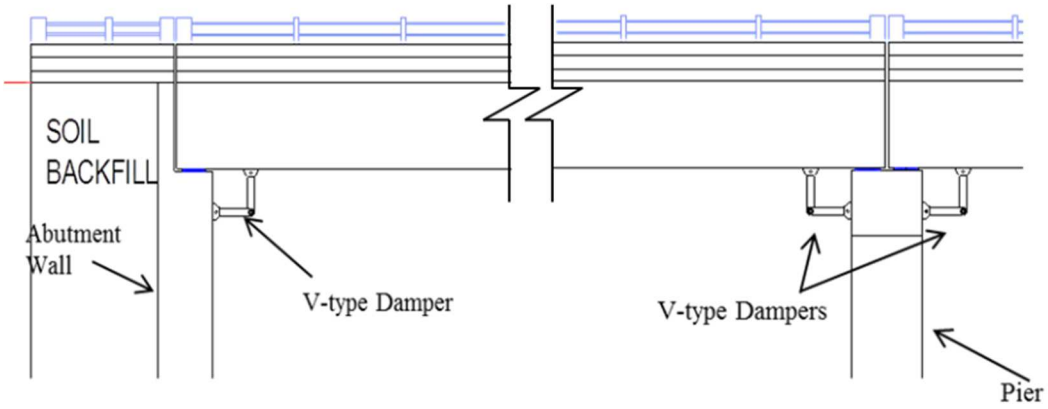

Figure 6-2 Connection scheme for V-type dampers.

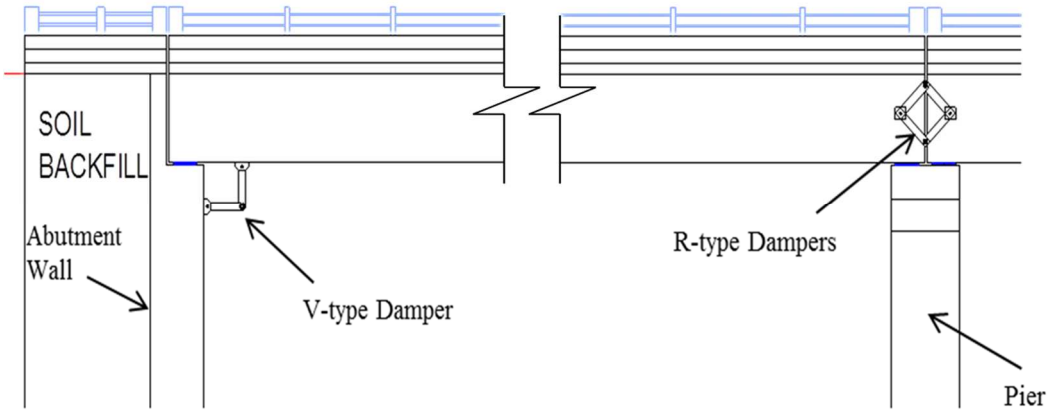

Figure 6-3 Connection scheme for R-type dampers.

6.4 Bridge Model

6.4.1 Bridge Description

Figure 6-5 shows the details of the simply supported bridge considered in this study. The bridge has 4 spans of 25 m each and the total length is 100 m. These are typical simply supported bridges commonly found in Nepal. The bridge is supported on 3 piers and 2 abutments. The piers are of circular geometry with 1.6 m diameter. The total height of the bridge piers from the top of foundation is 6 m. The bridge deck is slab on girder type construction with 3 girders of 2 m depth. The total weight of each 25 m deck is 2.13 MN. The

details of deck and pier to deck connections are presented in Figure 6.6. The deck is supported on elastomeric bearings of area 0.4 m by 0.3 m and thickness of 0.05 m. The piers and abutments are provided with shear keys that inhibit the lateral movement of bridge decks. The abutment is a seating type with back wall of 2 m in height and 7.2 m in width. The length of the seat at the abutment is 0.94 m. All the bridge piers and both the abutment rest on a well foundation of diameter 6 m and depth 13 m.

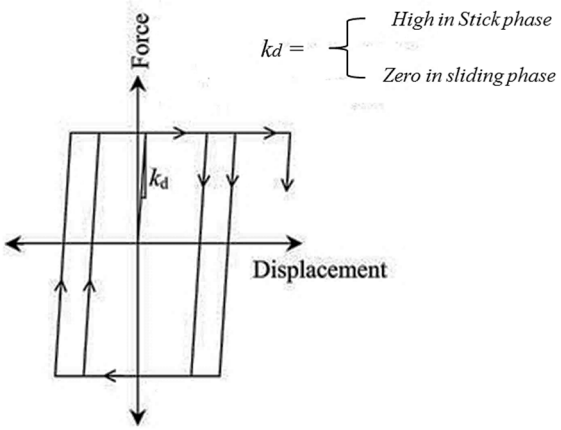

Figure 6-4 Force-displacement relationship for RFHD.

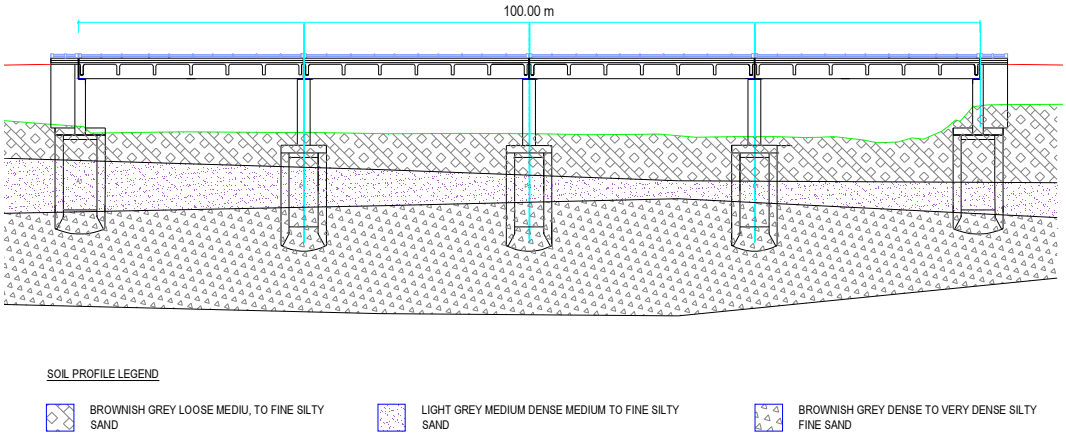

Figure 6-5 Sectional view of the bridge.

6.4.2 Numerical Modelling

In this study, 2-D finite element models of the bridge is developed. The geometrical property of the bridge is calculated based on the details of the bridge designs illustrated in Figure 6-6. The superstructures of an isolated bridge are usually designed to remain elastic under seismic events. Therefore an elastic beam-column element with the calculated properties is used to model the bridge deck. The piers are modelled using nonlinear beam-column element. Fiber element modelling, also known as discretized-section model for non-linear analyses, is used

to represent non-linear behavior of the reinforced concrete bridge piers. Reinforced concrete sections are constructed from three materials, namely unconfined concrete, confined concrete and reinforcing steel. The unconfined and confined concrete behavior is modelled using the nonlinear concrete model that follows the constitutive relationship proposed by Mander et al. (1988) and the cyclic rules proposed by Martinez-Rueda and Elnashai (1997). The confinement effects provided by the lateral transverse reinforcement are incorporated through the rules proposed in (Mander et al., 1988), whereby constant confining pressure is assumed throughout the entire stress-strain range. To represent the behavior of the steel re-bars, Menegotto-Pinto steel model (Menegotto & Pinto, 1973) is used. The yield strength of the rebar is 500 MPa, and the elastic modulus, E_s is 200GPa. Reinforcement details of the piers are shown in Figure 6-6 (b).

The foundation of the bridge is assumed to be fixed at the top of well foundation. To simplify the problems, interaction between soil and the foundation of bridge structure is neglected in the present study. It is common in engineering practice to use a simplified bilinear model with kinematic hardening rules, as shown in Figure 6-7 (b), to represent the behavior of elastomeric bearings (Naeim & Kelly, 1999). The bilinear model can be completely described by the elastic stiffness, K_1, characteristic strength Q and post-yielding stiffness K_2. The characteristics strength Q of bearing is taken as 10% of the weight carried by bearings. This value has been widely accepted among the bearing designers (Ali & Adbel Ghaffer, 1995; Adbel Raheem, 2009). The elastic stiffness to post-yielding stiffness ratio, K_2/K_1 is taken as 0.10. The elastic stiffness of elastomeric bearings is taken as 13.25 MN/m, the post-yielding stiffness is 1.32 MN/m and the characteristic strength is 98.60 KN.

Pounding between two decks or deck and abutment is modelled using a linear impact spring element with gap of 25mm. The stiffness of impact element K_i, and the impact force F_i at the impact spring element are expressed as

$$K_i=\gamma\frac{AE}{L} \tag{6.5}$$

$$F_i=K_i\cdot\Delta u \tag{6.6}$$

where Δu is the relative closing displacement between the adjoining bridge superstructures beyond the provided gap width. In Equation (6.5), A is the sectional area of the deck, γ is the ratio of impact spring stiffness to the stiffness of the superstructure and E is the modulus of elasticity of the deck material. In this study γ is taken as 2 based on the previous studies on similar bridges (Adbel Raheem, 2009; Ruangrassamee & Kawashima, 2003). The stiffness of

the impact spring is calculated to be 7884 MN/m. Abutment of the bridge is modelled using linear spring. The stiffness of abutment spring, K_{abut} used in the analysis is 174 MN/m. The abutment springs get activated only in passive direction of the abutment.

The mechanical model of as-built bridge and bridge installed with V-type and R-type RFHD are illustrated in Figure 6-7 (a), (b) and (c), respectively. In the figure, RLink*i*L and RLink*i*R refer to the rigid link connecting the i_{th} pier with the deck on the left and right side of the i_{th} pier, respectively; AbutSpr1 is the abutment spring at abutment 1, Br2L refers to the left bearing at Pier 2, Vtype2L refers to V-type RFHD at left side of Pier 2. Rtype 2 indicates R-type RFHD placed above pier 2.

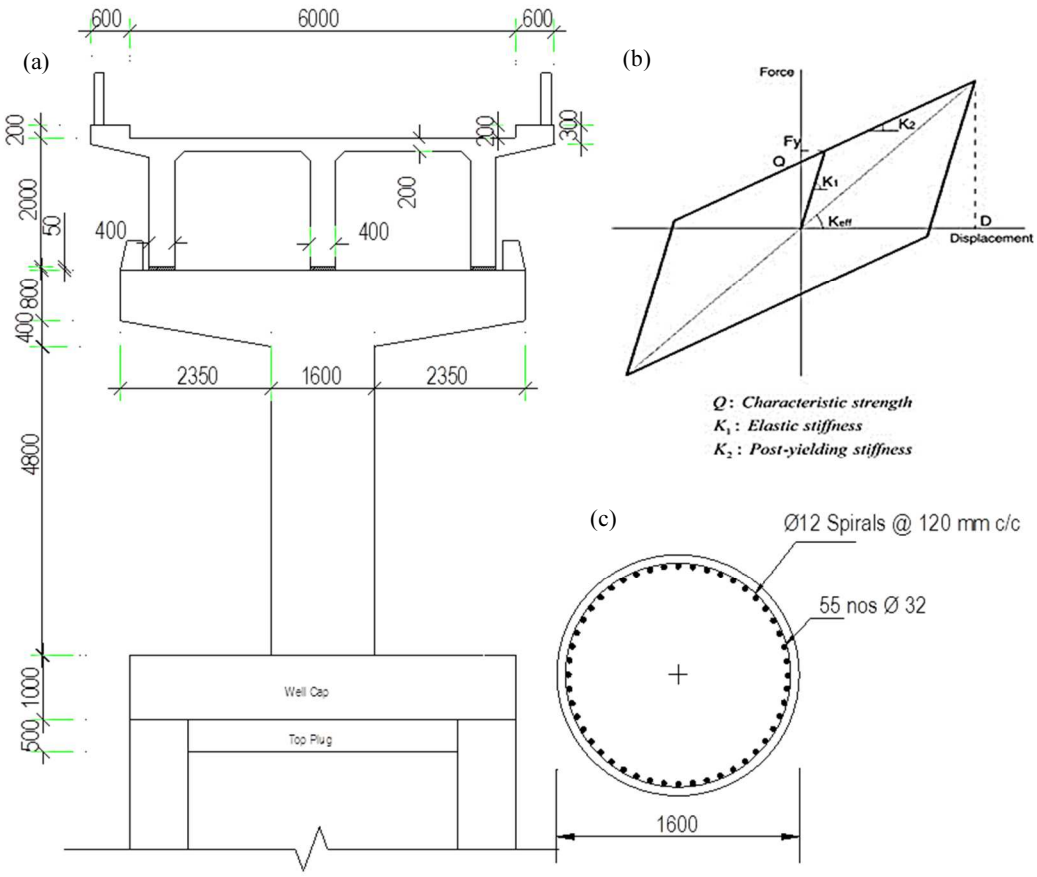

Figure 6-6 (a) Bridge geometrical details; (b) Hysteretic behaviour of elastomeric bearing and (c) Pier reinforcement details.

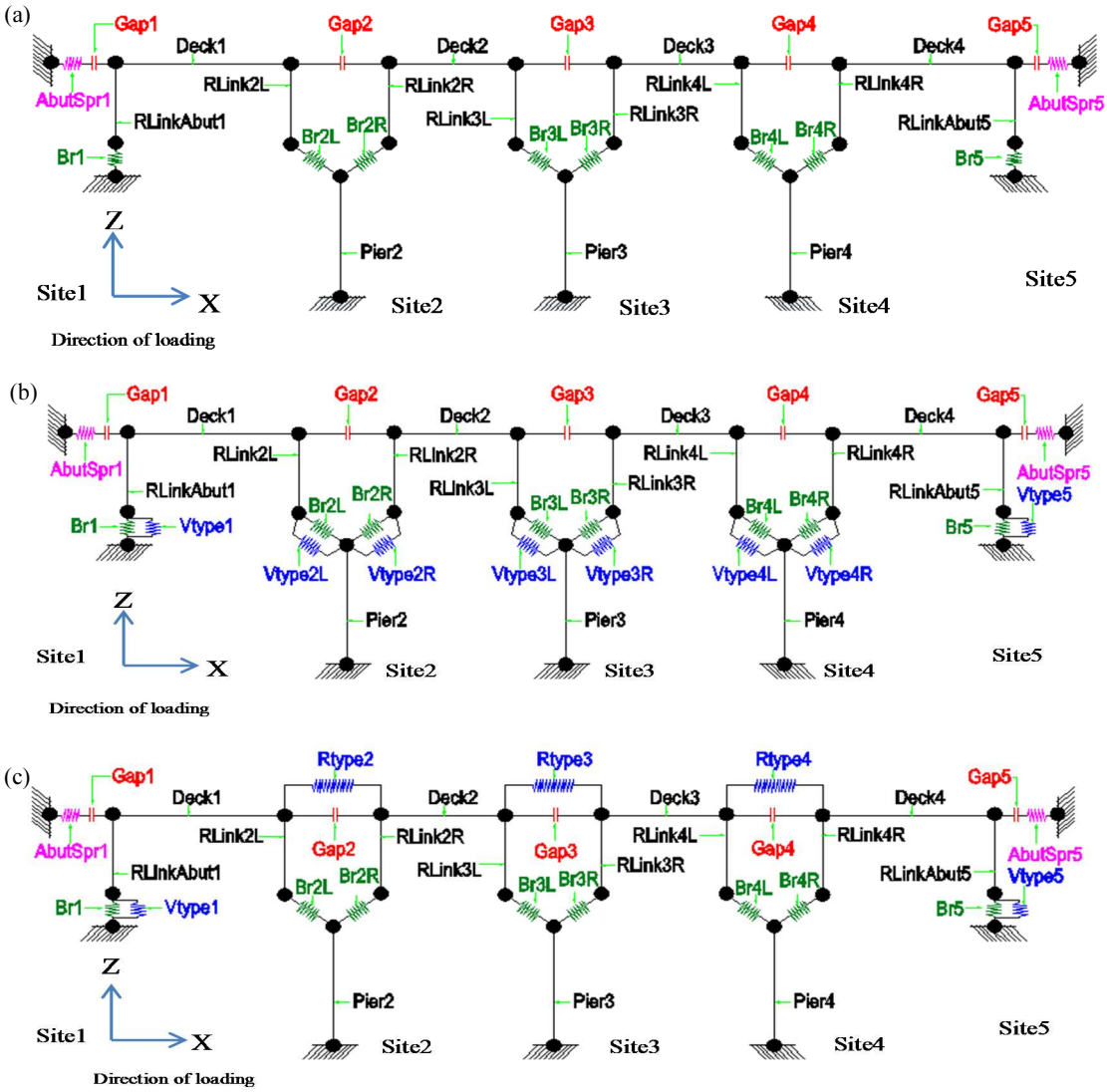

Figure 6-7 Mechanical model of (a) as-built bridge; (b) Bridge with V-type dampers and (c) Bridge with R-type dampers at intermediate joints.

6.5 Ground Motions

The method proposed by Bi and Hao (2012) is used to simulate spatially varying ground motion time histories. The ground motions are simulated to be compatible with the design response spectrum defined in Indian code IS1893 (2002) for Type III (soft soil) condition normalized to PGA 0.65g. The PGA value adopted in this study was determined in recent Probabilistic Seismic Hazards Analyses (PSHA) (Parajuli, 2009; Ram & Wang, 2013; Mahajan et al., 2010) for regions in Nepal and adjoining areas for rare earthquake events that should be used for designing lifeline bridge structures.

The spatial variation between ground motions recorded at two locations j and k on ground surface is modelled by a theoretical coherency loss function (Sobczky, 1991)

$$\gamma_{jk}(i\omega) = \left|\gamma_{jk}(i\omega)\right| \exp(-i\omega d_{jk} \cos\alpha / v_{app}) = \exp(-\beta\omega d_{jk}^2 / v_{app}) \cdot \exp(-i\omega d_{jk} \cos\alpha / v_{app}) \quad (6.7)$$

where β is a constant reflecting the level of coherency loss, d_{jk} is the distance between the two locations j and k in the wave propagation direction, f is the frequency in Hz, v_{app} is the apparent wave velocity, and α is the seismic wave incident angle. In this study, $\beta = 0.001$, v_{app} and α is assumed to be 500 m/s and 45°, respectively. The adopted value of β represents intermediate coherency losses of the spatial ground motions at supports of the bridge. To obtain a relatively unbiased response accounting for the random phase angles of ground motions, 5 sets of spatial ground motion time histories (referred as GM1 to GM5) are simulated independently. Sampling frequency is set to 100 Hz, and duration of the ground motion is 20.47 seconds in simulation. Figure 6-8 compares the response spectra of the simulated spatial ground motions with the target response spectrum. As shown, the response spectra of the simulated spatial ground motions at the five sites are all compatible with the design response spectrum.

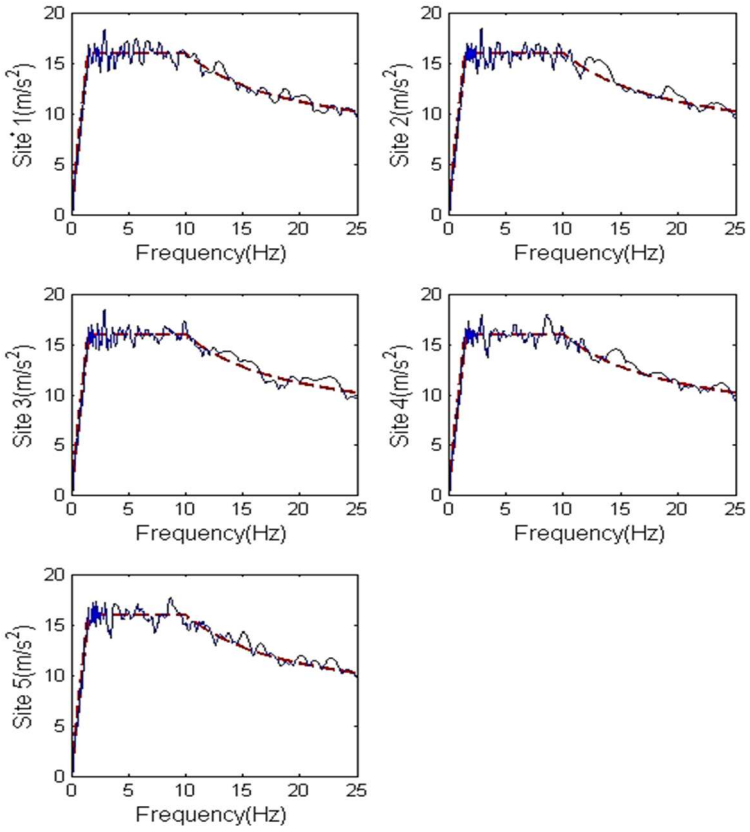

Figure 6-8 Comparison of response spectra of simulated ground motions with the design response spectra.

The comparison of the empirical coherency loss function defined by Eq. (6.7) between Site 1 and the other sites is presented in Figure 6-9. A good match can be observed except for $|\gamma_{15}|$

in the higher frequency range. This is expected since Site 5 is the furthest from site 1 and the spatial ground motions at these two sites are least correlated. The cross correlation between spatial motions or the coherency loss decreases with frequency, but the numerically calculated coherency loss between any two spatial ground motion time histories is more than 0.3. This is because the numerically calculated coherency loss has a threshold value of about 0.3-0.4, the value corresponding to the numerically calculated coherency loss between two white noise series as revealed in previous studies, e.g. Hao et al. (1989).

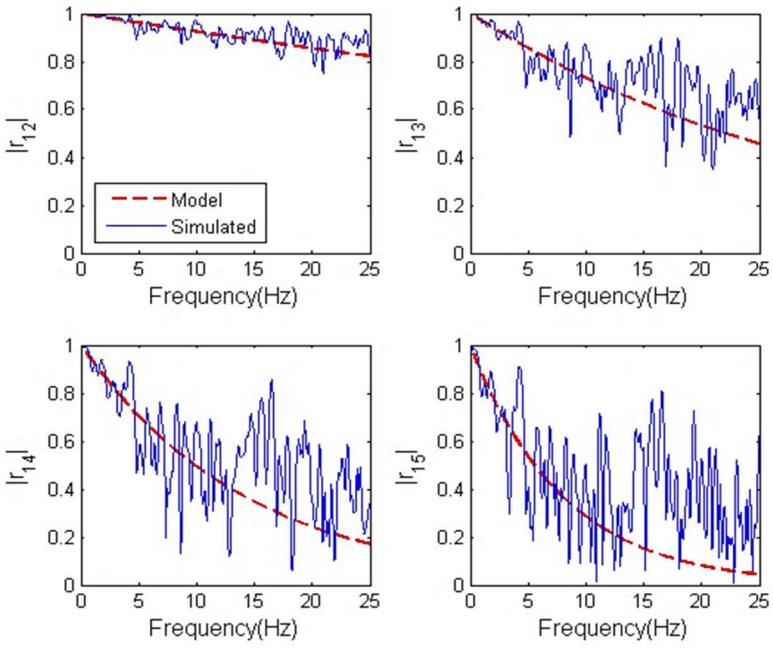

Figure 6-9 Ideal and simulated coherency losses.

6.6 Results and Discussions

6.6.1 Effects of Pounding

Prior to assessing the effectiveness of the friction hinge dampers, the effects of seismic pounding on the response of the structure must be understood. It is well-known that seismic pounding results in damaging impact between the adjacent bridge components, however, its effect on the relative opening displacements at joints of simply supported bridges subjected to non-uniform ground motions has not been well documented. As relative opening displacement may result in unseating damage, it is important to understand the influence of pounding on the relative opening displacement response. To study this, as built bridge model with expansion gap of 25 mm and assumed gap large enough to avoid contact between the adjacent bridge components are analyzed.

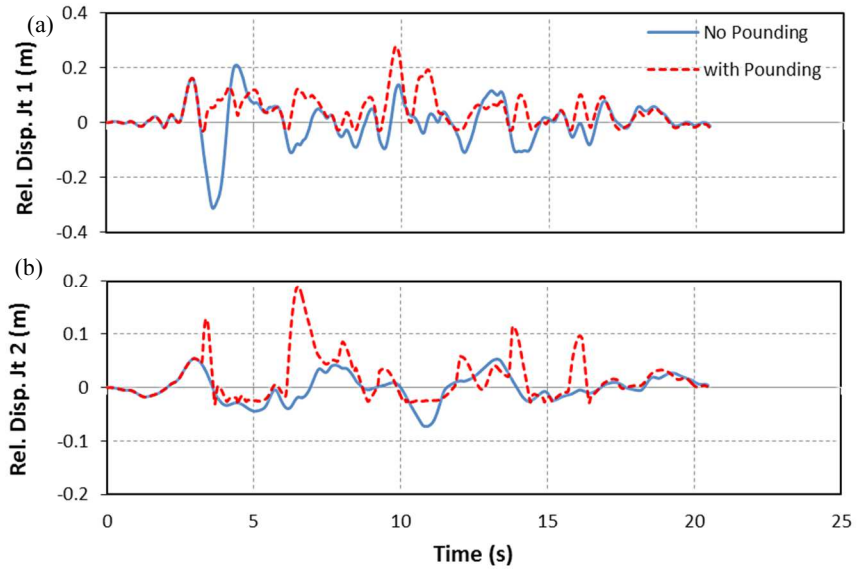

Figure 6-10 Relative displacements between adjacent decks at (a) joint 1 and (b) joint 2 with and without pounding.

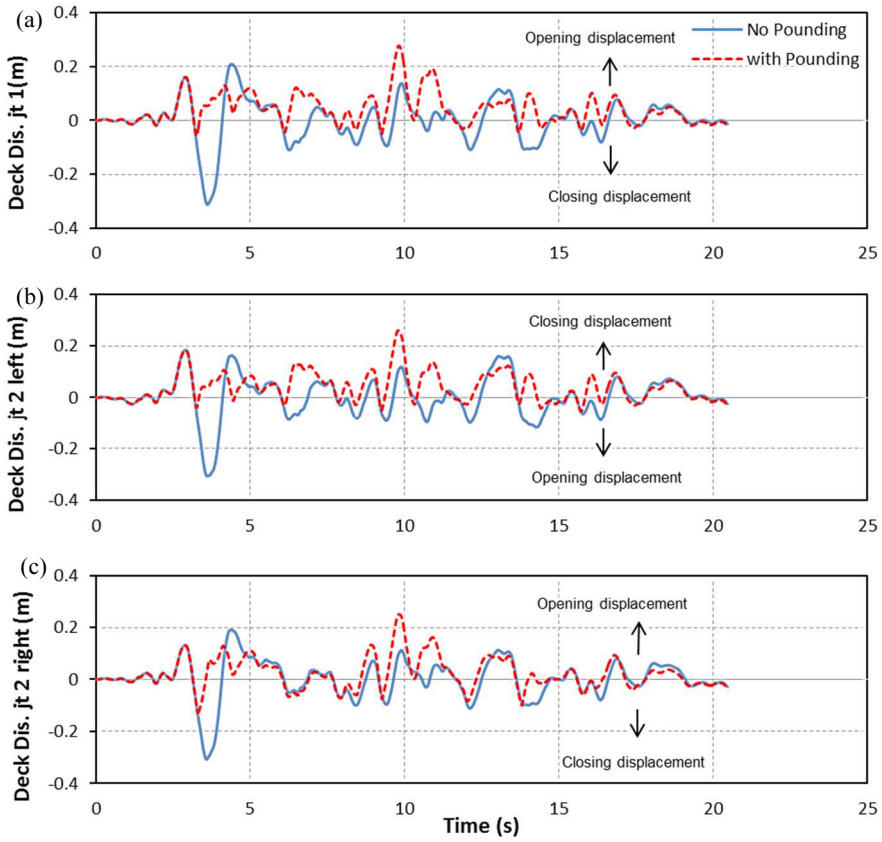

Figure 6-11 Relative displacements between bridge deck and supporting pier at (a) joint 1; (b) left side of joint 2 and (c) right side of joint 2 with and without pounding.

As shown in Figure 6-10, without pounding the deck could move beyond the gap size (negative or closing relative displacement more than 25 mm) and the response is more stable for the duration of the earthquake. When pounding occurs the closing relative movement is

limited approximately to 25mm at each joint as the gap closes. As shown in the figure, peak joint opening displacements at Joint 1 and Joint 2 due to pounding experience an increase of 33% and 250%, respectively. This indicates that the relative joint separations could be amplified by the pounding of adjacent segments. As a consequence, the unseating displacements (i.e. opening relative displacement between the bridge deck and supporting pier) of the bridge deck, as presented in Figure 6-11, may increase, which may lead to unseating failure of the bridge deck if the provided seat width is smaller than the unseating displacement.

6.6.2 Effectiveness of RFHD

To evaluate the effectiveness of the RFHD in bridge structures subjected to spatially varying ground motions, responses of the as-built bridge model and the bridge model with V-type damper are analyzed and compared. In this section, without losing generality only the case with the total damper slip force of 186kN, i.e. with two dampers with slip force 93 KN each placed at two outer girders of the deck as shown in Figure 6-12, is presented. The performance of the bridges is compared in terms of the peak and standard deviation of pounding forces, peak and standard deviation of relative displacement, residual displacement, bearing deformation and pier drift.

Figure 6-13 shows the peak pounding forces at five joints of the bridge for the two bridge models, i.e. as-built and with V-type dampers as shown in Figure 6-2. The middle point represents the mean peak pounding forces while vertical line represents the mean plus or minus one standard deviation of the peak pounding force at the bridge joints obtained with the 5 sets of independently simulated spatially varying ground motions. Thus the tip of the line represents the 84^{th} percentile value of peak pounding force while bottom end of the line represents the 16^{th} percentile value of the peak pounding force. As shown, the V-type dampers are effective in mitigating peak pounding forces at all joints of the bridge. Figure 6-14 compares the peak relative displacement at five joints of the bridges. The V-type dampers are also effective in reducing the peak relative opening of the joints. As shown the dampers significantly reduce the relative displacement at all joints except at joint 4, which has the least relative displacement without the dampers. This is because the dampers are effective only when the relative displacement is relatively large as damping capacity depends upon the opening of the joints and have only limited effect if the relative displacement is small as in the case for joint 4.

A factor that could limit the application of friction damper is its mechanical behavior which is likely to induce residual displacement in the structure that could limit the serviceability of

the bridge after an earthquake. In order to evaluate the residual deformation that dampers can induce at the bridge joints, residual deformations at all joints are measured and compared with the corresponding residual deformations of the as-built bridge model. As shown in Figure 6-15, residual deformations at joints are not significantly altered by use of the friction dampers. The residual deformation could widen the gap or completely close the gap, however, the calculated residual deformations are within a limited range (less than 3cm) for the considered ground motions, thus would not impede the traffic flow.

Damper constraints the movement of bridge deck and this limits the deformation on the bearings. Bearing deformations without dampers could be large and could result in the failure of the bearings, potentially generating vertical gaps between the two adjacent decks or deck and approach slab. This study verifies the failure of rubber bearing by observing its peak deformation. Though the bridge codes (Japan Road Association 2004) suggest 250% shear strain as the ultimate shear strain limits, the modern isolation bearings can sustain shear strain up to 400% before failure. In this study without losing generality, a failure criterion of shear strain 300% for rubber bearing is adopted as in a previous study (Zhu et al. 2004). Figure 6-16 shows the peak deformation of the bearing to five sets of simulated ground motions for two bridge models. As presented, the bearing deformations in as-built bridge model are large and most of the bridge bearing will be damaged due to the earthquake ground motions. Installing the V-type dampers significantly reduces the deformation demand of the bearings and limits the bearing deformations within the permissible limit.

Figure 6-17 compares the peak drift of the three piers of the two bridge models. As shown, applying the V-type dampers results in an increase in the drift of the bridge piers due to the transfer of forces from superstructure to the pier. However, this does not significantly affect the bridge pier responses as indicated by only the slight increase in the bridge drift because the slip force of the damper is relatively lower and damper dissipates some of the kinetic energy. Application of V-type dampers leads to slightly higher forces on the bridge piers, however, this would not significantly reduce the effectiveness of bridge isolation and only slight increase in peak displacement demand would be expected to bridge piers. Despite this undesirable influence on pier responses, the advantages of using friction dampers to mitigate relative displacement responses of bridge superstructures are obvious.

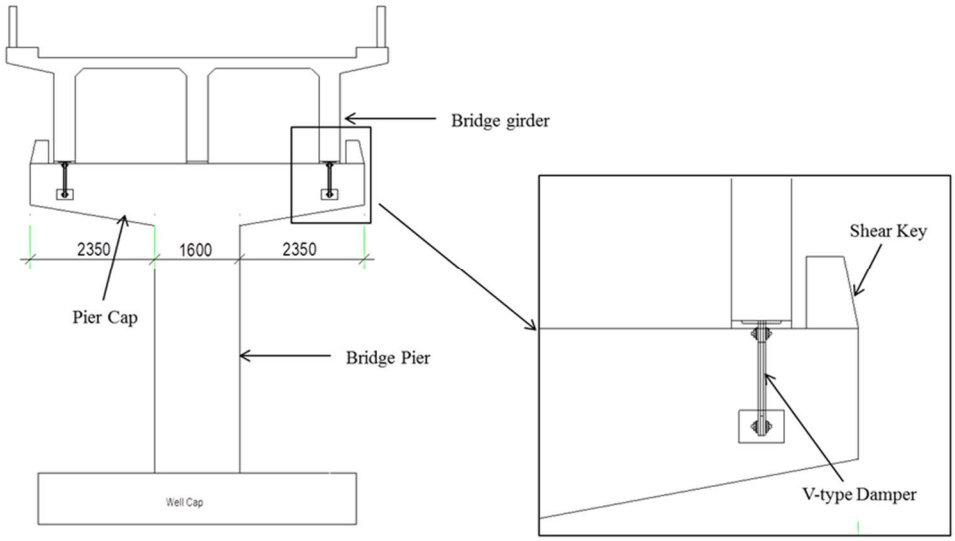

Figure 6-12 Symmetrical placement of dampers at outer bridge girders.

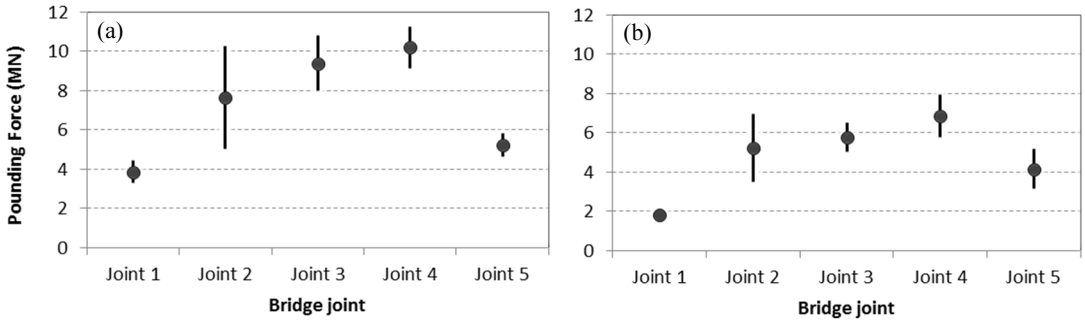

Figure 6-13 Pounding forces at five joints (a) as-built bridge; (b) Bridge with V-type RFHD.

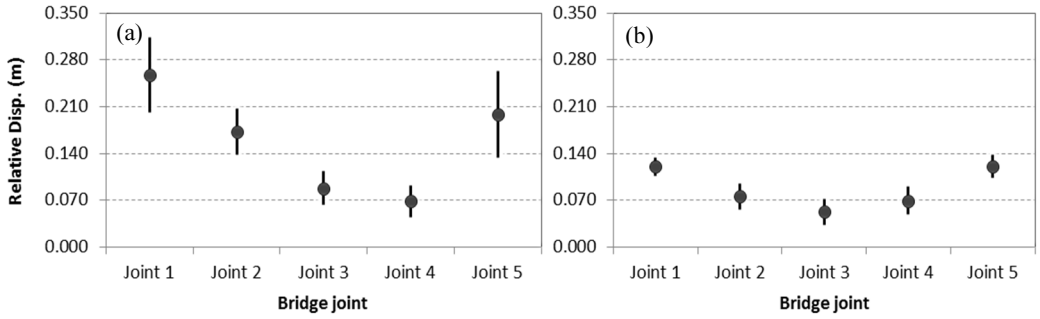

Figure 6-14 Relative displacement at five joints (a) as-built bridge; (b) bridge with V-type RFHD.

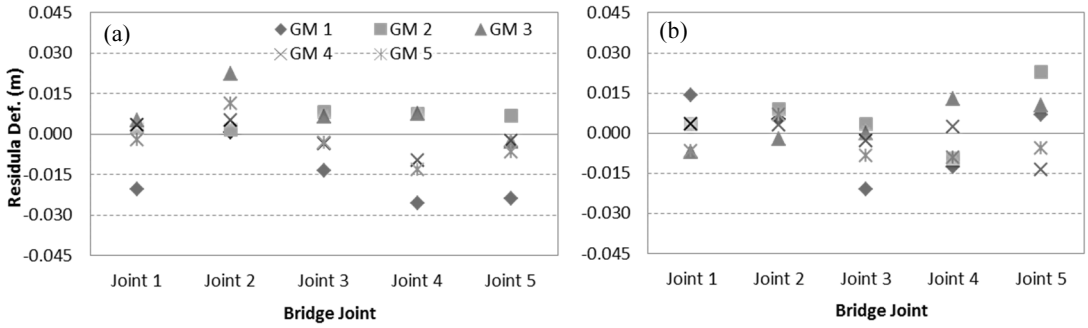

Figure 6-15 Residual displacement at five joint (a) as-built bridge; (b) bridge with V-type RFHD.

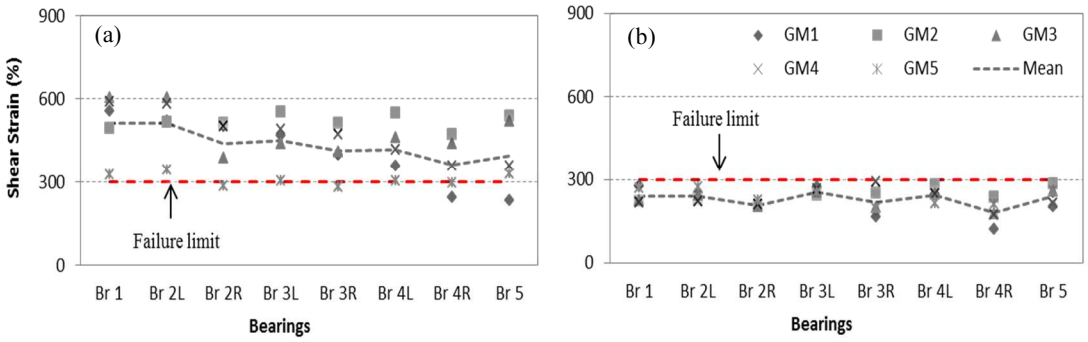

Figure 6-16 Peak deformation of bearings (a) as-built bridge; (b) bridge with V-type RFHD.

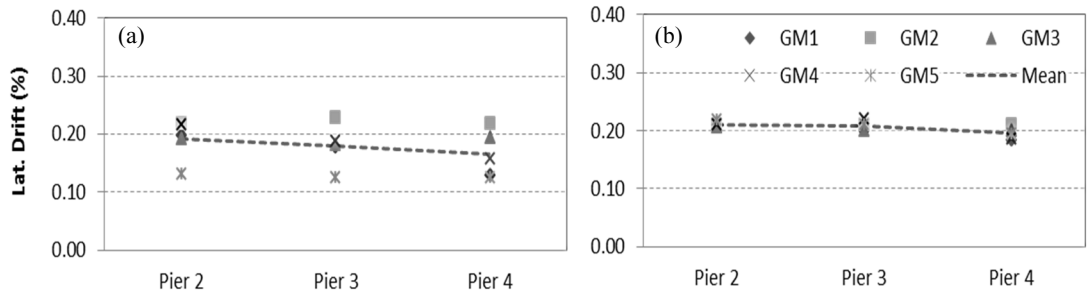

Figure 6-17 Comparisons of peak pier drifts (a) as-built bridge; (b) bridge with V-type RFHD.

6.6.3 Optimum Damper Slip Force

In order to find out the optimum slip force of the dampers to mitigate relative displacement responses without significantly increasing the pier responses, analyses are carried out with varying slip forces of the dampers. The slip forces of the dampers can be practically controlled by increasing or decreasing bolt pretension and/or by increasing or decreasing the number of friction plates. In this study, five damper slip forces, i.e. 93, 186, 280, 373 and 466 kN are considered to identify the effects of the damper slip force on the bridge response. This represents the normalized damper slip forces, defined as the ratio of slip force over weight of the bridge deck on bearing supports, of 0.09, 0.19, 0.28, 0.38 and 0.47, respectively. In order

to investigate the optimum slip force of the dampers normalized damper slip forces are used to compare the bridge responses.

Figure 6-18 compares the mean peak pounding forces and mean peak joint opening at five joints of the bridge for 5 sets of ground motions. As shown, the pounding forces and relative joint opening are significantly reduced due to the application of RFHD. In general, increasing the RFHD slip forces result in reductions of peak pounding forces and joint opening. However, the rate of pounding force and joint opening reduction decreases with the higher slip force. When the normalized slip force is larger than 0.28, further increasing the slip force has insignificant effect on reduction of pounding force and joint opening displacement. This is because, as will be discussed subsequently, the energy dissipated by the dampers reduces with the higher slip forces. The reduction in the energy dissipation reduces the effectiveness of dampers to mitigate pounding forces between adjacent bridge components.

The energy dissipated by the dampers is affected by the damper slip force. Figure 6-19 presents comparison of hysteretic responses of a damper, Vtype4R with normalized damper slip force of 0.09 and 0.47 subjected to GM2. It is observed that the increase in the slip forces could result in a reduction of damper deformation and in some cases the device may form an incomplete hysteretic loop, suggesting a reduction in energy dissipation as well as presence of some residual displacements. Comparison of bearing shear deformation and pier drift demand subjected to GM2 is presented in Figure 6-20 (a). As shown, the bearing deformations of the bridge model without dampers are large and exceed the ultimate limit state. Placing the dampers with the normalized damper slip forces of 0.09 reduces the bearing deformations; however the deformations are still large enough to result in bearing failure. Installing the dampers with the normalized damper slip forces of 0.19 or above reduces the shear deformations below the ultimate strain limit of 300%. The higher is the normalized slip forces of the dampers, the more is the reduction of bearing shear strain. However, when the normalized damper slip force is larger than 0.38, further increase in slip force has insignificant effect on bearing deformation. Figure 6-20 (b) shows that as the normalized slip force is larger than 0.19, further increase in the slip force results in an increase in the peak drift of the bridge piers. This is because large damper slip force reduces the effectiveness of bearing isolation of the bridge deck, therefore results in more seismic forces being transferred from bridge decks to the piers.

The above results indicate that increasing the damper slip force is generally beneficial to mitigating relative displacement responses, however, would also result in reduction of energy dissipation and larger pier responses. Therefore a balance needs be found for a practical application of dampers for better protection of not only the bridge super structures (decks) and

connection members (bearings), but also the bridge piers. The results presented also suggest that damper effectiveness is not significantly affected by slight variations in the slip force of dampers. Hence, small variations in optimum slip force over the life of the bridge do not warrant any adjustment or replacement of friction dampers.

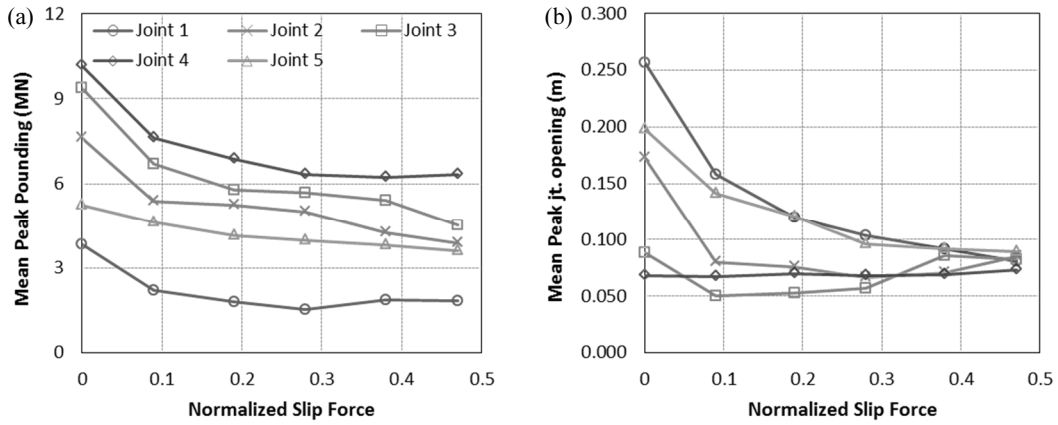

Figure 6-18 Comparison of (a) mean peak pounding forces; (b) mean peak joint opening.

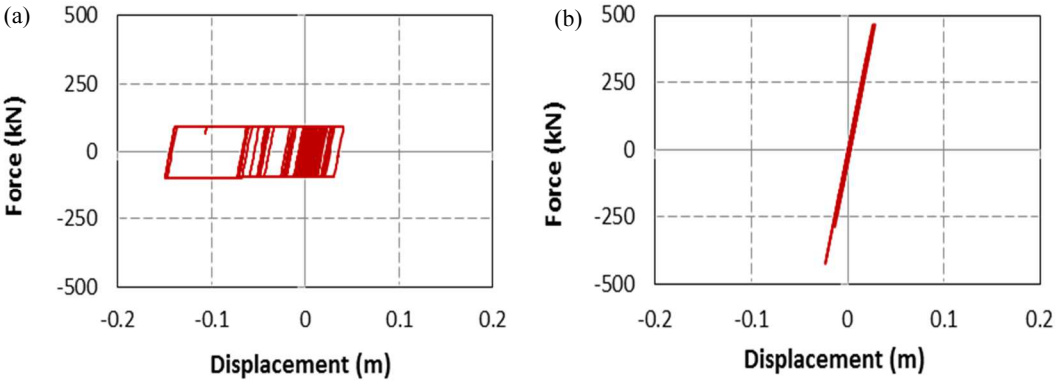

Figure 6-19 Comparisons of force-displacement curves of Vtype4R damper with normalized slip force (a) 0.09; (b) 0.47, subjected to GM2.

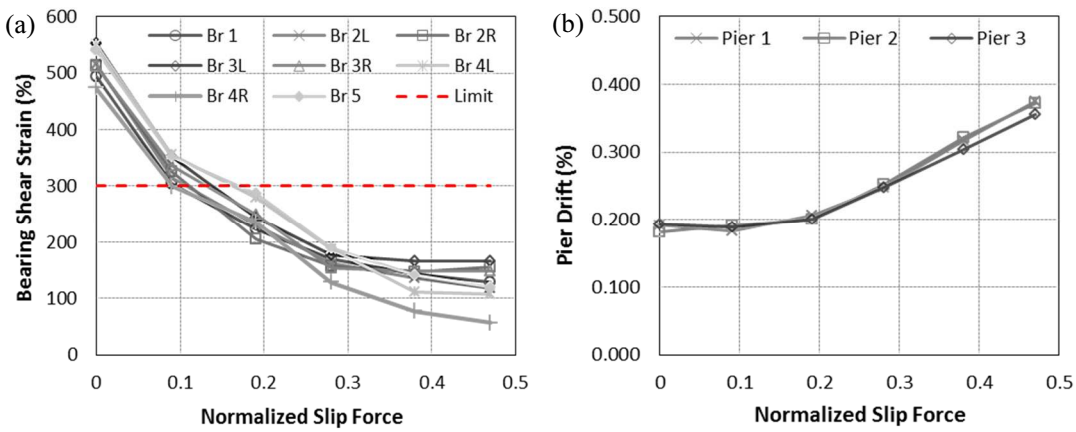

Figure 6-20 Comparison of (a) peak bearing deformations; (b) Pier drift subjected to GM2.

6.6.4 Effects of Damper Configuration

To investigate the effectiveness of damper types, responses of bridge model with applications of V-type and R-type dampers at the different joints are calculated and compared. The results corresponding to 5 normalized damper slip forces as described above subjected to the 5 sets of spatially varying ground motions are compared and discussed. Figure 6-21 (a) and (b) present the comparisons of mean peak pounding forces at joint 3 and mean peak joint opening at joint 1 and 3 for two damper types with varying normalized damper slip forces, respectively. As shown, V-type dampers are more effective in mitigating pounding impact and relative displacement at the joint as it is connected to the bridge piers. R-type dampers reduce peak opening joint displacement at joint 3 more effectively than V-type dampers. However, it should be noted that the peak joint opening at joint 3 is much smaller compared to that at joint 1. Figure 6-21 (c) and (d) present the comparison of shear strain in bearings and peak drift of three piers with two damper configurations to a set of spatially varying ground motion. V-type dampers are more effective than R-type dampers on mitigating bearing deformations, however, it also leads to transfer of large forces to bridge piers resulting in larger deformations. R-type dampers reduces the pier drift demand as connection is deck to deck and it dissipates some input energy by hysteretic response at superstructure of the bridge.

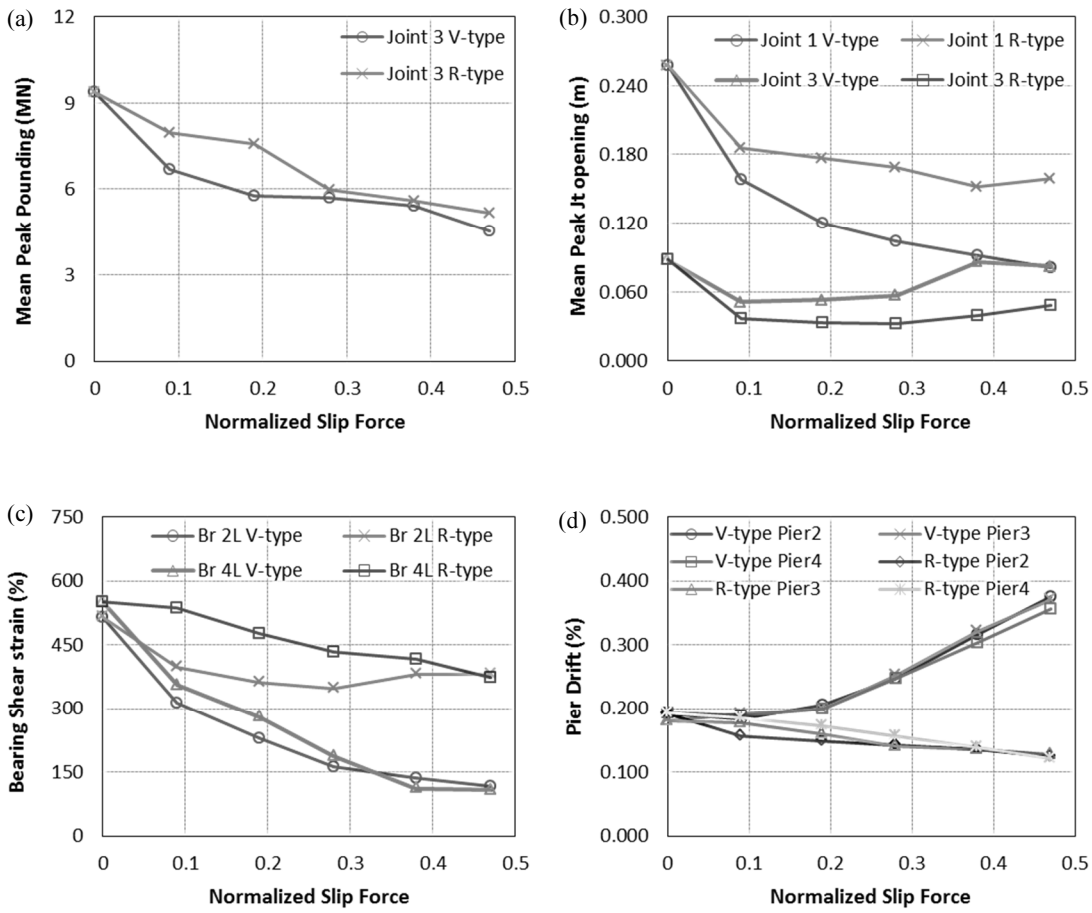

Figure 6-21 Comparison of (a) mean peak pounding force; (b) mean peak joint opening; (c) bearing shear strain; (d) pier drift demand for two damper configurations.

From the above results it can be concluded that, in general, V-type dampers are more effective in reducing pounding and joint opening at the bridge joints. It is to be noticed, however, that in the current numerical simulations in the case of V-type damper two friction hinge devices are used at the both sides of each joint connecting the deck to the pier, in the case of R-type damper only one friction hinge device with equal slip force as a single V-type unit is used to connect the two adjacent decks. This assumption implies the force required to make V-type damper connected joint move is two times of that required to make R-type damper to move.

The appropriate damper configuration to control the bridge responses thus depends upon responses of the most vulnerable components of the bridge. In the studied bridge the bearings are the weaker components thus V-type dampers that connects the deck with the piers are the appropriate retrofit device as this will lead to reduction of displacement and shearing strains of the bearings. However, more forces are transmitted to the bridge substructures. In case where protection of bridge superstructures from pounding and unseating damages are desired without transfer of additional forces to bridge piers, R-type dampers are the appropriate selection.

6.7 Conclusion

The paper presents investigations on the effectiveness of using RFHD to control responses of simply supported bridges subjected to non-uniform ground motions. Five sets of spatially varying ground motions compatible with the design spectrum and empirical coherency loss function along the supports of the bridge are used to simulate realistic relative displacement responses of the bridge. The bridge model is based on a typical Nepalese simply supported bridge. The study found that pounding between the adjacent bridge components could increase relative joint opening, thus enhancing the risk of unseating failures. The results presented in this paper suggest RFHD could be an ideal retrofit device to mitigate relative displacement induced damages, such as pounding and unseating damages, abutment back wall deformations and bearing failure. These devices are capable of reducing the response at bridge joints by dissipating some of the input energies.

For better mitigation of seismic responses of bridge, damper with optimum slip force should be provided. Increasing the slip force of the dampers beyond optimum slip force, in general, leads to slight reductions in bridge responses. However, it also increases the pier drift as more forces are transferred to the piers of the bridge. The result presented also shows the effectiveness of dampers to mitigate the relative displacement induced damages, such as pounding and unseating, are not significantly affected by small changes in optimum slip force of the dampers. Therefore, small variations on optimum slip forces of dampers during the life of the bridge do not warrant any adjustment or replacement of friction dampers.

V-type dampers are found to be more effective in mitigating pounding and relative opening displacement at bridge joints. The dampers are also significantly more effective in reducing the deformation demand of the bearings compared to the R-type dampers. However, V-type dampers could increase the drift demand of the piers because they transfer forces from the superstructure to the bridge piers. R-type dampers are relatively less effective on mitigating poundings, relative joint displacements and bearing deformations but their effectiveness on reducing the piers demands is superior compared to the V-type dampers.

6.8 References

Abdel Raheem, S. E. (2009). Pounding mitigation and unseating prevention at expansion joints of isolated multi-span bridges. *Engineering Structures*, *31*(10), 2345-2356.

Ali, H. E. M., & Abdel-Ghaffar, A. M. (1995). Modeling of rubber and lead passive-control bearings for seismic analysis. *Journal of Structural Engineering*, *121*(7), 1134-1144.

Bhaskararao, A. V., & Jangid, R. S. (2006). Seismic response of adjacent buildings connected with friction dampers. *Bulletin of Earthquake Engineering*, *4*(1), 43-64.

Bi, K., & Hao, H. (2012). Modelling and simulation of spatially varying earthquake ground motions at sites with varying conditions. *Probabilistic Engineering Mechanics*, *29*, 92-104.

Bi, K., & Hao, H. (2013). Numerical simulation of pounding damage to bridge structures under spatially varying ground motions. *Engineering Structures*, *46*, 62-76.

Chen, W., & Hao, H. (2013). Numerical study of blast-resistant sandwich panels with rotational friction dampers. *International Journal of Structural Stability and Dynamics*, *13*(06), 1350014.

Choi, E., Nam, T. H., & Cho, B. S. (2005). A new concept of isolation bearings for highway steel bridges using shape memory alloys. *Canadian Journal of Civil Engineering*, *32*(5), 957-967.

Chouw, N., & Hao, H. (2008). Significance of SSI and nonuniform near-fault ground motions in bridge response I: Effect on response with conventional expansion joint. *Engineering Structures*, *30*(1), 141-153.

Feng, M. Q., Kim, J. M., Shinozuka, M., & Purasinghe, R. (2000). Viscoelastic dampers at expansion joints for seismic protection of bridges. *Journal of Bridge Engineering*, *5*(1), 67-74.

Ghosh, G., Singh, Y., & Thakkar, S. K. (2011). Seismic response of a continuous bridge with bearing protection devices. *Engineering structures*, *33*(4), 1149-1156.

Guo, A., Li, Z., Li, H., & Ou, J. (2009). Experimental and analytical study on pounding reduction of base-isolated highway bridges using MR dampers. *Earthquake Engineering & Structural Dynamics*, *38*(11), 1307-1333.

IS 1893 (2002). *Criteria for Earthquake resistant Design of structures -Part 1: General provisions and buildings*, Bureau of Indian standard, India.

Jankowski, R., Wilde, K., & Fujino, Y. (2000). Reduction of pounding effects in elevated bridges during earthquakes. *Earthquake engineering & structural dynamics*, *29*(2), 195-212.

Japanese Road Association. (1996). Specifications for highway bridges, part V, seismic design. *Tokyo, Japan*.

Kim, J. M., Feng, M. Q., & Shinozuka, M. (2000). Energy dissipating restrainers for highway bridges. *Soil Dynamics and Earthquake Engineering*, *19*(1), 65-69.

Li, B., Bi, K., Chouw, N., Butterworth, J. W., & Hao, H. (2012). Experimental investigation of spatially varying effect of ground motions on bridge pounding. *Earthquake Engineering & Structural Dynamics*, *41*(14), 1959-1976.

Mahajan, A. K., Thakur, V. C., Sharma, M. L., & Chauhan, M. (2010). Probabilistic seismic hazard map of NW Himalaya and its adjoining area, India. *Natural hazards*, *53*(3), 443-457.

Mander, J. B., Priestley, M. J., & Park, R. (1988). Theoretical stress-strain model for confined concrete. *Journal of structural engineering*, *114*(8), 1804-1826.

Martínez-Rueda, J. E., & Elnashai, A. S. (1997). Confined concrete model under cyclic load. *Materials and Structures*, *30*(3), 139-147.

Menegotto, M., & Pinto, P.E. (1973). Method of analysis for cyclically loaded RC plane frames including changes in geometry and non-elastic behavior of elements under combined normal force and bending. In *Proc. of IABSE symposium on resistance and ultimate deformability of structures acted on by well-defined repeated loads*, Zurich, Switzerland.

Mualla, I. H., & Belev, B. (2002). Performance of steel frames with a new friction damper device under earthquake excitation. *Engineering Structures*, *24*(3), 365-371.

Mualla, I. H. (2000). Parameters influencing the behavior of a new friction damper device. In *SPIE's 7th Annual International Symposium on Smart Structures and Materials* (pp. 64-74). International Society for Optics and Photonics.

Nielsen, L. O., Mualla, I. H., & Iwai, Y. (2004, August). Seismic isolation with a new friction-viscoelastic damping system. In *13th World Conference on Earthquake Engineering, Vancouver, Canada*.

Otsuka, H., Unjoh, S., Terayama, T., Hoshikuma, J., & Kosa, K. (1996). Damage to highway bridges by the 1995 Hyogoken Nanbu earthquake and the retrofit of highway bridges in Japan. In *Proceedings of the 3rd US Japan Workshop on Seismic Retrofit of Bridge*.

Ozbulut, O. E., & Hurlebaus, S. (2010). Seismic assessment of bridge structures isolated by a shape memory alloy/rubber-based isolation system. *Smart Materials and Structures*, *20*(1), 015003.

Parajuli, H. (2009). *Dynamic analyses of low strength masonry houses based on site specific earthquake ground motions*, PhD Thesis, Kyoto University, Japan.

Ram, T. D., & Wang, G. (2013). Probabilistic seismic hazard analysis in Nepal. *Earthquake Engineering and Engineering Vibration*, *12*(4), 577-586.

Ruangrassamee, A., & Kawashima, K. (2003). Control of nonlinear bridge response with pounding effect by variable dampers. *Engineering Structures*, *25*(5), 593-606.

Shrestha, B., Hao, H., & Bi, K. (2014). Effectiveness of using rubber bumper and restrainer on mitigating pounding and unseating damage of bridge structures subjected to spatially varying ground motions.*Engineering Structures*, *79*, 195-210.

Shrestha, B., Hao, H., & Bi, K. (2015). Seismic response analysis of multiple-frame bridges with unseating restrainers considering ground motion spatial variation and SSI. *Advances in Structural Engineering*, *18*(6), 873-891.

Sobczky, K. (1991) *Stochastic Wave Propagation*. Kluwer Academic Publishers, Netherlands.

Takahashi, Y. (2012). Damage of rubber bearings and dampers of bridges in 2011 Great East Japan Earthquake, *In Proceedings of the International Symposium on Engineering Lessons Learned from the 2011 Great East Japan Earthquake*, Tokyo, Japan.

Vafai, A., Hamidi, M., & Ahmadi, G. (2001). Numerical modeling of MDOF structures with sliding supports using rigid-plastic link. *Earthquake engineering & structural dynamics*, *30*(1), 27-42.

Wilde, K., Gardoni, P., & Fujino, Y. (2000). Base isolation system with shape memory alloy device for elevated highway bridges. *Engineering structures*, *22*(3), 222-229.

Zhu, P., Abe, M., & Fujino, Y. (2004). Evaluation of pounding countermeasures and serviceability of elevated bridges during seismic excitation using 3D modeling. *Earthquake engineering & structural dynamics*, *33*(5), 591-609.

Zanardo, G., Hao, H., & Modena, C. (2002). Seismic response of multi-span simply supported bridges to a spatially varying earthquake ground motion. *Earthquake engineering & structural dynamics*, *31*(6), 1325-1345.

CHAPTER 7
PARAMETRIC STUDY OF SEISMIC PERFORMANCE OF SUPERELASTIC SHAPE MEMORY ALLOY REINFORCED BRIDGE PIERS

7.1 Abstract

One of the important measures of post-earthquake functionality of bridges after a major earthquake is residual displacement. In many recent major earthquakes large residual displacements resulted in demolition of bridge piers due to the loss of functionality. Replacing the conventional longitudinal steel reinforcement in the plastic hinge regions of bridge piers with superelastic shape memory alloy (SMA) could significantly reduce residual deformations. In this study numerical investigations on the performance of SMA Reinforced Concrete (RC) bridge bents to monotonic and seismic loading are presented. Incremental dynamic analyses are conducted to compare the response of SMA RC bents with steel RC bents considering the peak and the residual deformations after seismic events. Numerical study on multiple prototype bridge bents with single and multiple piers reinforced with superelastic SMA or conventional steel bars in plastic hinge regions are conducted. Effects of replacement of the steel rebar by SMA rebar on the performance of the bridge bents are studied. This paper presents results of the parametrical analyses on the effects of various design and geometric parameters, such as number and geometry of bents and reinforcement ratio of the RC SMA bridge bents on its performance.

7.2 Introduction

Reinforced concrete (RC) bridges designed to current seismic codes in the regions of high seismicity are susceptible to severe damage during large earthquakes, leading to the possibility of large residual displacements. During major earthquakes such as the Northridge 1994, Kobe 1995, Duzce 1999 and other events, it was found that bridge structures sustained high residual drifts rendering the bridge to be unserviceable. Consequently, post disaster rescue and relief operation were severely affected. The principal factor leading to the loss of serviceability was residual strains in steel reinforcement bars after an earthquake resulting in larger residual inclination of bridge piers. During the 1995 Kobe earthquake 88 bridge piers along the Hanshin expressway were demolished because of the large residual inclination even though some of those piers had experienced only light damage (Fujino et al., 2005). As a result there is a consensus among the engineering practitioners that the residual displacement has a greater significance in the overall structural performance of the infrastructure under earthquake loading.

As bridges are the key components in the transportation network for providing emergency services following an earthquake, it is necessary to minimize the loss of functionality by enhancing the performance of the bridges. During strong earthquakes steel reinforcements are expected to endure large plastic deformations under severe shakings to dissipate seismic energy. This inevitably leads to significant residual deformation that could make bridge structures unserviceable or unsafe. To address these problems innovative design methods capable of re-centering after an earthquake event are being explored since last few decades. One of such innovative methods is using a relatively new material for civil infrastructure system, superelastic Shape Memory Alloy (SMA) as reinforcement on structures. SMAs are able to undergo large strains and still recover their shape through either heating (shape memory effect) or stress removal (superelastic effect) (Wilson & Welsolowsky, 2005). In general, SMAs exhibit two distinct crystal structures or phases. These phases are Martensite, with the ability to completely recover residual strains by heating, and Austenite, with nominally zero residual strain when unloaded without the application of heat (Otsuka & Wayman, 1999). Superelastic behavior of SMA would be beneficial in many ways particularly for civil engineering applications, especially to reduce permanent deformation of structural components.

Previous studies have highlighted that superelastic SMA could be an ideal alternative material for use as reinforcement in RC structures to reduce the large residual deformation. Several studies have been conducted in recent years using the superelastic behavior of SMA by placing it in plastic hinge locations of Reinforced Concrete (RC) structures to mitigate the large residual deformations after strong earthquake shakings. Saaidi and Wang (2006) explored the effectiveness of using the superelastic SMA bars at plastic hinge regions of RC columns by conducting shake table experiments. Youssef et al. (2008) utilized SMA in the plastic hinge region of RC beam-column joints. Saaidi et al. (2009) compared the responses of SMA reinforced RC column with normal concrete and Engineered Cementitious Composite (ECC) to steel RC column under cyclic loading test. Cruz and Saiidi (2012) investigated the seismic performance of a large-scale four-span RC bridge incorporating innovative plastic hinges consisting of superelastic SMA and ECC using shake table tests. The above studies experimentally validate that SMA reinforcement in critical regions of concrete structures could significantly reduce the earthquake induced damages and dissipate adequate amount of energy. Billah and Alam (2012), Zafar and Andrawes (2012) numerically investigated hybrid SMA column with SMA bars at the plastic hinge regions as non-corroding reinforcement for ductile RC structures. Billah and Alam (2014) extended their study by assessing the seismic performance of SMA RC bridge piers using fragility function. Tazrav and Saaidi (2013, 2014) investigated performance of concrete columns with superelastic SMA bar and the effects of

key mechanical properties of one of the most commonly used SMA, Nickel Titanium (NiTi) bars on seismic performance of SMA RC bridge piers. Roh and Reinhorn (2010), Ehsan et al. (2015) investigated on the applications of SMA bars in precast segmental bridge columns to improve the hysteretic energy dissipation of the columns.

The above researches demonstrate that superelastic SMA could be a strong contender for use as reinforcements at plastic hinge regions of RC structures, which are prone to experience significant damages during strong seismic events with large residual deformation. However, conclusion based on investigation of a single RC column, usually of small scale may not give a conclusive result. The performances of realistic RC bridge bent having different geometries, and numbers of piers subjected to a suite of earthquake ground motions are inexistent. Moreover, previous studies have not focused on parametrically studying the influence of the replacement of steel reinforcement with SMA reinforcement on the performance of the bridge bents. Superelastic SMA bars have different characteristics compared to conventional steel reinforcement. For example, the modulus of elasticity SMA is, in general, 1/2 to 1/5 of steel reinforcement and yield strain are significantly higher than steel reinforcement. This variation in the properties of two kinds to reinforcements demands significant attention in order to better understand the performance of bridge piers with SMA reinforced compared to conventional piers. Presently, there are not any guidelines provided by the literatures on replacement of steel by SMA reinforcement. Previous studies mostly compared the performance of SMA RC bents with steel RC bents with either lower or similar moment capacity. However, this may result in higher peak drift of the SMA reinforced bridge piers compared to conventional steel reinforced pier due to lower modulus of elasticity of SMA bars. Previous studies have not parametrically studied the effect of reinforcement ratio of SMA bars on performance of the SMA bridge bents.

In this study, intensive analyses are conducted to compare the responses of concrete bridge bents with SMA reinforcements and conventional steel reinforcements subjected to different earthquake excitations. The behavior of the SMA piers under the monotonic loading are evaluated and compared against steel reinforced piers. Furthermore, incremental dynamic analyses are used to investigate the performance of superelastic SMA RC bents under seismic loading. To give a generalized observation, twelve models with variations in geometry, numbers of piers in a bridge bent and varying superelastic SMA rebar ratio are analyzed. To reduce the cost of the bridge, SMA reinforcements are placed at critical plastic hinge regions of bridge piers and connected to steel reinforcement using couplers. In this study numerical models are developed using fiber based element model on Seismostruct. The accuracy of the numerical models on predicting the response of SMA reinforced bridge piers are first validated

by comparing the results with the experimental shake table data of a bridge pier with SMA reinforcement (Saiidi & Wang, 2006). The purpose of the present study is to (1) compare the performance of the prototype bridge bents with steel and SMA reinforcements in terms of damage progression, peak deformations, residual deformation, and energy absorption capacity, and (2) compare parametrically the performance of SMA RC bents with varying reinforcement ratio to steel RC bents.

7.3 Validation of Numerical Model

In order to achieve realistic results validation and calibration of the numerical model is essential. In this study to validate the numerical model for inelastic dynamic time history analysis experimental study by Saiidi and Wang (2006) on a large-scale RC column conducted at the structure laboratory at the University of Nevada, Reno is used. The experiment is briefly described here. A RC column scaled to 1/4 with SMA reinforcements in the plastic hinge region was tested on a shake table. In the experiment NiTi bars, 356 mm long, were used as longitudinal reinforcement in plastic hinge area. Details of the experimental column are presented in Figure 7-1. The mechanical properties of the SMA bars, steel reinforcement and concrete are presented in Table 7-1. An axial load of 624 kN was applied, corresponding to an Axial Load Index (ALI) of 0.25, where the ALI is defined as the ratio of the axial load and the product of the gross column section and the specified concrete compressive strength. The NiTi bars provided the reinforcement in the lower 254 mm of the column. The column was subjected to a synthetic ground motion compatible to the Applied Technology Council 32 (Applied technology Council 1996) for medium soil (ATC-32-D). Peak ground acceleration (PGA) of the motion was 0.44g. The specimen was subjected to a series of scaled motions, the amplitudes of which were progressively increased. The specimen was subjected to 11 run of the ground motion excitation, with amplitude normalized to 15% for the first run to 300% for the last run of the ATC-32-D record amplitude. More detailed information of the experimental tests can be found in (Saiidi & Wang, 2006).

7.3.1 SMA model

The NiTi rebar are usually based on the equi-atomic compound of nickel and titanium. Beside the ability of tolerating large amounts of strain, shape-memory NiTi alloys show high stability in cyclic applications and are corrosion resistant. They also have a moderate solubility range, enabling changes in composition and alloying with other elements to modify both the shape-memory and mechanical characteristics. For commercial application and in order to improve its properties, a third metal is usually added to NiTi. Although two metals (nickel and titanium) are processed identically, a slight increase in nickel content improves the mechanical behavior

of SMA by depressing the transformation temperatures and improving the hysteretic energy dissipation capacity.

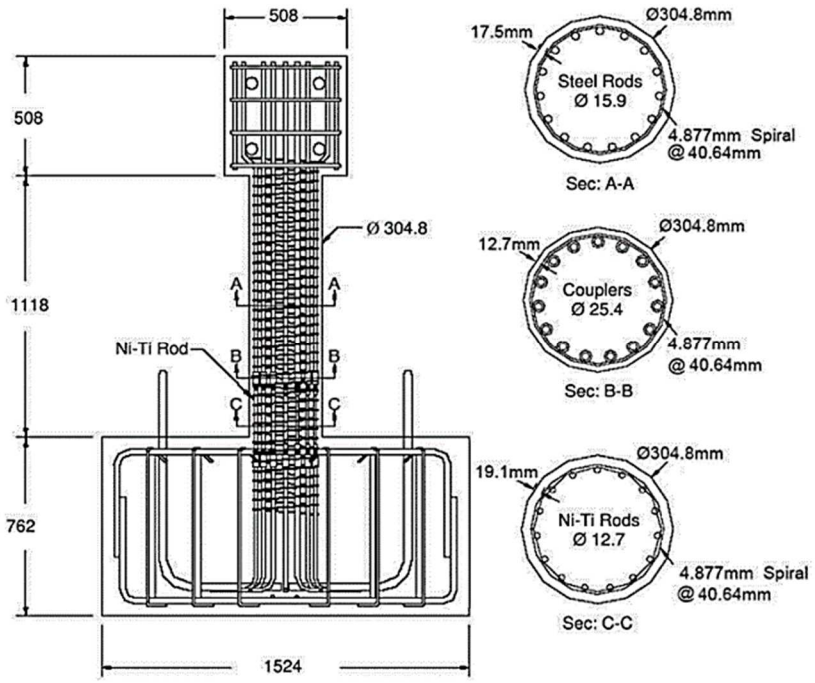

Figure 7-1 Details of SMA RC column (Saiidi & Wang, 2006).

In order to realistically represent the NiTi reinforcement, one dimensional uni-axial model for superelastic SMA programmed by Fugazza (2003) following the constitutive relationship proposed by Auricchio and Sacco (1997), implemented on Seismostruct program are used in numerical simulations. This model is capable of describing the force-deformation relationship of superelastic SMAs at constant temperature. The model is sufficiently accurate for the present study with respect to the temperature effects because unlike in other applications SMA bars is not exposed to ambient temperature and are insulated by a thick layer of concrete. A schematic of force deformation relationship of the SMA model used in this study is presented in Figure 7-2. The model is defined by six parameters namely modulus of elasticity, austenite to martensite starting stress, austenite to martensite finishing stress, martensite to austenite starting stress, martensite to austenite finishing stress and superelastic plateau strain. The six parameters adopted for this study are presented in Table 7-1. The SMA model represents an idealized behavior of the SMA material where a complete recovery of the original shape is achieved at the end of each cycle.

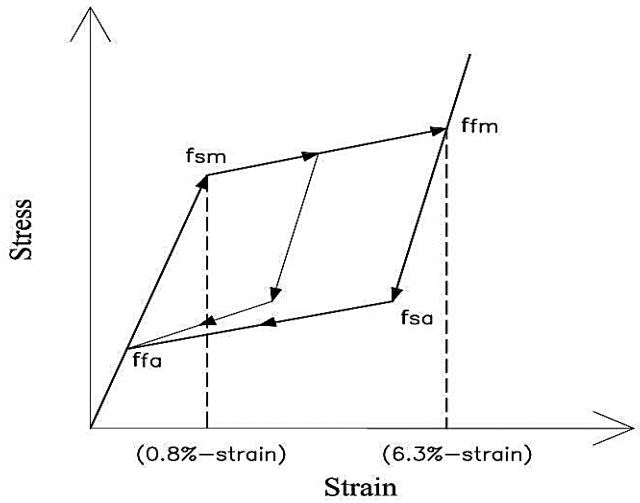

Figure 7-2 Constitutive model of superelastic SMA model.

7.3.2 Numerical model

Displacement based nonlinear beam column elements discretized into 12 frame elements are used to model the pier. Fiber modelling approach is employed to represent the distribution of inelasticity along the length and cross-sectional area of the member. The fiber section used for the column is discretized into core fiber for confined concrete, cover fiber for unconfined concrete and steel/SMA fiber for reinforcement bars. The material properties of confined and unconfined concrete is modelled using the constitutive relationship proposed by Mander et al. (1988) and the cyclic rules proposed by Martinez-Rueda and Elnashai (1997), respectively. Steel re-bars are modelled using Menegotto-Pinto (Menegotto & Pinto, 1973) steel model. The axial load is applied at the top of the pier as lumped mass. For the prototype bridges, as will be discussed later in the paper, the yield strength of the reinforcement is 414 MPa and the compressive strength of the concrete is 35 MPa. Bond slip effect in the longitudinal reinforcing steel is calculated based on the modified Wehbe's method (Wehbe et al., 1999; Vosoogi & Saiidi, 2010) and included in the form of moment-rotation spring at the end of the column using zero-length element. The modified Wehbe's bond slip model was applied and experimentally validated in the study of Saiidi and Ardakani (2012), Vosoogi and Saiidi (2010). Multi-linear link element in Seismostruct is used to represent the bond slip behavior of steel reinforcement. SMA reinforcements at the plastic hinge regions of the RC piers were connected to the steel reinforcements by using metallic couplers. In order to model slippage of SMA rebars inside the coupler, a bond slip model is incorporated in the numerical model of SMA reinforced bridge piers. The bond slip relation for SMA rebar obtained from the experimental study of Alam et al. (2010) and validated numerically in the study of Billah and Alam (2012) is adopted in this study. The bond slip element is modelled in Seismostruct using

modified Takeda hysteretic curve (Otani, 1974) as done in a previous study (Billah & Alam, 2012). The details of the finite element modelling are presented in

Figure 7-3.

Table 7-1 Material properties for SMA RC column

Material	Property	Value
Unconfined Concrete	Compressive strength (MPa)	43.8
	Strain at peak stress (%)	0.002
	Tensile strength (MPa)	0
Confined Concrete	Compressive strength (MPa)	43.8
	Strain at peak stress (%)	0.0025
	Tensile strength (MPa)	4.38
Longitudinal Steel	Yield Strength (MPa)	469
	Young's Modulus (MPa)	199000
Superelastic SMA	Modulus of Elasticity	48300
	Austenite to martensite starting stress, f_{sm} (MPa)	379
	Austenite to martensite finishing stress, f_{fm} (MPa)	405
	Martensite to austenite starting stress, f_{sa} (MPa)	180
	Martensite to austenite finishing stress, f_{fa} (MPa)	100
	Superelastic plateau strain (%)	5.5

7.3.3 Comparison of Results

The calculated displacement histories of experimental and numerical results for run 4, run 7 and run 11, which correspond to the base motion of ATC-32-D record amplified by 0.75, 2 and 3 times respectively, are presented in

Figure 7-4. As shown the numerical simulation results could capture the responses of the experimental tests accurately. The measured and simulated responses correlated well with reasonably close agreements for all the runs. Figure 7-5 compares the measured and the calculated cumulative hysteretic curve of the specimen. The maximum base shear and tip displacement measured were 77.2 kN and 65.6 mm compared to the calculated value of 84 kN and 62.8 mm, which represent a variation of 8.8% and 4.3% for base shear and tip displacement, respectively. The total energy dissipation obtained from the numerical study is 4.4% higher than the energy dissipation from the experimental study.

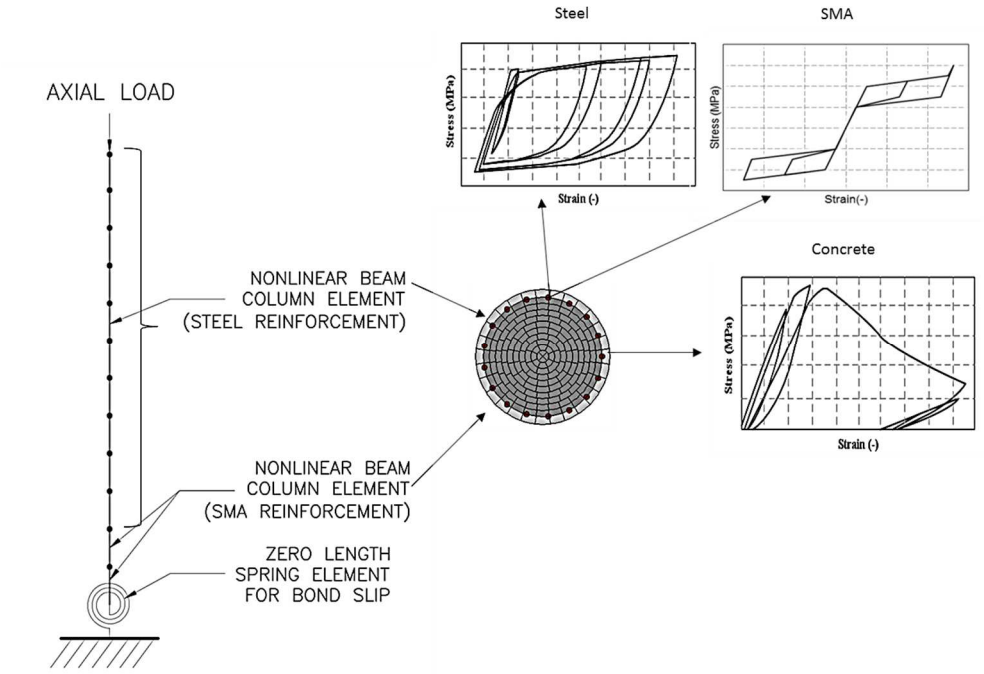

Figure 7-3 Finite element modelling of bridge piers.

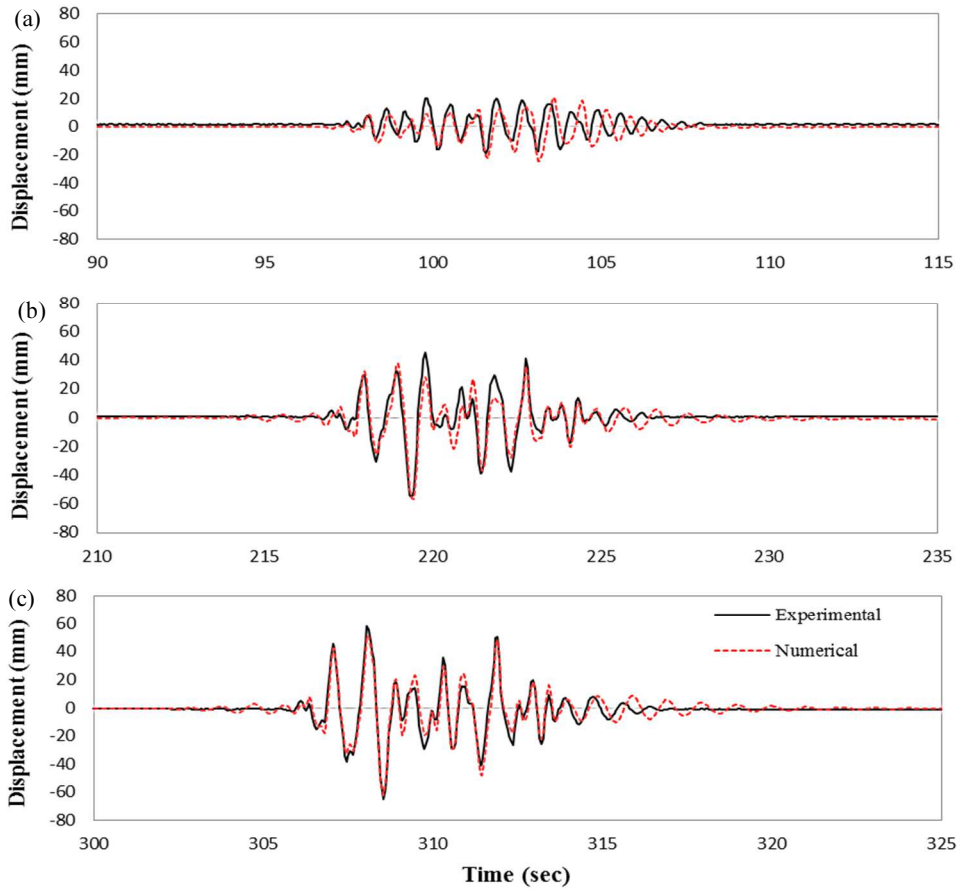

Figure 7-4 Comparison of displacement histories for (a) run 4; (b) run 7 and (c) run 11.

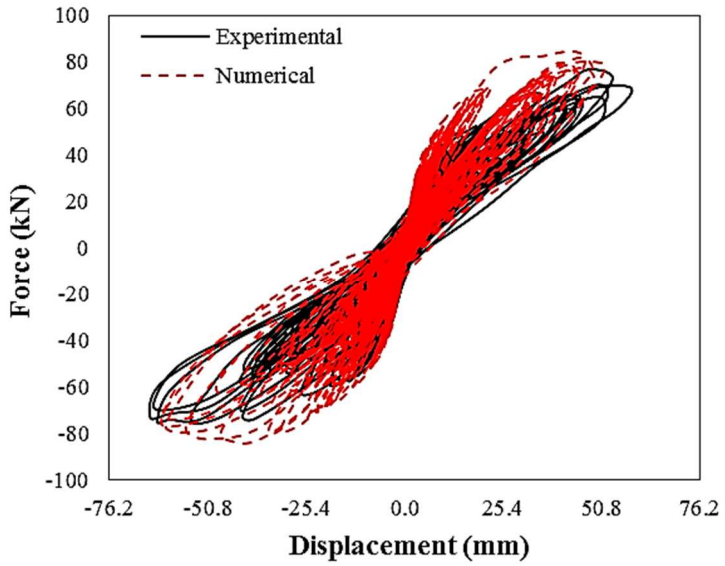

Figure 7-5 Comparison of measured (Saiidi & Wang, 2006) and calculated cumulative hysteretic curves.

7.4 Prototype Bridge Bents

To evaluate the performance of SMA RC bents, three typical prototype bridge bents with single and three piers are selected. Details of three bridge bents are presented in Table 7-2. Fundamental period of steel RC bents in transverse direction are 1.53 sec, 0.87 sec and 0.48 sec, respectively for B1-15, B1-10 and B3-7.72. B1-15 and B1-10 are single pier bents with pier height of 15 m and 10 m, respectively. All other geometrical features of the bents are the same. Both the bridge piers are reinforced with 64 numbers of 32 mm diameter rebars. B3-7.72 is a three pier bridge bent with height of the piers 7.72 m and diameter 1.22 m reinforced with 28 number 32 mm diameter rebar. For SMA reinforced pier three alternative reinforcement ratios in the plastic hinge region are considered so that the flexural capacity of the SMA RC piers are slightly lower, equal and slightly higher compared to the steel RC pier and are identified as SMA RC1, SMA RC2 and SMA RC3, respectively. SMA RC piers are designed such that yielding of the SMA reinforcement at plastic hinge occurs before yielding of steel reinforcement. This is achieved by providing slightly lower reinforcement ratio at plastic hinge region of SMA RC piers compared to the other region. This reduction in bar area ensures NiTi reinforcements yielding before the yielding of steel reinforcement and confines most of the inelastic behavior to the NiTi reinforcement. The reinforcement details at the plastic hinge regions for three alternatives SMA RC bridge piers are provided in Table 7-3. Structural details of the prototype bridge piers are presented in Figure 7-6. The plastic hinge length, L_p is calculated according to the relation given by Paulay and Preistley (1992):

$$L_p = 0.08L + 0.022 d_b f_y \quad (7.1)$$

where L is the length of the member in mm, d_b represents the bar diameter in mm, f_y is the yield strength of the rebars in MPa. Previously, Alam et al. (2008), O'Brien et al. (2007) showed that Paulay & Preistly (1992) equation could be used to reasonably estimate the plastic hinge length of SMA reinforced concrete elements. The length of the SMA reinforcement is equal to the plastic hinge length presented in Table 7-2.

Table 7-2 Properties of prototype bridge bents

Prototype	Height, L (m)	Diameter, D (m)	Axial Load	Aspect ratio (L/D)	Plastic hinge, Lp (m)
B1-15	15	1.8	7473	8.333	1.53
B1-10	10	1.8	7473	5.556	1.13
B3-7.72	7.72	1.22	13200	6.328	0.95

Table 7-3 Reinforcement details of bridge piers

Prototype	Steel RC detail (rebar %)	SMA RC 1 detail (rebar %)	SMA RC 2 detail (rebar %)	SMA RC 3 detail (rebar %)	Spiral Rebars (spacing c/c)
B1-15	64 D 32 (2.02)	64 D 28 (1.55)	74 D 32 (2.34)	60 D 40 (2.96)	D 20 (110 mm)
B1-10	64 D 32 (2.02)	64 D 28 (1.55)	74 D 32 (2.34)	60 D 40 (2.96)	D 20 (110 mm)
B3-7.72	28 D 32 (1.93)	28 D 28 (1.47)	36 D 32 (2.48)	32 D 40 (3.44)	D 16 (90 mm)

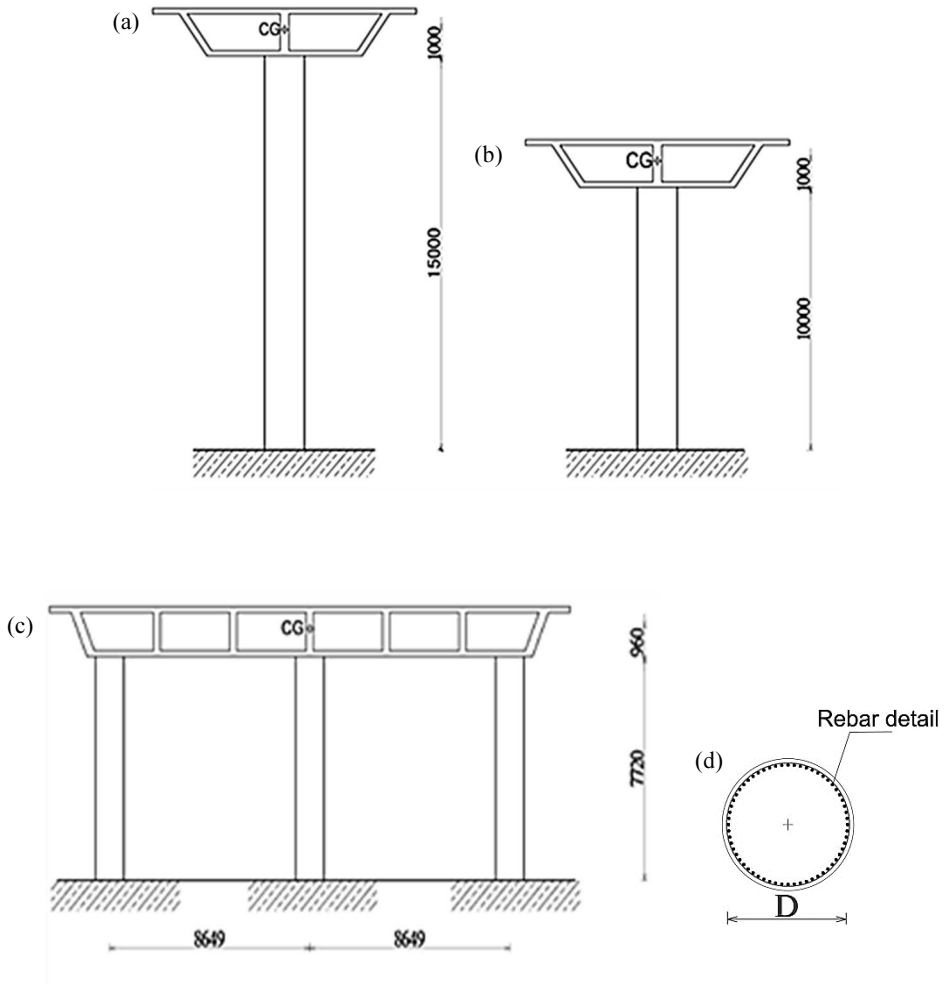

Figure 7-6 Prototype bridge piers (a) B1-15, (b) B1-10 (c) B3-7.72 (d) Typical bridge pier rebar detail (dimensions in mm).

7.5 Response to Monotonic Loading

Nonlinear pushover analyses are performed on the bridge bents in order to investigate response under displacement control lateral loading. In order to evaluate the response of the bridge piers to monotonic loading progression of damage on each bridge bents are compared. In this study, three damage states; longitudinal bar yielding, cover concrete spalling and crushing of core concrete are used to evaluate the response of the bridge bents. The yielding of steel and SMA rebar are taken as tensile strain of 0.0021 and 0.008, respectively. Strains at extreme rebar fibres are monitored to identify the yielding instances. Spalling of cover concrete is considered to occur once the compressive strain at extreme cover concrete fiber exceeds 0.0035. The crushing strain for core concrete is calculated based on the equation given by Pauley & Priestley (1988):

$$\varepsilon_{cu} = 0.004 + 1.4\,\rho_s f_{yh}\,\varepsilon_{sm}/f'_c \qquad (7.2)$$

where ε_{cu} is the ultimate compressive strain, ε_{sm} is steel strain at maximum tensile stress, f'_c is the concrete compressive strength in MPa, f_{yh} is the yield strength of transverse steel in MPa and ρ_s is the volumetric ratio of confining steel. The ultimate compressive strain of confined concrete for bent 1 and 2 is calculated to be 0.018 and for bent 3 is 0.015.

Figure 7-7 to Figure 7-9 presents base shear versus drift and moment versus rotation curves for bridge bents B1-15, B1-10 and B3-7.72, respectively. Yielding of longitudinal reinforcement, spalling of cover concrete and crushing of core concrete is also presented in the figures. The results presented suggest that the stiffness of the bents is quite similar until cracking of the concrete. Once the concrete has cracked, steel RC bents exhibits comparatively large stiffness compared to SMA RC bents due to the larger modulus of elasticity of steel reinforcement. For steel RC bents yielding of the rebar initiates at significantly lower drift/rotation compared to SMA RC bents as yielding strain of steel rebar are significantly lower compared to SMA rebar. The calculated drift at onset of yielding of steel rebar is 1.12%, 0.75% and 0.35% for bridge bents B1-15, B1-10 and B3-7.72, respectively. SMA rebar yielding initiated around 1.7%, 1.25% and 0.65% drift for SMA RC bents B1-15, B1-10 and B3-7.72, respectively. In SMA RC bents the yielding of SMA rebar and concrete cover spalling occurred at nearly similar drift levels. In case of SMA RC3 spalling of the cover concrete preceded the yielding of rebar. However, for steel RC bents the spalling of the concrete cover always occurs after the yielding of steel rebar with increase in drift or rotation. Crushing of the core concrete for both steel and SMA RC bents occurs more or less at similar drift.

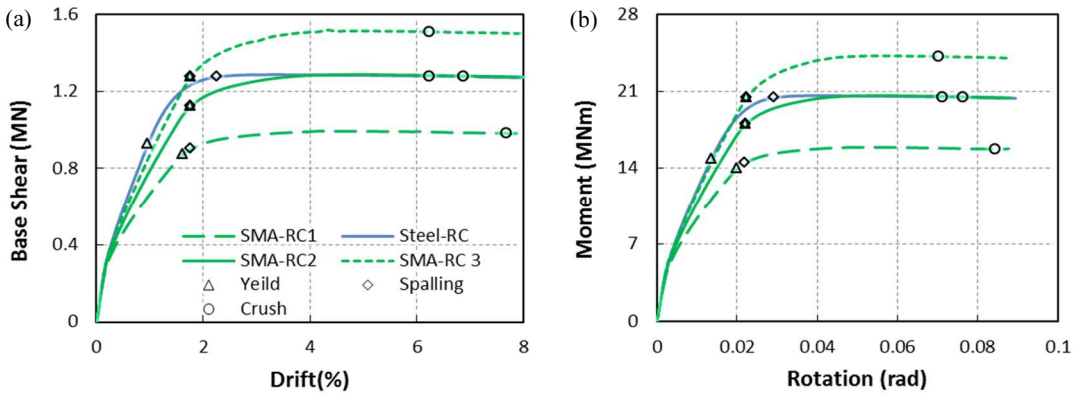

Figure 7-7 Base shear vs drift (a); and Moment vs rotation (b) curves for B1-15.

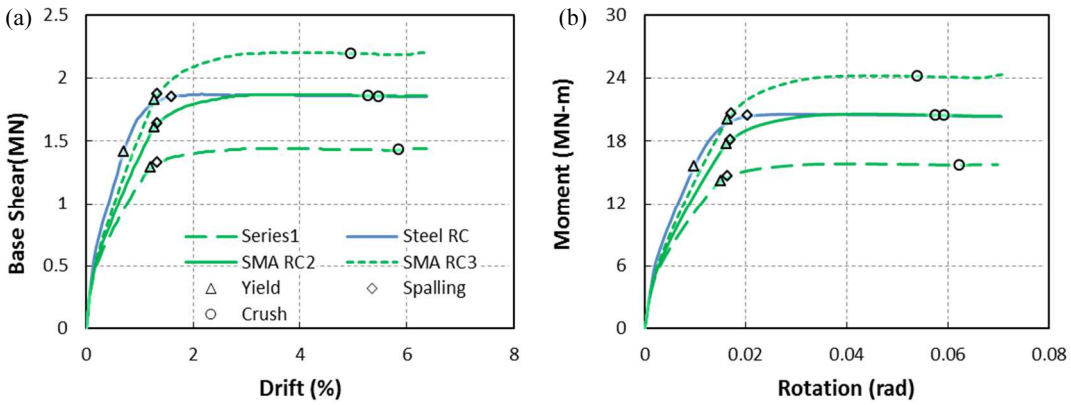

Figure 7-8 Base shear vs drift (a); and Moment vs rotation (b) curves for B2-10.

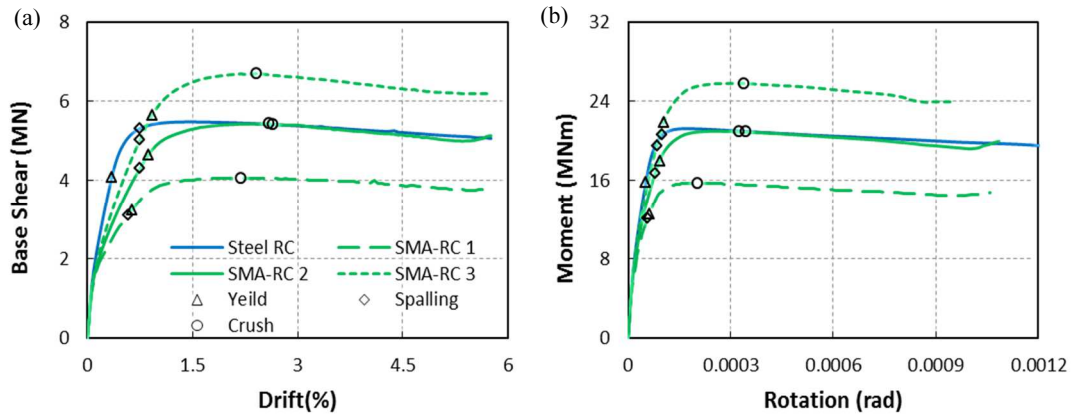

Figure 7-9 Base shear vs drift (a); and Moment vs rotation (b) curves for B3-7.72

7.6 Response of Seismic Motions

7.6.1 Ground Motions

To evaluate the response of the bridge bents to dynamic loading five recorded ground motions are used. The five ground motions listed in Table 7-4 are used to examine the response of bridge bents to dynamic loading. The selected ground motions have wide variation in the frequency contents, as highlighted by different spectral shapes presented in Figure 7-10, thus useful to evaluate the variation of performance of the prototype bridge bents.

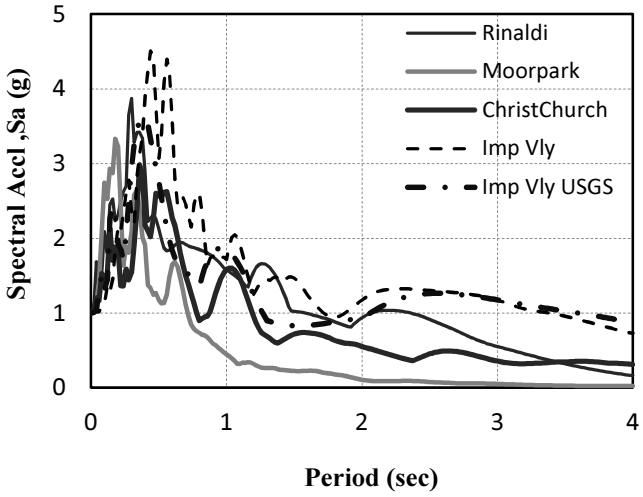

Figure 7-10 Normalized ground motion response spectra.

Table 7-4 Ground motion for seismic response analysis

No	Event	Station Site	Comp	PGA (g)	PGV (cm/s)
1	Imperial valley	USGS 0952	N-S	0.367	48.51
2	Imperial valley	Holtville PO	315	0.221	49.79
3	Northridge	Moorpark Fire Station	90	0.193	20.12
4	Northridge	Rinaldi receiving Stn	318	0.486	74.52
5	Christchurch, Feb 2011	CBGS	S01W	0.415	34.95

7.6.2 Incremental Dynamic Analysis (IDA)

The IDA method involves the bridge bents subjected to ground motions scaled to multiple levels of intensity, thus providing one or more load displacement curves (Vamvatsikos & Cornell, 2001). The dynamic pushover curve, which is a plot between the maximum drift and the maximum base shear obtained from the IDA for SMA and steel reinforced bridge piers are evaluated to compare their performance. Unlike the static counterpart the dynamic pushover incorporates the frequency content of the earthquake excitation in the response. For comparison of two kinds of bridge piers peak drift, residual drift and hysteretic energy dissipations of the bridge bents are observed. The ground motions are scaled from 0.15 g to 1.5 g at an interval of 0.15g. The analysis is terminated once the drift exceeds 8% to avoid numerical instability problem at higher drifts due to induced damages on the RC piers. Hence, the dynamic pushover curve presents the result for the selected ground motion starting from 0.15g to 1.5g or 8% drift limit, whichever is achieved first. The ground motions are applied in transverse direction of the bridge bents.

Figure 7-11 presents the dynamic pushover curves for bridge bent B1-15 for Rinaldi and Imperial Valley USGS ground motions. The presented result shows that there are only slight differences in the initial stiffness of the bridge piers. The cracked stiffness of the steel reinforced bridge piers is higher than the SMA RC bents, particularly SMA RC1, as the modulus of elasticity of SMA is approximately ¼ of that of the steel rebar and the reinforcement ratio in SMA RC1 is lower than steel RC bent. The result shows that performance of the structures is dependent on the ground motion frequency contents. For Rinaldi ground motion the drift observed in the steel RC bents are larger compared to the SMA RC bents, however, for the Imperial Valley USGS ground motion SMA RC1 resulted in larger drifts. The drift observed for SMA RC2 and SMA RC3 is lower compared to the steel RC pier. The reduction of stiffness resulting from the replacement of steel with SMA bars for SMA RC1 works similar to that of isolation system, by elongating the period and reducing the base shear as well as drift demand for some ground motions. However, for other ground motions, particularly those with high amplitude in long period range, such shift in period will have no benefit and the resulting drift will be higher than that of the steel reinforced piers. The drift demands of the bridge piers can be reduced by increasing SMA reinforcement as in case of SMA RC2 and SMA RC3. Figure 7-12 and Figure 7-13 also show the similar trend for the bent B1-10 subjected to Moorpark and Imperial Valley USGS ground motions and bent B3-7.72 subjected to Imperial Valley USGS and Rinaldi motions, respectively.

Comparison between the peak and residual drift responses of the SMA reinforced and steel reinforced bridge pier, B1-15, is shown in Figure 7-14 and Figure 7-15. As shown in Figure 7-14 (a), peak drift response for SMA RC bents is slightly lower than the steel RC bent for Rinaldi ground motion. For Moorpark, as presented in Figure 7-15 (a), the peak drift demand for SMA and steel reinforced piers are nearly similar. This again suggests that the peak drift responses of the bridge piers are dependent upon the particular ground motion. Unlike the peak drift responses, there is a clear difference in the residual drift. With the increase in intensity of ground motion steel reinforced bridge piers begin to sustain significant residual displacement. Though the SMA reinforced piers also sustained some residual drift, its performance is far superior compared to steel reinforced bridge piers. Performance of both the steel and SMA reinforced bridge bents in terms of peak and residual displacements are nearly the same at lower drift levels due to the limited inelastic response of steel reinforcement at these drifts. As the peak drift reached 2%, weakness of the steel reinforced piers are exposed. Residual drift increased dramatically for the steel reinforced piers beyond the 2% drift due to the inelastic deformation of reinforcements. However, for SMA RC bents increase in the residual drift is gradual due to the superelastic behavior of SMA reinforcement. As shown in Figure 7-14 (b) steel reinforced bridge pier sustained 4% of residual drift subjected to the peak

drift of 8%. SMA reinforced bridge piers sustained residual drift of less than 1% subjected to the peak drift of around 6.50%. Figure 7-15 (b) suggests that the re-centering behavior of SMA RC do not necessarily improve with higher ratio of SMA reinforcement. However, the sustained residual displacement are very small and do not have any significant impact on the performance of the SMA RC bridge bents as will be presented in subsequent section. These inconsistencies in the residual deformation are caused by slipping of SMA rebar inside the couplers. Figure 7-16 (a) and (b) show the hysteretic energy dissipation of bent B1-15 with two types of reinforcement for Rinaldi and Moorpark ground motion, respectively. These results show that the steel reinforced piers dissipate more energy than SMA RC1 piers at all intensity levels. The SMA reinforced piers with higher reinforcement ratio (SMA RC2 and SMA RC3) showed improved energy dissipation capacity and is comparable to that of steel RC piers at higher intensity. The increases in lateral strength of the SMA RC with increasing rebar ratio result in increase of energy dissipation capacity of the bridge bents and thus help to reduce the peak drift.

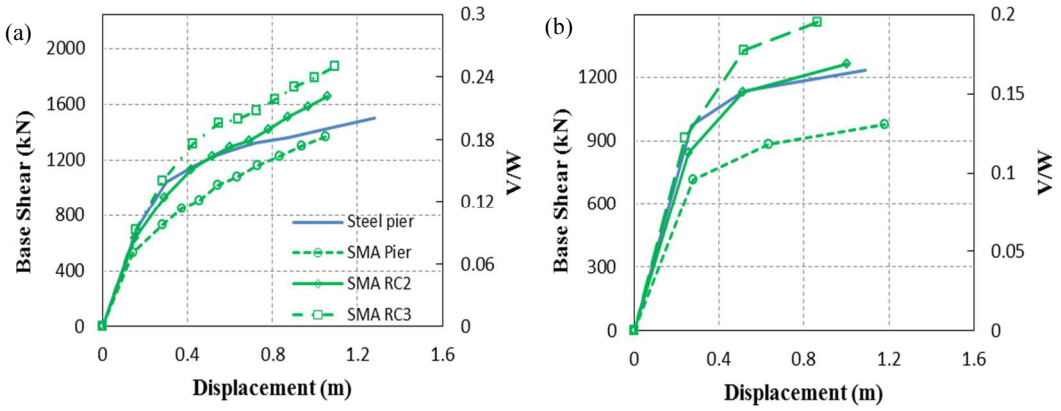

Figure 7-11 Dynamic Pushover curve for B1-15 corresponding to (a) Rinaldi, and (b) Imperial valley USGS ground motion.

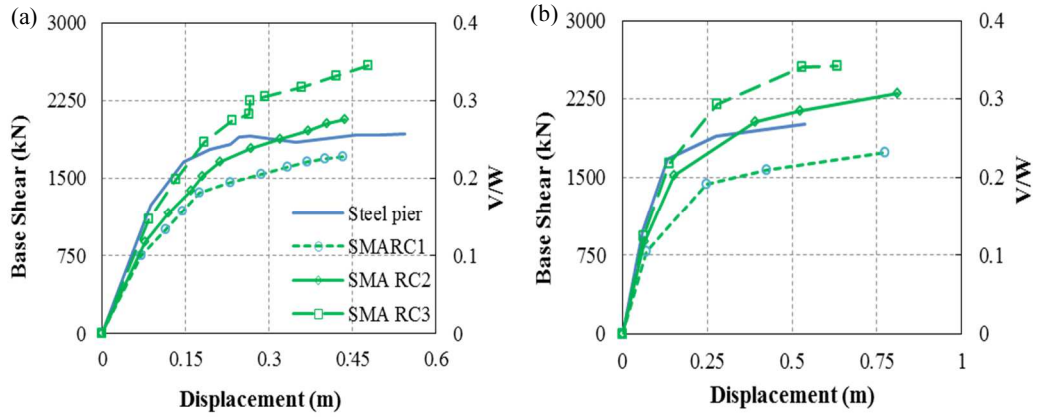

Figure 7-12 Dynamic Pushover curve for B1-10 corresponding to the (a) Moorpark; and (b) Imperial valley USGS ground motion.

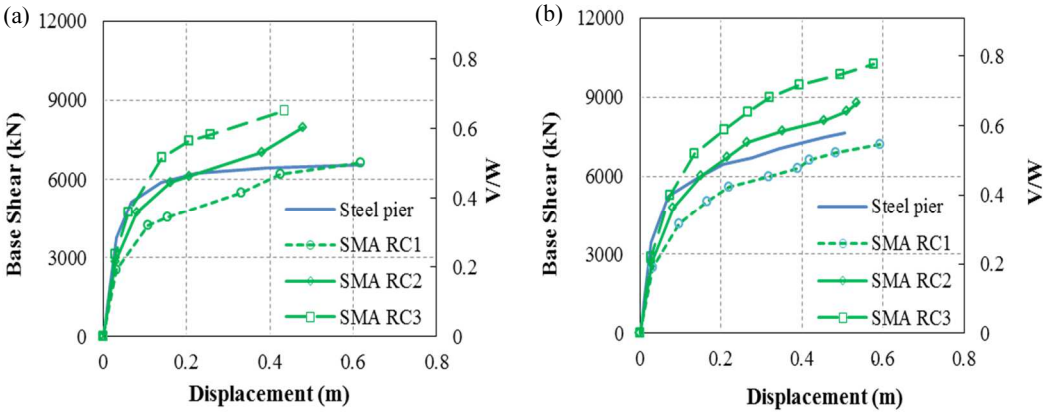

Figure 7-13 Dynamic Pushover curve for B3-7.72 corresponding to the (a) Imperial valley USGS; and (b) Rinaldi ground motion.

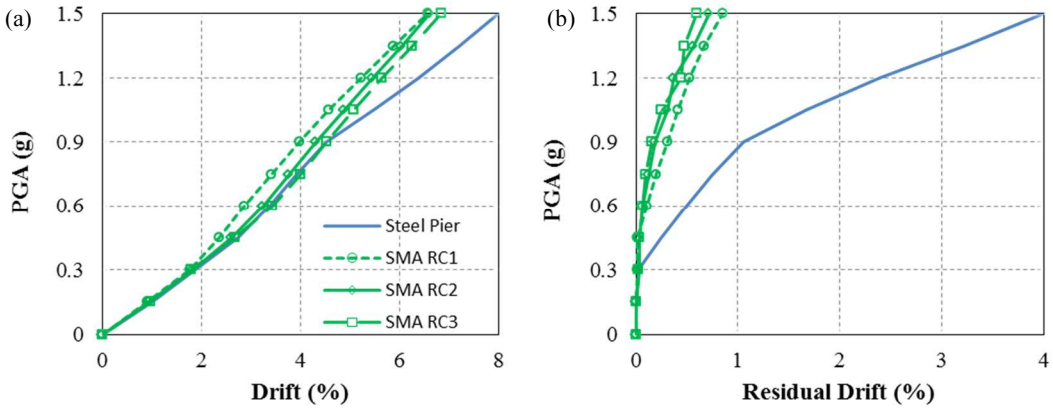

Figure 7-14 Peak drift demand (a) and Residual drift (b) for B1-15 to Rinaldi ground motion.

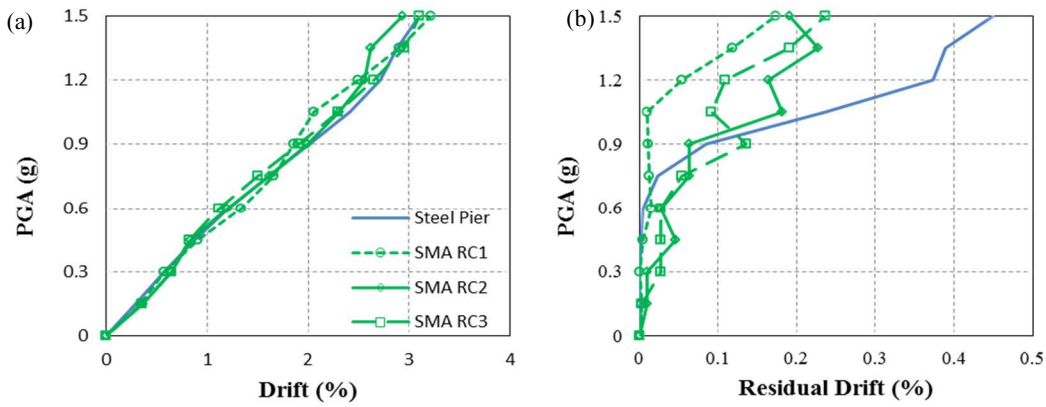

Figure 7-15 Peak drift demand (a) and Residual drift (b) for B1-15 to Moorpark ground motion.

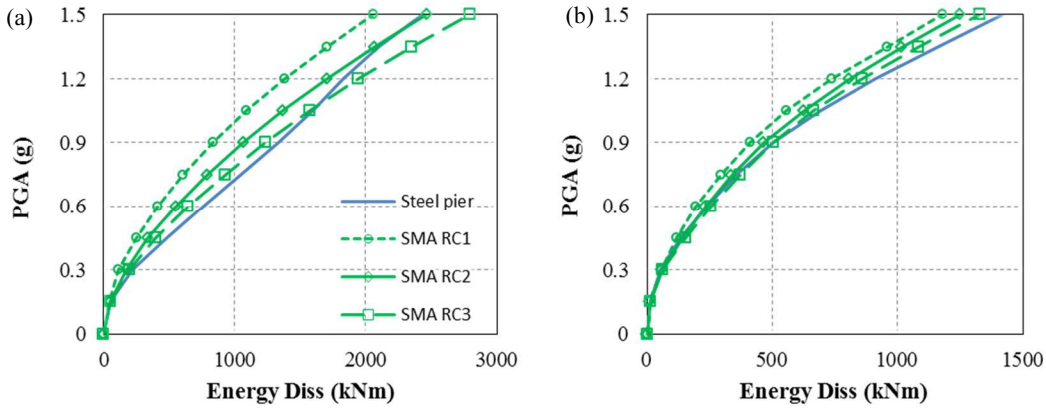

Figure 7-16 Comparison of hysteretic energy dissipation of B1-15 to (a) Rinaldi and (b) Moorpark ground motion.

7.6.3 Damage analysis

The results from the IDA are used to compare the level of damages that is observed on SMA and steel RC bents subjected to the selected ground motions. Five different damage states for the bridge piers based on the peak and residual drift is adopted as presented in Table 7-5. As described in HAZUS (1999), two extreme damage states, 'No' and 'Collapse' can be expressed by bridge's ability at yield state and ultimate state, respectively. The damage states defined are based on the recommendation of Dutta and Mander (1999) and Basoz and Mander (1999). Previous studies (Kim & Shinozuka, 2004) also used similar damage states for bridge bents similar to this study. In addition of using peak drift, this study used five damage states based on the residual displacement as well. Due to the lack of experimental data on residual damage measures, values based on the experimental investigation of O'Brien et al. (2007) and similar to that of the Japanese code for highway bridge design (Japan Road Association, 2006) are adopted in the present study. O'Brien et al. (2007), based on the observed damage under

the cyclic loading test, suggest that a residual drift below 0.25% would meet the serviceability requirement providing full functionality while a residual drift larger than 1% would be characterized as a collapse damage state since major repair or even demolition of the structure would be needed.

The result obtained from IDA of the bridge bents are categorized based on the damage state defined in Table 7-5. Figure 7-17 (a) and (b) present the comparison of damage state distribution of SMA and steel reinforced bridge bents based on the peak and residual displacements defined in Table 7-5 for bent B1-15 obtained from IDA. As discussed above, the IDA is conducted with PGAs varying from 0.15 g to 1.5 g with an increment of 0.15 g for the 5 ground motions defined above. The analysis, however, stops when the 8% peak drift is achieved or the PGA reaching 1.5 g. The number of the bridge bent response reaching prescribed damage level in IDA is also tabulated as shown in Figure 7-17 together with the histogram. The bar chart in Figure 7-17 presents the results from 37 time history analyses out of the possible 50 analyses (5 ground motions each with 10 PGA increment) for each type of bent, since for some ground motion 8% drift limits is reached well below PGA of 1.5 g. performance of bent B1-15 based on the damage state defined in Table 5 for both the SMA and steel reinforced bridge bents are presented in Figure 7-17 (a). In the graph the ordinate represents the frequency of the samples achieving the prescribed damage states and abscissa represents the damage states as defined in Table 7-5. Both the SMA and steel reinforced bridge bents have nearly similar number of cases experiencing the damage states in terms of the peak drift. There is only a small difference in the number of cases corresponding to the damage state 3 and 4, indicating again that the peak drift of the bent with two types of reinforcement are nearly similar. The results imply that the system with lower stiffness and lower hysteretic energy dissipation, i.e. the SMA RC1 reinforced pier, does not necessarily have greater displacement demands. The performance of SMA reinforced bridge piers improved slightly with higher ratio of SMA reinforcement (SMA RC2 and SMA RC3) compared to SMA RC1.

Table 7-5 Definition of damage state for bridge piers

Damage State	Peak drift (%)	Residual drift (%)
1.No	0-0.7	0-0.25
2. Minor	0.7-1.5	0.25-0.5
3. Intermediate	1.5-2.5	0.5-0.75
4. Extensive	2.5-5	0.75-1
5. Very severe	Above 5.0	Above 1.0

The differences of two types of bridge piers are, however, clearly evident in Figure 7-17 (b) which shows the comparison of the number of cases of bridge pier reaching different damage states in terms of residual displacements. Bridge piers reinforced with SMA bars at plastic hinge regions show good re-centering capacity. In no cases the SMA reinforced bridge piers experience damage state 5, i.e. residual displacement exceeding 1%. In contrary, as many as 9 cases are observed for the steel reinforced bridge piers that exceed the 1% drift limit. The residual displacement recovery of SMA reinforcement is also slightly improved with the higher SMA reinforcement ratio.

Figure 7-18 (a) and (b) compare the performance of bent B1-10 based on the peak and residual drift, respectively. Figure 7-18 (a) presents the damage state in terms of the peak drift. The results presented indicate that steel reinforced pier performs slightly better in terms of peak response than the SMA RC1 due to the higher stiffness and higher flexural strength. The performance of the SMA bridge pier with higher flexural capacity is similar to the steel reinforced bridge pier. However, as presented in Figure 7-18 (b) the performance of SMA RC bent based on the residual drifts is far superior compared to the steel reinforced bridge pier. Both the peak drift and residual drift of SMA reinforced bridge pier improved slightly with the use of higher SMA reinforcement ratio. Peak drift response of bent B3-7.72 as presented in Figure 7-19 (a) shows more cases of SMA RC bent experiencing damage state 4 and 5 than the steel reinforced piers with an exception of SMA RC3. Conversely, none of the case with SMA RC bents exceeding the damage state 1 is observed compared to 13 cases for steel reinforced bents as presented in Figure 7-19 (b). It should also be noted that bent B3-7.72, i.e. bents with 3 piers, experiences comparatively less residual drift compared to single pier bridges.

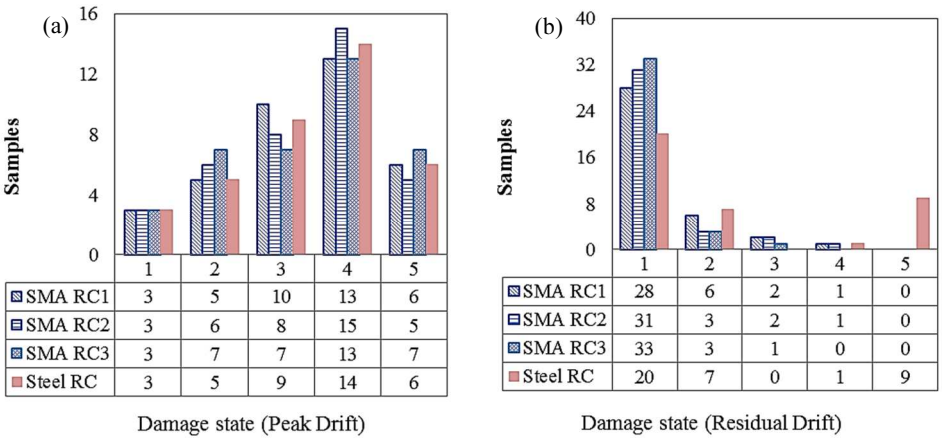

Figure 7-17 Comparison of histogram of damage state based on (a) Peak drift and (b) Residual drift for bent B1-15.

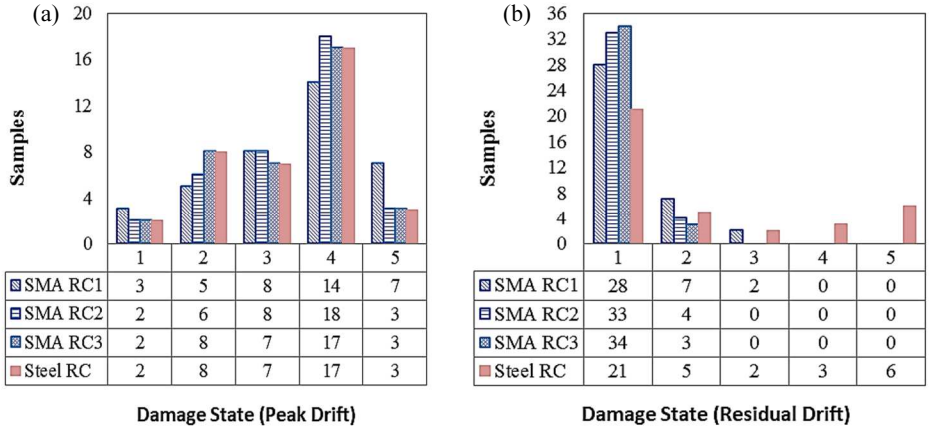

Figure 7-18 Comparison of histogram of damage state based of (a) Peak drift and (b) Residual drift for bent B1-10.

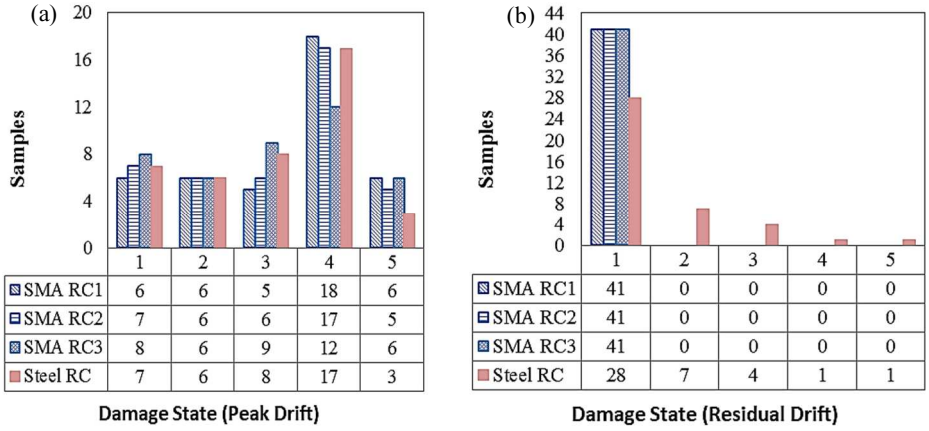

Figure 7-19 Comparison of histogram of damage state based on (a) Peak drift and (b) Residual drift for bent B3-7.72

In order to compare the capacity of SMA reinforcement in recovering the deformation, the mean of peak drift responses obtained for five damage states are plotted against respective mean residual drift for each of the bents. Figure 7-20 (a), (b) and (c) show the mean peak drift versus the corresponding mean residual drift at different damage state for B1-15, B1-10 and B3-7.72, respectively. The results in Figure 7-20 (a) shows that for bridge bent B1-15 with steel reinforcement at damage state 5 (bents having peak drift higher than 5%) the mean peak drift is 6.87% and the mean residual drift is 2.81%. Whereas for SMA reinforced bents, i.e. SMA RC1, SMA RC2 and SMA RC3 having rebar ratio of 1.55%, 2.34% and 2.93% respectively, at the same damage state having the mean peak drift of 6.2%, 6.23% and 5.76% have the mean residual drift of 0.54%, 0.58% and 0.29%, respectively. Similar results of significantly reduced residual drifts for SMA RC bents at nearly similar peak drift as Steel RC bents could also be observed in Figure 7-20 (a), (b) and (c) for B1-15, B1-10 and B3-7.72 at damage state 4 and 5. The results presented show that regardless of the height, natural period, reinforcement ratio and the numbers of piers, replacing steel reinforcements with SMA reinforcements in bridge bents at the plastic hinge locations are effective in reducing the residual displacement of the bridge piers. The results obtained in this study suggest that with SMA reinforcement at plastic hinge region, the residual drift could be reduced to approximately 1/4 for single pier bridge bent and approximately 1/6 for multi-pier bridge bent of that obtained for conventional steel reinforced bridge bents. This substantial reduction in residual drift implies the bridge piers can be easily repaired by replacing the damaged concrete after a major earthquake event. It is to be noticed again that the bridge bents with multiple columns has significantly lower residual drift though the peak drifts are comparable to the single column bents. The improved performance of the multiple column bridge bent may be attributable to the relatively higher redundancy of these bents in comparison to single column bents.

It should be noted that the response of the bridge bents should be evaluate considering peak drift, residual drift as well as the energy dissipation. Though the performance of SMA RC1 piers are slightly inferior to steel reinforced piers in terms of peak drift and hysteretic energy dissipation, its performance in reducing the residual drift is far superior to the conventional steel reinforced piers. The performance of SMA reinforced bridge piers in terms of peak drift, hysteretic energy dissipation and residual deformation improves with higher SMA reinforcement ratio.

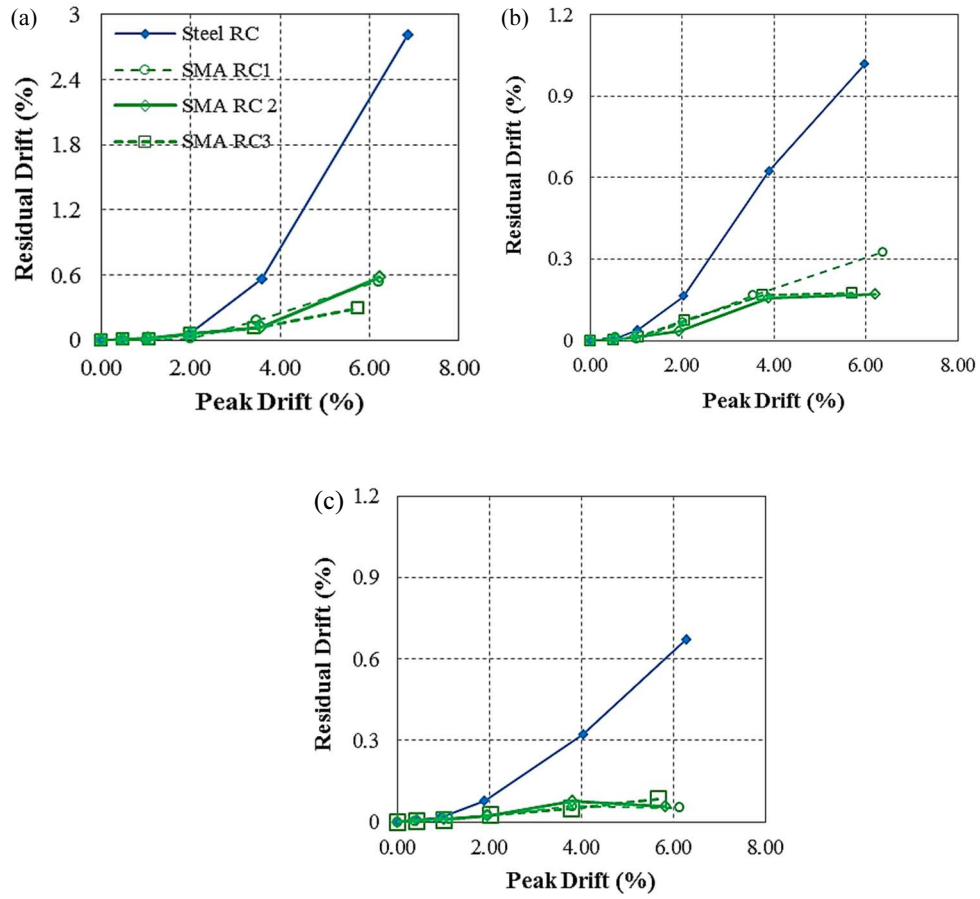

Figure 7-20 Peak drift versus Residual drift for (a) B1-15 (b) B1-10 and (c) B3-7.72.

7.7 Conclusion

This study parametrically compares the performance of SMA RC bridge bents with steel RC bridge bents using numerical analysis. Twelve prototype bridge bents representing three different geometries with single and multiple piers with SMA reinforcement or conventional steel reinforcement are modelled and analyzed under monotonic and seismic loading.

The response of the bridge bents to monotonic loading showed that progression of damage such as yielding of longitudinal rebar, spalling of concrete and crushing to core concrete could be different in SMA RC and steel RC bridge bents. Due to the low yielding strain steel rebar are subjected to yielding at relatively lower drift/rotation compared to SMA rebar. In steel RC bridge piers crushing of concrete occurs after substantial increase in drift beyond the initial yielding of rebar. Yielding and spalling of cover concrete occurs at nearly similar drift level in SMA RC bents and in case of SMA RC3 for B3-7.72 spalling of cover concrete preceded the yielding of SMA reinforcement. Spalling of cover concrete and crushing of core concrete for both SMA and steel RC bents initially at roughly similar drift levels.

The results from dynamic pushover analysis with various reinforcement ratio of superelastic SMA rebar and conventional steel rebar revealed that SMA-RC bridge piers are comparable to steel RC bridge bents in terms of peak drifts. However, the residual drifts of the SMA-RC bridge piers are significantly small compared to the steel RC bridge piers owing to the superelastic behavior of SMA bars. An increase of nearly 0.8% (SMA RC2) and 1.4% (SMA RC3) in rebar ratio in bents B1-15 and B1-10 resulted in reduction of peak and residual deformations. In some cases, however, it is found that SMA RC bents with higher reinforcement ratio may not necessarily result in lower residual drift. However, the calculated residual drift for those cases are quite small and have insignificant impact on the overall performance of the bridge bents. The increase in reinforcement ratio also improved the hysteretic energy dissipation of the bridge bents.

Damage Analysis of the bridge piers show that performance of SMA RC bridge bents with lower SMA rebar ratio (i.e. SMA RC1) is slightly inferior to steel-RC bridge piers in terms of performance based on peak drifts. However, significant improvements in performance based on residual drifts are obvious. With the increment in rebar ratio the performance of the SMA bridge bents in terms of both the peak and the residual deformations improved. The results also revealed that the multi-column bridge bent (B3-7.72) leads to relatively smaller residual displacement compared to single column bents, subjected to the ground motions considered in this study, owing to their higher redundancy. Moreover, the residual drift performance of the bent (B3-7.72) improves with the use of SMA rebar. The application of SMA reinforcement at plastic hinge region resulted in reduction of residual drift by approximately 1/4 of the steel RC bent with single piers and approximately 1/6 for bents with multiple columns.

This study verifies the promising performance of superelastic SMA as reinforcement for RC bridge bents through parametric investigation on the effects of important design and geometric parameters. However, few other design parameters such as fatigue of SMA reinforcement and cost effectiveness of SMA bars needs careful consideration in future investigations.

7.8 References

Alam, M.S., Youssef, M.A., & Nehdi, M. (2008). Analytical Prediction of the Seismic behaviour of super elastic Shape Memory Alloy reinforced concrete elements, *Engineering Structures*, 30, 3399-3411.

Alam, M.S., Youssef, M.A., & Nehdi, M. (2010). Exploratory investigation on mechanical anchors for connecting SMA bars to steel or FRP bars, *Materials and Structures*, 43: 91-107.

Auricchio, F., & Sacco, E. (1997). A superelastic shape-memory alloy beam. *Journal of Intelligent material and Structures,* 8, 489-501.

Basoz, N., & Mander, J.B. (1999). *Enhancement of the highway transportation lifeline module in HAZUS*. Final Pre-Publication Draft (#7), National Institute of Building Science

Billah, A.H.M.M., & Alam, M.S. (2012) Seismic performance of concrete columns reinforced with hybrid shape memory alloy (SMA) and fibre reinforced polymer (FRP) bars. *Construction and Building Materials*, 28, 730-742.

Billah, A.H.M.M., & Alam, M.S. (2014). Seismic Fragility Assessment of Concrete Bridge Pier Reinforced with superelastic Shape memory Alloy. *EERI Earthquake Spectra*, (Online version).

Dutta, A., & Mander, J.B. (1998). *Seismic fragility analysis of highway bridges*. In: Proceeding s of the INCEDE-MCEER center-to-center workshop on earthquake engineering frontiers in transportation systems: 311-325.

Cruz Noguez, & C.A., Saiidi, M. (2011). Shake-table studies of a four-span bridge model with advanced materials. *Journal of Structural Engineering*, 138, 183-192.

Fujino, Y., Satoko, H., & Abe, M. (2005). Damage Analysis of Hanshin Expressway viaducts during 1995 Kobe Earthquake. I: Residual Inclination of Reinforced concrete Piers. *Journal of Bridge Engineering*, 10, 45-53.

Fugazza, D. (2003). *Shape-memory alloy devices for earthquake engineering: Mechanical properties, constitutive modelling and numerical simulations*. Master's Thesis, University of Pavia, Italy.

HAZUS (1999). *Earthquake loss estimation methodology. Technical manual HAZUS99-SR2*. Washington (DC): National Institute of Building Sciences for the Federal Emergency Management Agency.

Japan Road Association (2006). *Specifications for Highway Bridges*. Japan Road Association, Japan.

Kim, S.H., & Shinozuka, M. (2004). Development of fragility curves of bridges retrofitted by column jacketing. *Probabilistic Engineering Mechanics*, 19, 105-112.

Mander, J.B., Nigel Priestley, M.J., & Park, R. (1988). Theoretical stress-strain model for confined concrete, *Jour of Struct Eng*, 114, 1804-1826.

Martínez-Rueda, E.J., & Elnashai, A.S. (1997). Confined concrete model under cyclic load, *Materials and Structures,* 30, 139-147.

Menegotto, M., & Pinto, P.E. (1973). *Method of analysis of cyclically loaded RC plane frames including changes in geometry and non-elastic behaviour of elements under combined normal force and bending*. Symposium on the Resistance and Ultimate deformability of Structures acted on by well-defined repeated loads, IABSE, Zurich, Switzerland, 15-22

Nikbakht, E., Rashid, K., Hejazi, F., & Osman,S.A. (2015). Applications of shape memory alloy bars in self-centering precast segmental columns as seismic resistance. *Structure and Infrastructure Engineering, 11, 297-309.*

O'Brien, M., Saiidi, M., & Sadrossadat-Zadeh, M. (2007). *A study of concrete bridge columns using Innovative materials subjected to cyclic loading.* CCEER, Dept. of Civil Engineering, University of Nevada, Reno, Nevada, Report no. CCEER-07-01

Otani, S. (1974). *A Computer program for inelastic response of R/C frames to earthquakes*. Civil Engineering Studies, Report UILU-Eng-74-2029, 1974. University of Urbana-Champaign, USA.

Paulay, T., & Priestley, M.N.J. (1992), *Seismic Design of Reinforced Concrete and Masonry Building*. New York, John Wiley & Sons, Inc.

Roh, H., & Reinhorn, A.M. (2010). Hysteretic behaviour of precast segmental bridge piers with superelastic shape memory alloy bars. *Engineering Structures,* 32, 3394-3403.

Saiidi, M., & Wang, H. (2006). An Exploratory Study of Seismic Response of Concrete Columns with Shape Memory Alloys Reinforcement. *ACI Structural Journal*, 103, 436-443.

Saiidi, M., O'Brien, M., & Sadrossadat-Zadeh, M. (2009). Cyclic Response of Concrete Bridge Column Using Superelastic Nitinol and Bendable Concrete. *ACI Structural Journal*, 106, 69-77.

Saiidi, M.S., & Ardakani, S.M.S. (2012). An analytical study of residual displacements in RC bridge columns subjected to near-fault earthquakes. *Bridge Structures*, 8, 35-45.

Seismosoft Inc (2012) *Seismo-struct User Manual for version 6.*

Tazarv, M., & Saiidi, M. (2013). Analytical studies of the seismic performance of a full-scale SMA-reinforced bridge column. *International Journal of Bridge Engineering*, 1, 37-50.

Tazarv, M., & Saiidi, M. (2014). Reinforcing NiTi superelastic SMA for Concrete structures. *Journal of Structural Engineering,* (Online version).

Vamvastsikos, D., & Cornell, A.C. (2001). Incremental dynamic analysis. *Earthquake Engineering and Structural Dynamics*, 31, 491-514.

Vosooghi, A., & Saiidi, M.S. (2010). *Post-Earthquake Evaluation and Emergency Repair of Damaged RC bridge Columns using CFRP Materials.* Center for Civil Engineering Earthquake Research, Dept. of Civil Engineering, University of Nevada, Reno, Nevada, Report No. CCEER-10-05.

Wehbe, N., Saiidi, M., & Sander, D. (1999). Seismic Performance of rectangular bridge column with moderate confinement. *ACI Structural Journal*, 96, 248-259.

Wilson, J.C., & Wesolowsky, M.J. (2005). Shape Memory Alloys for Seismic Response Modification: A State-of-the-Art Review. *EERI Earthquake Spectra*, 21, 569-601.

Youssef, M.A., Alam, & M.S., Nehdi, M. (2008). Experimental Investigation on the seismic behaviour of beam-column joints reinforced with superelastic Shape Memory Alloy. *Journal of Earthquake Engineering*, 12, 1205-1222.

Zafar, A., & Andrawes, B. (2012). Incremental dynamic analysis of concrete moment resisting frames reinforced with shape memory composite bars. *Smart Material and Structures*, 21, 025013.

CHAPTER 8
PERFORMANCE-BASED SEISMIC ASSESSMENT OF SUPERELASTIC SHAPE MEMORY ALLOY REINFORCED BRIDGE PIERS CONSIDERING RESIDUAL DEFORMATIONS

8.1 Abstract

The application of superelastic Shape Memory Alloy (SMA) reinforcement in plastic hinge regions of bridge piers has been proven to reduce the residual displacement after a strong shaking owing to its unique shape recovery characteristics. However, the maximum deformation of the piers could increase due to the relatively lower modulus of elasticity of SMA bars and lower hysteretic energy dissipation capacity. In this context, the paper applies a recently formulated probabilistic performance-based seismic assessment methodology that considers both the maximum and the residual deformation simultaneously to evaluate the performance of SMA reinforced bridge piers.

8.2 Introduction

Reinforced concrete (RC) bridge piers with high ductility capacity are designed and constructed in regions of high seismicity to avoid collapse of the supported bridge superstructure during strong ground shaking. While the reinforced concrete bridge piers are likely to avoid collapse, it could result in significantly large residual displacements following an extreme earthquake event. During past major earthquakes, such as 1994 Northridge earthquake in the USA, 1995 Kobe earthquake in Japan, 2010 Maule earthquake in Chile, numerous bridge piers were demolished due to the large residual deformations that made them impossible to return to their initial un-deformed position (Kawashima & Unjoh, 1997; Kawashima et al., 2011; Fujino et al., 2005). Consequently, there is a consensus among researchers and practicing engineers on the importance of residual (permanent) displacement on the seismic performance and post-earthquake functionality of RC structures (Saiidi & Ardakani, 2012; Ramirez & Miranda, 2012). Recently, significant research investments have been made to improve the seismic performance of the bridge piers using advanced structural systems with re-centering properties, such as unbonded post-tensioned bridge columns and superelastic SMA reinforced elements. These advanced structural systems and materials can improve the seismic performance under the seismic loads and ensure the post-earthquake functionality of bridges.

This study focuses on the performance-based evaluation of piers with superelastic SMA in the plastic hinge region, hereafter referred as SMA RC pier. Recently, SMAs have found significant applications in civil engineering due to their unique ability to sustain large

deformations and return to their original shape by heating (shape memory effect) or through removal of stress (superelastic effect). Particularly, the superelastic behavior of SMA is of the greatest interest as no external power source is required for it to bring to the original shape. Superelastic bars are capable of regaining its original shape through a crystalline phase transformation under stress change when the phase transformation temperature is sufficiently below the operating temperature. Since the discovery of first SMA in 1963, a large number of alloys have been investigated for shape memory behavior. Specifically, Nickel Titanium (NiTi) based alloys have been mostly used in commercial applications because of its several advantages such as large strain recovery, high energy dissipation and excellent corrosion resistance. Some of the commercial applications of NiTi SMA include eyeglass frames, cellular phone antennas, under wire for women's brassieres and SMA actuator for transmission fluid control in automative (Wu & Schetky, 2000). NiTi SMA are also frequently used in medical applications, such as cardiovascular devices, orthopedic devices and surgical instruments (Machado & Savi, 2003).

Many recent studies (Cruz Noguez & Saiidi, 2011; Saiidi & Wang, 2006; Youssef et al., 2008; Saiidi et al., 2009) have experimentally explored the performance of RC structures with superelastic NiTi reinforcement in critical plastic hinge regions. The above experiments found that superelastic SMA reinforcements could significantly improve the performance of RC structures by largely reducing the residual deformation and are capable of dissipating an adequate amount of energy. While other investigators (Billah & Alam, 2012, 2014; Tazarv & Saiidi, 2014, 2015; Shrestha et al., 2015; Shrestha & Hao, 2015) used numerical analyses to investigate the performance of RC structures with superelastic NiTi bars. In addition to the above studies, a few recent studies have focused on the application of Cu-based superelastic SMA as reinforcement for RC elements (Varela & Saiidi, 2014; Hosseini et al., 2015; Shrestha et al., 2013). The wide operating temperature along with the lower cost and ease to machine are the attractive features of Cu-based alloy compared to the NiTi (Zhang et al., 2009; Shrestha et al., 2013; Shrestha et al., 2016; Gencturk & Hosseini, 2014). These researchers have comprehensively approved the superior performance of SMA RC elements in terms of reducing the residual deformation. However, owing to the lower modulus of elasticity of the SMA reinforcement and lower hysteretic energy dissipations, the maximum displacement in the SMA RC piers could be higher than the steel counterpart (Tazarv & Saiidi, 2014; Shrestha & Hao, 2015; Nakashoji & Saiidi, 2014; Varela & Saiidi, 2014). This disparity in performance of the two systems (SMA RC and steel RC piers) for two response variables (maximum and residual deformation) clearly highlights the need for collective consideration of both the variables for proper evaluation of seismic performance.

In recent years, the earthquake engineering community has been focusing attention on the performance-based engineering approach in order to predict and manage better the post-earthquake functionality and condition of structures. Performance-based seismic design requires that the structural system should be capable of meeting various performance levels over the full range of earthquake demands. To explicitly relate the bridge seismic vulnerability with performance objectives, it is necessary to evaluate its seismic fragility considering multi-level performance criteria. A performance objective is typically defined when a set of structural and/or non-structural performance level is coupled with different intensities of seismic input. Earlier guidelines (FEMA 273; SEAOC, 1995) represented performance levels in discrete forms in terms of one or multiple response indices, usually given by maximum responses. Little attention was given to the permanent (residual) state of structural elements. To include residual deformation to the performance level Pampanin et al. (2003) and Christopolous et al. (2003) proposed Residual Deformation Damage Index (RRDI) as an additional performance indicator. Pampanin et al. (2002) further developed the study by proposing the use of a three-dimensional performance matrix, where the term "matrix" is used to refer to the combination of two dependent variables, Maximum Drift (MD) and Residual Drift (RD). Recently, Uma et al. (2010) formulated probabilistic framework of the aforementioned performance-based assessment approach including MD and RD. The authors derived the joined fragility curves expressing the probability of exceedance of performance levels defined by the pair of maximum and residual deformation using bivariate probability distribution.

In this paper, the above mentioned probabilistic framework is applied to assess the performance of typical RC bridge piers. Using the joined fragility curve the likelihood of seismic demand exceeding the predefined damage limits, expressed as probability of exceedance of the corresponding damage state, at a chosen seismic excitation level are identified for bridge piers with SMA and steel reinforcement. No such study that uses combined maximum and residual response indices to define the performance of SMA RC bridge piers could be found in the literature. As residual and maximum deformations are correlated variables, separate handling of these two performance indices may not provide a conclusive result. A suite of 30 near-fault ground motions with directivity effects are used for nonlinear response history analyses to generate the fragility curves.

8.3 Joined fragility function methodology

In the seismic fragility analyses of engineering facilities, the structural performance levels are commonly defined by a single measure of maximum response or cumulative damage (e.g., Choi et al., 2004; Alipour et al., 2010; Li et al., 2015). However, to achieve a more reasonable

seismic performance evaluation, the structural residual responses after an earthquake event should also be considered since the post-earthquake functionality of structures is of a great significance.

To simultaneously consider the structural performance measures of Residual Drift (RD) and Maximum Drift (MD), Pampanin et al. (2002, 2003) and Christopoulos et al. (2003) proposed a bivariate measure in the format of an RD-based performance matrix, the elements of which are identified as the performance level defined by a pair of RD and MD. For different ground motion intensities, a full three-dimensional performance domain can be represented as shown in Figure 8-1 (a); while for a specific ground motion intensity, the performance levels (PL (i, j)) considering the combination of RD (index i) and MD (index j) can be expressed in the X-Y plane as shown in Figure 8-1 (b).

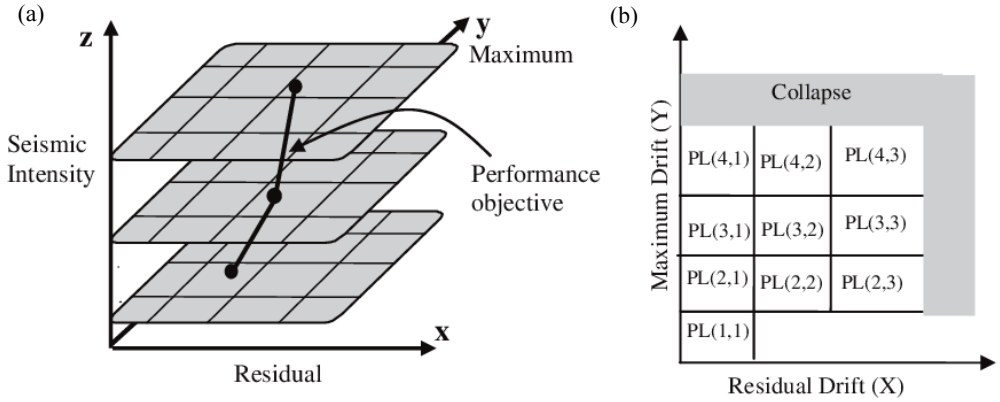

Figure 8-1 Three dimensional performance matrix considering the combination of RD and MD associated with seismic intensity (Pampanin et al., 2002, 2003).

Uma et al. (2010) extended the three-dimensional matrix approach to compute the performance levels as a function of the combined probability distribution of RD and MD by defining a probabilistic seismic demand model, which allows the estimation of experiencing a given combination of RD and MD conditioned on a ground motion intensity level. Within the proposed procedure, the exceedance probability of damage measure (DM) conditioned on intensity measure (IM), namely $P[DM \mid IM]$ is expressed as

$$P[DM \mid IM] = \int\int P[DM \mid EDP_{RD,MD}] \mid dP[EDP_{RD,MD} \mid IM] \tag{8.1}$$

where $P[DM|EDP_{RD,MD}]$ denotes the probability of a specific DM in combination with a performance level determined by the pair of engineering demand parameter (EDP) values and $dP[EDP_{RD,MD}|IM]$ denotes the probability density function of EDPs under a certain value of IM. In this study, the MD and RD of RC bridge piers under earthquake excitations are chosen as the pair of EDPs in the seismic fragility analyses. Equation (1) can be employed to calculate

the seismic fragilities under different performance levels with the consideration of joint occurrence of MD and RD.

Due to the advantage in simultaneously modelling the uncertainties in the EDPs, the concept of multivariate distribution response curve (Moehle et al., 2004) is commonly employed to represent the joint probability distribution of two random variables. In the present study, a single bivariate lognormal distribution is utilized as the joint probability density function (PDF) to represent the joint occurrence of a pair of RD and MD under a certain ground motion intensity level. The joint PDF for the bivariate lognormal distribution of RD (X) and MD (Y) can be expressed as (Uma et al, 2010)

$$f_{X,Y}(x,y)=\frac{0.5}{xy\pi\zeta_X\zeta_Y\sqrt{1-\rho^2}}*\exp\left\{-\frac{0.5}{1-\rho^2}\left[\frac{(\log x-\lambda_X)^2}{\zeta_X^2}-\frac{2\rho(\log x-\lambda_X)(\log y-\lambda_Y)}{\zeta_X\zeta_Y}+\frac{(\log y-\lambda_Y)^2}{\zeta_Y^2}\right]\right\} \quad (8.2)$$

where λ_X, λ_Y and ζ_X, ζ_Y are the lognormal mean and lognormal standard deviation of X (RD) and Y (MD), respectively; ρ denotes the linear correlation coefficient between the two response indices of RD and MD.

By conducting the double integration over the joint PDF in the interval from zero to corresponding drift limits of RD and MD, the probability of reaching or being within a performance level, namely PL (i, j) can be obtained as

$$PL(i,j)=\int_0^{MD_i}\int_0^{RD_j} f_{X,Y}(x,y)dxdy \quad (8.3)$$

where MD_i and RD_j represent the drift limits of RD and MD, respectively. It is evident that the exceedance probability of a performance level (P_{ij}), namely the seismic fragility function can be calculated by subtracting PL (i, j) from 1, namely

$$P_{ij}=1-PL(i,j)=1-\int_0^{MD_i}\int_0^{RD_j} f_{X,Y}(x,y)dxdy \quad (8.4)$$

With Equations (8.2) and (8.4), the joined seismic fragility of bridge piers considering both RD and MD can be calculated. The above-described method is employed to evaluate the joined seismic fragility of steel and SMA RC bridge piers considering both RD and MD in the following sections.

8.4 Bridge Piers Description

In this study, numerical investigations on a couple of typical Californian bridge piers, representing the majority of RC highway overpass bridges in California (Ketchum et al.,

2004), is used for the analysis. The geometric and reinforcement details of the bridge piers are presented in Figure 8-2. The piers have a clear height of 15 m and 10 m, hereafter referred as Pier1 and Pier 2, respectively. An axial load of 7473 kN is lumped on the top of the bridge piers to represent the load of the superstructure. The fundamental period of the two typical RC bridge piers are 1.53 and 0.87 sec, respectively. The two steel RC piers are reinforced with 64 numbers of 32 mm diameter steel rebars. For SMA reinforced piers, the reinforcement in the plastic hinge region is replaced with 74 numbers of 32 mm diameter NiTi bars. 20 mm diameter spiral reinforcement with the pitch of 110 mm C/C is provided as transverse reinforcement. The SMA RC piers are designed to have a similar flexural strength as the steel RC bridge piers (Shrestha & Hao, 2015). NiTi bars are used only in the plastic hinge region of the SMA RC piers to reduce the cost. SMA RC piers are designed to have SMA reinforcement in plastic hinge area to yield before the yielding of the steel reinforcement so that most of the damages are confined in the plastic hinge region. The plastic hinge length, L_p is calculated according to the relation given by Paulay and Preistley (1992)

$$L_p = 0.08L + 0.022d_b f_y \quad (mm) \tag{8.5}$$

where L is the length of the member in mm, d_b represents the bar diameter in mm, f_y is the yield strength of the rebars in MPa. Previous studies (Alam et al., 2008; O'Brien et al., 2007) showed that Paulay and Preistly (1992) equation can reasonably estimate the plastic hinge length of SMA reinforced concrete elements.

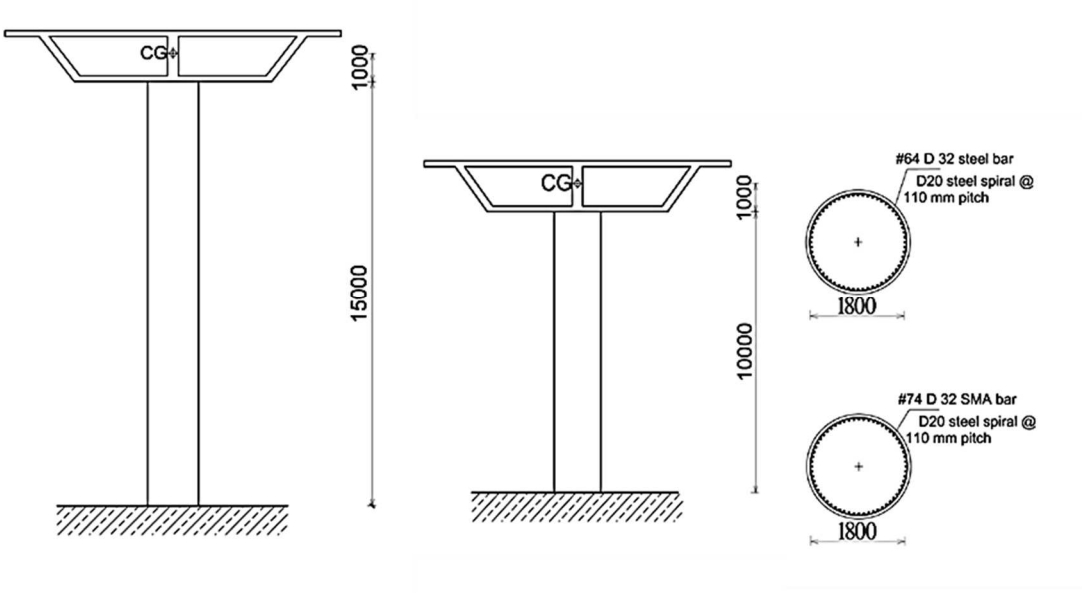

Figure 8-2 Prototype bridge piers.

8.5 Numerical Model

The numerical modelling of the bridge piers is conducted using Seismostruct software. Displacement based nonlinear beam-column elements discretized into 12 finite element frames are used to model the piers. Fiber modelling approach is employed to represent the distribution of inelasticity along the length and cross-sectional area of the member. The fiber section used for the column is discretized into core fiber for confined concrete, cover fiber for unconfined concrete and steel/SMA fiber for reinforcement bars. The material properties of confined and unconfined concrete are modelled using the constitutive relationship proposed by Mander et al. (1988) and the cyclic rules proposed by Martínez-Rueda and Elnashai (1997), respectively. Steel rebar are modelled using Menegotto-Pinto (1973) steel model.

The yield strength of the reinforcement is 414 MPa and the compressive strength of the concrete is 35 MPa. Wehbe's bond-slip model proposed by Wehbe et al. (1999) is used to calculate the bond-slip deformations (yield penetration) of the rebar in the steel reinforced columns. Bond slip effect is included in the form of moment-rotation spring at the end of the column using a zero-length element. The bond-slip spring is modelled by using a trilinear curve (Vosooghi & Saiidi, 2010) composed of the bilinear idealized curve followed by an extension branch with zero stiffness. The trilinear curve was constructed by connecting the origin, effective yield point and predicted ultimate point followed by the extension branch. The trilinear curve was used to account for the higher actual ultimate strain of confined concrete than the predicted ultimate strain by Mander et al. (1988) stress-strain model (Vosooghi & Saiidi, 2010; Johnson et al., 2006). A multi-linear element in Seismostruct is used to represent the bond slip behavior.

To model the slippage of SMA rebars inside the coupler, a bond-slip model is incorporated in the analytical model of SMA reinforced bridge piers. The bond slip relation for SMA rebar was obtained from the experimental study of Alam et al. (2010), which was validated numerically by Billah and Alam (2012). The bond slip element was modelled in Seismostruct using a link element with modified Takeda hysteretic curve (Otani, 1974), as done in the previous study (Billah & Alam, 2012). The details of the finite element modelling are presented in Figure 8-3. Detailed discussion on numerical modelling and validation of the numerical model is presented in a previous study (Shrestha & Hao, 2015). The authors verified the numerical model using the experimental study of Saiidi and Wang (2006).

8.5.1 NiTi SMA Model

The NiTi rebar is usually based on the equi-atomic compound of Nickel and Titanium. Besides the ability to tolerate large amounts of strain, shape memory NiTi alloys show high stability

in cyclic applications and are corrosion resistant. They also have a moderate solubility range, enabling changes in composition and alloying with other elements to modify both the shape memory and mechanical characteristics. For commercial application and in order to improve its properties, a third metal is usually added to NiTi. Although two metals (Nickel and Titanium) are processed identically, a slight increase in Nickel content improves the mechanical behavior of SMA by depressing the transformation temperatures and improving the hysteretic energy dissipation capacity.

Manufacturing of NiTi alloys is not easy, and many machining techniques can be used only with difficulty. This characteristic is the reason for the expensive cost of NiTi alloys. Despite this disadvantage, the excellent mechanical properties of NiTi alloy have made them the most frequently used SMA material for the commercial applications.

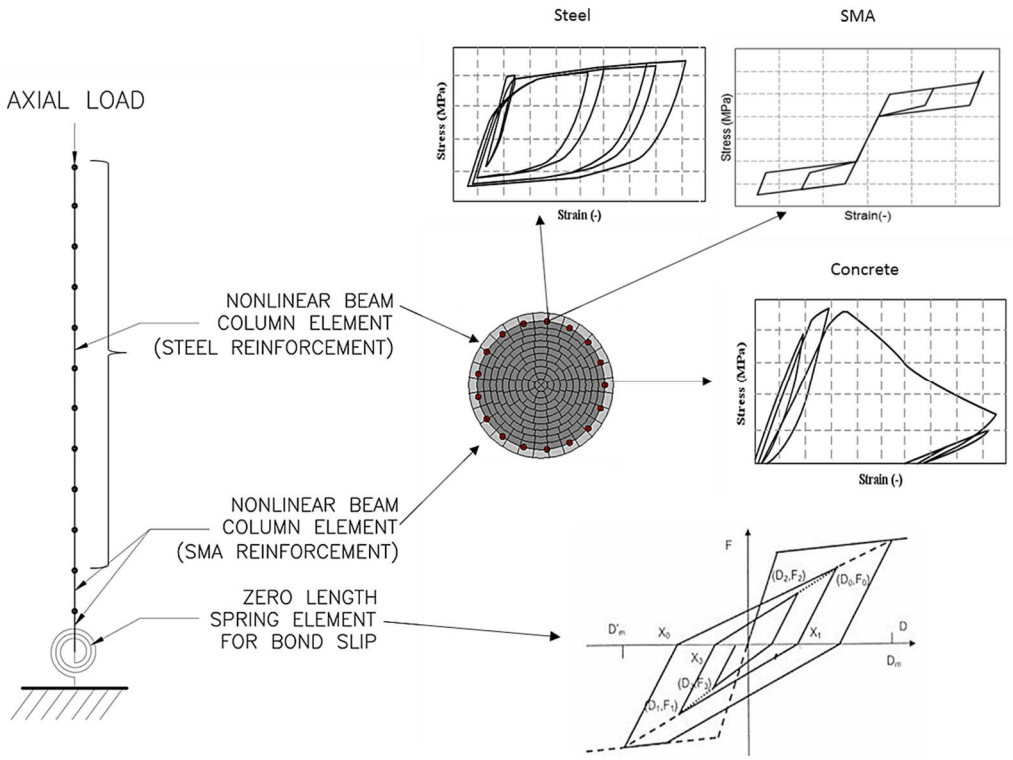

Figure 8-3 Finite Element modelling of bridge piers.

In order to realistically represent the NiTi reinforcement, one dimensional uni-axial model for superelastic SMA, programmed by Fugazza (2003) following the constitutive relationship proposed by Auricchio and Sacco (1997), implemented on Seismostruct program are used in numerical simulations. This model is capable of describing the constitutive model of superelastic SMAs at a constant temperature. The model is sufficiently accurate for the present study with respect to the temperature effects because unlike in other applications where the SMA is exposed to ambient temperature, SMA reinforcements are insulated by a thick layer

of concrete. A schematic of force-deformation relationship of the SMA model used in this study is presented in Figure 8-4. The model is defined by six parameters that are given in Table 8-1. The SMA model represents an idealized behavior of the SMA material where a complete recovery of the original shape is achieved at the end of each cycle.

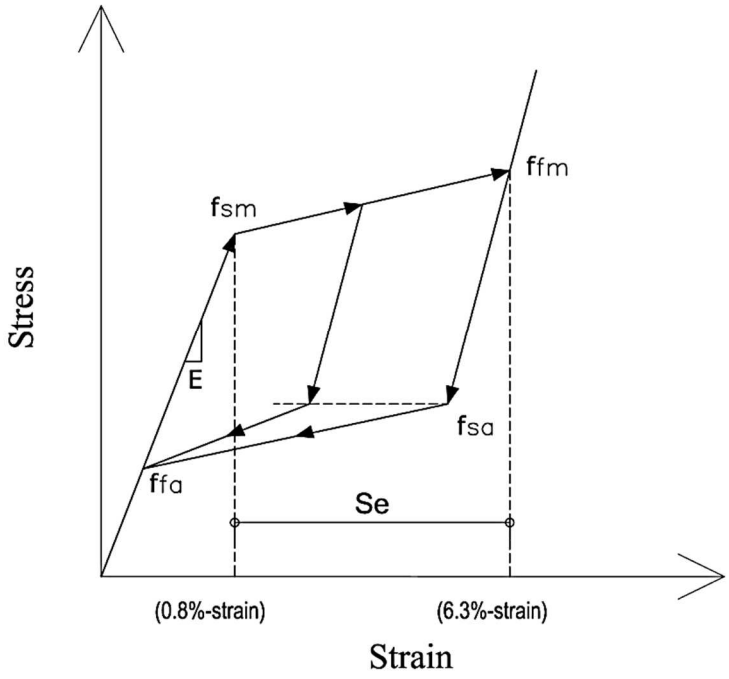

Figure 8-4 Constitutive model of superelastic SMA model.

Table 8-1 Material properties for SMA RC column

Material	Property	Value
Superelastic SMA	Modulus of Elasticity, E (MPa)	48300
	Austenite to martensite starting stress, fsm (MPa)	379
	Austenite to martensite finishing stress, ffm (MPa)	405
	Martensite to austenite starting stress, fsa (MPa)	180
	Martensite to austenite finishing stress, ffa (MPa)	100
	Superelastic plateau strain, Se (%)	5.5

8.6 Ground motions

Recent earthquake records have shown that in the proximity of an active fault, ground motions are significantly affected by the faulting mechanism, direction of rupture propagation relative to the site, e.g., forward directivity. These near-fault ground motions often contain a strong and long period velocity pulse that could cause severe structural damage. These types of ground motions may generate high demands that force the structures to dissipate this input

energy with few large displacement excursions. Previous investigations (Phan et al., 2007; Choi et al., 2010] found that the most unique measured response characteristic of RC bridge piers subjected to near-fault ground motions was the significant residual displacement even under moderate motions. The high amplitude velocity pulse due to the fault-normal component of the near fault motions could generate large displacement on one side. Generally, this displacement is only partially recovered due to a lack of reversed pulse, thus leading to a significant residual displacement (Phan et al., 2007; Choi et al., 2010).

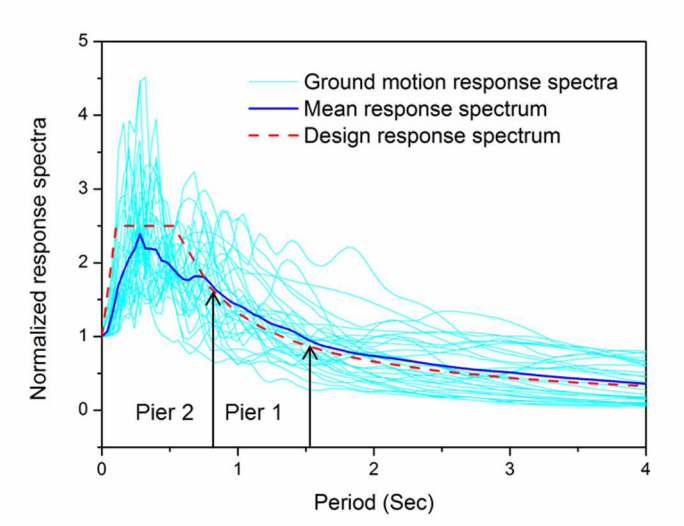

Figure 8-5 5% damped response spectra and comparison of mean spectra and design spectra.

A total of 30 near-fault earthquake ground motions with the forward directivity effects, extracted from the Pacific Earthquake Engineering Research (PEER) database and as given in Table 8-2, are considered for the response history analysis. The ground motions were recorded for events with magnitude ranging from 6.4-7.4, with the closest distances to the fault of rupture varying from 0.7-15.9 km. All the ground motions were recorded at site C and D according to the NEHRP provision (FEMA 273). The Peak Ground Acceleration (PGA) of the selected ground motions varies from 0.13-0.84 g. The normalized response spectra for 5% damping of the ground motions are presented in Figure 8-5. The mean spectrum of the response spectra is also plotted in the same figure. Figure 8-5 also shows the comparison of the mean spectrum to the IBC (2009) design spectrum for soil category C at the bridge site. The site for the bridge is taken from a previous investigation (Lee & Billington, 2011). The bridge site is located in Oakland, California, with a latitude and longitude of 37.80 N × 122.30 W. The site is located within 10 km of the Hayward Fault. Good matching between the normalized design spectrum and normalized mean spectrum could be observed for periods longer than 0.70 sec. The fundamental periods of the two piers are also plotted in the figure for the indicative purpose.

Table 8-2 Details of selected near-fault records

Record No	Year	Earthquake	M_W	Station	Dist. (km)	Site Class*	PGA (g)
1	1979	Imperial-Valley	6.5	Brawley Airport	11.3	D	0.16
2	1979	Imperial-Valley	6.5	El Centro Array #3	13.8	D	0.22
3	1979	Imperial-Valley	6.5	El Centro Diff. Array	5.6	D	0.35
4	1979	Imperial-Valley	6.5	El Centro Imp. Co. Cent.	7.6	D	0.23
5	1979	Imperial-Valley	6.5	Holtville Post Office	8.8	D	0.22
6	1999	Kocaeli	7.4	Duzce	11.0	D	0.31
7	1989	Loma Prieta	7.0	Gilroy STA #2	4.5	D	0.37
8	1989	Loma Prieta	7.0	Gilroy STA #3	6.3	D	0.37
9	1994	Northridge	6.7	Rinaldi Rec. Stn.	8.6	D	0.84
10	1994	Northridge	6.7	Slymar Con. Sta	6.1	D	0.83
11	1979	Imperial-Valley	6.5	El Centro Array #7	3.1	D	0.46
12	1994	Northridge	6.7	Jensen Filt. Plant	6.2	D	0.42
13	1994	Northridge	6.7	Newhall LA Fire Stn.	7.1	D	0.58
14	1994	Northridge	6.7	Sylmar Olive View Hos.	6.4	D	0.84
15	1987	Superstition Hills	6.4	Parachute Test Site	0.7	D	0.45
16	1994	Northridge	6.7	Newhall Pico Canyon	7.1	D	0.45
17	1989	Loma Prieta	7.0	Corralitos	5.1	D	0.64
18	2004	Parkfield	6.4	Cholame 1E	6.5	D	0.47
19	2004	Parkfield	6.4	Cholame 5W (Sta 5)	10.0	D	0.21
20	2004	Parkfield	6.4	Fault Zone 1	3.4	D	0.50
21	2004	Parkfield	6.4	Gold Hill 1W	0.8	D	0.13
22	1992	Cape Mendocino	7.1	Petrolia, General Store	15.9	C	0.66
23	1992	Erzincan	6.7	Erzincan	2.0	C	0.50
24	1999	Chi-Chi	7.6	CHY028	7.3	D	0.82
25	1999	Chi-Chi	7.6	CHY101	11.1	D	0.44
26	1999	Chi-Chi	7.6	TCU049	4.5	D	0.25
27	1999	Chi-Chi	7.6	TCU053	6.7	D	0.14
28	1979	Imperial-Valley	6.5	El Centro Array #4	6.8	D	0.36
29	1995	Kobe	6.7	KJMA	0.6	C	0.82
30	1979	Loma Prieta	7.0	Gilroy STA #2	10.9	C	0.36

8.7 Numerical Results and Discussion

In this study, Incremental Dynamic Analyses (IDA) using the selected suite of earthquake records are performed to study the seismic responses and fragilities of the example SMA and steel RC bridge piers considering both RD and MD. The seismic intensity level are increased by scaling up the ground motion PGA to 10 different levels, i.e., from 0.15-1.5 g. At each PGA level, the RDs and MDs of steel and SMA RC bridge piers subjected to the 30 recorded ground motions are calculated using the nonlinear time history analyses. It should be noted that the PGA is the optimum choice of ground motion IM due to its efficiency, practicality and sufficiency in the structural seismic fragility analyses (Padgett et al., 2008; Zhang & Huo, 2009; Billah et al., 2012). Therefore, PGA is selected as the IM in the present study.

8.7.1 Seismic Response Analysis

The difference between the seismic responses of steel and SMA RC bridge piers are firstly investigated. The displacement time histories of Pier1 with SMA and steel reinforcement subjected to the ground motion record 25 at PGA level of 0.6g is plotted in Figure 8-6. It can be observed that the SMA RC pier showed a significantly better response in terms of recovering the drift at the end of the ground motion, indicated by the lower RD. Though the MD of the SMA RC pier is slightly higher than that of the steel RC pier owing to the lower stiffness of SMA reinforcement and lower hysteretic energy dissipations, the RD of the piers is significantly lower than its steel counterpart. The MD and the RD are calculated for the 30 selected ground motions at each intensity levels. The distribution of RD with respect to MD at PGA level of 0.45 g for SMA RC Pier1 and steel RC Pier1 are presented in Figure 8-7 (a) and (b), respectively. As presented, both the SMA RC and steel RC piers have nearly similar value with regard to the MD. While a sizable increase in the value of RD is observed in the steel RC pier in comparison to the SMA RC pier.

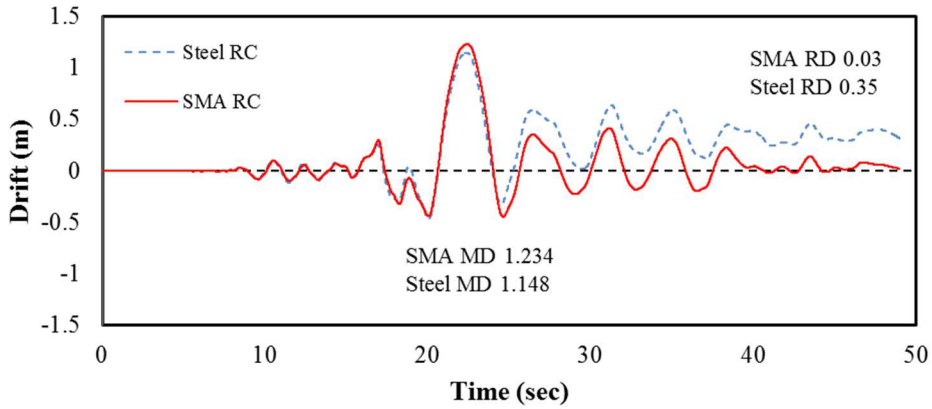

Figure 8-6 Displacement time histories of the bridge piers analysed at PGA 0.6g of record 25.

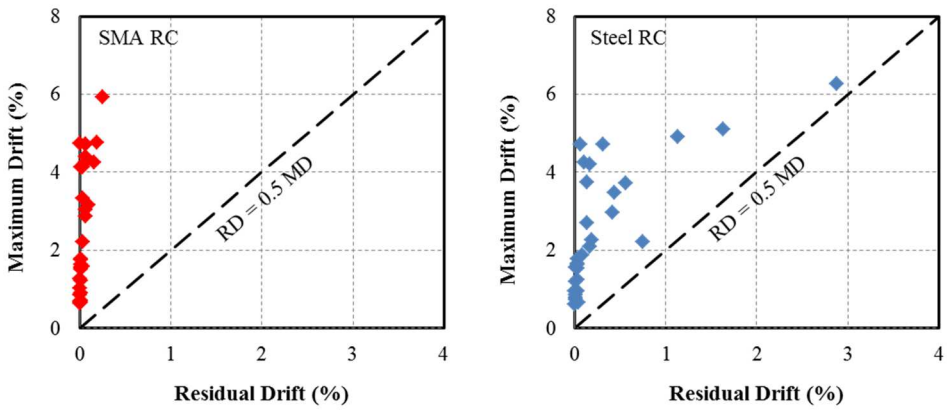

Figure 8-7 MD versus RD relation at PGA = 0.45g for SMA RC Pier 1 and steel RC Pier 1.

8.7.2 Seismic Fragility Analysis

The joined seismic fragility curves of the steel and SMA RC bridge piers are generated using the methodology introduced previously. The damage limit states for MD and RD defined in the fragility analysis are shown in Table 8-3. A five by five matrix based Performance Levels (PLs) are defined based on the combination of MD and RD performance of the piers. For the limit states based on MD, accepted values from previous investigations are adopted (Kim & Shinozuka, 2004; Dutta & Mander, 1999). Additionally, five damage states based on the RD are also defined. For the definition of the damage states tentative values suggested by previous investigations (O'Brien et al., 2007; Pampanin et al., 2002; Shrestha & Hao, 2015) and bridge design codes (JRA, 2006) are used. A threshold of 0.25% of RD is defined below which the piers will meet the serviceability requirement providing full functionality. While a RD of 1% is taken as an upper threshold requiring the demolition of the piers since repair work is extremely difficult. To elaborate, the probability of exceedance of PL (3,3) is the probability of MD>2.5% and RD>0.75%. It is also to be noticed that PLs defined by a given maximum drift ratio limit with lower residuals might represent the lesser damage state compared to the PLs with the same maximum drift ratio limit with larger residual drift limits.

Table 8-3 Definition of performance levels

Peak Drift(%) limit state (i)	Residual drift(%) limit state(j)				
	RD < 0.25	0.25< RD < 0.50	0.50< RD < 0.75	0.75< RD < 1.00	RD > 1.00
MD < 0.7	PL (1,1)	PL (1,2)	PL (1,3)	PL (1,4)	PL (1,5)
0.7 < MD < 1.5	PL (2,1)	PL (2,2)	PL (2,3)	PL (2,4)	PL (2,5)
1.5 < MD < 2.5	PL (3,1)	PL (3,2)	PL (3,3)	PL (3,4)	PL (3,5)
2.5 < MD < 5	PL (4,1)	PL (4,2)	PL (4,3)	PL (4,4)	PL (4,5)
MD > 5	PL (5,1)	PL (5,2)	PL (5,3)	PL (5,4)	PL (5,5)

With the defined damage limit states and the computed bridge responses (RDs and MDs), the conditional probability for the steel and SMA RC piers to exceed each performance level corresponding to each PGA value can be calculated with Equations (8.2) and (8.4). The joined fragility curves are generated by fitting the exceedance probability values with a lognormal cumulative distribution function. The effect of SMA and pier geometry on the joined fragility curves are investigated in detail.

8.7.2.1 Effect of SMA on Fragility Curve

The probability of exceedance corresponding to PL (3,2) and PL (4,2) for the SMA and steel RC Pier1 are compared in Figure 8-8. It is interesting to note that while considering lower performance level, i.e. PL (3,2), the similar fragility can be observed for both the piers. However, differences between the two piers are distinctly visible at higher performance level PL (4,2). Figure 8-9 compares the fragility curves obtained for various PLs (PL (2,2), PL (3,2), PL (4,2), PL (5,2)) for SMA RC and steel RC bridge pier. It can be observed that the fragility of the SMA RC piers is relatively higher at lower PLs (PL (2,2)). However, as the higher PLs are considered the performance of the SMA RC is improved. This behavior is because of the response of the steel RC piers that are characterized by slightly lower MD, but higher RD as compared to the SMA RC piers. At lower PLs, the pier responds within the elastic range or may incur small inelastic deformations with negligible residual deformations thus fragility curves of SMA RC are relatively higher than steel RC piers. As the residual displacement increases at higher PLs due to the increase in inelastic deformations, the performance of the steel RC piers gradually worsen in comparison to the SMA RC piers, thus results in relatively higher fragility curve for steel RC piers at higher PLs.

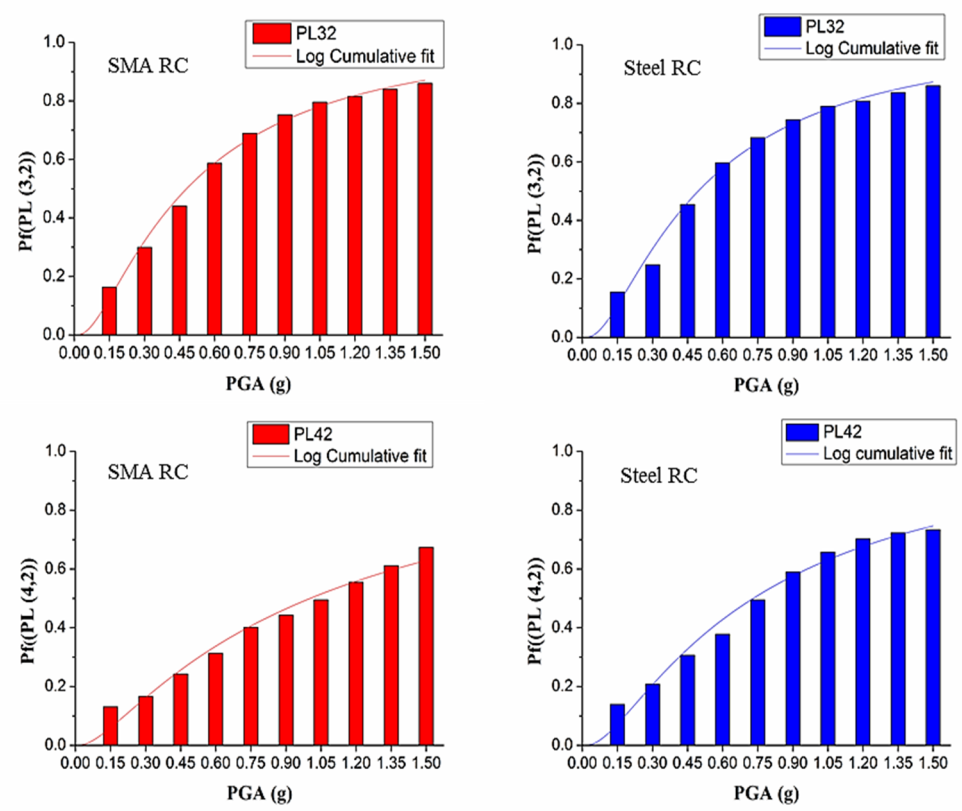

Figure 8-8 Probability of exceedance of PL (3,2) and PL (4,2) for SMA and steel RC Pier 1.

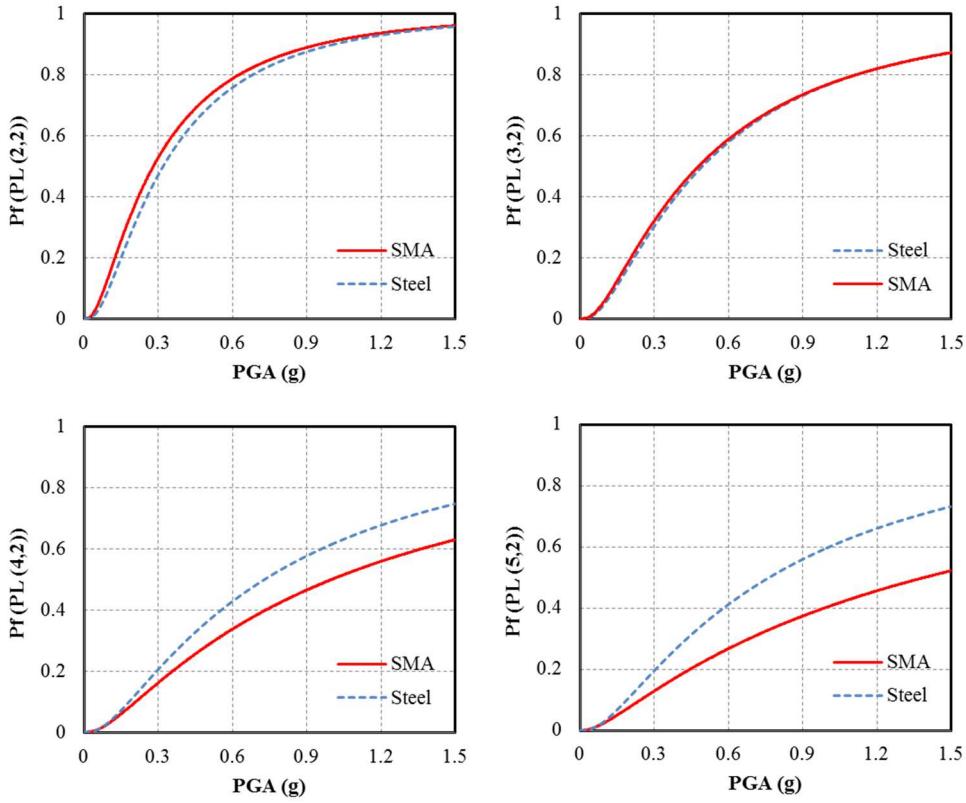

Figure 8-9 Comparison of the fragility curves at various PLs for Pier 1.

8.7.2.2 Effect of pier geometry on fragility curve

Comparisons between the fragility curves of Pier1 and Pier2 are made to evaluate the performance of steel and SMA reinforced bridge piers at various PLs. Figure 8-10 presents the comparison of the fragility curves for the piers at PL (2,1) and PL (3,1). As shown in the figure, Pier1 has a higher probability of exceedance of the performance level at lower intensity levels. On the contrary, at higher intensity levels Pier2 has a higher probability of exceedance. This dissimilarity of performances at lower intensity levels is because of the higher stiffness of the Pier2 resulting in relatively lower drifts at a lower intensity. However, as the higher intensity is considered the system with the higher stiffness attracts larger forces resulting in higher drift demands and consequently the higher fragility. Thus, the fragility curves for Pier1 and Pier2 intersects one another at a certain level of excitation. It is also to be noted that fragility curves for SMA piers are slightly higher compared to the steel counterparts for both the piers at the lower PLs (i.e. PL (2,1)) due to the reasons described previously. For PL (3,1) the probability of exceedance of SMA pier is similar to steel pier for Pier1 and marginally higher than steel pier for Pier2.

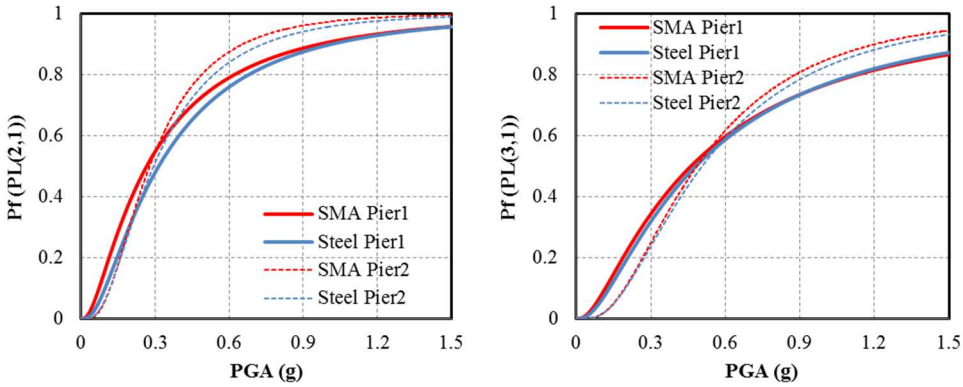

Figure 8-10 Comparison of the fragility curves at lower PLs for Pier 1 and Pier 2.

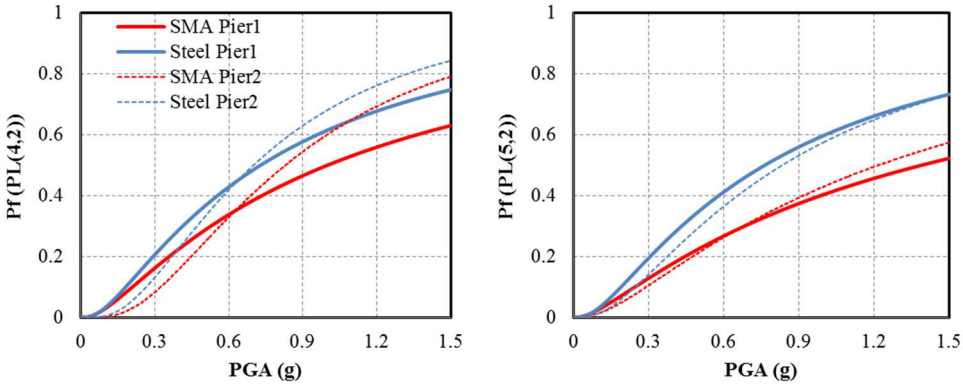

Figure 8-11 Comparison of the fragility curves at higher PLs for Pier 1 and Pier 2.

Figure 8-11 presents the comparison of the fragility curves for the piers at PL (4,2) and PL (5,2). As shown, the SMA piers outperform the steel piers at higher PLs due to its superior performance in residual deformation recovery. The response pattern of higher probability of exceedance of Pier1 at lower intensity levels and vice-versa is also clearly evident at PL (4,2). However, the pattern is less distinctive at PL (5,2) particularly for steel RC piers as the fragility curve of Pier1 converges with the fragility curve of Pier2 only at the highest intensity level (i.e., PGA 1.5 g).

To derive a comparison from the presented fragility curves of the studied piers, the median values of the fragility (50% probability of exceedance) of SMA and steel RC piers at PL (2,1) and PL(4,1) with respect to the ground motion intensity (PGA) for Pier1 are presented in Figure 8-12. As shown, at the lower PL the median value of probability for steel pier corresponds to a higher PGA than SMA pier; however, at higher PL the steel pier are much more fragile compared to the SMA pier. The median value of fragility is achieved for steel and SMA piers at PGA of 0.32 g and 0.27 g, respectively at PL (2,1), and at PGA of 0.60 g and 0.90 g, respectively at PL (4,1). Table 8.4 compares the PGA corresponding to the median values of the probability of exceedance at various PLs for the piers with steel and SMA

reinforcements. As shown at the lower PLs the ground motion intensity required to achieve the median value of probability of exceedance for SMA RC piers is slightly lower than that for the steel RC piers, suggesting better performance of steel RC piers. However, as the higher PLs are considered the required PGA for reaching the median value of the fragility for SMA RC piers improves significantly relative to the steel RC piers. As presented in the table, SMA RC piers start to outperform the steel RC piers at PL (4,3) and gradually the difference between the piers with two types of reinforcement increases with the PLs. It is interesting to note that the PGA corresponding to the median value for PL (5,1) for the piers are lower than that for PL (4,4) for Pier1. It should be noted that for a chosen system, at a given probability of exceedance, the higher intensity measure indicates a lower damage state and vice-versa. Therefore, for Pier1 PL (5,1) defined by a higher MD and a lower RD might represent a lesser damage state compared to PL (4,4) with slightly lower MD but higher RD. However, the above argument does not apply for the Pier2.

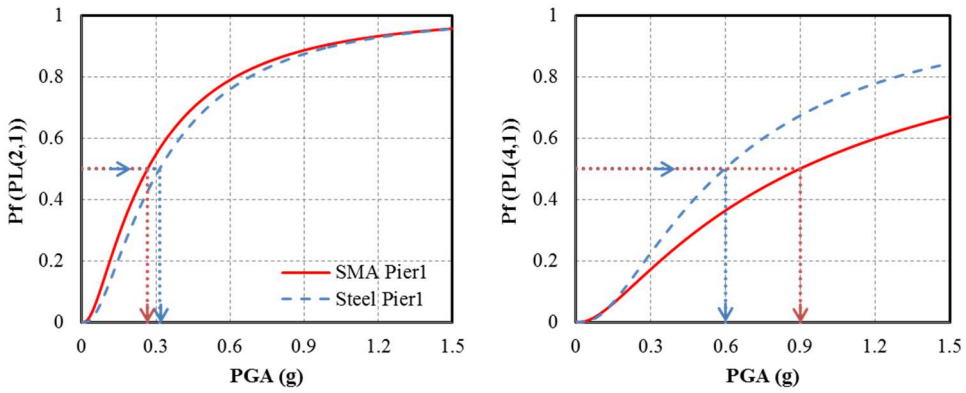

Figure 8-12 Comparison of the median value of probability of exceedance at PL (2,1) and PL (4,1) for Pier 1.

Table 8-4 Comparison of the ground motion PGA required to achieving the median value of probability of exceedance for the piers corresponding to different PLs (g).

Piers	PL (1,1)	PL (2,2)	PL (3,2)	PL (3,3)	PL (4,3)	PL (4,4)	PL (5,1)	PL (5,2)
SMA RC Pier1	0.14	0.28	0.48	0.49	1.00	1.31	1.08	1.39
Steel RC Pier1	0.15	0.32	0.50	0.50	0.73	0.93	0.62	0.77
Difference (%)	-7%	-13%	-4%	-2%	37%	31%	74%	81%
SMA RC Pier2	0.15	0.29	0.50	0.50	0.84	0.86	1.10	1.22
Steel RC Pier2	0.15	0.30	0.52	0.52	0.73	0.75	0.74	0.83
Difference (%)	0%	-3%	-4%	-4%	15%	13%	49%	47%

8.8 Conclusion

Shape Memory Alloy (SMA) reinforcement bars have been significantly researched in recent as a plausible replacement of conventional steel reinforcement bars. The objective of this paper is to conduct a performance-based seismic assessment of bridge piers with SMA and steel reinforcement considering the combined maximum and residual deformations. A recently formulated probabilistic framework that uses three-dimensional performance matrix combining the maximum and the residual deformation to define performance levels and performance objective at the different level of seismic intensity is utilized to fulfil the objective. Joined fragility curves, representing the probabilities of exceedance of the performance level defined by a pair of maximum and residual deformations, are developed for the bridge piers.

The results signify the need of considering the residual deformations in the performance of the structures. Neglecting the residual deformation, while evaluating the seismic performance of structures, may not provide a realistic depiction of the performance. The results show that at lower performance levels steel RC bridge piers with the higher initial stiffness and energy dissipation capacity perform slightly better than the SMA RC piers. This result could be attributed to the relatively lower maximum deformation of the steel RC piers and to the insignificant residual deformations at these performance levels. However, the SMA RC piers have the lower probability of exceedance at higher performance level as residual deformation along with the maximum deformations have an influence on the fragility curve at these levels. The results also indicate that the Pier2 with higher stiffness have a lower probability of exceedance at all the performance levels at lower seismic ground motion intensities than Pier1. On the contrary, at higher intensities the opposite results are observed due to the stiffer pier attracting higher seismic forces. The results presented advocate the benefits of using SMA reinforcement in the plastic hinge region of bridge piers to limit the damages, particularly those constructed at moderate-high seismicity regions.

This study focuses on the uncertainty in the ground motions to produce the fragility curves. Other sources of uncertainties arising from material properties of SMA/steel reinforcement and concrete are not considered. This is because it is well understood that variations of earthquake ground motions are more significant than those of structural parameters (Padgett & DesRoches, 2007; Kwon & Elnashai, 2006). Moreover, fatigue behavior of SMA reinforcements is not considered either. Future works will focus on these limitations of the present study.

8.9 References

Alam, M. S., Youssef, M. A., & Nehdi, M. (2008). Analytical prediction of the seismic behaviour of superelastic shape memory alloy reinforced concrete elements. *Engineering Structures*, *30*(12), 3399-3411.

Alam, M. S., Youssef, M. A., & Nehdi, M. L. (2010). Exploratory investigation on mechanical anchors for connecting SMA bars to steel or FRP bars. *Materials and structures*, *43*(1), 91-107.

Alipour, A., Shafei, B., & Shinozuka, M. (2010). Performance evaluation of deteriorating highway bridges located in high seismic areas. *Journal of Bridge Engineering*, *16*(5), 597-611.

Auricchio, F., & Sacco, E. (1997). A superelastic shape-memory-alloy beam model. *Journal of intelligent material systems and structures*, *8*(6), 489-501.

Billah, A. M., & Alam, M. S. (2012). Seismic performance of concrete columns reinforced with hybrid shape memory alloy (SMA) and fiber reinforced polymer (FRP) bars. *Construction and Building Materials*, *28*(1), 730-742.

Billah, A. M., Alam, M. S., & Bhuiyan, M. R. (2012). Fragility analysis of retrofitted multicolumn bridge bent subjected to near-fault and far-field ground motion. *Journal of Bridge Engineering*, *18*(10), 992-1004.

Billah, A. H. M., & Alam, M. S. (2015). Seismic fragility assessment of concrete bridge pier reinforced with superelastic shape memory alloy. *Earthquake Spectra*, *31*(3), 1515-1541.
Choi, E., DesRoches, R., & Nielson, B. (2004). Seismic fragility of typical bridges in moderate seismic zones. *Engineering Structures*, *26*(2), 187-199.

Choi, E., DesRoches, R., & Nielson, B. (2004). Seismic fragility of typical bridges in moderate seismic zones. *Engineering Structures*, *26*(2), 187-199.

Choi, H., Saiidi, M. S., Somerville, P., & El-Azazy, S. (2010). Experimental study of reinforced concrete bridge columns subjected to near-fault ground motions. *ACI Structural Journal*, *107*(1), 3-12.

Christopoulos, C., Pampanin, S., & Nigel Priestley, M. J. (2003). Performance-Based Seismic Response of Frame Structures Including Residual Deformations Part I: Single-Degree of Freedom Systems. *Journal of Earthquake Engineering*, *7*(01), 97-118.

Cruz Noguez, C. A., & Saiidi, M. S. (2011). Shake-table studies of a four-span bridge model with advanced materials. *Journal of Structural Engineering*, *138*(2), 183-192.

Dutta, A., & Mander, J. B. (1998, June). Seismic fragility analysis of highway bridges. In *Proceedings of the INCEDE-MCEER center-to-center project workshop on earthquake engineering Frontiers in transportation systems* (pp. 22-23).

Federal Emergency Management Agency (FEMA) (1997) FEMA 273, NEHRP Guidelines for the Seismic Rehabilitation of Buildings. Washington, D.C.

Fujino, Y., Hashimoto, S., & Abe, M. (2005). Damage analysis of Hanshin Expressway viaducts during 1995 Kobe earthquake. I: Residual inclination of reinforced concrete piers. *Journal of Bridge Engineering*, *10*(1), 45-53.

Fugazza, D. (2003). Shape-memory alloy devices for earthquake engineering: Mechanical properties, constitutive modelling and numerical simulations. Master's Thesis, University of Pavia, Italy.

Gencturk, B., & Hosseini, F. (2014, July). Use of Cu-based superelastic alloys for innovative design of reinforced concrete columns. In *10th US National Conf. on Earthquake Engineering*.

Hosseini, F., Gencturk, B., Lahpour, S., & Gil, D. I. (2015). An experimental investigation of innovative bridge columns with engineered cementitious composites and Cu–Al–Mn superelastic alloys. *Smart Materials and Structures*, *24*(8), 085029.

International Code Council, et al. (2009). International building code. International Code Council.

Japan Road Association. (2006) Specifications for Highway Bridges. Japan.

Johnson, N., Saiidi, M.S., & Sanders, D. (2006). Large-Scale Experimental and Analytical Seismic Studies of a Two-Span Reinforced Concrete Bridge System. Report No. CCEER-06-02, Dept. of Civil Engineering, Univ. of Nevada, Reno, Nevada.

Kawashima, K., & Unjoh, S. (1997). The damage of highway bridges in the 1995 Hyogo-ken nanbu earthquake and its impact on Japanese seismic design. *Journal of Earthquake Engineering*, *1*(03), 505-541.

Kawashima, K., Unjoh, S., Hoshikuma, J. I., & Kosa, K. (2011). Damage of bridges due to the 2010 Maule, Chile, Earthquake. *Journal of Earthquake Engineering*, *15*(7), 1036-1068.

Ketchum, M., Chang, V., and Shantz, T. (2004). Influence of design ground motion level on highway bridge costs. Report No. Lifelines 6D01, Pacific Earthquake Engineering Research Center, University of California, Berkley, California.

Kim, S. H., & Shinozuka, M. (2004). Development of fragility curves of bridges retrofitted by column jacketing. *Probabilistic Engineering Mechanics*, *19*(1), 105-112.

Kwon, O. S., & Elnashai, A. (2006). The effect of material and ground motion uncertainty on the seismic vulnerability curves of RC structure. *Engineering structures*, *28*(2), 289-303.

Lee, W. K., & Billington, S. L. (2011). Performance-based earthquake engineering assessment of a self-centering, post-tensioned concrete bridge system. *Earthquake Engineering & Structural Dynamics*, *40*(8), 887-902.

Li, C., Hao, H., Li, H., & Bi, K. (2015). Seismic Fragility Analysis of Reinforced Concrete Bridges with Chloride Induced Corrosion Subjected to Spatially Varying Ground Motions. *International Journal of Structural Stability and Dynamics*, 1550010.

Machado, L. G., and M. A. Savi. "Medical applications of shape memory alloys." *Brazilian Journal of Medical and Biological Research* 36.6 (2003): 683-691.

Mander, J. B., Priestley, M. J., and Park, R. (1988). Theoretical stress-strain model for confined concrete. *Journal of Structural engineering,* 114(8), 1804-1826.

Martínez-Rueda, J. E., & Elnashai, A. S. (1997). Confined concrete model under cyclic load. *Materials and Structures*, *30*(3), 139-147.

Menegotto, M., and Pinto, P.E. (1973). Method of analysis of cyclically loaded RC plane frames including changes in geometry and non-elastic behaviour of elements under combined normal force and bending. Symp. on the Resistance and Ultimate deformability of Structures acted on by well-defined repeated loads, IABSE, Zurich, Switzerland, 15-22.

Moehle, J., Stojadinovic, B., Der Kiureghian, A., & Yang, T. Y. (2005). An Application of PEER Performance-Based Earthquake Engineering Methodology, Research Digest No. 2005-1. *Pasadena, California*.

Nakashoji, A., and Saiidi, M.S. (2014). Seismic performance of Squared Nickel-Titanium reinforced ECC column with Headed couplers. Report No. CCEER-14-05, Dept. of Civil Engineering, University of Nevada, Reno, Nevada.

O'Brien. M., Saiidi, M. S., Sadrossadat-Zadeh, M. (2007) A study of concrete bridge columns using Innovative materials subjected to cyclic loading. Report no. CCEER-07-01, Dept. of Civil Engineering, University of Nevada, Reno, Nevada.

Otani, S. (1974). SAKE, A Computer Program for Inelastic Response of R/C Frames to earthquakes. Report UILU-Eng-74-2029, Civil Engineering Studies, University of Illinois at Urbana-Champaign, Illinois.

Padgett, J. E., & DesRoches, R. (2007). Sensitivity of seismic response and fragility to parameter uncertainty. *Journal of Structural Engineering*, *133*(12), 1710-1718.

Padgett, J. E., Nielson, B. G., & DesRoches, R. (2008). Selection of optimal intensity measures in probabilistic seismic demand models of highway bridge portfolios. *Earthquake Engineering & Structural Dynamics*, *37*(5), 711-725.

Pampanin, S., Christopoulos, C., and Priestley, M. J. N. (2002). Residual deformations in the performance based seismic assessment of frame structures. Research Report ROSE-2002/02, European School for Advanced Studies in Reduction of Seismic Risk, University of Pavia, Italy.

Pampanin, S., Christopoulos, C., & Nigel Priestley, M. J. (2003). Performance-based seismic response of frame structures including residual deformations Part II: Multi-degree of freedom systems. *Journal of Earthquake Engineering*, *7*(01), 119-147.

Paulay, T., and Priestley, M.J.N. (1992). Seismic Design of Reinforced Concrete and Masonry Buildings, John Wiley & Sons Inc., New York.

Phan, V., Saiidi, M. S., Anderson, J., & Ghasemi, H. (2007). Near-fault ground motion effects on reinforced concrete bridge columns. *Journal of structural engineering*, *133*(7), 982-989. Ramirez, C. M., & Miranda, E. (2012). Significance of residual drifts in building earthquake loss estimation. *Earthquake Engineering & Structural Dynamics*, *41*(11), 1477-1493.

Saiidi, M. S., & Wang, H. (2006). Exploratory study of seismic response of concrete columns with shape memory alloys reinforcement. *ACI Structural Journal*, *103*(3), 436.

Saiidi, M. S., O'Brien, M., & Sadrossadat-Zadeh, M. (2009). Cyclic response of concrete bridge columns using superelastic nitinol and bendable concrete.*ACI Structural Journal*, *106*(1), 69. Saiidi, M. S., & Ardakani, S. M. (2012). An analytical study of residual displacements in RC bridge columns subjected to near-fault earthquakes.*Bridge Structures*, *8*(1), 35-45.

SEAOC Vision 2000 Committee. (1995). Performance-based seismic engineering. *Structural Engineers Association of California, Sacramento, California*.

Shrestha, K. C., Saiidi, M. S., & Cruz, C. A. (2015). Advanced materials for control of post-earthquake damage in bridges. *Smart Materials and Structures*, *24*(2), 025035.

Shrestha, K. C., Araki, Y., Nagae, T., Koetaka, Y., Suzuki, Y., Omori, T., Sutou Y., Kainuma R., & Ishida, K. (2013). Feasibility of Cu–Al–Mn superelastic alloy bars as reinforcement elements in concrete beams. *Smart Materials and Structures*, 22(2):025025.

Shrestha, B., & Hao, H. (2015). Parametric study of seismic performance of superelastic shape memory alloy-reinforced bridge piers. *Structure and Infrastructure Engineering*, 1-14. (Available on-line)

Shrestha, B., Hong, H., & Bi, K. (2016). Devices for protecting bridge superstructures from pounding and unseating damages: an overview. *Structure and Infrastructure Engineering*. (In press)

Tazarv, M., & Saiidi, M. S. (2013). Analytical studies of the seismic performance of a full-scale SMA-reinforced bridge column. *Int. J. Bridge Eng*, *1*(1), 37-50.

Tazarv, M., & Saiid Saiidi, M. (2014). Reinforcing NiTi superelastic SMA for concrete structures. *Journal of Structural Engineering*, *141*(8), 04014197.

Uma, S. R., Pampanin, S., & Christopoulos, C. (2010). Development of probabilistic framework for performance-based seismic assessment of structures considering residual deformations. *Journal of Earthquake Engineering*, *14*(7), 1092-1111.

Varela, S., & Saiidi, M. S. (2014). Dynamic performance of novel bridge columns with superelastic CuAlMn shape memory alloy and ECC. *Int. J. Bridge Eng*, *2*(3), 29-58.

Wu, M. H., & Schetky, L. M. (2000). Industrial applications for shape memory alloys. In *Proceedings of the international conference on shape memory and superelastic technologies* (pp. 171-182).

Vosooghi, A., and Saiidi, M.S. (2010). Post-Earthquake Evaluation and Emergency Repair of Damaged RC bridge Columns using CFRP Materials. Report No. CCEER-10-05, Dept. of Civil Engineering, University of Nevada, Reno, Nevada.

Wehbe, N. I., Saiidi, M. S., & Sanders, D. H. (1999). Seismic performance of rectangular bridge columns with moderate confinement. *Structural Journal*,*96*(2), 248-258.

Youssef, M. A., Alam, M. S., & Nehdi, M. (2008). Experimental investigation on the seismic behavior of beam-column joints reinforced with superelastic shape memory alloys. *Journal of Earthquake Engineering*, *12*(7), 1205-1222.

Zhang, J., & Huo, Y. (2009). Evaluating effectiveness and optimum design of isolation devices for highway bridges using the fragility function method. *Engineering Structures*, *31*(8), 1648-1660.

Zhang, Y., Hu, X., & Zhu, S. (2009). Seismic performance of benchmark base-isolated bridges with superelastic Cu–Al–Be restraining damping device. *Structural Control and Health Monitoring*, *16*(6), 668-685.

CHAPTER 9
CONCLUSION AND RECOMMENDATIONS

9.1 Main Contributions

The objective of this research is to investigate pounding and unseating damages on bridges subjected to spatially varying ground motion and to explore effectiveness of various mitigation methods to reduce the vulnerability during earthquake events. Large-scale testing was conducted to identify the influences of spatially varying ground motion on pounding responses of the adjacent bridge segments along with the effectiveness of the mitigation devices. Moreover, effectiveness of various pounding and unseating damage mitigation devices was investigated numerically. Furthermore, bridge piers with superelastic SMA reinforcement were studied to address the problem arising from the residual deformation of conventional steel reinforced bridge piers. The major conclusions made from these works are detailed below.

Review of devices to mitigate pounding and unseating damages

An overview of the devices applied or proposed to mitigating damages on bridge structures resulting from excessive relative displacement at expansion joints is presented. Up-to-date information on experimental and numerical works along with the present state-of-practice on these devices, such as restrainers, dampers and other devices, is presented in the review. The merits and limitations of these devices for practical applications are discussed in detail, which would help design engineers to choose and design appropriate devices to mitigate relative displacement induced damages.

Shake table studies of pounding and unseating damages

In this study, pounding response of adjacent bridge frames subjected to spatially varying ground motions are investigated using shake table experiments and numerical analyses. Pounding damages at the bridge joints, as observed during strong earthquakes, are simulated in the laboratory using shake table array system on two-frame bridge models scaled to1:6. The mechanisms resulting in pounding damages along with spikes in the acceleration time history are discussed. The experimental studies and accompanying numerical investigations clearly demonstrated that adjusting the fundamental periods of adjacent bridge structures close to each other are not sufficient to avoid damages resulting from pounding and unseating. The results from parametrical studies also show that spatially varying ground motions result in severest response and considering only the wave passage effects are not sufficient as this would lead to underestimation of the responses.

Effectiveness of using rubber bumpers and restrainers

The effectiveness of using two types of restrainers (SMA and Steel) combined with the rubber bumpers on mitigating pounding and unseating damages to the adjacent bridge components are studied. SMA restrainers are found to be more effective in restricting the bridge joint opening and residual joint opening. The rubber bumpers are found to be effective in alleviating large pounding impacts. However, the rubber bumpers also result in more numbers of poundings due to the reduction of the gap width and also increase the duration of impact. Applying SMA restrainers along with rubber bumpers are found to be the most effective in mitigating damaging impacts as well as large opening relative displacements.

Seismic Response analysis of multiple-frame bridge with unseating restrainers

Parametric studies on the response of multiple-frame bridges with unseating restrainers are conducted using nonlinear finite element models subjected to spatially varying ground motion. Spatially varying ground motions, though reduce seismic demands on the piers of the bridge frames, have detrimental effects on relative displacement responses. Design method of restrainers that considers only the uniform ground motions could significantly underestimate the required stiffness and strength of the restrainers when subjected to spatially varying ground motions. It is also identified that the recommendation provided by the bridge codes to adjust the fundamental period of adjacent bridge segments close to each-other is indispensable to alleviate the relative displacement induced damages. However, this recommendation alone is not sufficient to prevent damages at bridge joints due to the relative displacements induced by spatially varying ground motions. Though SSI usually results in an increase in the absolute drift of the bridge frames, the relative displacement between the bridge segments could reduce due to the increase in flexibility and fundamental period of adjacent frames leading to in phase response between adjacent bridge frames.

Effectiveness of rotational friction hinge dampers

Rotation friction hinge dampers could be an ideal retrofit device to mitigate the relative displacement induced damages in base-isolated simply supported bridges. Moreover, these devices are also effective in reducing the shear strain of base-isolators thus preventing the bearing failure. Optimum slip forces of the dampers to mitigate the relative displacement induced damages and bearing failure are calculated for the studied bridge. It is also found that effectiveness of the dampers is not significantly affected by small changes in optimum slip forces, which are expected during the lifetime of the dampers. V-type dampers are found to be more effective in mitigating relative displacement induced damages and the bearing shear strains. However, these dampers could increase the drift of piers as forces from superstructures are transferred to the piers. R-type damper would be a suitable choice to limit the forces

transferred to the piers; however, it is comparatively less effective on mitigating pounding, unseating, and bearing shear deformations.

Parametric study of seismic performance of superelastic SMA reinforced bridge piers

Seismic performance of SMA RC bridge bents is parametrically compared with steel RC bridge bents. Twelve prototype bridge bents representing three geometries with single and multiple piers with superelastic SMA or steel reinforcement are analyzed under monotonic and seismic loading. It is found that major difference in their performance under monotonic loading is the yielding drift. Owing to the lower yielding strain of steel, rebars of conventional bridge piers yield at relatively lower drift/rotation compared to SMA rebar. It is revealed that SMA reinforced bridge piers have comparable performance to steel reinforced bridge piers regarding the peak drifts. However, the residual drifts of the SMA RC bridge piers are significantly smaller than that of steel RC bridge piers. The bridge bents with superelastic SMA reinforcement at plastic hinge region showed a significant reduction in residual drifts compared to steel reinforced bridge bents. In the case of bridge bents with single piers, residual drift reduced to approximately 1/4 of that observed for steel RC bents and for bridge bents with multiple bridge piers it reduced to almost 1/6.

Performance-based assessment of superelastic SMA reinforced bridge piers

A performance-based seismic assessment of bridge piers with superelastic SMA reinforcement considering the combined maximum and residual deformation limit states is presented. A recently formulated probabilistic framework that uses three-dimensional performance matrix to combine the maximum and the residual deformation to define performance levels and performance objective at the different level of seismic intensity is used. The results emphasize the need for considering the residual deformation in the performance of the structures so that safety and serviceability after the seismic event could be considered simultaneously in the structural performance assessment. It is found that at lower performance levels the steel RC bridge piers with higher initial stiffness and energy dissipation capacity performs slightly better than SMA RC piers. However, SMA RC bridge piers outperform steel RC bridge piers at higher performance levels. The results highlight the benefits of using SMA reinforcement at the plastic hinge region of bridge piers constructed in moderate-high seismicity regions.

9.2 Recommendations for future works

Despite the extensive research work that has been performed in the study, many topics would benefit from further research attention. The following list highlights topics of particular interest and relevance to the subjects discussed in this thesis.

1. Large scale experiments are conducted to investigate pounding and unseating damages that could arise in adjacent bridge segments subjected to spatially varying ground motions. Though an attempt is made to reproduce a realistic bridge model as far as possible, due to the limitation few compromises, e.g. neglecting of abutment effects, are made. Moreover, many other parameters such as bridge geometry, soil site condition, SSI and skewness that could have a significant effect on pounding response between the adjacent bridge segments are not considered due to various constraints. It is envisaged that future testing would address these factors.

2. Experimental investigations are required to identify the effectiveness of using the combination of shock absorbing devices and restrainers to mitigate the pounding and unseating damages. However, it is also to be noted that natural rubber bumpers, commonly used as a shock absorber, have durability issues and needs replacement after a period of few years. It is desirable to use shock absorber that can last for the entire lifespan of the bridge.

3. Although significant research works have already been carried to formulate a design method of seismic restrainers, as highlighted in this study such efforts are not sufficient as these do not consider the relative displacement induced by spatial variability of ground motions. As the spatial variation of earthquake ground motions is inevitable along the supports of extended structures such as bridges, more focus should be provided into this.

4. The effectiveness of rotational friction hinge dampers to mitigate relative displacement induced damages on bridge structures should be evaluated in the laboratory, and more numerical investigation should be carried out considering the three dimension bridge models. Additionally, presently used friction dampers could suffer from residual deformations. Evaluation of the effects of these residual deformations on the performance of the dampers is necessary under repeated earthquake event, which is likely to occur during aftershock events. Moreover, some modification on the device to enable the dampers to re-center automatically after an earthquake event are welcomed.

5. The mechanical properties of superelastic SMA could vary significantly due to the differences in mechanical processes involved in its manufacturing. The effects of the influence of mechanical properties of SMA on its responses to earthquake loadings needs to be studied. Another critical factor that affects the response of SMA is its

fatigue behavior. Further studies on the influence of fatigue behavior of SMA on the seismic response of SMA RC bridge piers are essential.

BIBLOGRAPHY DISCLAIMER

Every reasonable effort has been made to acknowledge the owners of copyright material. I would be pleased to hear from any copyright owner who has been omitted or incorrectly acknowledged.

APPENDIX I

STATEMENTS OF THE CO-AUTHORS

To Whom It May Concern

I, Bipin Shrestha, contributed (conducted the thorough review of literature and wrote the manuscript which was revised and edited by other co-authors) to the paper entitled (Devices for protecting bridge superstructures from pounding and unseating damages: an overview).

(_____)

I, as a Co-Author, endorse that this level of contribution by the candidate indicated above is appropriate.

(Prof. Hong Hao) (_____)

(Dr. Kaiming Bi) (_____)

To Whom It May Concern

I, Bipin Shrestha, contributed (prepared details and conducted the experimental study with help of other co-authors, carried out numerical investigation and finally wrote the manuscript which was revised and edited by other co-authors) to the paper entitled (Experimental and numerical analyses on pounding interaction between adjacent bridge frames subjected to spatially varying ground motions).

()

I, as a Co-Author, endorse that this level of contribution by the candidate indicated above is appropriate.

(Mr. Li-Xiang He) (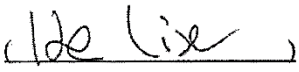)

(Prof. Hong Hao) (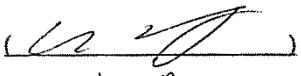)

(Dr. Kaiming Bi) (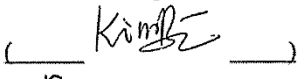)

(Prof. Wei-Xin Ren) ()

To Whom It May Concern

I, Bipin Shrestha, contributed (conducted the numerical investigation and wrote the manuscript which was revised and edited by other co-authors) to the paper entitled (Effectiveness of using rubber bumper and restrainer on mitigating pounding and unseating damage of bridge structures subjected to spatially varying ground motions).

(_____)

I, as a Co-Author, endorse that this level of contribution by the candidate indicated above is appropriate.

(Prof. Hong Hao) (_____)

(Dr. Kaiming Bi) (_____)

To Whom It May Concern

I, Bipin Shrestha, contributed (conducted the numerical investigation and wrote the manuscript which was revised and edited by other co-authors) to the paper entitled (Seismic response analysis of multiple-frame bridges with unseating restrainers considering ground motion spatial variation and SSI).

(_____)

I, as a Co-Author, endorse that this level of contribution by the candidate indicated above is appropriate.

(Prof. Hong Hao) (_____)

(Dr. Kaiming Bi) (_____)

To Whom It May Concern

I, Bipin Shrestha, contributed (conducted the numerical investigation with help of the co-authors, wrote the manuscript which was revised and edited by other co-authors) to the paper entitled (On the effectiveness of rotational friction hinge damper to control responses of multi-span simply supported bridge to non-uniform ground motions).

(_____)

I, as a Co-Author, endorse that this level of contribution by the candidate indicated above is appropriate.

(Prof Hong Hao) (_____)

(Mr. Nazman HJ Ibrahim) (_____)

(Dr. Kaiming Bi) (_____)

To Whom It May Concern

I, Bipin Shrestha, contributed (conducted the numerical investigation, wrote the manuscript which was revised and edited by other co-authors) to the paper entitled (Parametric study of seismic performance of super-elastic shape memory alloy-reinforced bridge piers).

()

I, as a Co-Author, endorse that this level of contribution by the candidate indicated above is appropriate.

(Prof. Hong Hao) (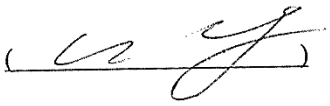)

To Whom It May Concern

I, Bipin Shrestha, contributed (conducted the numerical investigation, derived the fragility curved with the help of the second author, wrote the manuscript which was revised and edited by other co-authors) to the paper entitled (Performance-based seismic assessment of superelastic shape memory alloy reinforced bridge piers considering residual deformations).

(_____)

I, as a Co-Author, endorse that this level of contribution by the candidate indicated above is appropriate.

(Mr. Chao Li) (_____)

(Prof. Hong Hao) (_____)

(Prof. Hong-Nan Li) _____

APPENDIX II

COPYRIGHT CLEARANCE

The proof of the rights, granted by Elsevier for the publication that forms a chapter of this thesis, to reproduce the contribution in the thesis are attached below.

ELSEVIER LICENSE
TERMS AND CONDITIONS

Mar 29, 2016

This is a License Agreement between Bipin Shrestha ("You") and Elsevier ("Elsevier") provided by Copyright Clearance Center ("CCC"). The license consists of your order details, the terms and conditions provided by Elsevier, and the payment terms and conditions.

All payments must be made in full to CCC. For payment instructions, please see information listed at the bottom of this form.

Supplier	Elsevier Limited The Boulevard,Langford Lane Kidlington,Oxford,OX5 1GB,UK
Registered Company Number	1982084
Customer name	Bipin Shrestha
Customer address	6 Nightjar Lane Langford, WA 6147
License number	3801690450262
License date	Feb 03, 2016
Licensed content publisher	Elsevier
Licensed content publication	Engineering Structures
Licensed content title	Effectiveness of using rubber bumper and restrainer on mitigating pounding and unseating damage of bridge structures subjected to spatially varying ground motions
Licensed content author	Bipin Shrestha,Hong Hao,Kaiming Bi
Licensed content date	15 November 2014
Licensed content volume number	79
Licensed content issue number	n/a
Number of pages	16
Start Page	195
End Page	210
Type of Use	reuse in a thesis/dissertation
Portion	full article
Format	print
Are you the author of this Elsevier article?	Yes
Will you be translating?	No
Title of your thesis/dissertation	Numerical and Experimental study of pounding damages in adjacent bridge structures subjected to spatially varying ground motion and its mitigation method
Expected completion date	Apr 2016
Estimated size (number of pages)	180